Title
Non-standard Amino Acids for Synthetic Polypeptide-based Biomaterials

Author
Benavides, Isaac Augusto

Publication Date
2022

Peer reviewed|Thesis/dissertation

UNIVERSITY OF CALIFORNIA

Los Angeles

Non-standard Amino Acids for Synthetic Polypeptide-based Biomaterials

A dissertation submitted in partial satisfaction of the

requirements for the degree Doctor of Philosophy

in Chemistry

by

Isaac Benavides

2022

ABSTRACT OF THE DISSERTATION

Non-standard Amino Acids for Synthetic Polypeptide-based Biomaterials

by

Isaac Benavides

Doctor of Philosophy in Chemistry

University of California, Los Angeles, 2022

Professor Timothy J. Deming, Chair

Synthetic polypeptides are protein-mimetic materials that have been studied intensely for their potential biomedical applications. Advancements in polypeptide synthesis and peptide chemistries have enabled the design of structurally diverse biomaterials for a wide-range of applications. Their peptide bond backbone imbues the polymers with excellent biocompatibility while the relationship between amino acid residue and backbone structure permits the design of highly organized, supramolecular structures for biological applications. This dissertation describes recent advancements in synthetic polypeptides preparation, incorporation of non-standard amino acids, and the design of stimuli-responsive materials in Chapter 1. The promise of synthetic polypeptides for the biomedical field and development of new biomaterials is demonstrated throughout this dissertation.

Chapter 2 describes the preparation of poly(L-homoserine), **S^{H}**, a non-ionic, water-soluble polypeptide for use in diblock copolypeptide assemblies. Characterization of **S^{H}** properties revealed a disordered conformation that was maintained with increasing molecular weight, physiologically relevant ionic strength, and across a wide range of pH. The preparation of poly(L-homoserine)-*b*-poly(L-serine) amphiphilic diblock copolypeptides resulted in ordered assembly into unilamellar vesicles, highlighting the potential of **S^{H}** as a water-solubilizing segment for biomaterial design.

Chapter 3 describes the first successful synthesis of high molecular weight poly(dehydroalanine), **A^{DH}**, via a soluble poly(L-cysteine) precursor. The unique α,β-unsaturation of the planar dehydroalanine residues made **A^{DH}** an intriguing target for conformational studies and side-chain chemistries for further modification. Investigations into the preferred conformation of **A^{DH}** revealed a new “hybrid coil” containing aspects of both a 2_5-helix and 3_{10}-helix in the solid and solution state. The soluble poly(L-cysteine) precursor allowed preparation of **A^{DH}-**containing statistical and diblock colypeptides that are highly reactive towards amine and thiol nucleophiles, which provide a useful functional handle for the introduction of biologically relevant moieties. Adding to the intrigue of **A^{DH}**, characterization of the homopolymer spectroscopic properties reveal an extraordinary blue fluorescence, potentially useful for the design of label-free fluorescent biomaterials for imaging applications**.**

Chapter 4 focuses on the design of PEG-*b*-polypeptide based complex coacervate core micelles, C3Ms, for oligonucleotide delivery. Pegylated cationic, α-helical poly(S-alkyl-L-homocysteine) copolymers were prepared and characterized for single-stranded oligonucleotide complexation and release. Optimization of the

copolymer composition and length resulted in highly stable, nano-scale C3Ms when complexed with poly(adenylic acid), poly(A). Characterization of the poly(A)-C3Ms revealed a monomodal size distribution with excellent poly(A) encapsulation efficiency, (>90%). The stimuli-responsive nature of the poly(A)-C3Ms was showcased by triggering release of the oligonucleotide cargo in the presence of other multivalent anions and basic pH.

The dissertation of Isaac Benavides is approved.

William M. Gelbart

Joseph A. Loo

Andrea M. Kasko

Timothy J. Deming, Committee Chair

University of California, Los Angeles

2022

TABLE OF CONTENTS

LIST OF TABLES

LIST OF FIGURES

List of Abbreviations

PEG_{113}-b-5b$_x$	PEG_{113}-*b*-poly(*S*-(3-(2-L-valine amido)ethoxy)-2-hydroxypropyl)-L-homocysteine hydrochloride)
PEG_{113}-b-5c$_x$	PEG_{113}-*b*-poly(*S*-(3-(2-L-leucine amido)ethoxy)-2-hydroxypropyl)-L-homocysteine hydrochloride)
A	poly(L-alanine)
A^{DH}	poly(dehydroalanine)
tBu-Glu	γ-tert-butyl glutamate
C3Ms	complex coacervate core micelles
C^{BCM}	poly(S-(tert-butoxycarbonylmethyl)-L-cysteine)
C^{CM}	poly(S-carboxymethyl-L-cysteine)
CD	circular dichroism
Đ	dispersity
Dha	dehydroalanine
DI	deionized
DMF	dimethyl formamide
DMSO	dimethyl sulfoxide
d-TFA	deuterated trifluoroacetic acid
E^B	poly(γ-tert butyl-L-glutamate)
Et-Hse	O-propionyl-L-homoserine
FITC	fluorescein isothiocyanate
FTIR	fourier transform infrared spectroscopy
K	poly(L-lysine)
GPC	gel permeation chromatography
HFIP	hexafluoroisopropanol
HMDS	bis(trimethylsilyl) amine
iPr-Hse	O-isobutyryl-L-homoserine
KTFA	potassium trifluoroacetate
LCST	lower critical solution temperature
LSCM	laser scanning confocal microscopy
M	poly(L-methionine)
M:I	monomer to initiator ratio
Me-Hse	O-acetyl-L-homoserine
MeOH	methanol
M_n	number average molecular weight
M^o	poly(L-methionine sulfoxide)
mPEG-NCO	monomethoxy polyethylene glycol isocyanate
MWCO	molecular weight cutoff
$NaHCO_3$	sodium bicarbonate
NCA	α-amino acid *N*-carboxyanhydride
NMR	nuclear magnetic resonance
OEG	oligoethylene glycol

PEC	polyelectrolyte complex
PEG	poly(ethylene glycol)
Ph-Hse	O-benzoyl-L-homoserine
poly(A)	poly(adenylic acid)
PPM	post-polymerization modification
R-Hse	side-chain protected L-homoserine amino acid
ROP	ring-opening polymerization
S	poly(L-serine)
S^H	poly(L-homoserine)
SPPS	solid phase peptide synthesis
tBu-Hse	O-pivaloyl-L-homoserine
tBu-S	O-pivaloyl-L-serine
TEA	triethyl amine
TFA	trifluoroacetic acid
THF	tetrahydrofuran
TMS-Cl	trimethylsilyl chloride
TPP	sodium tripolyphosphate
UV	ultraviolet

Acknowledgements

I would first like to acknowledge and thank my advisor, Dr. Tim Deming for his support and patience along my journey to become a successful researcher. Throughout my personal ups and downs and a global pandemic, he constantly pushed me to keep moving forward and maintain a high level of focus. Without his guidance and steady hand, I would not have made it this far. I deeply appreciate his help.

My time in the Deming Lab introduced me to my lab mates and friends in the program. Alex Wollenberg, Pesach Perlin, Eric Raftery, and Yintao Sun were incredibly welcoming and helped me navigate the turbulent waters of graduate school. I must give a special shout-out to Wendell Scott for his constant support and willingness to stand by my side as we made our way through some of the most chaotic times our lives.

I would also like to thank my committee members, Dr. William Gelbart, Dr. Joseph Loo, and Dr. Andrea Kasko for helping build me into a competent researcher and offering me invaluable advice. To my undergraduate research advisor, Dr. Susan Gillmor, thank you for taking me under your wing as a clueless undergraduate seeking to learn how to ask better questions. Without your faith in me, I would never have made it to UCLA.

To my family, I cannot thank you enough. The strength and bravery of my parents Hector Benavides and Estela Ballesteros to leave their homes in Mexico and move to America with nothing gave me the courage to face any challenges. If they can build a new life with absolutely nothing to their names and no understanding of the language or culture, I have no excuse to not do all I can to succeed and make them proud. To my brother and sister, Hector and Mitzi, thank you for paving the way for me to understand the importance of education and hard work. I am only one head of our three-headed beast.

Finally, I would like to thank my partner Katherine Van Story for always praising me at my highest and comforting me at my lowest. This is our success.

Vita

Education

2014
The George Washington University

B.S. Chemistry

2018

University of California, Los Angeles

M.S. Chemistry

Research Experience

2016-2021
Graduate Student Researcher
University of California, Los Angeles
Professor Timothy J. Deming

2013-2015
Undergraduate Researcher
The George Washington University
Dr. Susan D. Gillmor

Work Experience

2021-Present

Lead Scientist
Bluefin Foods Inc.

2015-2016

Research Associate I

MesoScale Diagnostics

Publications

Benavides, I.A.; Deming, T.J. Poly(L-homoserine), a water-soluble, non-ionic polypeptide for use in diblock copolypeptide self-assemblies. In preparation

Benavides, I.A.; Raftery, E.D.; Bell, A.G.; Evans, D.; Scott, W.A.; Houk, K.N.; Deming, T.J. Poly(dehydroalanine): synthesis, properties and functional diversification of a fluorescent polypeptide. *J. Amer. Chem. Soc.* **2022**, *144* (9), 4214-4223

Scott, W.A.; **Benavides, I.A**.; Deming, T.J. Highly stable complex coacervate core micelles for oligonucleotide encapsulation and delivery via PEG-***b*-**poly(S-alkyl-homocysteine) copolymers complexation. In preparation

Chapter 1: Synthetic polypeptide-based biomaterials: preparation and applications

1.1 Introduction to polypeptides

Proteins encompass a diverse field of functional and structural biomolecules. Their biological properties include transport, structural support, and signaling, among various other functions.[1] Synthesized from long chains of amino acids linked through peptide bonds, proteins feature an astounding ability to transition from primary sequences into highly defined tertiary and quaternary structures, forming a unique relationship between sequence and function. The primary amino acid sequence determines which secondary structure motifs, including α-helices and β-sheets, form through non-covalent interactions that organize into the protein's tertiary structure, bound together through side chain interactions. The 21 canonical amino acids with distinctive chemical functionalities can be incorporated into sequences with countless iterations, allowing nature to dictate highly specific molecular and cellular interactions.[2]

Due to their versatility, researchers have tried to harness the power of proteins, inspiring refined methods to prepare these macromolecules.[3-4] Polypeptide synthesis mostly relies on three distinct techniques: recombinant protein expression for larger proteins, solid phase peptide synthesis for shorter, sequence-specific peptides that can be linked into larger peptides through step-growth coupling, and ring opening polymerization of α-amino acid N-carboxyanhydrides.

1.2 Current approaches for protein, peptide, and polypeptide synthesis

1.2.1 Recombinant protein expression

When larger proteins are desired in mass quantities, recombinant protein expression is a useful tool. Here, scientists can identify and clone DNA sequences specific for the target protein. Depending on the target protein and post-translational

modification needed, prokaryotic or eukaryotic cells are used. The DNA sequences are then introduced into the expressing cell.[5-7] The cell can then produce mass quantities of the expressed protein, allowing the researcher to isolate and purify the protein. Recombinant protein expression has provided several therapeutic proteins[8], including insulin, improving the quality of life for millions of people suffering from diabetes. This technique works extremely well for producing naturally occurring proteins; however, when non-canonical amino acids are introduced, the cells may not tolerate it as well, leading to lower quality and quantities of protein.[9-10]

1.2.2 Step-wise peptide synthesis

Synthesis and isolation of smaller peptides or polypeptides does not require recombinant protein expression. Instead, chemists rely on step-wise peptide synthesis, where a sequence specific peptide can be prepared using coupling chemistries between protected amino acids.[2] Initially, solution based peptide synthesis was utilized, but this required isolation after each coupling reaction, a tedious and inefficient process. Improvements on step-wise peptide synthesis relied on solid state peptide synthesis, where insoluble resin beads with a functional amine or hydroxyl handle are used prepare the peptide of interest one amino acid at a time.[1] This technique immobilizes the growing peptide chain on the resin bead and relies on step-wise addition of N-protected amino acids to the N-terminus of the growing chain using coupling agents. Once the peptide chain is completed, the final product is cleaved from the resin bead and released for further modification.

Solid phase peptide synthesis allows high levels of control over amino acid sequence, giving chemists the ability to produce desired peptide sequences and

introduce non-canonical amino acids. However, this technique suffers from difficulty synthesizing larger peptides (>50 amino acids) and requires tedious processes after each coupling step to ensure complete addition of the amino acid, leading to issues with incomplete or incorrect peptide sequences and poor yield.[3] Improvements to the accessibility of longer, higher molecular weight peptides via synthetic approaches has led to the use of native chemical ligation for assembly of smaller peptide sequences into larger protein targets.[11] The principle of native chemical ligation (NCL) involves a thioester on the C-terminus of one peptide and a cysteine residue on the N-terminus of another peptide. These residues undergo a reversible *trans*-thioesterification via nucleophilic attack of the cysteine residue's thiol side group on the thioester, forming a thioester linkage between the two peptides. The thioester then undergoes a rapid S→N acyl shift to create the peptide bond. NCL allows coupling of unprotected peptides in aqueous media at neutral pH, thereby improving the peptide's solubility, coupling efficiency, and stability. Continued improvements to NCL techniques have reduced the need for an L-cysteine residue at the ligation site, including desulfurization techniques to ligate at Ala junctions[12], ligation at a Met junction[13], and synthesis of thiolated amino acids followed by subsequent desulfurization.[14-16] NCL technology has rapidly improved size and length limitations of solid phase peptide synthesis to access large peptides and proteins with over 350 residues.[17-20]

1.2.3 Ring-opening polymerization of *N*-carboxyanhydrides

Recombinant protein engineering and step-wise synthesis are incredibly powerful tools to prepare sequence specific proteins and peptides. However, when high molecular weight polypeptide structures that don't require sequence specificity are

desired, ring opening polymerization (ROP) of NCAs is a highly efficient method.[21-23] While sequence specificity is required for the folding of peptide chains into a protein's tertiary structure, repeats of the same amino acid can form secondary structures[24], i.e. α-helices, β-sheets, and disordered segments, without the need for specific sequences.[24-26] For example, poly(L-methionine)[27] and poly(L-leucine)[28] are known to form α-helices, poly(L-serine)[29] and poly(L-cysteine)[30] assemble into β-sheets, and the ionic poly(L-glutamate)[31] and poly(L-lysine)[28] possess disordered conformations in aqueous environments. Chemists have used these structural motifs to their advantage, preparing multi-block copolypeptides of differing secondary structures, leading to supramolecular architectures such as hydrogels, vesicles, and micelles.[25-26, 32-33] Using ROP of α-amino acid *N*-carboxyanhydrides (NCA), researchers can prepare large quantities of polypeptide based biomaterials valuable for biological applications (Figure 1.1).

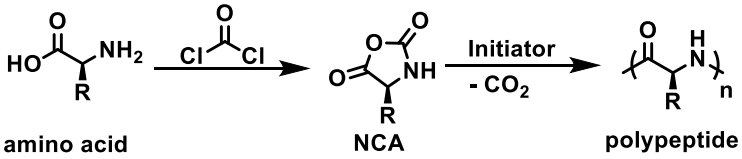

Figure 1.1. Polypeptide synthesis via ring-opening polymerization of NCAs

1.2.4 Preparation of polypeptides from NCAs

NCAs are commonly prepared through cyclization of amino acids using phosgene to form the heterocycle.[34] The resulting cyclic monomer is then purified through recrystallization and/or anhydrous column chromatography to remove impurities, including HCl, unreacted amino acids, and unwanted side products.[35] Adding to the versatility of NCA polymerization, amino acids with reactive side groups can be

selectively protected prior to cyclization, giving researchers a path to convert canonical and non-standard amino acids into NCAs and subsequent polypeptides. The use of acid scavenging groups such as α-pinene or triethylamine with chlorotrimethylsilane allows the preparation of acid-sensitive NCAs, further adding to the library of available NCAs for polypeptide synthesis.[36-37]

Polymerization of NCAs require an initiating species to begin propagation through nucleophilic ring-opening or basic activation of NCAs. Although amines are the most commonly used initiators for NCA polymerization, the preparation of block copolypeptides and hybrid block copolymers is difficult to control. This difficulty is due to two initiation mechanisms happening simultaneously, nucleophilic attack and base activation (Figure 1.2).[38-39] Here, an amine initiator can act as a nucleophile, opening the ring, causing the loss of CO_2, and releasing an N-terminal amine to continue propagating the chain. The initiating amines can also act as a base by deprotonating an NCA and activating the monomer for chain growth. Since the polymerization can switch back and forth between propagation mechanisms, the prepared polypeptides often have different structures and compositions than those predicted by the monomer feed ratio. Optimal polymerization conditions for NCAs and their respective polymers needs to be determined empirically as differences in solubility and reactivity affect their polymerization kinetics and propensity for chain-terminating side reactions. Techniques to improve these polymerization conditions include low temperatures, reduced pressure, and solvent selection, leading to a narrow size distribution of polymer chains (dispersity) and better control over the degree of polymerization. Work by the Cheng group addressed some of the limitations of amine-initiated polymerizations through the

development of bis(trimethylsilyl)amine (HMDS) as a new NCA initiator.[40] Here, the labile silazane bond and trimethylsilyl activation of the NCA carbonyl dramatically improved length control and dispersity. Continued efforts to improve reaction kinetics led to the use of LiHMDS as an activated initiator.[41-42]

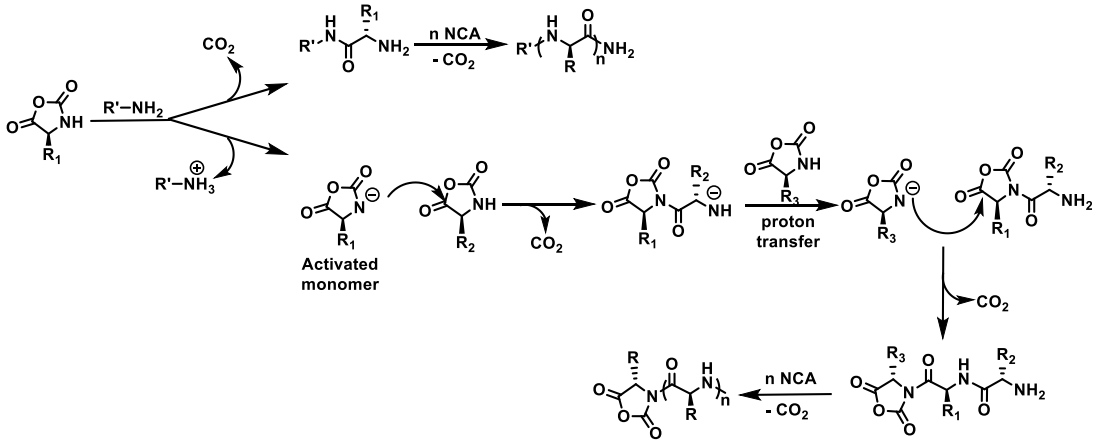

Figure 1.2. Amine-initiated polymerization of NCAs

1.2.5 Transition metal initiators for α-amino acid N-carboxyanhydride polymerization

Development of transition metal initiators for ring opening polymerization of NCAs have enabled access to high molecular weight polypeptides with narrow dispersities at high polymerization growth rates by dramatically improving control over the addition of NCA monomers to active polymer chain ends.[43] Deming and coworkers studied several transition metals to initiate living polymerizations of NCAs. Their initial metal initiator studies centered on bpyNi(COD) initiator precursor solutions, where bpy = 2,3'-bipyridine and COD = 1,5-cyclooctadiene, capable of producing high molecular weight block copolypeptides.[32] Further work with these nickel-based initiators focused on active divalent nickel complexes containing an amido-amidate functionality.[32] These complexes allow introduction of a wide range of end group functionalities, which are useful for post-polymerization modifications through click chemistries.[44]

Later work by the Deming group concentrated on the zerovalent $Co(PMe_3)_4$ complex as an initiator precursor.[45-46] $Co(PMe_3)_4$ initiated NCA polymerizations at a faster rate than the nickel based initiator precursor and was highly compatible with a wide-range of common and newly designed NCAs. The mechanism of initiation and propagation was studied in detail and was found to proceed as follows (Figure 1.3). First, the oxidative insertion of the metal initiator into the anhydride ring across the C-O bond results in the loss of carbon monoxide, creating a 5-membered ring. The addition of a second NCA forms a six-membered amido-alkyl metallacycle after the loss of two equivalents of CO_2. Subsequent addition of the next NCA is followed by proton transfer from the amide proton to the metal bound carbon, which results in a five-membered amido-amidate metallacycle. This five-membered ring serves as the propagating species, where each NCA addition follows the same CO_2 loss and proton migration, further extending the polypeptide chain. Clever work by the Deming group demonstrated the ability to use transition metal initiators in tandem to also produce brush type grafted polypeptides.[47] They successfully prepared cylindrical polypeptide brushes through $Co(PMe_3)_4$ initiation of NCAs containing alloc-α-aminoamide side groups that were subsequently activated *in situ* by addition of depeNi$(COD)_2$, where depe = 1,2-bis(diethylphosphino)ethane), to graft side-chain segments with high brush density, indicating efficient initiation and propagation.

There has been recent interest in N-substituted glycine N-carboxyanhydrides for polypeptoid, e.g. poly(sarcosine) aka poly(*N*-methyl glycine), synthesis, but these cannot be polymerized using the $Co(PMe_3)_4$ precursor since an N-H bond is needed to generate the propagating species. However, recent work by the Kramer group

confirmed that nickel amido-amidate propagating species are capable of initiating controlled polymerization of L-proline NCA and other N-substituted glycine N-carboxyanhydrides that lack N-H bonds previously assumed to be necessary for proton transfer during propagation using these complexes. Using this knowledge, metal amido-amidate metallacycles have been confirmed to provide controlled synthesis of polypeptide and polypeptoid (aka polypept(o)id) containing multiblock copolymers.[48] While the mechanism of initiation and propagation of N-alkyl NCAs is not currently understood, access to biologically useful polypeptoids such as poly(sarcosine), desired for its poly(ethylene glycol) PEG-like stealth properties, will give researchers more avenues to design improved polypept(o)ide-based biomaterials.[49-51]

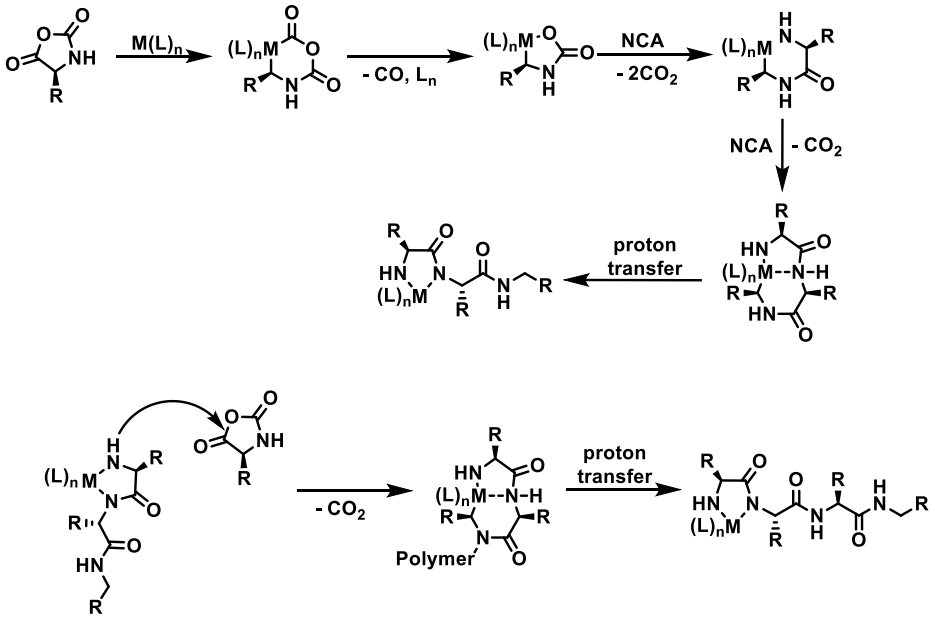

Figure 1.3. Cobalt and nickel mediated initiation and propagation of NCA monomers

1.3 Introduction of non-standard amino acids into polypeptide-based biomaterials

The ability to synthesize biomaterials from polypeptides relies on the diversity of amino acid side chains. The 21 naturally occurring amino acids offer a wide-variety of functional groups desirable for specific applications, including hydrophobicity, ionic

charge, and reactive functional groups. However, non-standard amino acid incorporation into synthetic polypeptides gives researchers even more control over specific polymer properties and structure, enabling the design and optimization of biomaterials for biological and clinical applications, including hydrogels, nanoparticles, vesicles, and coacervates.[21, 52] These materials can be designed to respond to physiologically relevant stimuli – pH triggers, redox environments, enzyme recognition, among many others, and are often combined to form multi-responsive polypeptides.[53]

Introduction of non-standard amino acids into polypeptides via ROP relies on two techniques, synthesis and polymerization of functional monomers or post-polymerization modification (PPM). The functional monomer approach ensures complete incorporation of a target residue at desired monomer ratios and segments within the polymer. In addition, multiple functionalized monomers can be polymerized at once, making polymer design a more straight-forward approach. However, this approach is often limited by difficulty synthesizing new monomers and the rigorous purification needed. Finally, even after preparation of a new monomer, polymerization may not be well-tolerated due to poor solubility of the active polypeptide chains or slow polymerization kinetics.

Post-polymerization modification offers an indirect route to desired functionalities, relying on well-characterized and easily polymerized monomers. While PPM can suffer from incomplete functionalization, optimization of coupling chemistries can approach near-quantitative modification. Click chemistry has proven especially useful for PPM, relying on azide-alkyne cycloaddition, thiol-e/yne, and amidations, enabling high efficiency reactions in mild conditions.[54-55] Work by the Deming group has focused on

thioethers as a clickable handle. The thioether group is present in naturally occurring L-methionine, and can undergo modifications to introduce new functionalities, charge, and conformational changes.[27, 30, 56-57] Poly(L-methionine), either as a homopolymer or copolymer, can undergo a variety of modifications as a reactive precursor. Alkylation via alkyl halides, alkyl triflates, and epoxides results in cationic sulfonium salts while also introducing a new functional group. Furthermore, the transition from thioether to sulfonium after alkylation can be harnessed to improve water-solubility and induce a conformational change, switching from an α-helix favoring, hydrophobic residue to a disordered favoring, hydrophilic residue. The thioether groups can also be reversibly oxidized from the hydrophobic, α-helix forming poly(L-methionine) to the water-soluble, disordered poly(L-methionine sulfoxide), while further oxidation to the sulfone reverts the chain back to a water-insoluble α-helix. Thus, poly(L-methionine) modifications are an excellent example of synthetic polypeptide PPM for biomaterial development. The modifications are useful in the preparation of non-fouling hydrogels for neural progenitor stem cells[58], enzyme responsive vesicles[59], and sugar conjugation for cell recognition.[60] In addition, the Deming group has also focused on thiol-ene chemistries around poly(L-homoallylglycine), based on the corresponding functional NCA monomer, that can be modified to introduce desired chemical moieties and thioether groups, available for further modification.[61]

1.4 Stimuli-responsive polypeptides

In biological systems, proteins are capable of extraordinary tasks, responding to an ever-changing environment to aid in cellular processes via catalysis, structural support, and signaling. This stimuli-responsiveness can be adapted to synthetic

polypeptides, utilizing the variety of amino acid functionalities and their corresponding secondary structures to create “smart” materials. Polypeptides can be designed to respond to changes in temperature, redox environments, pH, and enzymes. Using these stimuli, researchers can prepare biomaterials capable of rapid change in structure and assembly, useful for biological applications such as stem cell therapies and drug and gene delivery.

Thermo-responsiveness is considered a key target feature, due to the large difference between ambient temperature and physiological temperature.[62] This trigger can be integrated into thermo-responsive materials through the use of lower critical solution temperature (LCST) containing polymers, transitioning from soluble to insoluble polymer as the temperature increases. PEG-*b*-poly(L-alanine) is a well studied polymer capable of forming thermogels in water, capable of encapsulating stem cells in a 3D suspension through its sol-gel transition and inducing cell differentiation with the inclusion of growth factors.[63] In this example, the poly(L-alanine) segment drives the sol-gel transition at physiological temperatures while the PEG segment improves the water-solubility of the resulting hydrogel. Entirely polypeptide-based thermogels are garnering increased attention due to their biodegradability. These thermoresponsive polymers often rely on oligoethylene glycol repeats, where the initially water-soluble oligoethylene glycol (OEG) units shed their sphere of hydration and aggregate as temperature increases, leading to water-insoluble polymers.[64] Polypeptides can be designed with OEG units or by modification of reactive polypeptide residues[56, 65-66]. Work by the Deming group sought to understand the relationship between the number of OEG side-chain length and OEG terminal groups – including hydroxyl, acetyl, methyl

and ethyl - and their influence on LCST characteristics.[56] Using poly(L-methionine) as the parent polymer, OEG pendants with the variable terminal groups were attached via epoxide addition to the thioether groups. The number of OEG repeats and terminal group identity imparted a predictable effect on LCST, giving researchers a modular approach towards controlling the soluble to gel transition temperature of thermo-responsive polypeptides. Work by the Tang group focused poly(γ-4-(allyloxycarbonyl)benzyl-L-glutamate) that was further modified to contain a linear OEG pendant or Y-shaped OEG pendant per glutamate residue.[65] The effect of OEG length and structure – linear vs Y-shaped – was studied to determine its influence on hydrophilicity and LCST. The branched, Y-shaped pendants elevated the LCST to physiologically relevant temperatures when compared to linear OEG-modified polypeptide with the same amount of OEG units. Here, the Y-shaped OEG pendants increase the interactions between the solvating water molecules and the polypeptide side chain, resulting in improved hydrophilicity while retaining its LCST character. Continued focus into the structure and modifications of synthetic polypeptide side-chain functional groups will enable researchers to fine-tune thermoresponsive behavior for future biomedical applications.

Redox sensitive polypeptides can be designed to respond to reducing intracellular spaces or oxidative environment of cancerous and neurodegenerative tissues. [67-70] Sulfur containing polypeptides, including poly(L-cysteine) and poly(L-methionine), are highly sensitive to redox conditions. Under oxidative conditions, poly(L-cysteine) forms disulfide bridges[69, 71] while oxidation of hydrophobic, α-helical poly(L-methionine) results in water-soluble, disordered poly(L-methionine sulfoxide). The

disulfide bridges formed from oxidation of poly(L-cysteine) to poly(L-cystine) and their homologs are reversible chemical cross-links convenient for nanostructure formation and subsequent disassembly in a reducing environment, useful for drug and gene encapsulation and delivery *in vivo*.[69] Poly(L-methionine) has proven to be an extremely valuable polypeptide capable of switchable conformations under redox stress. Vesicles based on water-soluble poly(L-methionine sulfoxide) were formed and could then be reduced by methionine reductase enzymes, causing the rupture of vesicles and cargo release.[59]

Polypeptides designed to respond to changes in pH are valuable due to differences in the physiological pH of diseased tissues, endosomes and lysosomes, and the intra/extracellular space. These pH changes can trigger assembly and disassembly of nanostructures containing pH-sensitive residues, including poly(L-histidine), to improve cargo release.[72-73] The Wan group designed a pH-responsive nanoparticle containing poly(L-histidine) to deliver a chemotherapeutic drug.[72] At physiological pH, the poly(L-histidine) residues were deprotonated and the drug-loaded nanoparticles remained assembled. Once the nanoparticles were internalized into weakly acidic endosomes, the poly(L-histidine) residues became protonated, which triggered endosomal escape through the proton sponge effect, and caused nanoparticle disassembly and subsequent drug release into the intracellular space.

Negatively charged cell membranes can be targeted with cationic polypeptides that can disrupt and penetrate the membrane, enabling targeted intracellular delivery.[74] The Kataoka group has focused heavily on gene and drug delivery using polypeptide based polyion complexes (PIC).[75-76] Due to the negatively charged phosphate backbone

of oligonucleotides, new cationic polypeptides are increasingly being developed for gene delivery via polyion complexation.[77] Positively charged polypeptides in PICs can interact with anionic cell membranes and release bound oligonucleotides into the permeabilized cell, which significantly increases gene delivery efficiency.[74, 78-79] The Yin group developed fluorinated α-helical polypeptides containing guanidinium groups for siRNA complexation and delivery in acute lung injury patients.[80] Here, poly(γ-4-propargyloxybenzyl-L-glutamate), PPOBLG, was modified with perfluoroalkyl groups or guanylated via azide-alkyne click chemistry. These bifunctional α-helical cationic polypeptides can complex siRNA and aid in cell membrane penetration, while the perfluoroalkyl groups help penetrate through the mucus layer covering the surface of lung tissue. Huang and coworkers prepared pH-responsive random copolymer poly(L-glutamic acid-*co*-L-lysine) nanoparticles for cisplatin delivery for cancer therapies.[81] By manipulating the glutamate to lysine copolymer composition and cisplatin loading, the initially negatively charged nanoparticles were able to switch their surface charge from anionic to cationic in the acidic tumor extracellular environment (pH 6.5 – 7.2), releasing the cisplatin which resulted in increased HeLa cell killing.

1.5 Conclusions and Future Perspectives

The excellent material properties of synthetic polypeptides make them highly desirable for biomedical applications. Indeed, the chemical diversity of amino acids coupled with the superb biocompatibility and degradation of the peptide backbone have led to the advancement of improved diagnostic and therapeutic biomaterials. The development of transition metal initiators by the Deming group and subsequent improvements have enabled controlled and living polymerizations of α-amino acid NCA

monomers. Advances in polypeptide chemistries have also allowed the introduction of non-standard amino acids with diverse functional groups, necessary for the continued development of unique biomaterials. Additionally, improved understanding of the relationship between polypeptide composition and secondary structure has led to the design of ordered self-assemblies and stimuli-responsive materials. These synthetic polypeptide-based materials can enhance binding and release of sensitive cargos, improve interactions between biomaterials and biological environments *in vitro* and *in vivo*, and create switchable supramolecular structures that are highly responsive to their environment.

Although the field of polypeptide chemistry and ordered assembly continues to progress in leaps and bounds, focus on improvements in the cost and synthesis of large quantities of synthetic polypeptides is needed. NCA monomer synthesis suffers from tedious procedures and requires stringent purification and storage conditions to obtain controlled polymerization. These barriers will need to be lowered for synthetic polypeptides to make economical sense for their wide-spread application in the biomedical field. However, based on recent advances, it is not far-fetched to say that synthetic polypeptides will play a major role in the near future of biomaterials.

1.6 References

1. Palomo, J. M. *RSC Adv.* **2014,** *4* (62), 32658-32672.

2. Jaradat, D. S. M. M. *Amino Acids* **2018,** *50* (1), 39-68.

3. Varnava, K. G.; Sarojini, V. *Chem. Asian J.* **2019,** *14* (8), 1088-1097.

4. Santino, F.; Petruzzelli, R.; Zhao, J.; Boanini, E.; Gentilucci, L. *Sustain. Chem. Pharm.* **2021,** *24*, 100540.

5. Rosano, G. L.; Morales, E. S.; Ceccarelli, E. A. *Protein Sci*. **2019,** *28* (8), 1412-1422.

6. Mattanovich, D.; Branduardi, P.; Dato, L.; Gasser, B.; Sauer, M.; Porro, D. *Recomb. Gene Exp*. **2012**, 329-358.

7. Overton, T. W. *Drug Discov. Today* **2014,** *19* (5), 590-601.

8. Kerkar, K.; Tiwari, M.; Tiwari, D. K.; Kerkar, S. Industrial Scale Production of Important Therapeutic Proteins Using Bacterial Expression System. Springer Singapore: **2021**; pp 183-202.

9. Specht, E.; Miyake-Stoner, S.; Mayfield, S. *Biotechnol. Lett.* **2010,** *32* (10), 1373-1383.

10. Anné, J.; Maldonado, B.; Van Impe, J.; Van Mellaert, L.; Bernaerts, K. *J. Biotech*. **2012,** *158* (4), 159-167.

11. Kulkarni, S. S.; Sayers, J.; Premdjee, B.; Payne, R. J. *Nat. Rev. Chem.* **2018,** *2* (4), 0122.

12. Yan, L. Z.; Dawson, P. E. *J. Am. Chem. Soc.* **2001,** *123* (4), 526-533.

13. Tanaka, T.; Wagner, A. M.; Warner, J. B.; Wang, Y. J.; Petersson, E. J. *Angew. Chem. Int. Ed.* **2013,** *125* (24), 6330-6333.

14. Cergol, K. M.; Thompson, R. E.; Malins, L. R.; Turner, P.; Payne, R. J. *Org. Lett.* **2014,** *16* (1), 290-293.

15. Sayers, J.; Thompson, R. E.; Perry, K. J.; Malins, L. R.; Payne, R. J. *Org. Lett.* **2015,** *17* (19), 4902-4905.

16. Thompson, R. E.; Chan, B.; Radom, L.; Jolliffe, K. A.; Payne, R. J. *Angew. Chem. Int. Ed.* **2013,** *125* (37), 9905-9909.

17. Clark, R. J.; Craik, D. J. *Peptide Science* **2010,** *94* (4), 414-422.

18. Torbeev, V. Y.; Kent, S. B. *Angew. Chem. Int. Ed.* **2007,** *46* (10), 1667-1670.

19. Masania, J.; Li, J.; Smerdon, S. J.; Macmillan, D. *Org. Biomol. Chem*. **2010,** *8* (22), 5113-5119.

20. Jiang, W.; Zhang, B.; Fan, C.; Wang, M.; Wang, J.; Deng, Q.; Liu, X.; Chen, J.; Zheng, J.; Liu, L. *Cell Discov.* **2017,** *3* (1), 1-7.

21. Song, Z.; Han, Z.; Lv, S.; Chen, C.; Chen, L.; Yin, L.; Cheng, J. *Chem. Soc. Rev.* **2017,** *46* (21), 6570-6599.

22. Cheng, J.; Deming, T. J. *Peptide-based materials* **2011**, 1-26.

23. Kricheldorf, H. R. Polymerization of NCAs: Physical Aspects. In *α-Aminoacid-N-Carboxy-Anhydrides and Related Heterocycles*, Springer: **1987**; pp 158-209.

24. Song, Z.; Fu, H.; Wang, R.; Pacheco, L. A.; Wang, X.; Lin, Y.; Cheng, J. *Chem. Soc. Rev.* **2018,** *47* (19), 7401-7425.

25. Deming, T. J. *Hierarchical Macromolecular Structures: 60 Years after the Staudinger Nobel Prize II* **2013**, 1-37.

26. Deming, T. J. *Adv. Mater.* **1997,** *9* (4), 299-311.

27. Kramer, J. R.; Deming, T. J. *Biomacromolecules* **2012,** *13* (6), 1719-1723.

28. Breedveld, V.; Nowak, A. P.; Sato, J.; Deming, T. J.; Pine, D. J. *Macromolecules* **2004,** *37* (10), 3943-3953.

29. Bohak, Z.; Katchalski, E. *Biochem.* **1963,** *2* (2), 228-237.

30. Zhu, S.; Xue, R.; Yu, Z.; Zhang, X.; Luan, S.; Tang, H. *Biomacromolecules* **2021,** *22* (3), 1211-1219.

31. Rodríguez-Hernández, J.; Lecommandoux, S. *J. Am. Chem. Soc.* **2005,** *127* (7), 2026-2027.

32. Deming, T. J. *Nature* **1997,** *390* (6658), 386-389.

33. Deming, T. J. *Adv. Drug Deliv. Rev.* **2002,** *54* (8), 1145-1155.

34. Leuchs, H. *Ber. Dtsch. Chem. Ges.* **1906,** *39* (1), 857-861.

35. Kramer, J. R.; Deming, T. J. *Biomacromolecules* **2010,** *11* (12), 3668-3672.

36. Smeets, N. M. B.; Van Der Weide, P. L. J.; Meuldijk, J.; Vekemans, J. A. J. M.; Hulshof, L. A. *Org. Process Res. Dev*. **2005,** *9* (6), 757-763.

37. Kricheldorf, H.; Greber, G. *Chem. Ber.* **1971,** *104*, 3131.

38. Kricheldorf, H. R.; Von Lossow, C.; Schwarz, G. *J. Polym. Sci. A Polym. Chem.* **2006,** *44* (15), 4680-4695.

39. Kricheldorf, H.; Penczek, S. Models of biopolymers by ring-opening polymerization. *CRC Press: Boca Raton, FL*. **1990**, 46-62.

40. Lu, H.; Cheng, J. *J. Am. Chem. Soc.* **2008,** *130* (38), 12562-12563.

41. Salas-Ambrosio, P.; Tronnet, A.; Since, M.; Bourgeade-Delmas, S.; Stigliani, J.-L.; Vax, A.; Lecommandoux, S.; Dupuy, B.; Verhaeghe, P.; Bonduelle, C. *J. Am. Chem. Soc.* **2021,** *143* (10), 3697-3702.

42. Wu, Y.; Zhang, D.; Ma, P.; Zhou, R.; Hua, L.; Liu, R. *Nat. Commun.* **2018,** *9* (1), 1-10.

43. Deming, T. J. *J. Polym. Sci. A Polym. Chem.* **2000,** *38* (17), 3011-3018.

44. Sparks, B. J.; Ray, J. G.; Savin, D. A.; Stafford, C. M.; Patton, D. L. *Chem. Comm*. **2011,** *47* (22), 6245-6247.

45. Deming, T. J.; Curtin, S. A. *J. Am. Chem. Soc.* **2000,** *122* (24), 5710-5717.

46. Deming, T. J. *Macromolecules* **1999,** *32* (13), 4500-4502.

47. Rhodes, A. J.; Deming, T. J. *J. Am. Chem. Soc.* **2012,** *134* (47), 19463-19467.

48. Detwiler, R. E.; Schlirf, A. E.; Kramer, J. R. *J. Am. Chem. Soc.* **2021**.

49. Birke, A.; Ling, J.; Barz, M. *Prog. Polym. Sci.* **2018,** *81*, 163-208.

50. Heller, P.; Birke, A.; Huesmann, D.; Weber, B.; Fischer, K.; Reske-Kunz, A.; Bros, M.; Barz, M. *Macromol. Biosci.* **2014,** *14* (10), 1380-1395.

51. Bleher, S.; Buck, J.; Muhl, C.; Sieber, S.; Barnert, S.; Witzigmann, D.; Huwyler, J.; Barz, M.; Süss, R. *Small* **2019,** *15* (50), 1904716.

52. Johnson, J. A.; Lu, Y. Y.; Van Deventer, J. A.; Tirrell, D. A. *Curr. Opin. Chem. Biol*. **2010,** *14* (6), 774-780.

53. Song, Z.; Tan, Z.; Cheng, J. *Macromolecules* **2019,** *52* (22), 8521-8539.

54. Perlin, P.; Scott, W. A.; Deming, T. J. *Biomacromolecules* **2019,** *21* (1), 126-132.

55. Rhodes, A. J.; Deming, T. J. *Macro Lett.* **2013,** *2* (5), 351-354.

56. Gharakhanian, E. G.; Deming, T. J. *J. Phys. Chem*. **2016,** *120* (26), 6096-6101.

57. Gharakhanian, E. G.; Deming, T. J. *Biomacromolecules* **2015,** *16* (6), 1802-1806.

58. Wollenberg, A.; O'shea, T.; Kim, J.; Czechanski, A.; Reinholdt, L. G.; Sofroniew, M.; Deming, T. *Biomaterials* **2018,** *178*, 527-545.

59. Rodriguez, A. R.; Kramer, J. R.; Deming, T. J. *Biomacromolecules* **2013,** *14* (10), 3610-3614.

60. Wollenberg, A. L.; Perlin, P.; Deming, T. J. *Biomacromolecules* **2019,** *20* (4), 1756-1764.

61. Perlin, P.; Gharakhanian, E. G.; Deming, T. J. *Chem. Comm*. **2018,** *54* (48), 6196-6199.

62. Stuart, M. A. C.; Huck, W. T. S.; Genzer, J.; Müller, M.; Ober, C.; Stamm, M.; Sukhorukov, G. B.; Szleifer, I.; Tsukruk, V. V.; Urban, M.; Winnik, F.; Zauscher, S.; Luzinov, I.; Minko, S. *Nat. Mater.* **2010,** *9* (2), 101-113.

63. Patel, M.; Park, S.; Lee, H. J.; Jeong, B. *Tissue Eng. Regen. Med*. **2018,** *15* (5), 521-530.

64. Chua, G. B.; Roth, P. J.; Duong, H. T.; Davis, T. P.; Lowe, A. B. *Macromolecules* **2012,** *45* (3), 1362-1374.

65. He, X.; Zhou, R.; Ge, C.; Ling, Y.; Luan, S.; Tang, H. *Eur. Polym. J.* **2019,** *112*, 547-554.

66. Chen, C.; Wang, Z.; Li, Z. *Biomacromolecules* **2011,** *12* (8), 2859-2863.

67. Jing, T.; Li, T.; Ruan, Z.; Yan, L. *J. Mater. Sci.* **2018,** *53* (21), 14933-14943.

68. Hoang, Q. T.; Lee, D.; Choi, D. G.; Kim, Y.-C.; Shim, M. S. *J. Ind. Eng. Chem*. **2021,** *95*, 101-108.

69. Chen, Y.-F.; Chang, C.-H.; Lin, C.-Y.; Lin, L.-F.; Yeh, M.-L.; Jan, J.-S. *Colloids Surf. B .* **2018,** *165*, 172-181.

70. Deng, C.; Zhang, Q.; Guo, J.; Zhao, X.; Zhong, Z. *Adv. Drug Deliv. Rev.* **2020**.

71. Raftery, E. D.; Gharkhanian, E. G.; Ricapito, N. G.; McNamara, J.; Deming, T. J. *Chem. Asian J.* **2018,** *13* (22), 3547-3553.

72. Pan, J.; Lei, S.; Chang, L.; Wan, D. *J. Mater. Sci.* **2019,** *54* (2), 1692-1702.

73. Wang, P.; Liu, W.; Liu, S.; Yang, R.; Pu, Y.; Zhang, W.; Wang, X.; Liu, X.; Ren, Y.; Chi, B. *J. Biomater. Sci. Polym. Ed*. **2020,** *31* (3), 277-292.

74. Zhang, R.; Zheng, N.; Song, Z.; Yin, L.; Cheng, J. *Biomaterials* **2014,** *35* (10), 3443-3454.

75. Harada, A.; Kataoka, K. *Macromolecules* **1995,** *28* (15), 5294-5299.

76. Harada, A.; Kataoka, K. *Macromolecules* **1998,** *31* (2), 288-294.

77. Kim, B. S.; Naito, M.; Chaya, H.; Hori, M.; Hayashi, K.; Min, H. S.; Yi, Y.; Kim, H. J.; Nagata, T.; Anraku, Y. *Biomacromolecules* **2020,** *21* (10), 4365-4376.

78. Yin, L.; Song, Z.; Kim, K. H.; Zheng, N.; Tang, H.; Lu, H.; Gabrielson, N.; Cheng, J. *Biomaterials* **2013,** *34* (9), 2340-2349.

79. Yin, L.; Tang, H.; Kim, K. H.; Zheng, N.; Song, Z.; Gabrielson, N. P.; Lu, H.; Cheng, J. *Angew. Chem.* **2013,** *125* (35), 9352-9356.

80. Ge, C.; Yang, J.; Duan, S.; Liu, Y.; Meng, F.; Yin, L. *Nano Lett.* **2020,** *20* (3), 1738-1746.

81. Huang, Y.; Tang, Z.; Zhang, X.; Yu, H.; Sun, H.; Pang, X.; Chen, X.. *Biomacromolecules* **2013,** *14* (6), 2023-2032.

Chapter 2: Poly(L-homoserine), a water-soluble, non-ionic polypeptide for use in diblock copolypeptide self-assemblies

2.1 Abstract

Water-soluble, biodegradable, and biocompatible polymers are of high interest as potential alternatives to PEG for applications *in vivo*. Here, we report studies on poly(L-homoserine), **S^{H}**, a water-soluble, non-ionic polypeptide that was synthesized via transition-metal initiated ring-opening polymerization. Side-chain protected L-homoserine *N*-carboxyanhydride, **R-Hse** NCA (**R** = protecting group), monomers were prepared in a straightforward manner in high yield and werewere used to obtain **S^{H}** homopolypeptides and **S^{H}** containing diblock copolypeptides withwith controlled lengths via living polymerization. **S^{H}** was found to adopt a disordered conformation in aqueous media, which did not change with different chain lengths, across a wide range of pH, or in the presence of high ionic strength media. Amphiphilic diblock copolypeptides of poly(L-homoserine)-*b*-(L-serine), **S^{H}-*b*-S**, were found to assemble into unilamellar vesicles in aqueous media, which showcases the ability of poly(L-homoserine) to serve as a non-ionic, water-solubilizing segment in block copolypeptide assemblies.

2.2 Introduction

There is a need for new benign polymers for biomedical applications that possess of the desirable combination of good water-solubility, biocompatibility, and biodegradability.[1] Several water-soluble synthetic polymers have been studied for biomedical uses, including poly(vinyl alcohol), poly(oxazolines), and poly(ethylene glycol) (PEG), but all suffer from non-degradability, leading to tissue accumulation and potential immunogenic effects.[2-4] Despite its longstanding reputation as a biocompatible polymer with stealth-like properties, PEG has been observed to accumulate in several organs, including the liver, spleen, and lungs.[5] Due to its wide-spread use in clinical

applications, an increasing percentage of the population have developed an allergic response to PEG, potentially limiting its continued use as a biocompatible polymer in humans.[6] In the COVID-19 era, vaccine manufactures have relied on PEG to improve stability and circulation time of their formulations. However, reports of anaphylaxis and allergic responses have identified PEG hypersensitivity as a likely culprit.[7] A victim of its own success, the prevalence of PEG in foods, cosmetics and pharmaceutical formulations has led to undesirable immunogenicity, creating a need for development of new water-soluble, biodegradable polymers with improved biocompatibility. Specifically, synthetic polypeptides have been increasingly studied as biomedical polymers for drug and gene delivery, tissue engineering, and other biomaterials applications due to their biocompatibility, wide variety of functional groups, and biodegradability.[8-12] To obtain hydrophilicity, proteins, peptides, and polypeptides often rely on incorporation of ionic amino acids, such as L-lysine and L-glutamic acid. However, due to their charged side chains, these amino acids can adsorb to other biological macromolecules or cell surfaces, leading to recognition by the immune system and subsequent removal via the foreign body response.[1, 13] Unnatural non-ionic, water-soluble polypeptides have been synthesized using oligo(ethylene glycol)-functionalized polymers of L-lysine[14], L-glutamate[15], and L-serine[16]. Indeed, the water-solubilizing potential of di(ethylene glycol)-functionalized poly(L-lysine) was demonstrated by preparing amphiphilic block copolypeptides and assembling into spherical vesicles. Nonetheless, there remain unknowns about the degradability of unnatural polypeptides, while the reliance on oligo(ethylene glycol) raises the same PEG disadvantages mentioned previously. To address these issue, the Deming group has led the development of poly(L-methionine

sulfoxide), **M^{O}**, as a non-ionic, biodegradable, water-soluble polypeptide with non-fouling properties.[17] **M^{O}** has been effectively used as a water solubilizing component in diblock copolypeptide vesicles and hydrogels.[18-20] These entirely polypeptide-based materials assemble through microphase separation driven by the hydrophobic interactions of non-polar segments, including poly(L-leucine) and poly(L-phenylalanine). Recent efforts to identify new non-ionic, hydrophilic polypeptides have centered on poly(L-serine), **S**; yet its propensity to form β-sheet aggregates in both water and common organic solvents render it unsuitable for this use.[21-22] Work by Yang et al. focused on converting racemic D,L-serine to an α-amino acid *N*-carboxyanhydride (NCA) followed by polymerization to give water-soluble poly(D/L-serine).[23] The racemic polypeptide backbone prevents folding into β-sheets which disfavors chain aggregation. Sun et al. also improved the solubility of poly(L-serine) by incorporating small amounts D-serine into the backbone of the polymer during synthesis, and applied this polymer toward the cryopreservation of blood.[24] Similarly, Zhang and coworkers showed how poly(D/L-serine) and poly(D/L-β-homoserine) based materials can act as water-soluble and biocompatible materials with minimal signs of a foreign-body response.[25-26] In these studies, the polypeptide chain ends were reacted with a diacrylate cross-linker to form implantable hydrogels upon UV irradiation. *In vivo* studies on implanted poly(D/L-serine) hydrogels revealed negligible inflammatory responses at least 3 months after implantation which indicated successful mitigation of the foreign-body response. However, all of the approaches described above rely on racemic poly(D/L-serine) polypeptide backbones that are known to be highly susceptible to rapid hydrolysis in mildly alkaline aqueous solutions of pH 8-9, which may limit how they can be

incorporated into a biomaterial design.[27-28] In addition, many of these strategies rely on side-chain protected poly(D/L-serine) during their preparation, which give polypeptides prone to premature degradation to insoluble and reactive dehydrolanine residues via β-elimination.[29] It is also worth noting that D-serine is a known neurotransmitter and is highly biologically active, potentially limiting biomedical applications of these polymers due to off-target effects upon chain degradation.[30]

Recent focus on polypeptides composed of amino acid homologs has revealed a close relationship between side chain length and chain conformation.[31-36] For example, poly(L-cysteine) is known to form β-sheets in aqueous environments. However, extending every side chain by one methylene unit to give poly(L-homocysteine) changes the preferred conformation to α-helical, which improves polymer solubility and makes the side chains more accessible for further modification.[37-39] Similarly, limited prior studies on optically pure poly(L-homoserine), **S^{H}**, revealed that it is water-soluble and α-helical in N, N-dimethylformamide (DMF) and hexafluoroisopropanol (HFIP), strikingly different from water-insoluble, β-sheet forming poly(L-serine).[40-42] In addition, the homologation of serine to homoserine prevents β-elimination and degradation of **S^{H}**, improving polymer stability while retaining its biocompatibility.[29] Here, we present an improved synthetic method for preparation of well-defined poly(L-homoserine) with controlled chain lengths. First, L-homoserine was readily transformed into side-chain protected **R-Hse** NCA monomers (**R** = protecting group), in high yield. **R-Hse** NCA monomers were found to undergo living polymerization via transition metal-initiated ring opening polymerization, yielding **S^{H}** with controlled lengths and low dispersity after deprotection of side-chains. Despite its optically purity, **S^{H}** was found to adopt a

disordered conformation in aqueous media. In addition, **S^{H}** was readily incorporated as a non-ionic, hydrophilic segment into amphiphilic diblock copolypeptides through sequential polymerization of NCAs. As an example, diblock copolypeptides of poly(L-homoserine)-*b*-(L-serine), **S^{H}-*b*-S**, were prepared and found to assemble into unilamellar vesicles in aqueous media, highlighting the potential of this methodology for preparation of biomaterials containing **S^{H}** segments. Overall, water-soluble, non-ionic **S^{H}** contains many of the previously mentioned desired properties to be a suitable PEG alternative.

2.3 Results and discussion

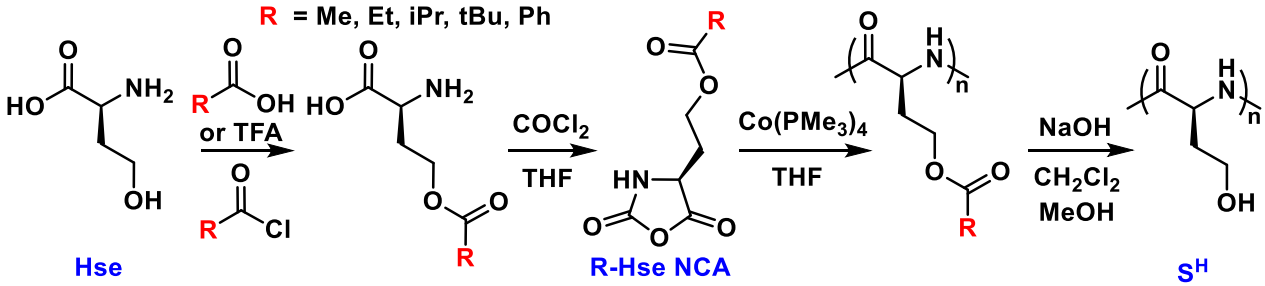

Figure 2.1. Synthesis of L-homoserine (Hse) derivatives, their corresponding **R-Hse** NCA monomers, and polymerization of NCAs to give poly(L-homoserine) (**S^{H}**) after side-chain deprotection.

To prepare **S^{H}**, we first needed to prepare a suitable **R-Hse** NCA monomer. The -hydroxyl side-chain group of **Hse** was protected in order to improve polymer solubility in organic solvents while also preventing undesirable side reactions during NCA synthesis and polymerization. Consequently, the hydroxyl group of L-homoserine, **Hse**, was directly acylated with a variety of reagents, which was accomplished directly without protection of the carboxyl and amine groups. Side-chain protected Hse derivatives were subsequently cyclized into the corresponding **R-Hse** NCAs, which were then polymerized to obtain protected **S^{H}** (Fig. 2.1). Keeping in mind the need for sufficient

solubility of the protected poly(O-acyl-L-homoserine) during polymerization in organic solvents, **Hse** was protected with increasingly hydrophobic acyl groups to improve solubility and prevent aggregation during polymerization (Table 2.1). To select the optimal **R-Hse** NCA we focused on the following characteristics: 1) high NCA yield, 2) facile NCA purification, and 3) good solubility of resulting polypeptide in THF. Of the five NCA monomers prepared and studied, each suffered from drawbacks that limited their suitability for controlled polymerization. While **Me-Hse** and **tBu-Hse** NCAs could be obtained in high yield and were readily purified, they produced polypeptides that gelled during polymerization, which limited chain growth. Both **Et-Hse** and **iPr-Hse** NCAs were obtained as oils, which complicated purification of these moisture sensitive molecules. Finally, **Ph-HSe NCA** gave a soluble polypeptide, but the NCA could only be prepared in low yields mainly due to inefficiency in the amino acid protection step.

NCA	**NCA Isolated Yield (%)**	**NCA Physical State**	**Highest M:I with complete monomer conversion**	**Reaction Mixture State**	**[a]Polypeptide Isolated Yield (%)**
Me-Hse	70	Solid	60	Gel	90
Et-Hse	40	Oil	100	Fluid	90
iPr-Hse	40	Oil	60	Fluid	***
Ph-Hse	18	Solid	20	Fluid	***
tBu-Hse	65	Solid	60	Gel	88
$tBu_{0.9}/Me_{0.1}$-Hse	NA	Solid	80	Fluid	93

Table 2.1**. R-Hse** NCA monomer and polymerization characteristics. All NCA polymerizations were in anhydrous THF at 50 mg/mL using $Co(PMe_3)_4$ initiator. The polymerizations wwere performed at ambient temperature in a N_2 filled glove box for 1-2 hours. [a] Indicates yield at highest M:I. NA = not applicable. *** = not measured.

Of the five NCAs studied, **Me-Hse** and **tBu-Hse NCAs** were identified as the most promising since they were obtained in high yields and with high purity. The gelation of **Me-S^{H}** and **tBu-S^{H}** homopolymers in THF was likely due to interchain aggregation. Previous studies on α-helical poly(L-methionine) synthesis in THF revealed similar behavior, where high molecular weight chains were found to aggregate and gel.[18] Due to aggregation, controlled addition of subsequent NCAs is hindered, preventing controlled chain extension. To prevent gelation of poly(L-methionine), 10 mol% of Ala NCA was added as a comonomer to give poly(L-methionine$_{0.9}$-*stat*-L-alanine$_{0.1}$), which remained soluble at high molecular weights. Inspired by these results with poly(L-methionine), **tBu-Hse** and **Me-Hse** NCAs at a 9:1 molar ratio, respectively, were copolymerized using Co(PMe$_3$)$_4$ initiator to give the statistical copolymer poly(pivaloyl-L-homoserine$_{0.9}$-*stat*-acetyl-L- homoserine$_{0.1}$) **tBu$_{0.9}$/Me$_{0.1}$-S^{H}**. At a monomer to initiator (M:I) ratio of 80:1, **tBu$_{0.9}$/Me$_{0.1}$-S^{H}** remained soluble during the polymerization with no signs of aggregate formation even after all monomer had been consumed (Table 2.1). This 9:1 mixture of NCAs was also found to undergo living polymerization using Co(PMe$_3$)$_4$ in THF to give **tBu$_{0.9}$/Me$_{0.1}$-S^{H}** with controlled chain lengths (Fig 2.2a). ^{1}H NMR and^{13}C NMR spectra analysis of **tBu$_{0.9}$/Me$_{0.1}$-S^{H}** confirmed the expected composition, and ^{1}H NMR was also used to determine molecular weights of polypeptides via end-group analysis. Gel permeation chromatography (GPC) analysis of **tBu$_{0.9}$/Me$_{0.1}$-S^{H}** showed the chains possess monomodal distributions with low dispersity (Fig 2.2b). FTIR analysis of **tBu$_{0.9}$/Me$_{0.1}$-S^{H}** in the solid-state was consistent with an α-helical or disordered chain conformation with minimal β-sheet content (Fig 2.2c). Circular dichroism analysis of **tBu$_{0.9}$/Me$_{0.1}$-S^{H}** in HFIP gave a spectrum that was

consistent with an α-helical conformation, validating our hypothesis that this higher homolog of poly(L-serine) would adopt this conformation instead of forming β -sheets (Fig 2.2d).

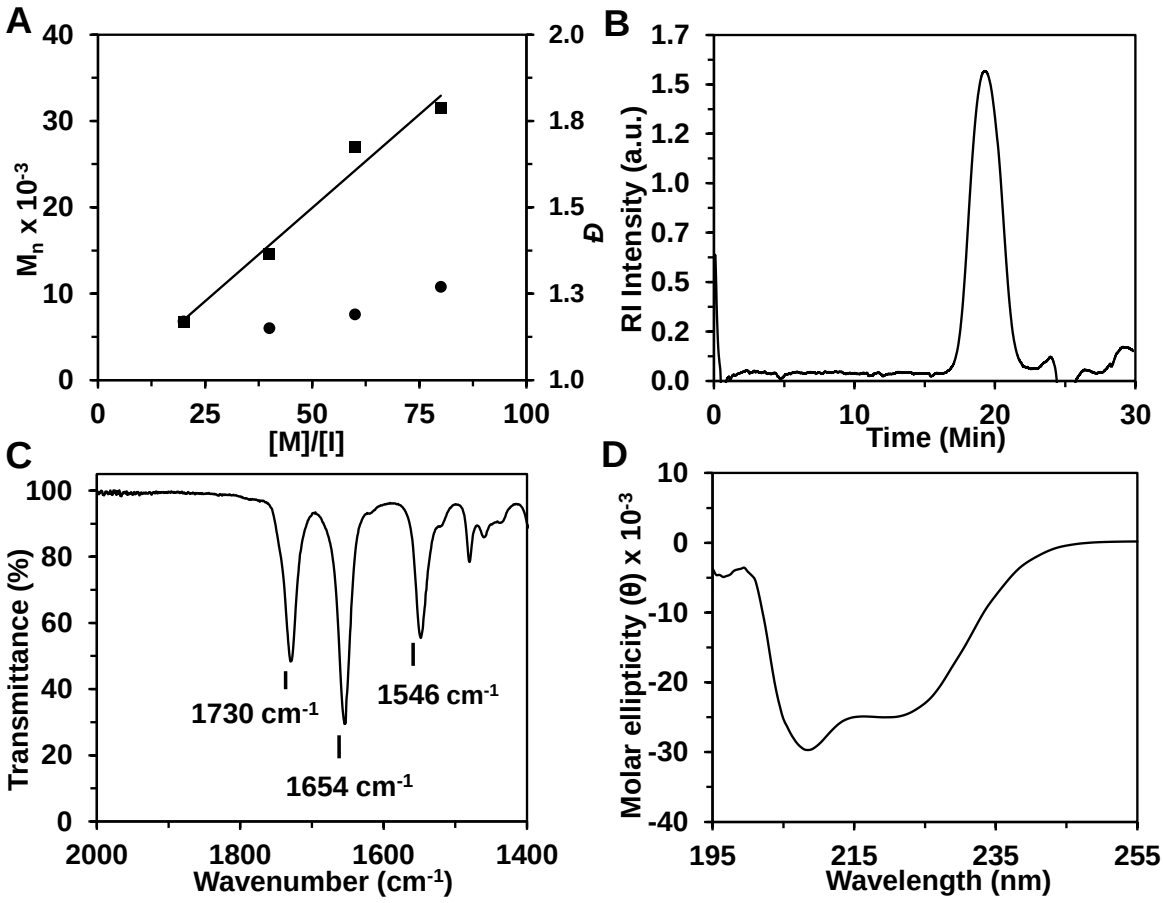

Figure 2.2. Synthesis and properties of poly(pivaloyl-L-homoserine$_{0.90}$-*stat*-acetyl-L-homoserine$_{0.10}$), **tBu/Me-S^{H}**. a) Variation in molecular weight, determined by ^{1}H NMR, and dispersity, determined by GPC, of **tBu/Me-S^{H}** as a function of monomer to initiator ratio (M:I) using Co(PMe$_3$)$_4$ in THF at 20 °C. b) GPC chromatogram of **tBu/Me-S$^{H}_{174}$** in HFIP containing 0.5% (w/w) KTFA. c) Solid State FTIR spectrum showing the amide band region of **tBu/Me-S$^{H}_{120}$**. The amide bands at 1654 and 1546 and cm^{-1} are indicative of α-helical or random coil conformations.[43] d) CD spectrum of **tBu/Me-S$^{H}_{47}$** (0.1 mg/mL) in HFIP at 22 °C. Minima at 208 and 224 nm are consistent with the polymer is adopting an α-helical conformation.[44]

To study the properties of **S^{H}**, protecting groups were removed from **tBu/Me-S^{H}** samples under basic conditions, and complete deprotection was confirmed by ^{1}H NMR and ^{13}C NMR. After deprotection and purification by dialysis, water-soluble **S^{H}** polypeptides were isolated as white solids by freeze-drying. To evaluate how chain length affects secondary structure, polypeptides of two different lengths were prepared, **S$^{H}_{47}$** and **S$^{H}_{100}$**. Solid-state FTIR analysis of **S$^{H}_{47}$** and **S$^{H}_{100}$** revealed two Amide I bands at 1647 cm^{-1} and 1611 cm^{-1}, which indicated the presence of two secondary structures (Fig 2.3). The Amide I and II bands at 1647 and 1538 cm^{-1} are consistent with random coil or α-helical conformations, while the Amide I band at 1611 cm^{-1} is consistent with a β-sheet conformation.[45] Based on these observations, increased chain length resulted in greater β-sheet content in the solid-state. Indeed, we found that freeze-dried **S^{H}** samples did not readily dissolve in DI water, and it was necessary to add a few drops of trifluoroacetic acid (TFA) to help solubilize these samples before diluting further in water. The TFA was able to disrupt β-sheet aggregates, and less than 5% TFA by volume was needed to solubilize freeze-dried **S$^{H}_{100}$** to give a final concentration of 50 mg/mL in water.

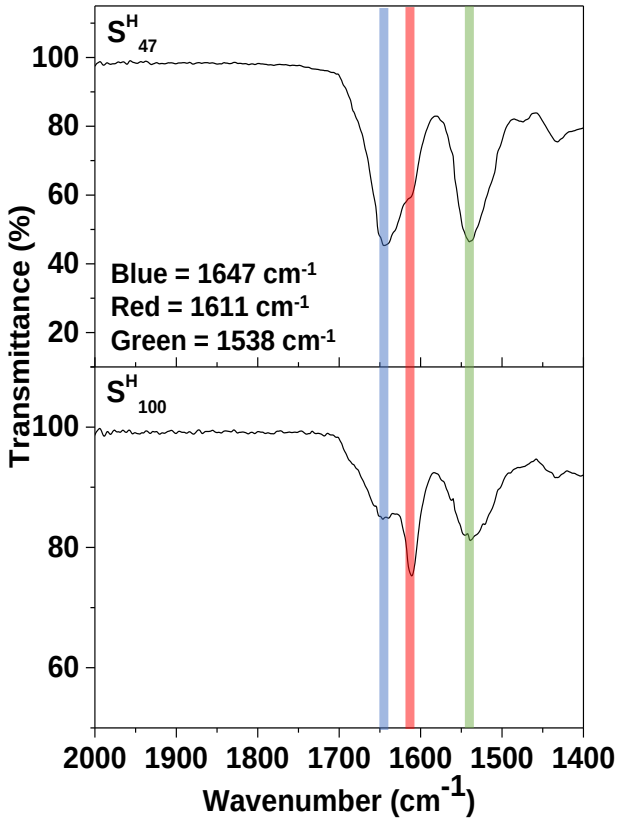

Figure 2.3. Solid state FTIR spectra showing amide band region of solid samples of **S^H_{47}** and **S^H_{100}.** The Amide I and II bands at 1647 cm^{-1} (blue) and 1538 cm^{-1} (green) are consistent with α-helical or random coil conformations.[43] The Amide I band at 1611 cm^{-1} (red) is consistent with a β-sheet conformation.[43]

To further study the water solubility and conformation of **S^H** in different conditions, CD spectra were recorded for aqueous solutions of **S^H** as functions of molecular weight, ionic strength, pH, and methanol content. For all CD analyses, negative Cotton effects were observed at 198 nm, indicating that optical purity was retained in the samples after deprotection, and that the chains primarily adopt disordered conformations in solution.[32, 34] Despite the partial β-sheet formation seen in the solid-state, aqueous solutions of **S^H_{47}** and **S^H_{100}** both showed similar disordered conformations, indicating that the solid-state β-structures were disrupted in water (Fig

2.4a). The disruption of solid-state β-strands to give disordered conformations in water has been noted before in previous work by the Deming Lab on derivates of poly(L-serine).[16] Here, solvation of the polypeptides by water molecules and increased steric bulk through ordered H-bonding around the chain backbone likely disrupts any ordered conformation.

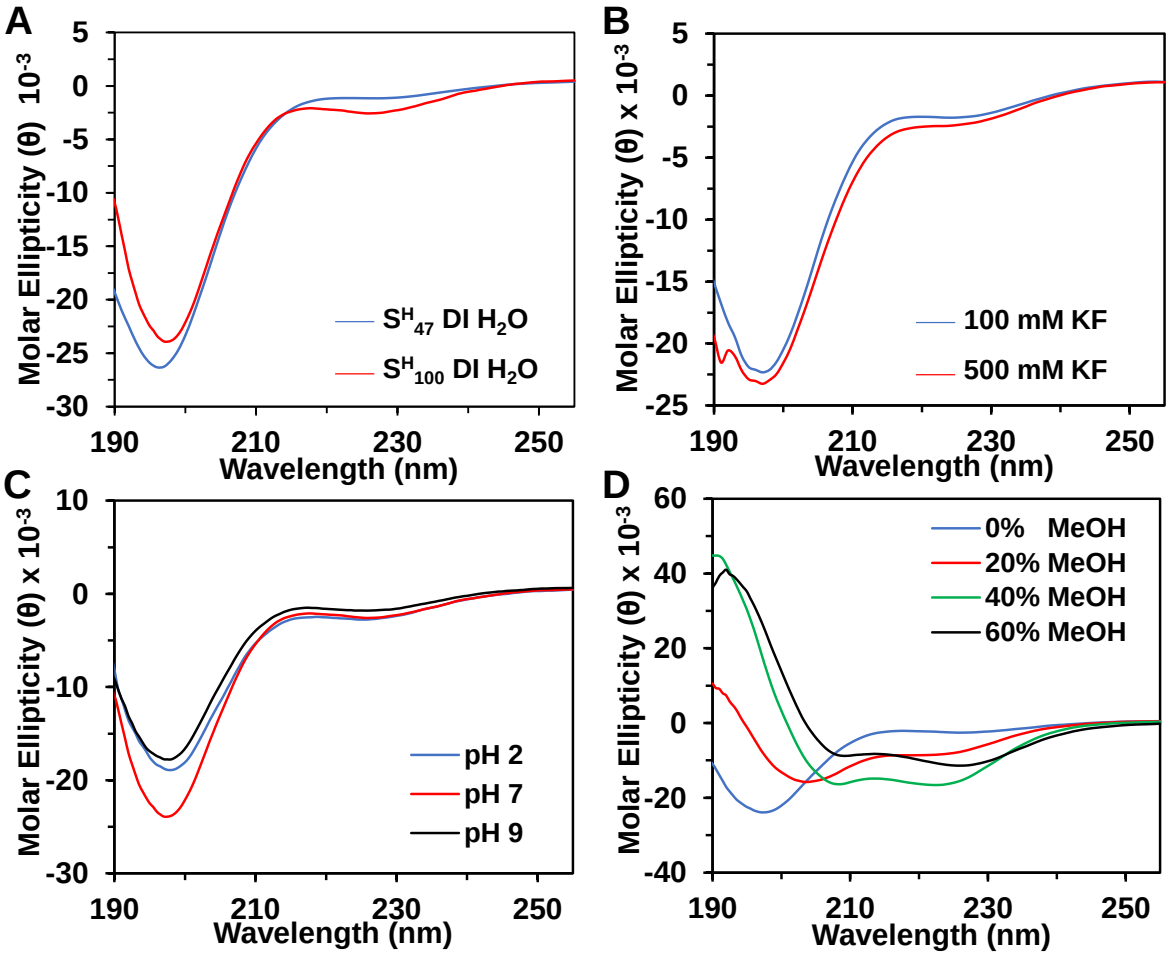

Figure 2.4. Conformational analysis of poly(L-homoserine), $\mathbf{S^H}$. a) CD spectra of $\mathbf{S^H_{47}}$ and $\mathbf{S^H_{100}}$ in DI water. b) CD spectra of $\mathbf{S^H_{100}}$ at pH 2, 5, and 9 in DI water. c) CD spectra of $\mathbf{S^H_{100}}$ in DI water containing either 100 mM or 500 mM KF. d) CD spectra of $\mathbf{S^H_{100}}$ in DI water containing 0, 20, 40 or 60% (v/v) methanol. For all CD spectra, polymer concentrations were 0.1 mg/mL and temperature was 22 °C.

Polypeptide conformations are stabilized by intramolecular noncovalent bonds, including hydrogen bonding of backbone amide groups and side-chain functional groups.[33] To study the influence of physiologically relevant ionic conditions, **S^{H}** was dissolved in aqueous media of increasing ionic strength. Potassium fluoride was selected as a model salt due to its low absorption between 190 and 210 nm, which reduced interference with the CD measurements. In water containing 500 mM KF, **S^{H}** remained disordered, showing that ionic media had no significant effect on the chain conformation (Fig. 2.4b). A distinct advantage of **S^{H}** as a water-soluble, non-ionic polypeptide is its lack of pH responsive side-chain groups that can cause undesirable conformation changes in acidic or basic conditions, which limits the utility of other hydrophilic ionic polypeptides, such as poly(L-lysine) and poly(L-glutamic acid). As expected, solution pH also had a minimal effect on the disordered chain conformation of **S^{H}** across a broad range (Fig. 2.4c).

Finally, to determine how water solvation of the hydroxyl-containing side chains in **S^{H}** influences chain conformation, **S^{H}** was dissolved in different aqueous media that contained increasing amounts of methanol. Chain conformations of these samples were determined using CD spectroscopy (Fig. 2.4d). Interestingly, as the polarity of the solvent was lowered by increasing methanol content, the chains were not found to adopt β-sheet conformations as seen in the solid-state. Instead, increasing methanol content resulted in adoptionof an α-helical conformation. Above 60% MeOH in water, **S^{H}** was insoluble, which prevented CD analysis at higher methanol fractions. The transition of **S^{H}** from disordered to α-helical conformations was likely due to decreased solvation

of the peptide backbone as hydrogen bonding between solvent and hydroxyl groups decreased.

Since non-ionic **S^H** is soluble in water and adopts a disordered conformation, we sought to use **S^H** to prepare amphiphilic diblock copolypeptides, where **S^H** would serve as the water-solubilizing segment (Fig. 2.5). L-methionine (Met) NCA and O-tert-butyl-L-serine (tBu-Ser) NCA were selected as different monomers for formation of water-insoluble segments that will drive self-assembly through microphase separation from water. The ability of **$tBu_{0.9}/Me_{0.1}$-Hse** NCAs to undergo controlled polymerization was further validated by their use in preparing diblock copolypeptides with Met NCA as either the initial or final segment. Secondary additions of NCA(s) to the active chain-ends of **$tBu_{0.9}/Me_{0.1}$-S^H** or **M** initial segments proceeded smoothly with full monomer conversions within 2 hours. Next, to confirm complete chain extensions and low dispersities, the diblock copolypeptides were analyzed by GPC. The poor solubility of the resulting diblock copolypeptides **$tBu_{0.9}/Me_{0.1}$-$S^H_{34}M_{109}$** and **$M_{42}tBu_{0.9}/Me_{0.1}$-S^H_{139}** in HFIP and other solvents necessitated methylation of the **M** segments prior to analysis. The **S^H** protecting groups were also removed to improve handling and ease of purification through dialysis (Fig. 2.6). During these modifications, **$S^H_{34}M^M_{109}$** was exposed to both basic and acidic conditions, as well as electrophilic reagents, without any degradation, which underscores the stability of **S^H** chains.

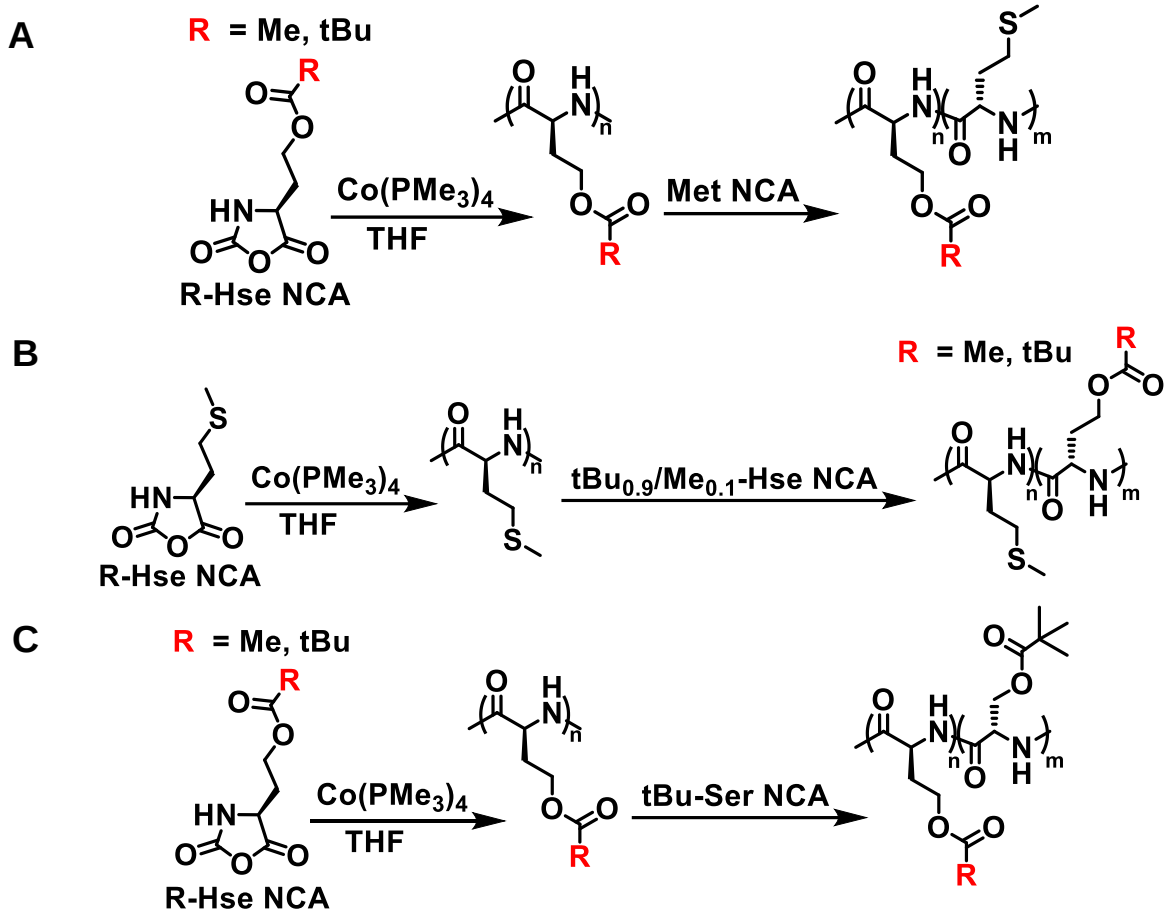

Figure 2.5. Scheme for preparation of **$tBu_{0.9}/Me_{0.1}$-S^H** containing diblock copolypeptides. a) **$tBu_{0.9}/Me_{0.1}$-$S^H_nM_m$** b) **$M_ntBu_{0.9}/Me_{0.1}$-S^H_n** c) **$tBu_{0.9}/Me_{0.1}$-S^H_ntBu-S_m**

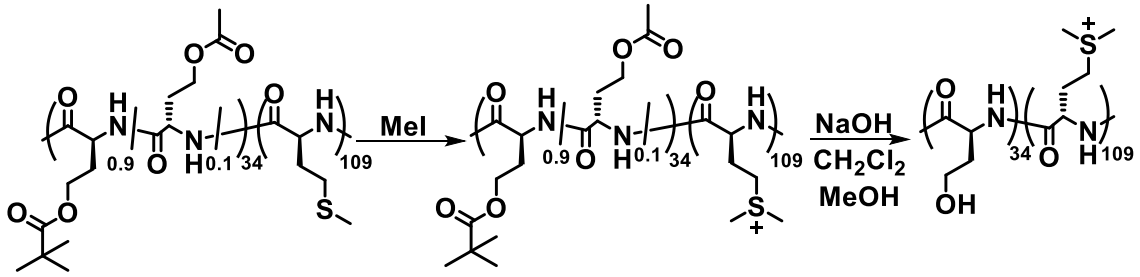

Figure 2.6. Scheme for preparation of **$S^H_{34}M^M_{109}$** for GPC analysis in HFIP with 0.5% (w/v) KTFA (sample concentration = 10 mg/mL).

First Segment			Second Segment		Diblock Copolypeptide[c]			
Monomer	eq.[a]	DP[b]	Monomer	eq.[a]	M_n[d] (kDa)	DP[d]	M_w/M_n[e]	Yield (%)[f]
$tBu_{0.9}/Me_{0.1}$-Hse NCA	20	34	Met NCA	60	20.4	143	1.23	90
Met NCA	20	42	$tBu_{0.9}/Me_{0.1}$-Hse NCA	60	30.6	181	1.28	92
$tBu_{0.9}/Me_{0.1}$-Hse NCA	50	110	tBu-Ser NCA	8	23.3	130	1.27	85

Table 2.2. GPC analysis of $\mathbf{S^H}$ containing block copolypeptides prepared using $Co(PMe_3)_4$ initiator in THF at 20 °C. [a] Indicates equivalents of monomer per $Co(PMe_3)_4$ initiator. [b] Degree of polymerization (DP) determined by end-group analysis after complete polymerization of first segments. [c] Data for diblock copolypeptides after complete polymerization of second segments. [d] Number average molecular weight (M_n) and DP determined by end-group analysis. [e] Determined by GPC-MALS. [f] Total isolated yield of diblock copolypeptides.

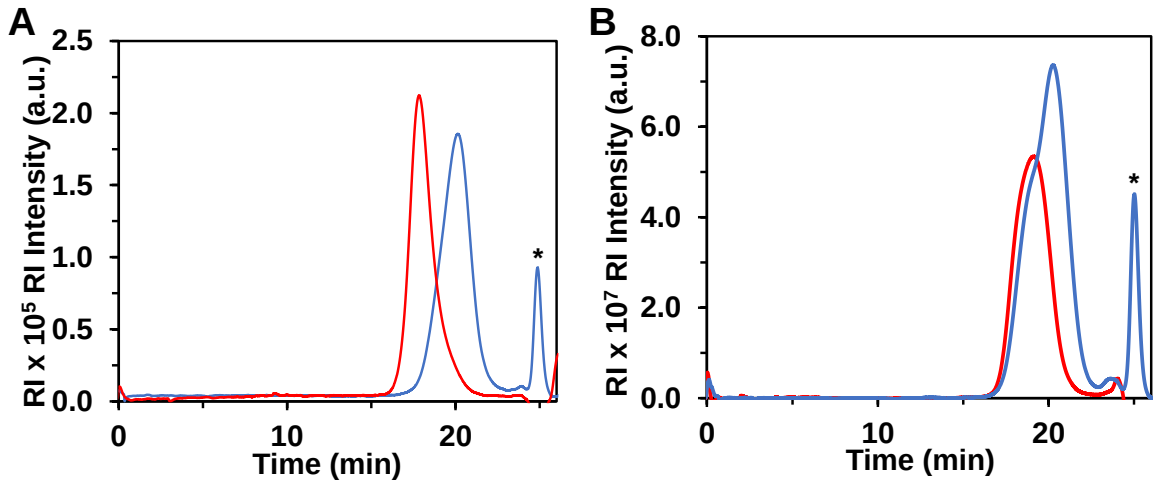

Figure 2.7. GPC chromatograms of $\mathbf{S^H}$ containing block copolypeptides in HFIP containing 0.5% (w/w) KTFA. a) Initial segment $\mathbf{S^H_{34}}$ (blue) and diblock copolypeptide $\mathbf{S^H_{34}M^M_{109}}$ (red). b) Initial segment $\mathbf{tBu_{0.9}/Me_{0.1}\text{-}S^H_{110}}$ (blue) and diblock copolypeptide $\mathbf{tBu_{0.9}/Me_{0.1}\text{-}S^H_{110}tBu\text{-}S_{20}}$ (red). * = solvent peak.

The data in Table 2.2 show that $\mathbf{tBu_{0.9}/Me_{0.1}\text{-}S^H}$ chains are suitable initiating segments for preparation of block copolypeptides. Comparison of the GPC traces for the first segment and final diblock copolypeptide of $\mathbf{S^H_{34}M^M_{109}}$ show the expected increase in molecular weight while retaining low dispersity, which indicate successful

chain extension (Fig. 2.7a). ^{1}H NMR and GPC analysis of the reverse sequence diblock copolypeptide where **tBu$_{0.9}$/Me$_{0.1}$-Hse** NCA monomers were added to the active **M** chains also showed chain extension via living polymerization (Table 2.2). GPC analysis of **tBu$_{0.9}$/Me$_{0.1}$-S$^{H}_{110}$tBu-S$_{20}$** did not require deprotection of the side chains due to good solubility of this copolymer in HFIP. Data in Table 2.2 and Fig. 2.7b demonstrate an increase in molecular weight after chain extension and a monomodal distribution for **tBu$_{0.9}$/Me$_{0.1}$-S$^{H}_{110}$tBu-S$_{20}$**, indicating the chain ends remained active and were able to add all **tBu-Ser** NCA monomers, despite the formation of β-sheet structures in the **tBu-S** segment. However, the β-sheet conformation of **tBu-S** prohibited controlled chain extensions when preparation of reverse sequence diblock copolypeptides was attempted.

After successful preparation of block copolypeptides containing **S^{H}** segments, a series of **S$^{H}_{m}$X$_{n}$** amphiphilic diblock copolypeptides were prepared, where **X** was either a **M** or **S** segment (Fig. 2.8), for study of their self-assembly in aqueous media. The block copolypeptide compositions and lengths were selected based on designs from earlier work, e.g. the vesicle forming **M$^{O}_{60}$ (F$_{0.5}$/L$_{0.5}$)$_{20}$** and hydrogel forming **(M$^{O}_{0.9}$/A$_{0.1}$)$_{180}$L$_{30}$.**[18-19] Unfortunately, despite variation of compositions and lengths in both **S$^{H}_{m}$** and **M$_{n}$** components, ordered self-assemblies were not obtained in aqueous media. Multiple assembly annealing techniques were attempted, including elevated temperature, dissolution in TFA followed by slow addition of water via dialysis, and prolonged agitation, yet all approaches yielded only disordered assemblies. In particular, all **M** containing samples were found to form large, micron scale irregular aggregates.

$S^H_mX_y$	Disperses in Water
$S^H_{170}M_{30}$	No
$S^H_{110}M_{13}$	No
$S^H_{110}M_{17}$	No
$S^H_{110}M_{20}$	No
$S^H_{60}M_{20}$	No
$S^H_{50}S_{10}$	Yes
$S^H_{97}S_{19}$	Yes
$S^H_{110}S_{14}$	Yes
$S^H_{110}S_{20}$	Yes
$S^H_{110}S_{27}$	Hazy

Figure 2.8. Library of $\mathbf{S^H}$ containing amphiphilic diblock copolypeptides screened for ability to disperse in water. Aqueous suspensions of $\mathbf{S^H_mS_n}$ were prepared from diblock copolypeptides at 1.0 mg/mL by dissolving in TFA before diluting and dialyzing extensively with DI water at room temperature.

On the other hand, many of the $\mathbf{S^H_mS_n}$ samples were found to disperse well in water at ambient temperature (Fig. 2.8). Of these, $\mathbf{S^H_{110}S_{20}}$ was identified by dynamic light scattering (DLS) as the most promising sample for assembly formation since aqueous suspensions contained particles with an average diameter of 290 nm (PDI = 0.35) after extrusion through 200 nm diameter pore size polycarbonate filters (Figure 2.9a). To visualize $\mathbf{S^H_{110}S_{20}}$ assemblies, $\mathbf{S^H_{110}S_{20}}$ N-terminal amines were labelled with fluorescein-5-isothiocyanate (FITC). $\mathbf{S^H_{110}S_{20}}$ was suspended in DI water at 1 mg/mL and briefly dispersed in a sonicator to reduce large particles. Individual z-axis image slices of the labelled assemblies in DI water were obtained using laser scanning

confocal microscopy (LSCM) and revealed the presence of fluorescent-rimmed circles of 2.9 ± 0.2 μm average diameter, which are characteristic for water filled vesicular assemblies (Figure 2.9b). Overall, the differences in solubility and self-assembly behavior between $\mathbf{S^H_mM_n}$ and $\mathbf{S^H_mS_n}$ in water may be due to a greater hydrophilicity of **S** segments as compared to the more hydrophobic **M** segments. Regardless, the ability to form vesicles with block copolypeptides using $\mathbf{S^H}$ as the water-soluble segment shows the potential for use of $\mathbf{S^H}$ containing polypeptide assemblies for downstream biomedical applications, including drug and gene delivery.

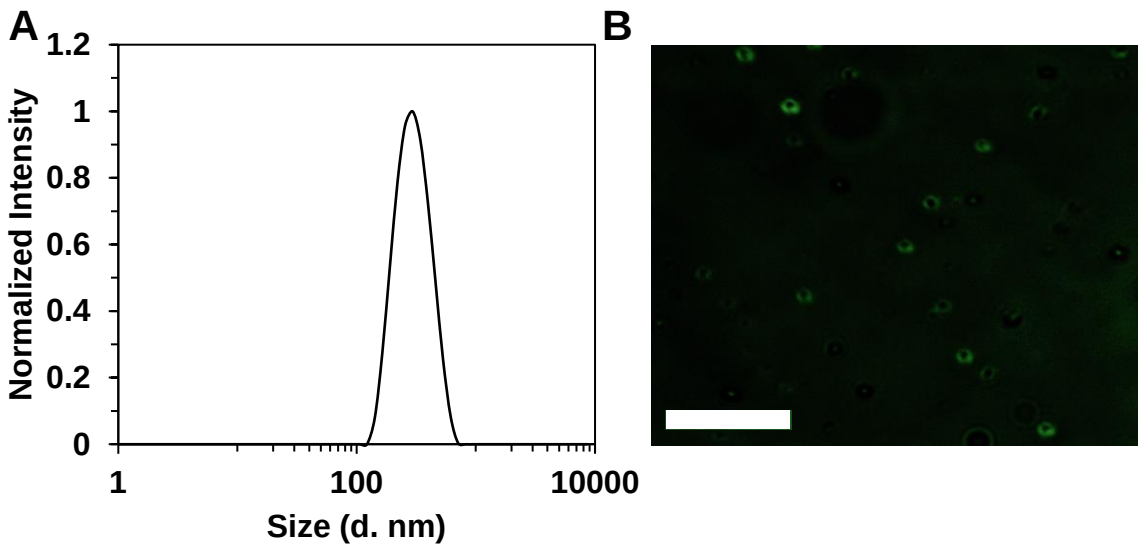

Figure 2.9. Assembly of diblock copolypeptide $\mathbf{S^H_{110}S_{20}}$ in DI water. a) DLS data for assemblies of $\mathbf{S^H_{110}S_{20}}$ at 2 mg/mL in DI water at 20 ^{o}C. b) LSCM image of fluorescein labeled 1% (w/v) $\mathbf{S^H_{110}S_{20}}$ vesicle suspension in DI water. Scale bar = 20 μm, optical z-slice = 700 nm.

2.4 Conclusion

PEG has long been the gold standard for a water-soluble, non-fouling polymer in biomaterials applications. However, its lack of degradability and increasing reports of immunogenic responses in clinical applications underscore the need for new

alternatives. Here we report **S^{H}** as a potential PEG alternative due to its water-solubility, non-ionic side chains, and potential biocompatibility and degradability of the peptide backbone. **Me-Hse** and **tBu-Hse** NCAs were prepared in few steps with high yield and purity and were readily copolymerized to give high molecular weight polypeptides with controlled chain lengths. Preparation of high molecular weight **tBu/Me-S^{H}** was possible since this copolymer adopts an α-helical conformation, as opposed to the the β-sheet aggregation typically seen with protected poly(L-serine) derivatives. The lack of **tBu/Me-S^{H}** chain aggregation allows efficient chain extension by addition of a second NCA to **tBu/Me-S^{H}** active chain ends to give diblock copolypeptides. While ordered self-assemblies in water could not be obtained from **S$^{H}_{m}$M$_{n}$** diblock copolypeptides due to their poor solubility, **S$^{H}_{m}$S$_{n}$** block copolypeptides of varying compositions dispersed well in water and could form vesicle assemblies. Downstream *in vitro* and *in vivo* studies will be necessary to learn more about **S^{H}** degradability and non-fouling properties. However, the results obtained here show that **S^{H}** should be considered as a promising candidate for biomedical applications where non-ionic, water-soluble polymer components are desired.

2.5 Experimental

2.5.1 Materials and methods

The following chemicals were used as received from commercial vendors: L-homoserine (Combi-Blocks), L-serine (Sigma-Aldrich), acetyl chloride (ACROS Organics), acetic acid (Fisher-Scientific), propionyl chloride (Sigma-Aldrich), propionic acid (Sigma-Aldrich), *i*-butyryl chloride (Honeywell Fluka), *i*-butyric acid (Sigma-Aldrich), benzoyl chloride (EM Science), trimethyl acetic chloride (ACROS Organics), sodium

methoxide (30 wt%) in methanol (ACROS Organics) trifluoroacetic acid (Oakwood), and 15% phosgene in toluene (Sigma–Aldrich). DI H_2O is in house deionized water. α-Methoxy-ω-isocyanoethyl-poly(ethylene glycol), mPEG-NCO (1 kDa), was prepared as previously reported.[46] NCA purifications[47] and polymerizations[48] were performed in an N_2 filled glove box using established techniques. Reactions at elevated temperature were controlled using a Corning PC 420D thermostat controlled hotplate equipped with a thermocouple probe. All reactions were performed under N_2 at 22 ºC unless otherwise described. THF and hexanes were degassed by sparging with nitrogen, and water was removed by passage through columns of dried alumina. Thin-layer chromatography was performed with EMD gel 60 F254 plates (0.25 mm thickness) and visualized using a UV lamp or ninhydrin stain. Column chromatography was performed using Silicycle Siliaflash G60 silica (60–200 mm). Silica used for chromatographic purification of NCA monomers was dried under vacuum at 250 °C for 48 hours and then stored in a dinitrogen filled glovebox. Dialysis was performed with regenerated cellulose tubing obtained from Spectrum labs. CD spectra were collected using 0.1 or 0.5 mg/mL solutions of polypeptide on an Olis DSM 10 spectrophotometer using a 0.1 cm path length quartz cuvette. DART-MS spectra were collected on a Thermo Exactive Plus MSD (Thermo Scientific) equipped with an ID-CUBE ion source at the low desorption setting and a Vapur Interface (IonSense). Both the source and MSD were controlled by Excalibur v. 3.0. Analytes were dissolved at 1.0 mg/mL in 1:3 THF:MeCN and spotted onto OpenSpot sampling cards (IonSense). Ionization was accomplished using He plasma with no additional ionization agents. Mass calibration was carried out using Pierce LTQ Velos ESI (+) and (-) ion calibration solutions (Thermo Fisher Scientific).

FTIR spectroscopy was performed on a ThermoScientific iS5 FTIR spectrometer or a JASCO FT/IR-4100 spectrometer. NMR spectroscopy was performed on a Bruker AV400 spectrometer. Tandem gel permeation chromatography/light scattering (GPC/LS) was performed using an SSI Accuflow Series III pump equipped with Wyatt DAWN EOS light scattering and Optilab REX refractive index detectors. Separations were achieved using 100 Å and 1000 Å PSS-PFG 7 μm columns at 30 ºC with 0.5% (w/w) potassium trifluoroacetate (KTFA) in 1,1,1,3,3,3-hexafluoroisopropanol (HFIP) as eluent and sample concentrations of 10 mg/ml.

2.5.2 Synthesis of Amino Acids and NCA Monomers

General procedures for O-acyl-L-homoserine derivatives

Method A. This method was adapted from a previously reported procedure.[4] A neat mixture of the desired acid chloride (8 mL) and its corresponding carboxylic acid (8 mL) were mixed in an equal volume ratio and cooled to 0 ºC in an ice bath before slowly adding L-homoserine (2.00 g, 16.8 mmol). The resulting heterogeneous mixture was stirred while allowing the ice bath to warm to ambient temperature. After 4 hours, the heterogeneous mixture was filtered under suction to remove excess solvent, washed with ether, and dried under vacuum to give a white solid. This solid was then dissolved with DI H_2O (50 mL) in a flat bottom flask and cooled in an ice bath before adjusting the pH to 6 by dropwise addition of 5 M NaOH in water. Water was then removed by rotary evaporation to give a white solid. In the same flask, boiling water was carefully added to the solid until just dissolved, before removing from the heat. Any insoluble material was removed by hot filtration. After the solution cooled down to ambient temperature, it was placed in a 4 ºC refrigerator and left overnight to promote crystallization. The resulting

small, dense white crystalline product was collected by washing with ice-water and drying to remove residual moisture.

Method B. L-homoserine (2.00 g, 16.8 mmol) was dissolved in trifluoroacetic acid (15 mL) and cooled to 0 ^{o}C in an ice bath before addition of the desired acid chloride (50.4 mmol). The reaction was let stir at ambient temperature for 16 hours, and was then placed under vacuum to remove solvent, resulting in a yellow, viscous liquid. DI H_2O (50 mL) was added to dilute the reaction mixture, which was stirred before cooling in an ice bath. The solution was adjusted to pH 6 by slow addition of 10M NaOH in water. Due to the large amount of residual TFA left in the solution, a considerable amount of 10M NaOH (*ca*. 15 mL) must be added to reach pH 6. Purification and crystallization of the product was accomplished using the same procedure as described in Method A.

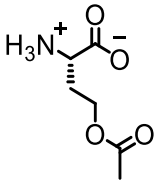

O-Acetyl-L-homoserine (Me-Hse) Prepared using Method A to give a white solid (75% yield). ^{1}H NMR (400 MHz, D_2O) δ 4.22 – 4.10 (m, 2H), 4.07 (t, *J* = 6.2 Hz, 1H), 2.28 – 2.16 (m, 2H), 1.97 (s, 3H). Spectrum in agreement with literature data.[49]

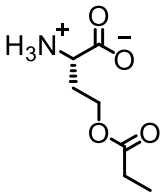

O-Propionyl-L-homoserine (Et-Hse) Prepared using Method A to give a white solid (70% yield). ^{1}H NMR (400 MHz, D_2O) δ 4.15 (t, *J* = 6.0 Hz, 2H), 3.74 (dd, *J* = 7.1, 5.3 Hz, 1H), 2.31 (q, *J* = 7.6 Hz, 2H), 2.23 – 2.03 (m, 2H), 0.98 (t, *J* = 7.6 Hz, 3H).

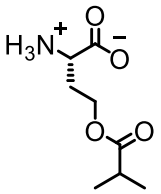

O-Isobutyryl-L-homoserine (iPr-Hse) Prepared using Method A to give a white solid (75% yield). ^{1}H NMR (400 MHz, D_2O) δ 4.22 – 4.07 (m, 2H), 3.90 (t, *J* = 6.3 Hz, 1H), 2.52 (hept, *J* = 7.0 Hz, 1H), 2.30 – 2.06 (m, 2H), 1.02 (d, *J* = 7.0 Hz, 6H).

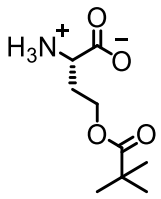

O-Pivaloyl-L-homoserine (tBu-Hse) Prepared using Method B to give a white solid (80% yield). ^{1}H NMR (400 MHz, D_2O) δ 4.18 – 3.98 (m, 3H), 2.31 – 2.11 (m, 2H), 1.02 (s, 9H).

O-Benzoyl-L-homoserine (Ph-Hse) Prepared using Method B to give a white solid (20% yield). ^{1}H NMR (400 MHz, D_2O) δ 6.91 (dt, *J* = 3.7, 2.6 Hz, 2H), 6.56 (dd, *J* = 8.4, 6.6 Hz, 1H), 6.41 (t, *J* = 7.8 Hz, 2H), 3.55 – 3.36 (m, 2H), 3.22 (t, *J* = 6.4 Hz, 1H), 1.57 – 1.29 (m, 2H).

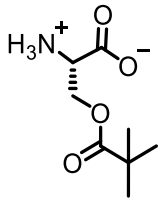

O-Pivaloyl-L-serine (tBu-Ser) Prepared using Method B to give a white solid (85% yield). ^{1}H NMR (400 MHz, D_2O) δ 4.58 (dd, *J* = 12.3, 4.1 Hz, 1H), 4.36 – 4.20 (m, 2H), 1.07 (s, 9H). Spectrum in agreement with literature data.[50]

Amino acid N-carboxyanhydride (NCA) monomers.

NCA monomers were prepared by adaptation of procedures previously reported for other NCA monomers.[47] ***Caution! Phosgene is extremely hazardous and all manipulations must be performed in a well-ventilated chemical fume hood with proper personal protection and necessary precautions taken to avoid exposure.***

After complete removal of solvents under vacuum on a Schlenk manifold, crude reaction

mixtures, in sealed Schlenk flasks under vacuum, were brought into a dinitrogen filled glovebox for purification. The method of purification varied for different monomers, as detailed below.

General procedures for purification of O-Acyl-L-homoserine *N*-carboxyanhydrides

Method A. This method was used to purify NCAs that are crystalline solids. Crude NCA was purified via anhydrous column chromatography in a dinitrogen filled glovebox using a solvent gradient of 25 to 33% THF in hexanes, followed by isolation of the purified NCA by solvent removal under vacuum. The resulting material was further purified by 2x recrystallization from THF/hexanes to give the NCA product as a white solid.

Method B. This method was used to purify to purify NCAs that are oils. Outside the glove box, an ice cold DCM solution of crude NCA (*ca*. 1 g in 15 mL) was washed rapidly in a separatory funnel with ice cold 5% $NaHCO_3$(aq) (10 mL) followed by ice cold DI H_2O (10 mL). The organic layer was collected and dried with sodium sulfate before being decanted into a Schlenk flask and the solvent removed under vacuum. The sealed flask was brought into a dinitrogen filled glovebox. The NCA was purified further via anhydrous column chromatography using 33% THF in hexanes to give the product, after removal of solvents, as a clear oil.

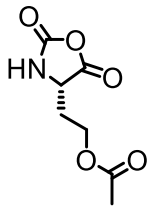

O-Acetyl-L-homoserine N-carboxyanhydride (Me-Hse NCA) Purified using Method A to give dense, white crystals (70% yield). ^{1}H NMR (400 MHz, $CDCl_3$) δ 6.54 (s, 1H), 4.46 – 4.35 (m, 2H), 4.16 (ddd, *J* = 12.0, 8.0, 4.3 Hz, 1H), 2.35 – 2.24 (m, 1H), 2.16 (dtd, *J* = 12.2, 7.9, 4.4 Hz, 1H), 2.09 (s, 3H). ^{13}C NMR (101 MHz, $CDCl_3$) δ 171.28, 169.65, 152.58, 59.76, 55.15, 30.52, 20.69. DART-MS m/z = 186.05 $[M - H]^-$ (calcd for

$C_7H_9NO_5$: 186.05). FTIR (solid): 1855 cm^{-1} (NCA anhydride), 1782 cm^{-1} (NCA anhydride), 1741 cm^{-1} (ester).

O-Propionyl-L-homoserine N-carboxyanhydride (Et-Hse NCA) Purified using Method B to give a colorless oil (40% yield). ^{1}H NMR (400 MHz, $CDCl_3$) δ 6.39 (s, 1H), 4.51 – 4.39 (m, 1H), 4.36 (ddd, *J* = 7.8, 4.6, 1.1 Hz, 1H), 4.15 (ddd, *J* = 11.9, 7.8, 4.2 Hz, 1H), 2.44 – 2.23 (m, 3H), 2.21 – 2.05 (m, 1H), 1.14 (t, *J* = 7.6 Hz, 3H). ^{13}C NMR (101 MHz, $CDCl_3$) δ 174.68, 169.63, 152.50, 59.57, 55.11, 30.58, 27.31, 8.88. DART-MS m/z = 200.06 $[M - H]^-$ (calcd for $C_8H_{11}NO_5$: 200.06). FTIR (neat oil): 1855 cm^{-1} (NCA anhydride), 1785 cm^{-1} (NCA anhydride), 1739 cm^{-1} (ester).

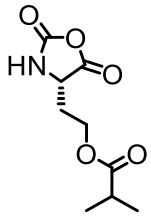

O-Isobutyryl-L-homoserine N-carboxyanhydride (iPr-Hse NCA) Purified using Method B to give a colorless oil (40% yield). ^{1}H NMR (400 MHz, $CDCl_3$) δ 6.66 (s, 1H), 4.50 – 4.27 (m, 2H), 4.16 (ddd, *J* = 12.0, 7.7, 4.4 Hz, 1H), 2.67 – 2.46 (m, 1H), 2.30 (ddt, *J* = 16.0, 6.8, 4.6 Hz, 1H), 2.17 (dtd, *J* = 12.1, 7.7, 4.4 Hz, 1H), 1.28 – 1.03 (m, 6H). ^{13}C NMR (101 MHz, $CDCl_3$) δ 177.43, 169.54, 152.40, 59.50, 55.00, 33.87, 30.63, 18.83. DART-MS m/z = 214.08 $[M - H]^-$ (calcd for $C_9H_{13}NO_5$: 214.08). FTIR (neat oil): 1855 cm^{-1} (NCA anhydride), 1786 cm^{-1} (NCA anhydride), 1739 cm^{-1} (ester).

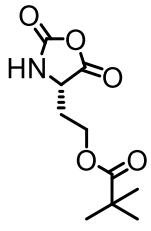

O-Pivaloyl-L-homoserine N-carboxyanhydride (tBu-Hse NCA) Prepared using Method A to give needle-like crystals (65% yield). ^{1}H NMR (400 MHz, $CDCl_3$) δ 6.12 (s, 1H), 4.45 (ddd, *J* = 11.8, 7.8, 3.9 Hz, 1H), 4.29 (ddd, *J* = 8.4, 4.5, 1.4 Hz, 1H), 4.19 – 4.03 (m, 1H), 2.39 – 2.23 (m, 1H), 2.19 – 2.02 (m, 1H), 1.21 (s, 9H). ^{13}C NMR (101 MHz, $CDCl_3$) δ 179.03, 169.33, 152.14, 59.59, 54.90, 38.88, 30.82, 27.06. DART-MS m/z = 228.10 $[M - H]^-$ (calcd for $C_{10}H_{15}NO_5$: 200.06). FTIR (solid): 1859 cm^{-1} (NCA anhydride), 1781 cm^{-1} (NCA anhydride), 1737 cm^{-1} (ester).

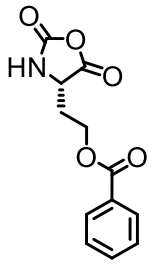

O-Benzoyl-L-homoserine N-carboxyanhydride (Ph-Hse NCA) Prepared using Method A to give a white solid (18% yield). ^{1}H NMR (400 MHz, $CDCl_3$) δ 8.00 (dt, *J* = 8.5, 1.5 Hz, 2H), 7.64 – 7.54 (m, 1H), 7.51 – 7.41 (m, 2H), 6.57 (s, 1H), 4.67 (ddd, *J* = 11.8, 7.6, 4.0 Hz, 1H), 4.41 (ddd, *J* = 11.7, 7.1, 4.4 Hz, 2H), 2.49 – 2.37 (m, 1H), 2.31 – 2.19 (m, 1H). ^{13}C NMR (101 MHz, $CDCl_3$) δ 169.30, 166.90, 151.88, 133.73, 129.75, 128.97, 128.67, 60.09, 54.98, 31.20. DART-MS m/z = 262.08 $[M - H]^-$ (calcd for $C_{13}H_{13}NO_5$: 262.08). FTIR (solid): 1839 cm^{-1} (NCA anhydride), 1772 cm^{-1} (NCA anhydride), 1731 cm^{-1} (ester).

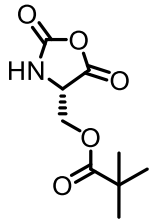

O-Pivaloyl-L-serine N-carboxyanhydride (tBu-Ser NCA) Prepared using Method A to give needle-like crystals (70% yield). ^{1}H NMR (400 MHz, $CDCl_3$) δ 6.19 (s, 1H), 4.71 (dd, *J* = 12.1, 2.9 Hz, 1H), 4.53 (t, *J* = 3.0 Hz, 1H), 4.27 (dd, *J* = 12.1, 3.2 Hz, 1H), 1.20 (s, 9H). ^{13}C NMR (101 MHz, $CDCl_3$) δ 178.42, 167.31, 152.29, 61.14, 57.71, 38.97, 26.94. DART-MS m/z = 214.08 $[M - H]^-$ (calcd for $C_9H_{13}NO_5$: 214.08). FTIR (solid): 1859 cm^{-1} (NCA anhydride), 1781 cm^{-1} (NCA anhydride), 1737 cm^{-1} (ester).

2.5.3 Preparation of poly(L-homoserine) using different NCA precursors

General procedure for polymerization of O-acyl-L-homoserine NCAs. The synthesis of poly[(O-pivaloyl-L-homoserine)$_{0.9}$-*stat*-(O-acetyl-L-homoserine)$_{0.1}$]$_n$, **(tBu$_{0.9}$/Me$_{0.1}$-S^{H})$_n$**, is used as an example. All polymerization reactions were performed in a dinitrogen filled glove box using anhydrous solvents. tBu-Hse and Me-Hse NCAs were dissolved separately in THF (50 mg/mL) before mixing at the desired molar ratio. To a solution of tBu$_{0.9}$/Me$_{0.1}$-Hse NCAs in THF (50 mg/mL) was added an aliquot of $Co(PMe_3)_4$ solution in THF (20 mg/mL) to give the desired monomer to initiator ratio.

Once mixed, the reaction was let stand at ambient temperature for 1-2 h, and completion of polymerization was confirmed by FTIR by monitoring the disappearance of NCA bands at 1840 cm^{-1} and 1790 cm^{-1}. An aliquot (200 µL) of the polymer solution was removed for molecular weight determination by end-group analysis (*vide infra*). The polymerization mixture was removed from the glove box and polypeptide was precipitated by addition of the mixture to excess 0.1M aqueous HCl with vigorous stirring for 1 hr. The suspension was centrifuged at 3000 rpm to recover the solid polymer and the supernatant was discarded. The pellet was washed once more with 0.1M HCl and then 3x with DI water before lyophilizing to yield **$(tBu_{0.9}/Me_{0.1}\text{-}S^H)_n$** as a white solid.

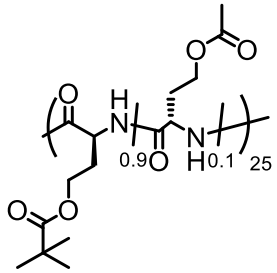

Poly[(O-pivaloyl-L-homoserine)$_{0.9}$-*stat*-(O-acetyl-L-homoserine)$_{0.1}$]$_{25}$, $(tBu_{0.9}/Me_{0.1}\text{-}S^H)_{25}$ Obtained in 93% yield. ^{1}H NMR (400 MHz, TFA-d) δ 4.95 (d, *J* = 5.3 Hz, 25H), 4.34 (d, *J* = 5.4 Hz, 50H), 2.52 – 2.08 (m, 62H), 1.31 (s, *J* = 7.6 Hz, 190H). ^{13}C NMR (126 MHz, TFA-d) δ 183.23, 173.26, 61.46, 51.47, 39.09, 30.53, 25.75, 18.69.

General procedure for deprotection of poly(O-acyl-L-homoserine) and poly(O-acyl-L-serine). Deprotection of **$(tBu_{0.9}/Me_{0.1}\text{-}S^H)_n$** is used as an example. To a solution of **$(tBu_{0.9}/Me_{0.1}\text{-}S^H)_n$** in DCM (50 mg/mL) was added two equivalents of NaOMe (30% NaOMe in MeOH) per ester group, and the mixture was stirred for 8 h to give a white suspension. Complete precipitation of solids was then achieved by addition of the reaction mixture to excess diethyl ether. After washing the solids two times with diethyl ether, the precipitate was collected by centrifugation at 3000 rpm and dried under

vacuum. TFA was added to help dissolve the dried polymer, which was then diluted with water (final ratio of 1:9 TFA:Water) before transferring to a 2000 MWCO dialysis bag. The resulting soluble polymer was dialyzed first against saturated $NaHCO_3$ (aq) (2 water changes for 48 h) and DI H_2O (4 water changes for 48 h) before lyophilization to recover poly(L-homoserine)$_n$, $\mathbf{S^H_n}$, as a fluffy, white solid (90% yield).

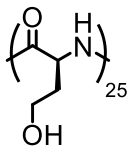

Poly(L-homoserine)$_{25}$, $\mathbf{S^H_{25}}$ Obtained in 90% yield. ^{1}H NMR (400 MHz, D_2O) δ 4.41 – 4.21 (m, 23H), 3.69 – 3.39 (m, 50H), 2.06 – 1.62 (m, 50H). FTIR (solid): 1643 cm^{-1} (Amide I), 1539 cm^{-1} (Amide II).

General procedure for end-capping of polypeptides with PEG chains. The general procedure of polymerization of O-Acyl-L-homoserine NCAs was followed. Once polymerization was determined to be complete by FTIR, a solution of α-methoxy-ω-isocyanoethyl-poly(ethylene glycol), PEG-NCO (MW = 1000 Da, 3 eq per $Co(PMe_3)_4$) in THF was added to an aliquot of the polymerization mixture inside a dinitrogen filled glovebox. The reaction was let stand overnight before removing from the glovebox. The completed reaction was precipitated by addition to excess 0.1M aqueous HCl with vigorous stirring for 1 hr. The mixture was centrifuged at 3000 rpm to recover the solid polymer and the supernatant was discarded. The solid polymer was washed once more with 0.1M HCl and then 3 times with DI water to remove unconjugated PEG-NCO before lyophilizing to yield the PEG-endcapped polypeptide as a white solid. Molecular weight of the polypeptide (M_n) was determined by ^{1}H NMR using the integral of the polyethylene oxide repeat of known length as a standard to obtain polypeptide lengths.[46]

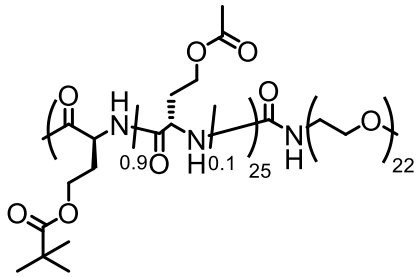

Poly[(O-pivaloyl-L-homoserine)$_{0.9}$-*stat*-(O-acetyl-L-homoserine)$_{0.1}$]$_{25}$-*block*-poly(ethyleneglycol)$_{22}$, (tBu$_{0.9}$/Me$_{0.1}$-S^{H})$_{25}$-PEG$_{22}$ ^{1}H NMR (400 MHz, TFA-d) δ 4.95 (s, 125H), 4.37 (d, *J* = 7.0 Hz, 50H), 3.99 (s, 88H), 3.67 (s, 3H), 2.51 – 2.12 (m, 59H), 1.35 (s, 213H).

General procedure for block copolypeptide preparation. All polymerization reactions were performed in a dinitrogen filled glovebox using anhydrous solvent. To a solution of tBu$_{0.9}$/Me$_{0.1}$-Hse NCA mixture in THF (50 mg/mL), an aliquot of Co(PMe$_3$)$_4$ solution in THF (20 mg/mL) was added to obtain the desired monomer to initiator ratio. The reaction was let stir at ambient temperature for 1 hr. Complete consumption of NCAs was confirmed by FTIR. An aliquot (200 µL) of the polymer solution was removed for molecular weight determination by end-group analysis. The desired amount of Met NCA or tBu-Ser NCA in THF (50 mg/mL) was added to the reaction mixture, which was let react for an additional 1 hr. FTIR was used to confirm complete consumption of NCA. The resulting solution was removed from the glovebox and the block copolypeptide was precipitated and washed using the method described above for polymerization of O-acyl-L-homoserine NCAs. The sample was then lyophilized to give the product as a white solid.

General procedure for methylation of Met residues in diblock copolypeptides. To convert Met residues in **tBu$_{0.9}$/Me$_{0.1}$-S$^{H}_{34}$M$_{109}$** to S-methyl-Met sulfonium residues, the diblock copolypeptide was suspended in DI water at 20 mg/mL containing iodomethane (3 eq. per Met residue). The reaction was protected from light with

aluminum foil and stirred vigorously for 5 days at ambient temperature. After the reaction was completed, the copolymer was transferred to a 2000 MWCO dialysis bag and dialyzed against sodium metabisulfite in DI water (0.75 mM, 1 day) to remove iodine impurities, NaCl in DI water (35 mM, 2 days) to remove iodide counterions, and DI water (2 days), to remove residual NaCl. Dialysis water was changed twice per day. The copolymer was then freeze-dried to produce a white, fluffy solid (95% yield). The protected Hse residues were deprotected following the deprotection procedure described above.

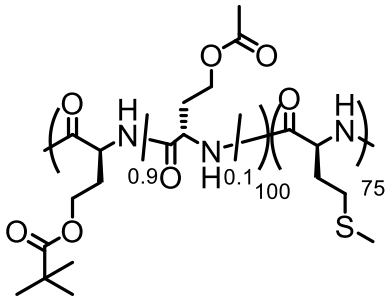

Poly[(O-pivaloyl-L-homoserine)$_{0.9}$-*stat*-(O-acetyl-L-homoserine)$_{0.1}$]$_{100}$-*block*-poly(L-methionine)$_{75}$, (tBu$_{0.9}$/Me$_{0.1}$-S^{H})$_{100}$(M)$_{75}$. ^{1}H NMR (400 MHz, TFA-d) δ 4.93 (br s, 175H), 4.31 (br s, 230H), 2.72 (br s,125H), 2.35 (br s, 146H), 2.20 (br m, 386H), 1.29 (s, 915H).

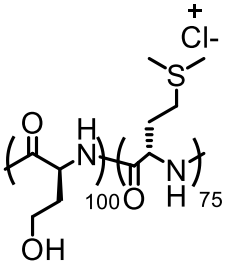

Poly[(L-homoserine)$_{100}$-*block*-poly(S-methyl-L-methionine sulfonium chloride)$_{75}$, (S^{H})$_{100}$(M^{M})$_{75}$. ^{1}H NMR (400 MHz, TFA-d) δ 5.03 (br s, 175H), 4.12 (br s, 200H), 3.69 (br s, 135H), 3.13 (s, 380H), 2.73-2.57 (br m, 140H), 2.41 (br s, 100 H), 2.21 (br s, 100H).

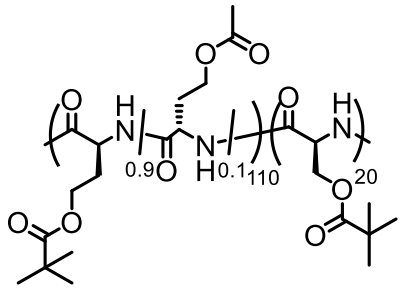

Poly[(O-pivaloyl-L-homoserine)$_{0.9}$-*stat*-(O-acetyl-L-homoserine)$_{0.1}$]$_{110}$-*block*-poly(O-pivaloyl-L-serine)$_{20}$, (tBu$_{0.9}$/Me$_{0.1}$-S^{H})$_{110}$(tBu-S)$_{20}$ ^{1}H NMR (400 MHz, TFA-d) δ 5.24 (s, 20H), 4.93 (br m, 120H), 4.57 (s, 41H), 4.33 (br m, 220H), 2.35 (br m, 139H), 2.22 (br m,135H), 1.29 (s, 863H), 1.27 (s, 178H).

2.5.4 Poly(L-homoserine) Characterization

Circular dichroism of copolypeptides.

Circular dichroism spectra (from 190 to 250 nm) were recorded in a quartz cuvette of 0.1 cm path length with samples prepared at 0.1 mg/mL in the chosen solvent. All spectra were recorded as an average of 3 scans. The spectra are reported in units of molar ellipticity [θ] (deg·cm^2 ·dmol^{-1}). The formula used for calculating molar ellipticity, [θ], was [θ] = (θ x 100 x MW)/(c x l) where θ is the experimental ellipticity in millidegrees, MW is the average molecular weight of a residue in g/mol, c is the peptide concentration in mg/mL; and l is the cuvette pathlength in cm.

Dynamic light scattering (DLS) measurements.

Samples were prepared at 0.2% (w/v) in DI water before extruding through a series of polycarbonate filters of decreasing pore size: 1000, 400, and 200 nm. DLS samples were prepared in disposable plastic cuvettes (ZEN0118 and ZEN0040). Dynamic light scattering measurements were performed on a Malvern Panalytical Zetasizer Nano ZS and measured using a non-invasive backscattering angle of 173°.

Fluorescent probe conjugation to $S^{H}_{110}S_{20}$.

Fluorescein 5(6)-isothiocyanate (FITC) was conjugated to the N-terminal amine groups of polypeptide chains. $S^{H}_{110}S_{20}$ was dissolved at 10 mg/mL in DMF. FITC was dissolved in DMF at 10 mg/mL and added to the polypeptide solution at a 5:1 molar ratio of FITC per polypeptide chain. The reaction was covered in foil and left overnight. The FITC labelled polypeptide was dialyzed extensively against isopropanol, isopropanol/DI water (1:1), and DI water to ensure removal of unconjugated FITC.

Laser scanning confocal microscopy (LCSM) of fluorescently labeled vesicles.

LSCM images of copolypeptide samples were taken on a Leica Inverted TCS-SP1 MP-Inverted Confocal and Multiphoton Microscope. The FITC labelled $S^{H}_{110}S_{20}$ was prepared at 1% (w/v) in DI water, dispersed in a bath sonicator for 10 min to disrupt large particles, and visualized on glass slides with a spacer between the slide and coverslip (Secure Seal Imaging Spacer, Grace Bio-labs). Imaging of the xy plane with a z-slice of 700 nm revealed the presence of green fluorescent rings, consistent with formation of water-filled vesicles.

2.5.6 Spectral Data

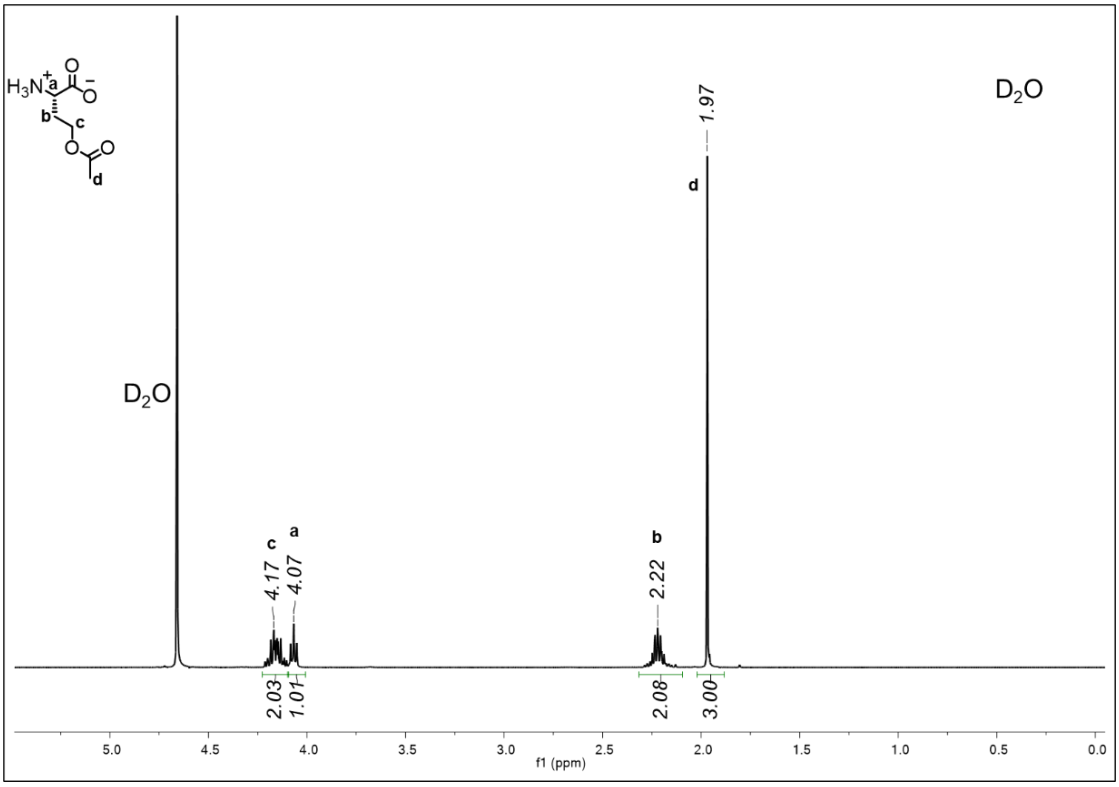

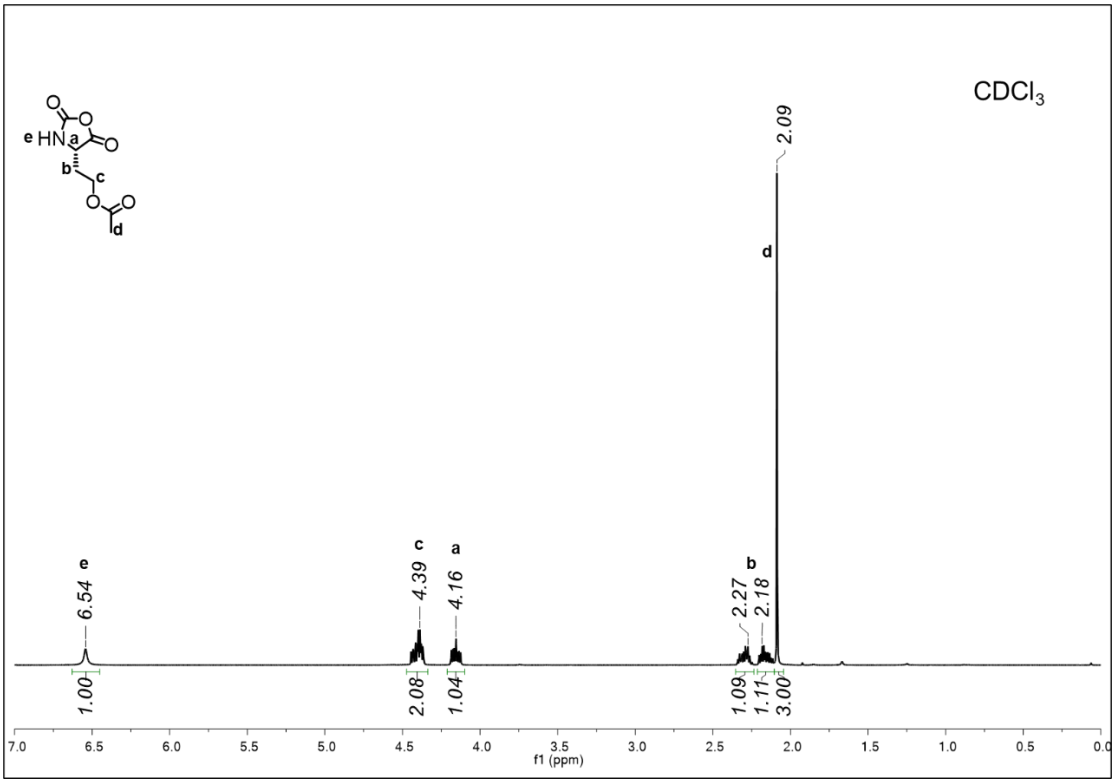

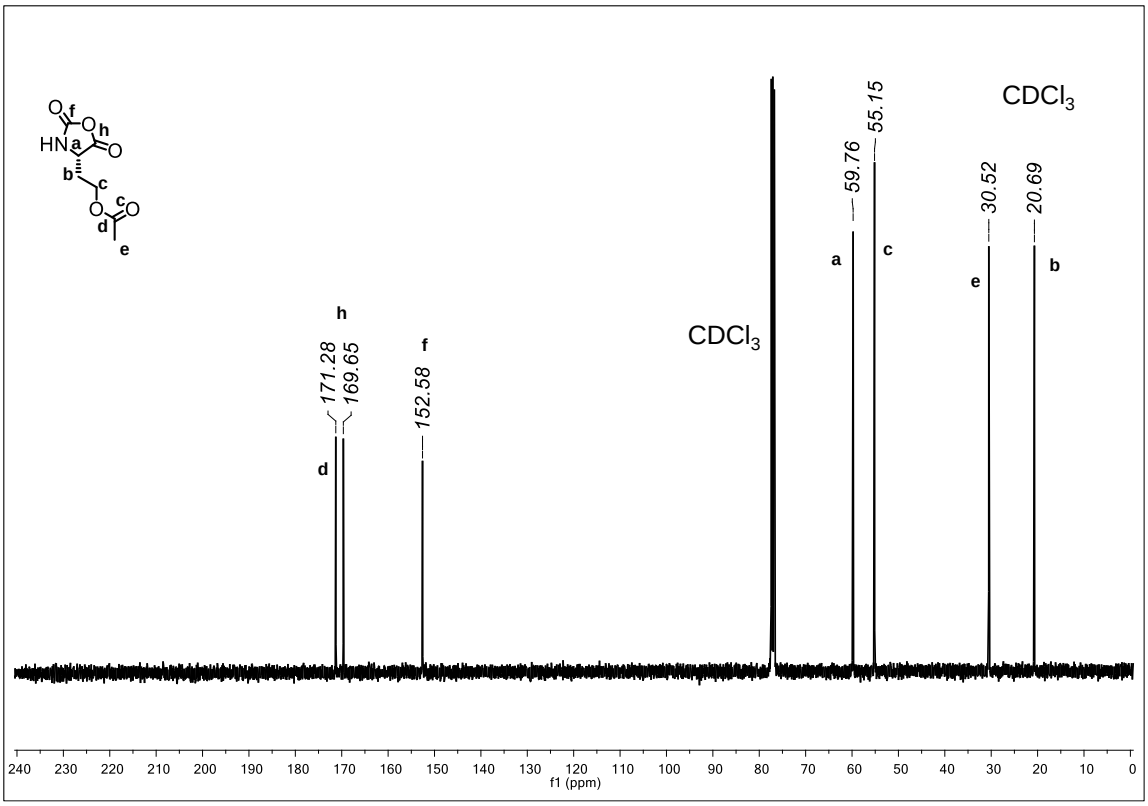
CDCl3
CDCl3
171.28
169.65
152.58
59.76
55.15
30.52
20.69
f1 (ppm)

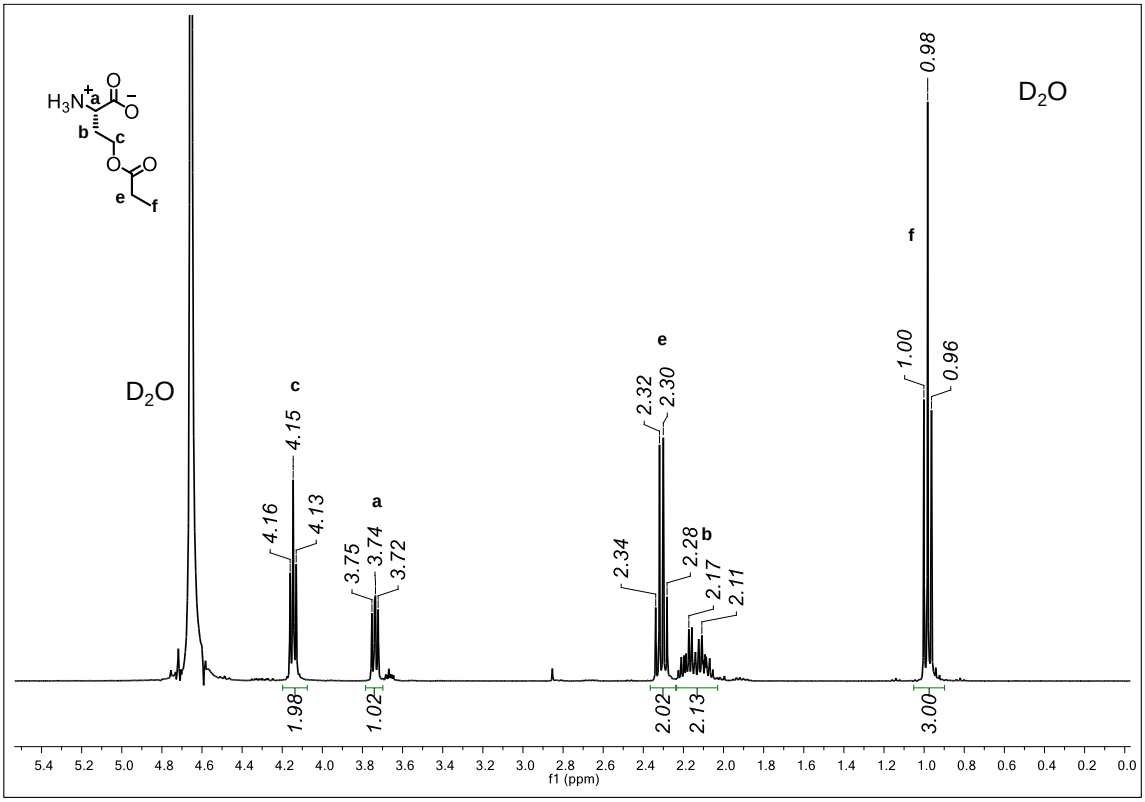
D2O
D2O
4.16
4.15
4.13
3.75
3.74
3.72
2.34
2.32
2.30
2.28
2.17
2.11
1.00
0.98
0.96
1.98
1.02
2.02
2.13
3.00
f1 (ppm)

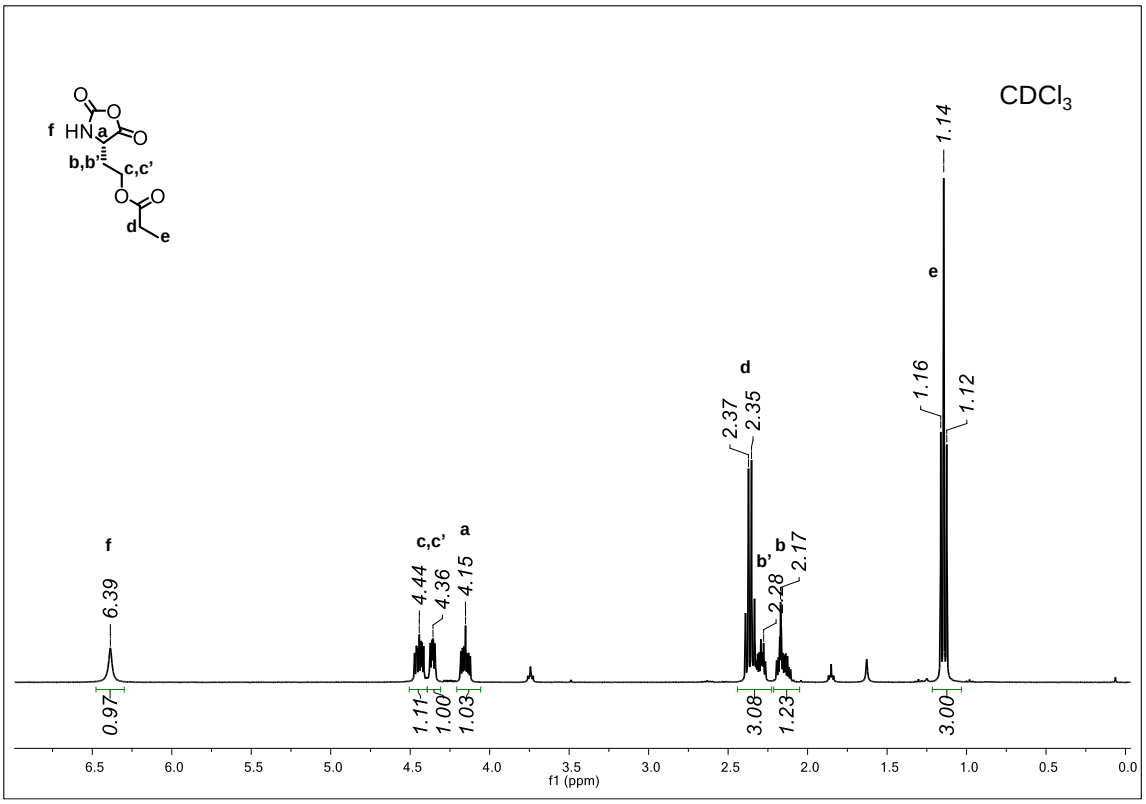
CDCl3
f
HN
a
b,b'
c,c'
d
e
6.39
4.44
4.36
4.15
2.37
2.35
2.28
2.17
1.16
1.14
1.12
0.97
1.11
1.00
1.03
3.08
1.23
3.00
f1 (ppm)

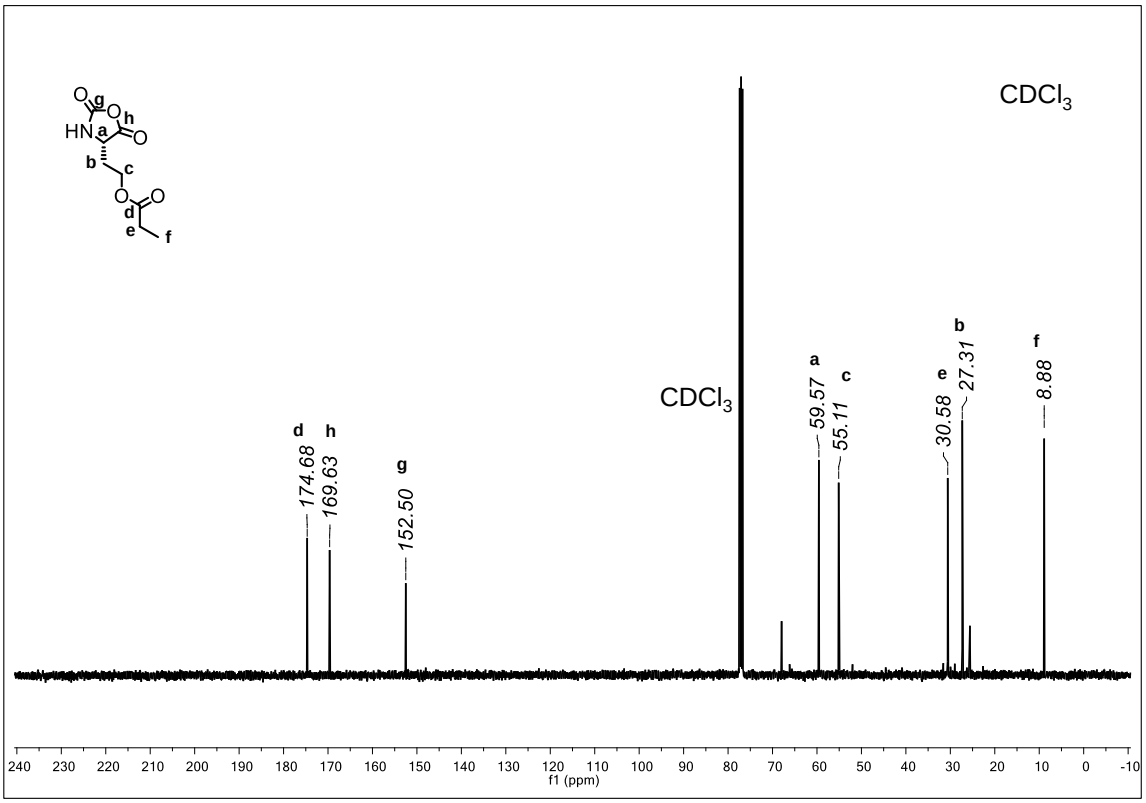
CDCl3
g
h
HN
a
b
c
d
e
f
174.68
169.63
152.50
59.57
55.11
30.58
27.31
8.88
f1 (ppm)

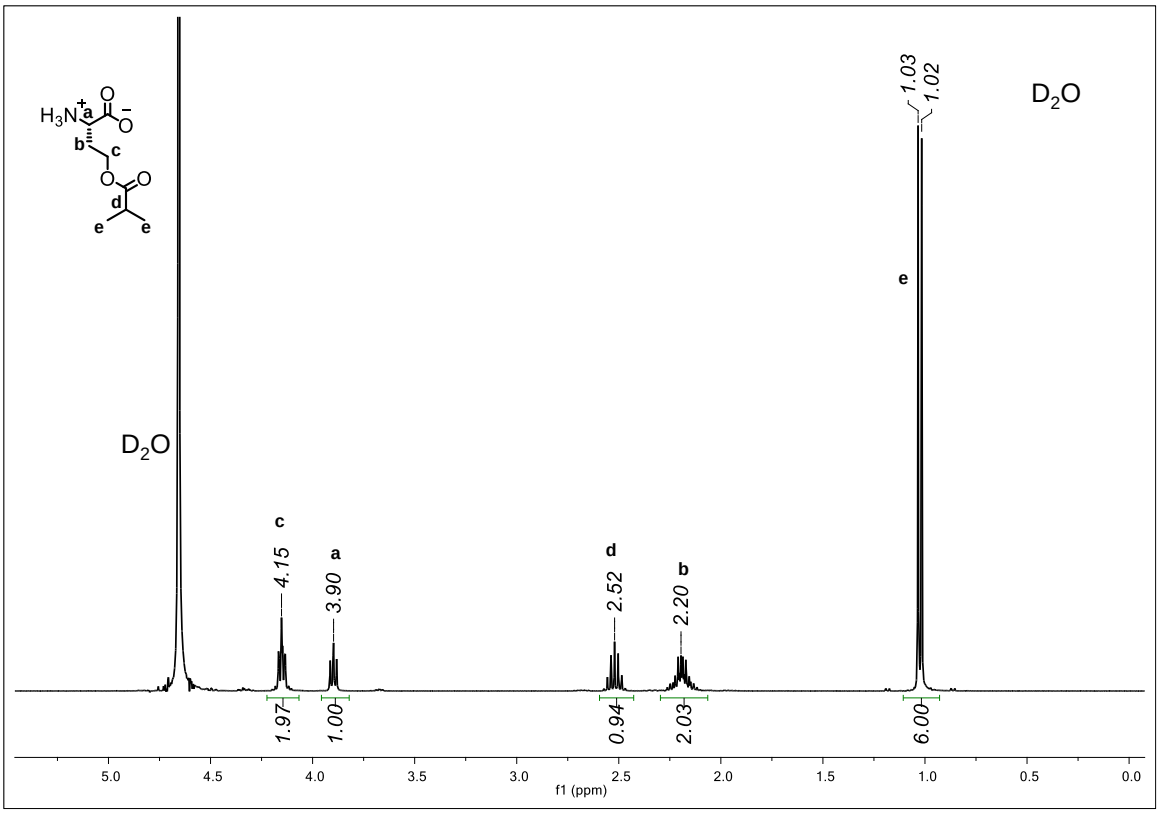
D2O
1.03
1.02
e
D2O
c
4.15
a
3.90
d
2.52
b
2.20
1.97
1.00
0.94
2.03
6.00
5.0
4.5
4.0
3.5
3.0
2.5
2.0
1.5
1.0
0.5
0.0
f1 (ppm)

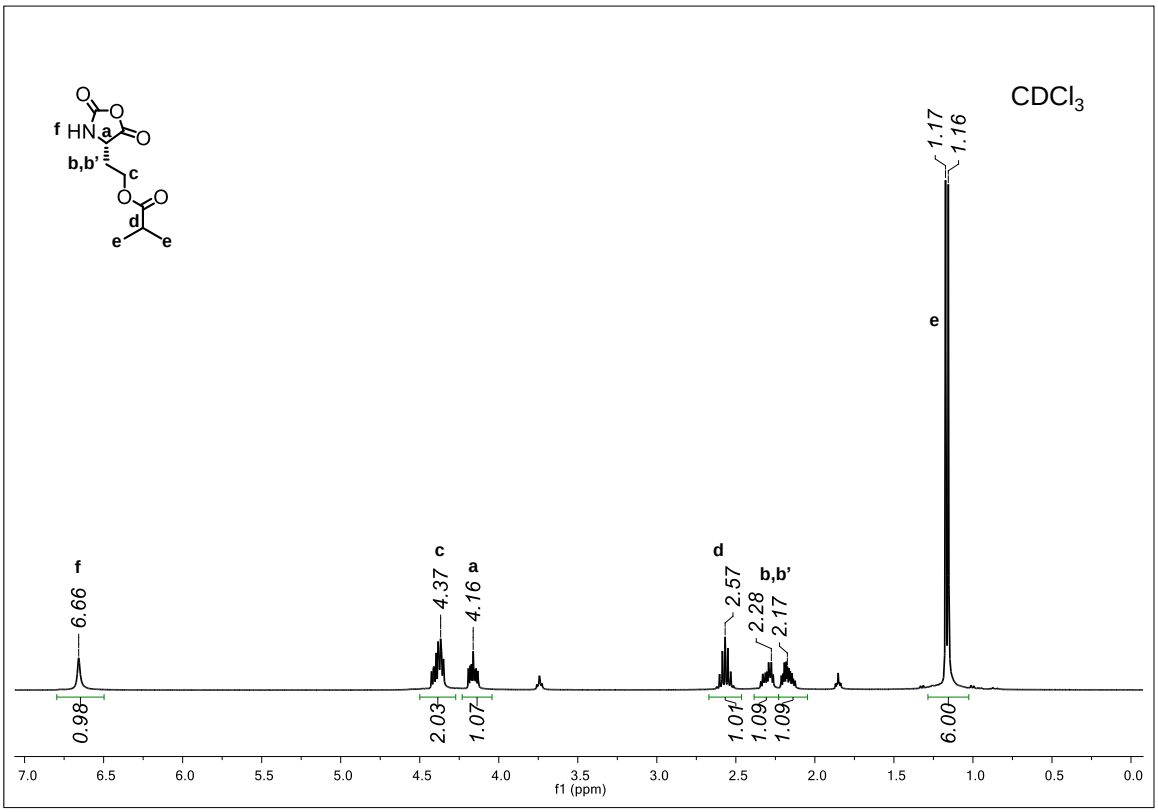
CDCl3
f HN a
b,b'
c
d
e e
1.17
1.16
e
f
6.66
c
4.37
a
4.16
d
2.57
2.28
2.17
b,b'
0.98
2.03
1.07
1.01
1.09
1.09
6.00
7.0
6.5
6.0
5.5
5.0
4.5
4.0
3.5
3.0
2.5
2.0
1.5
1.0
0.5
0.0
f1 (ppm)

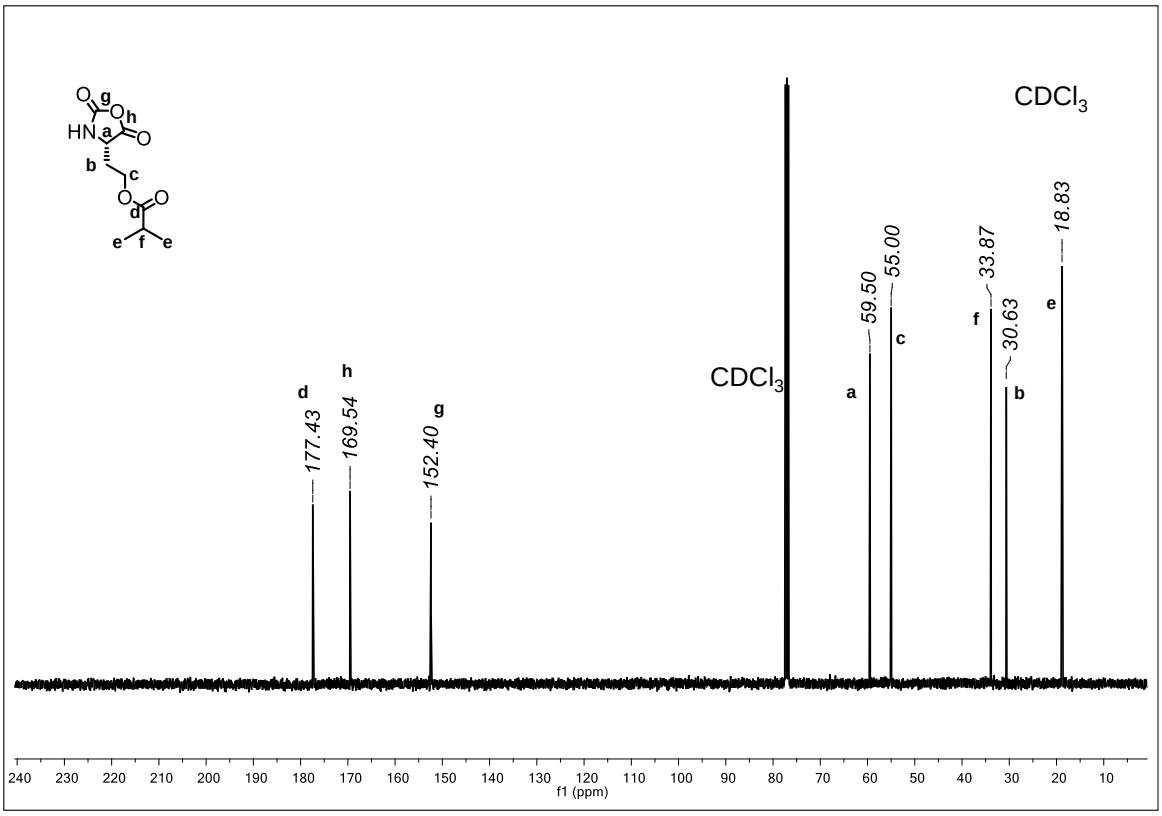
CDCl3
CDCl3
d
177.43
h
169.54
g
152.40
a
59.50
c
55.00
f
33.87
b
30.63
e
18.83
240 230 220 210 200 190 180 170 160 150 140 130 120 110 100 90 80 70 60 50 40 30 20 10
f1 (ppm)

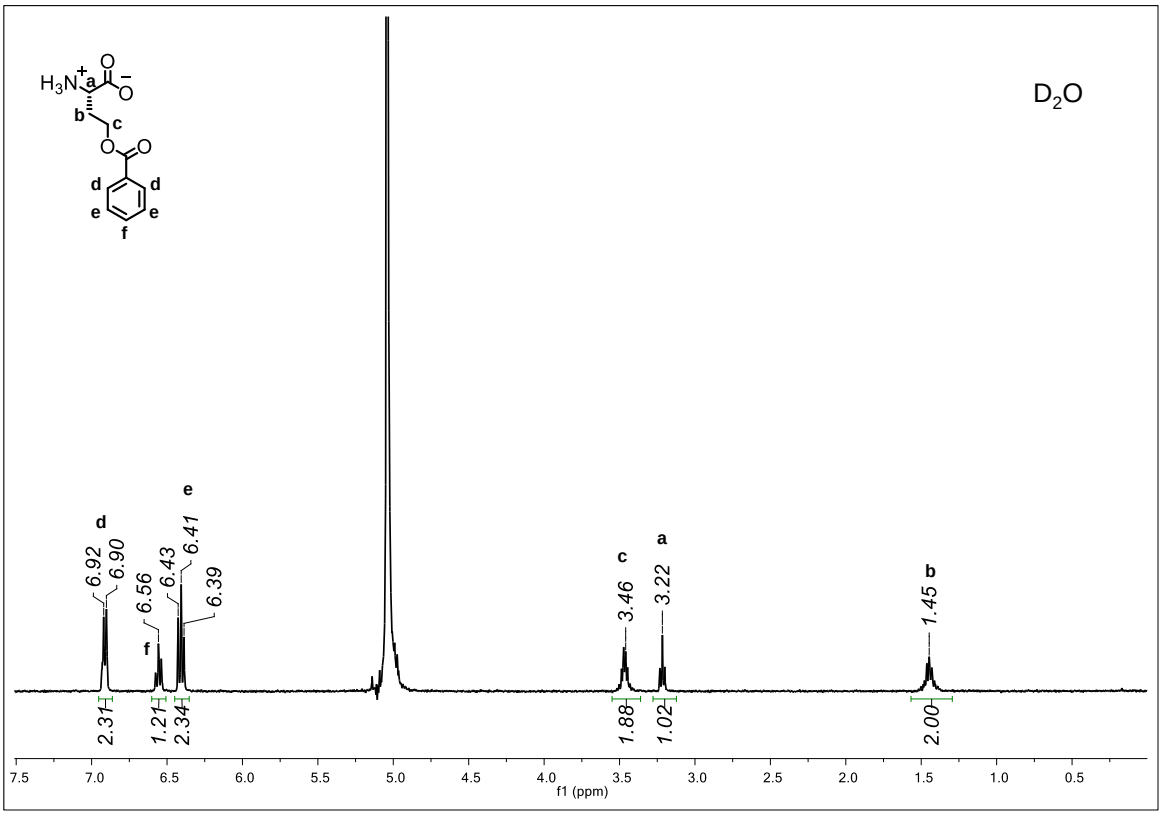
D2O
d
6.92
6.90
6.56
f
e
6.43
6.41
6.39
c
3.46
a
3.22
b
1.45
2.31
1.21
2.34
1.88
1.02
2.00
7.5 7.0 6.5 6.0 5.5 5.0 4.5 4.0 3.5 3.0 2.5 2.0 1.5 1.0 0.5
f1 (ppm)

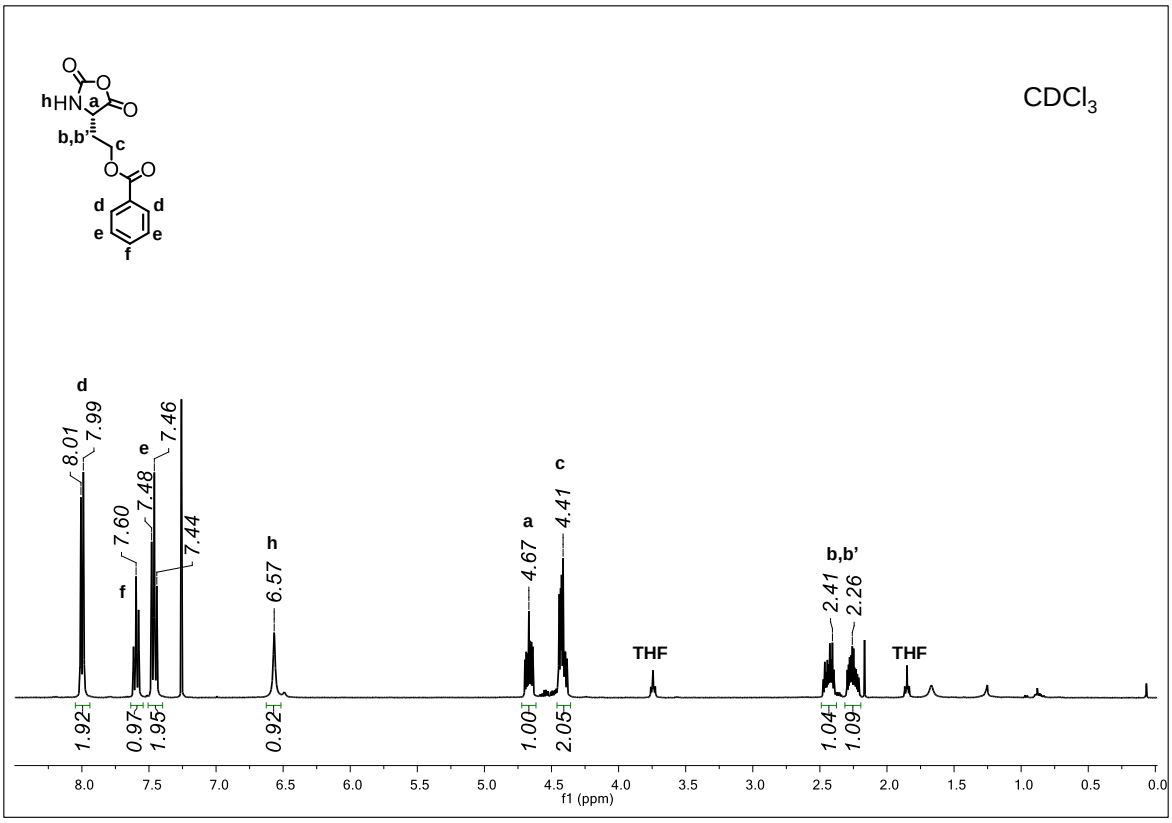
CDCl3
hHN a
b,b'
c
d
e
f
d 8.01
7.99
e 7.48
7.46
7.60
f
7.44
h 6.57
a 4.67
c 4.41
THF
b,b' 2.41
2.26
THF
1.92H
0.97H
1.95H
0.92H
1.00H
2.05H
1.04H
1.09H
f1 (ppm)

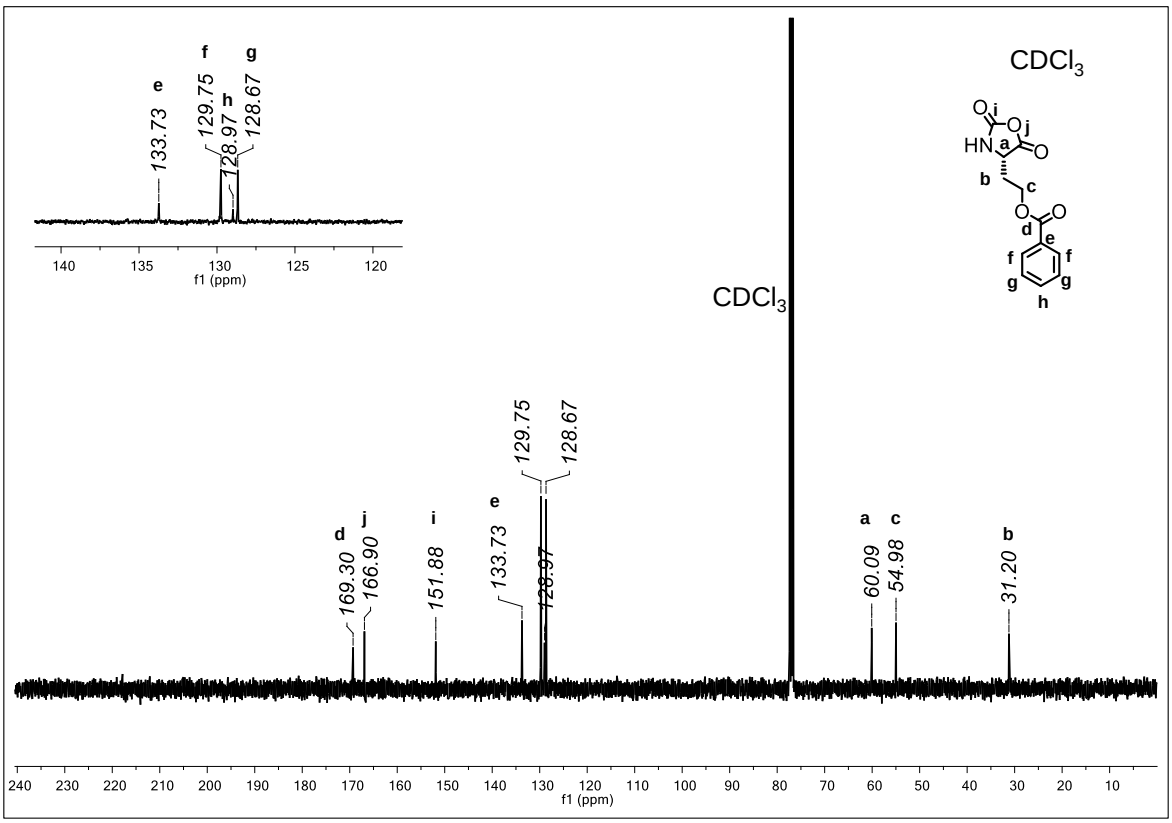
f g
e
h
133.73
129.75
128.97
128.67
f1 (ppm)
CDCl3
i j
HN a
b
c
d
e
f
g
h
CDCl3
129.75
128.67
d j i e
169.30
166.90
151.88
133.73
128.97
a c b
60.09
54.98
31.20
f1 (ppm)

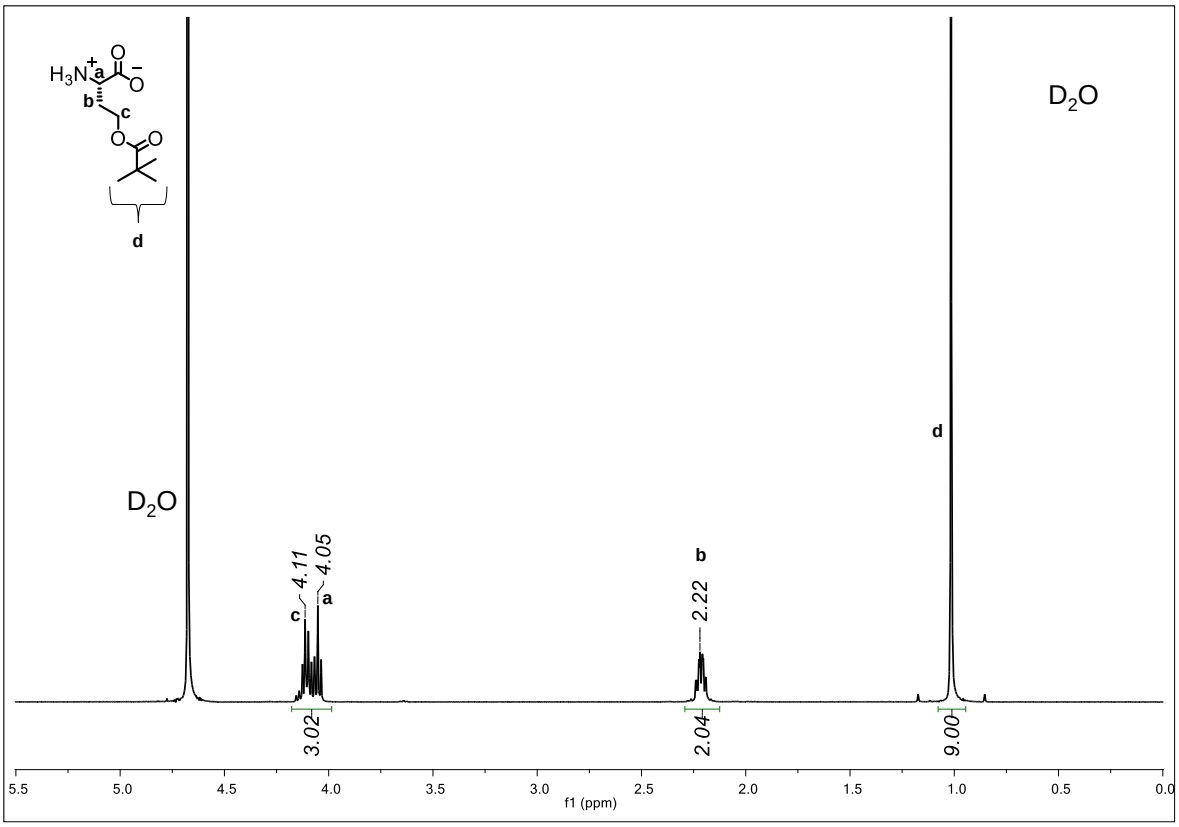
D2O
D2O
d
b
2.22
c
4.11
a
4.05
3.02
2.04
9.00
f1 (ppm)

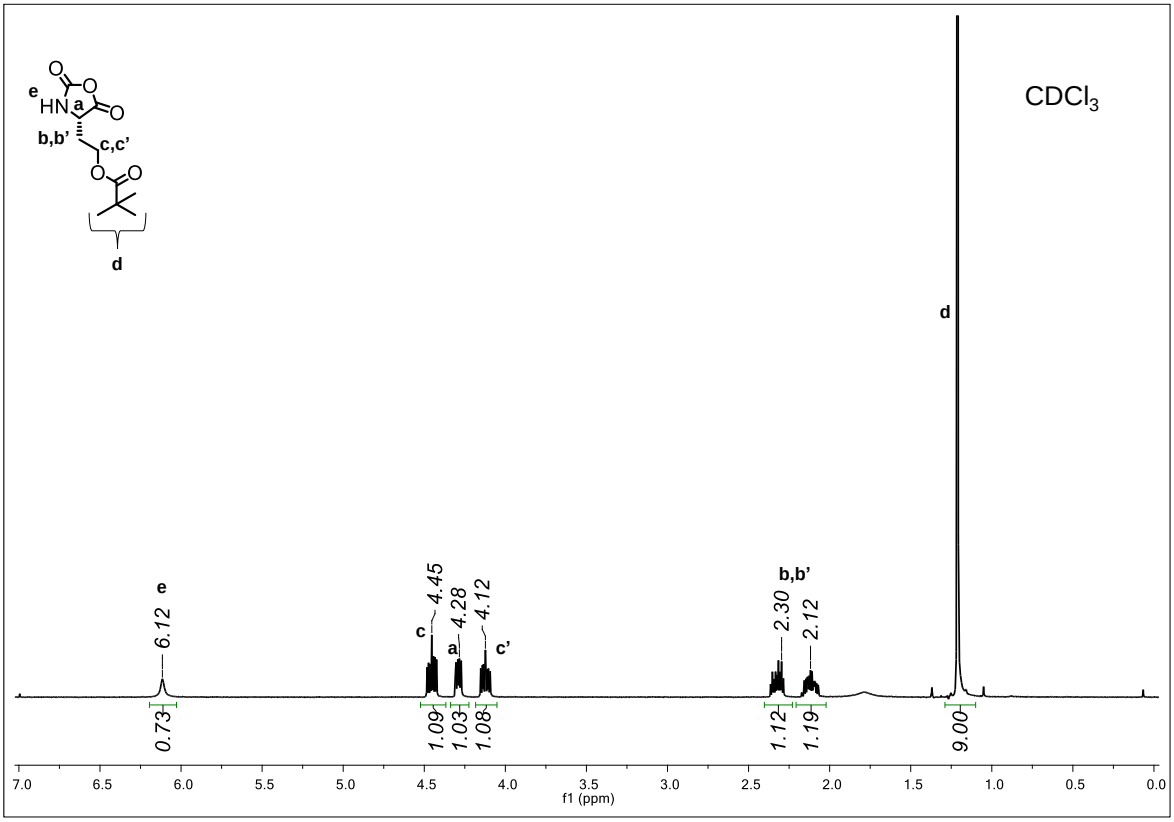
CDCl3
e
6.12
c
4.45
a
4.28
c'
4.12
b,b'
2.30
2.12
d
0.73
1.09
1.03
1.08
1.12
1.19
9.00
f1 (ppm)

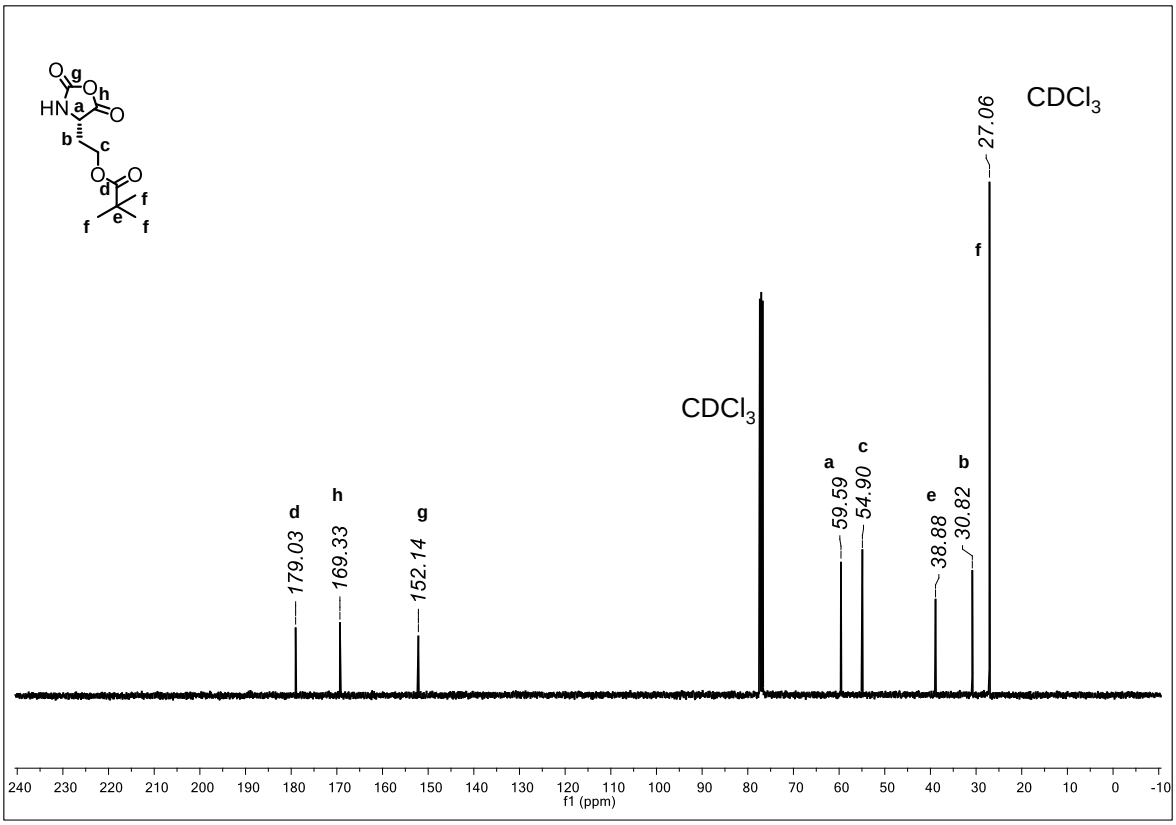
CDCl3
CDCl3
27.06
f
a
c
b
e
d
h
g
59.59
54.90
38.88
30.82
179.03
169.33
152.14
f1 (ppm)

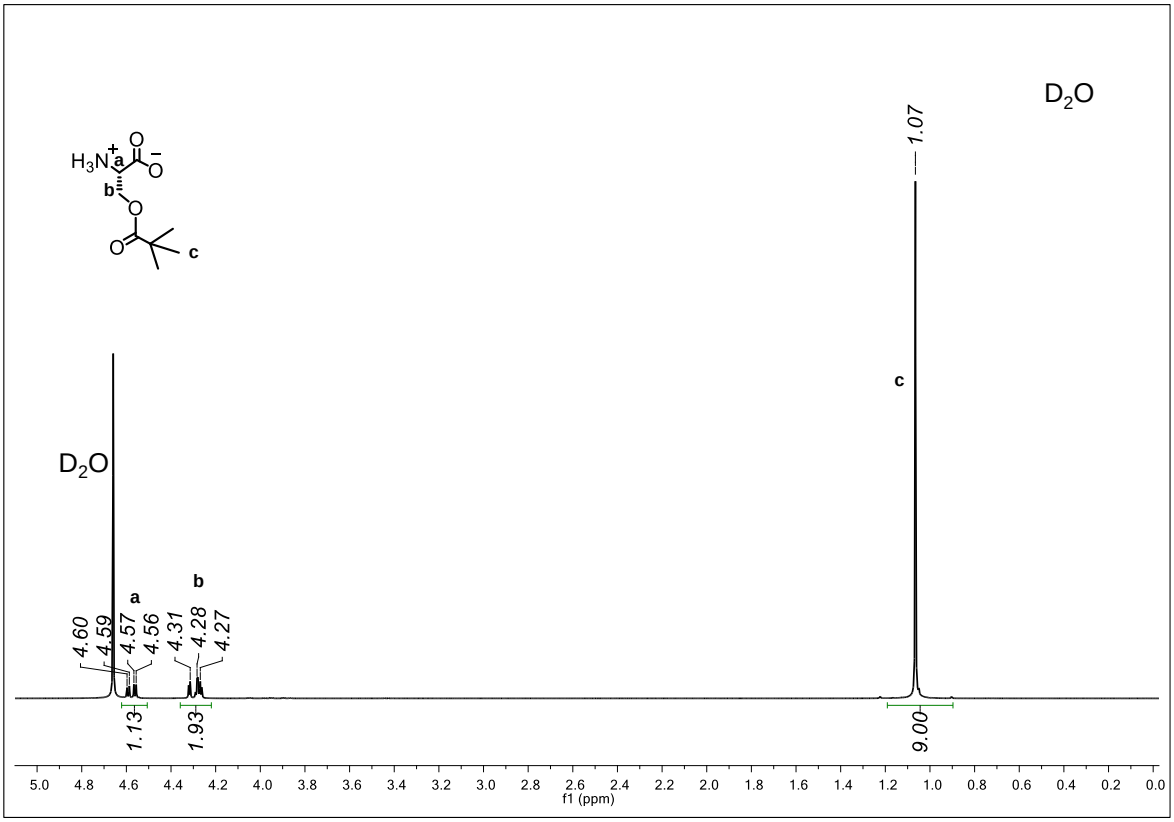
D2O
1.07
c
D2O
b
a
4.60
4.59
4.57
4.56
4.31
4.28
4.27
1.13
1.93
9.00
f1 (ppm)

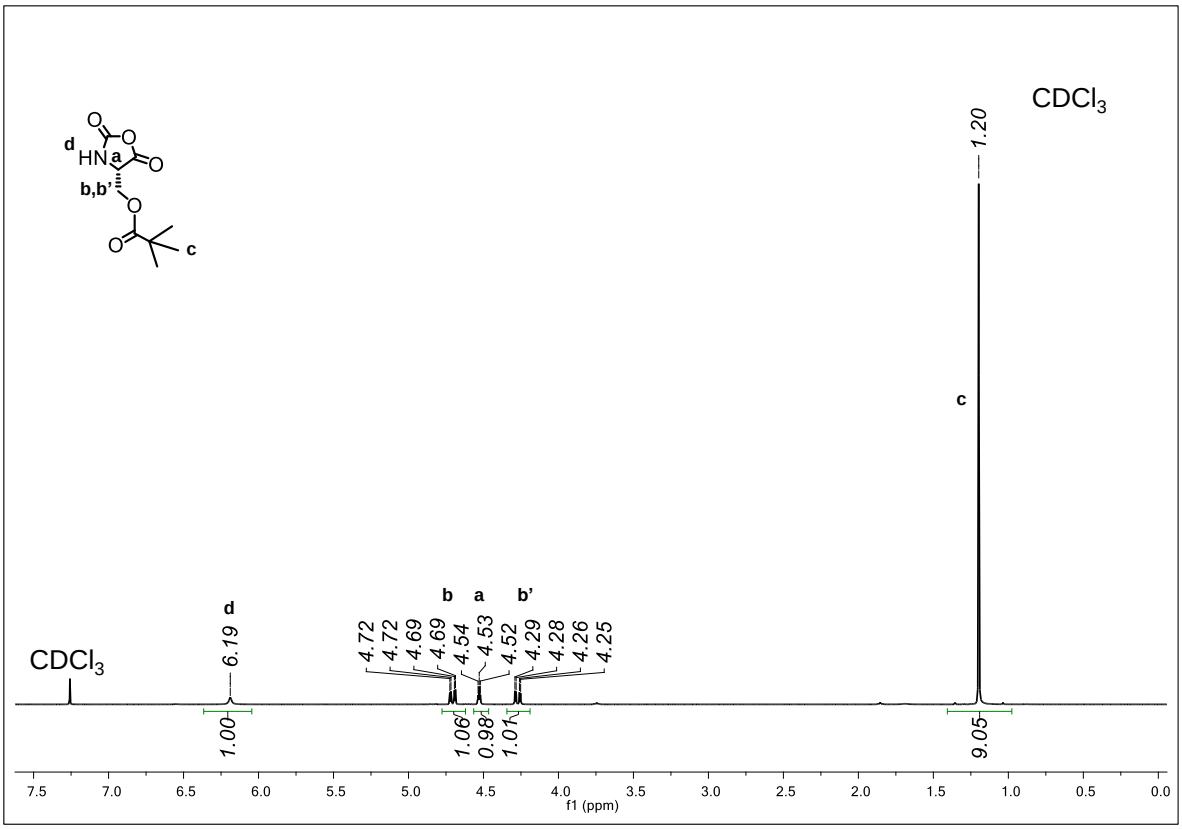
CDCl3
1.20
c
d
6.19
b a b'
4.72
4.72
4.69
4.69
4.54
4.53
4.52
4.29
4.28
4.26
4.25
CDCl3
1.00
1.06
0.98
1.01
9.05
7.5 7.0 6.5 6.0 5.5 5.0 4.5 4.0 3.5 3.0 2.5 2.0 1.5 1.0 0.5 0.0
f1 (ppm)

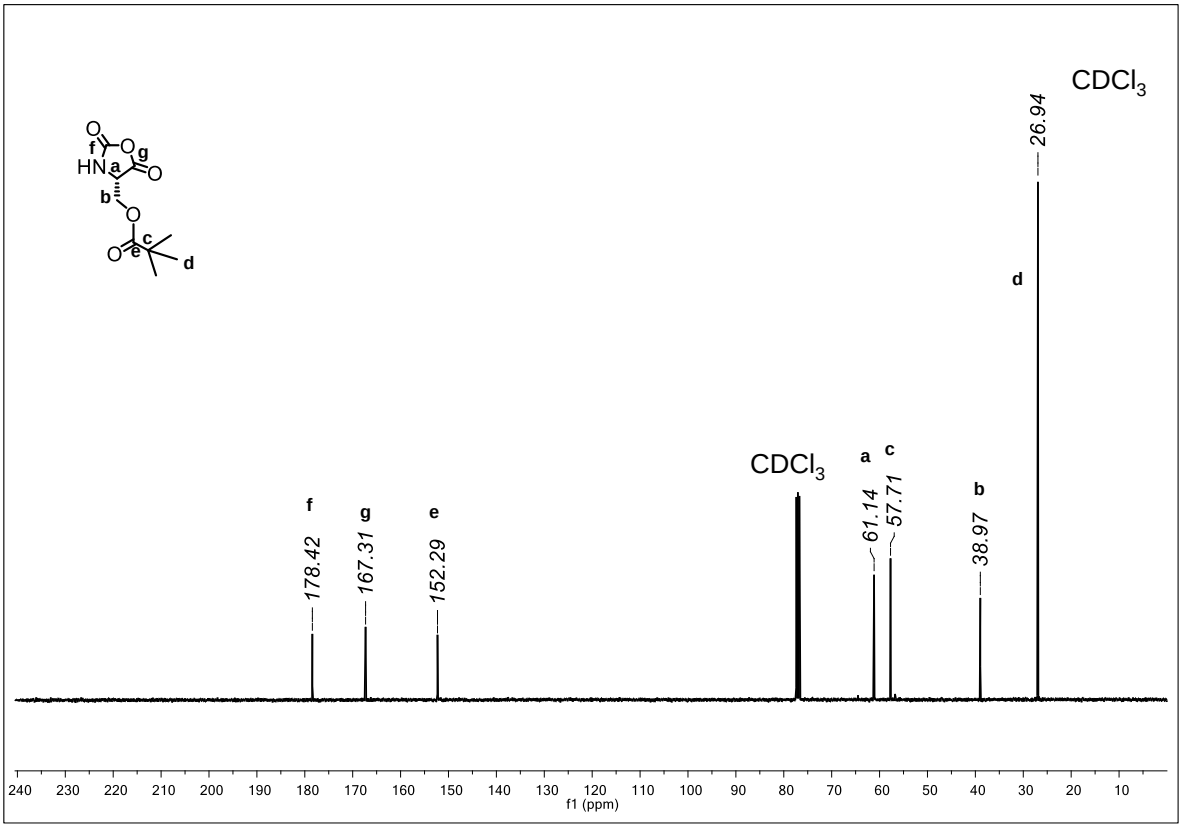
CDCl3
26.94
d
f
178.42
g
167.31
e
152.29
CDCl3
a
61.14
c
57.71
b
38.97
240 230 220 210 200 190 180 170 160 150 140 130 120 110 100 90 80 70 60 50 40 30 20 10
f1 (ppm)

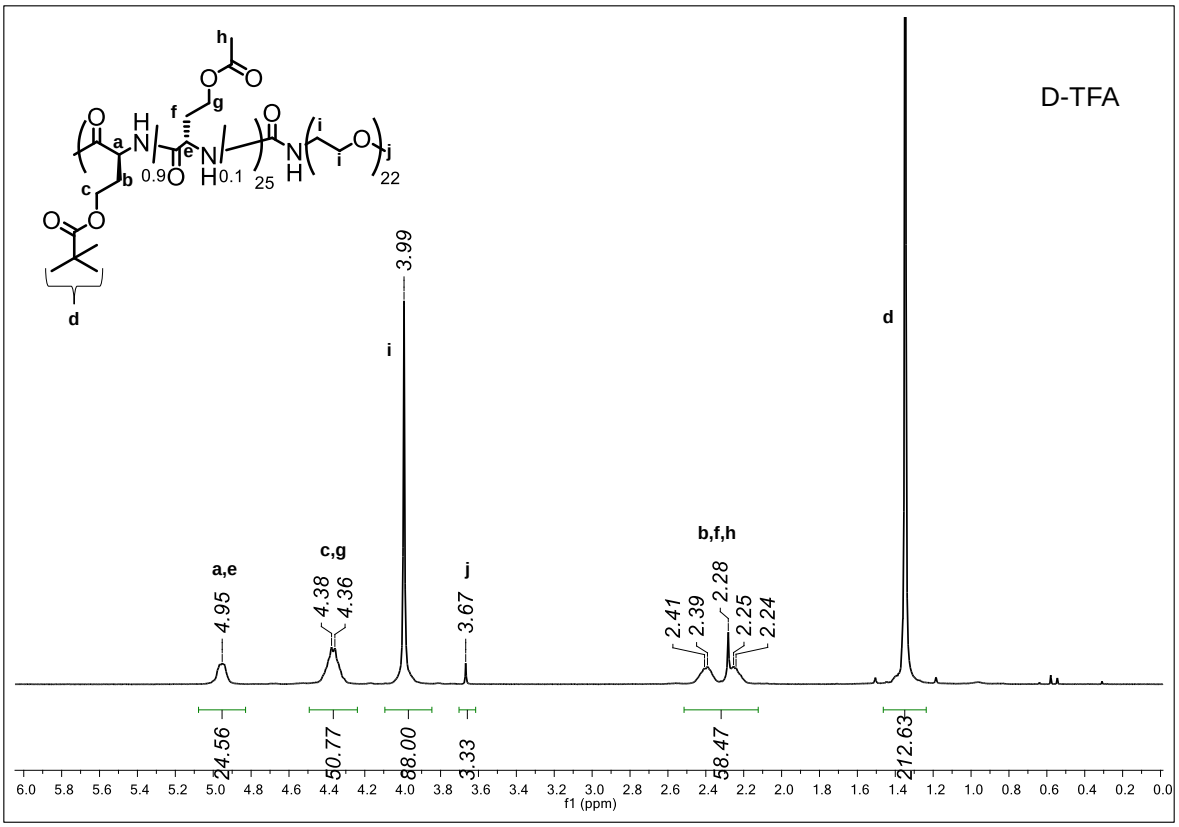
D-TFA
a,e
c,g
i
j
b,f,h
d
4.95
4.38
4.36
3.99
3.67
2.41
2.39
2.28
2.25
2.24
24.56
50.77
88.00
3.33
58.47
212.63
f1 (ppm)

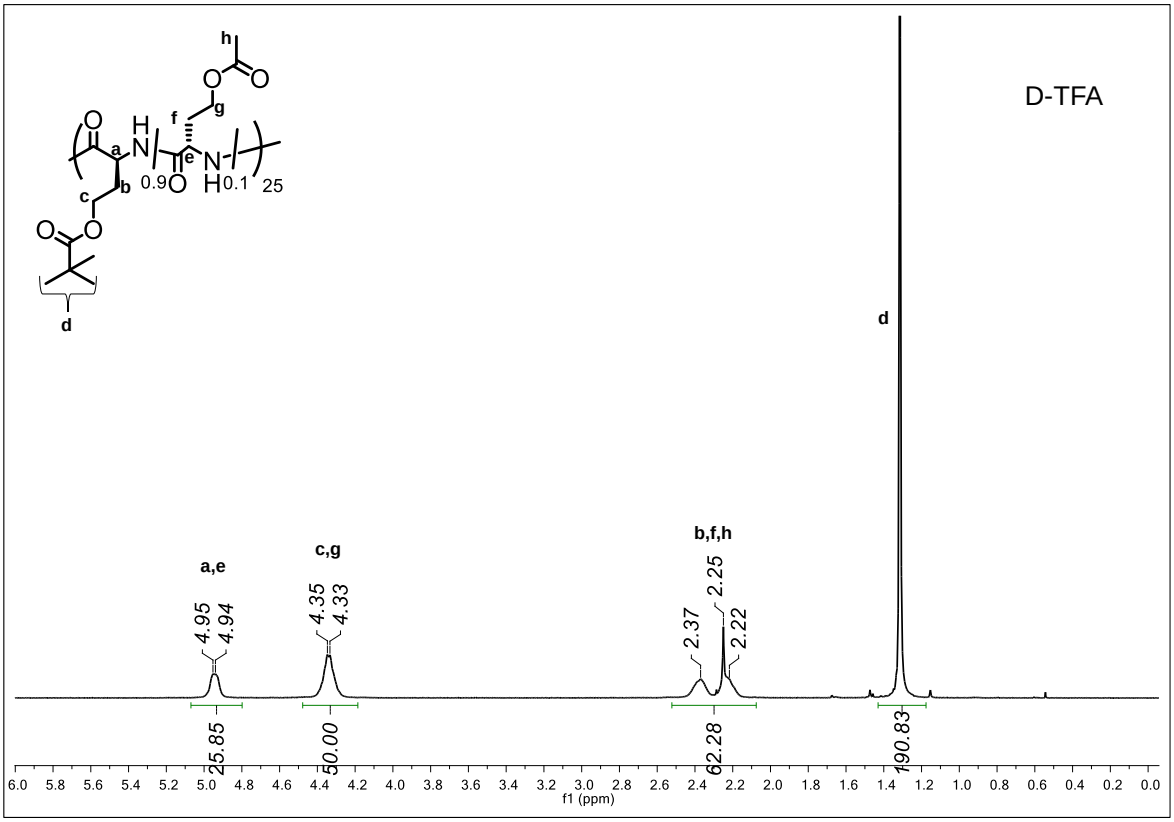
D-TFA
a,e
c,g
b,f,h
d
4.95
4.94
4.35
4.33
2.37
2.25
2.22
25.85
50.00
62.28
190.83
f1 (ppm)

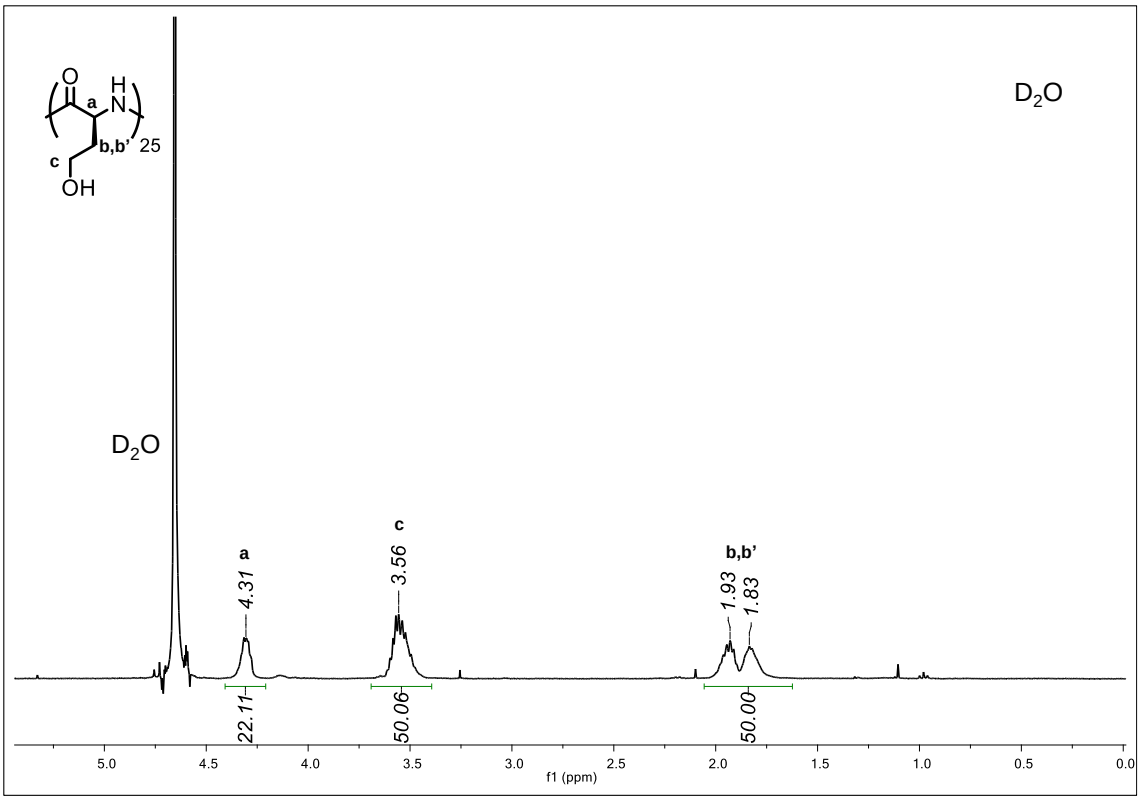
D2O
D2O
a
4.31
c
3.56
b,b'
1.93
1.83
22.11
50.06
50.00
f1 (ppm)

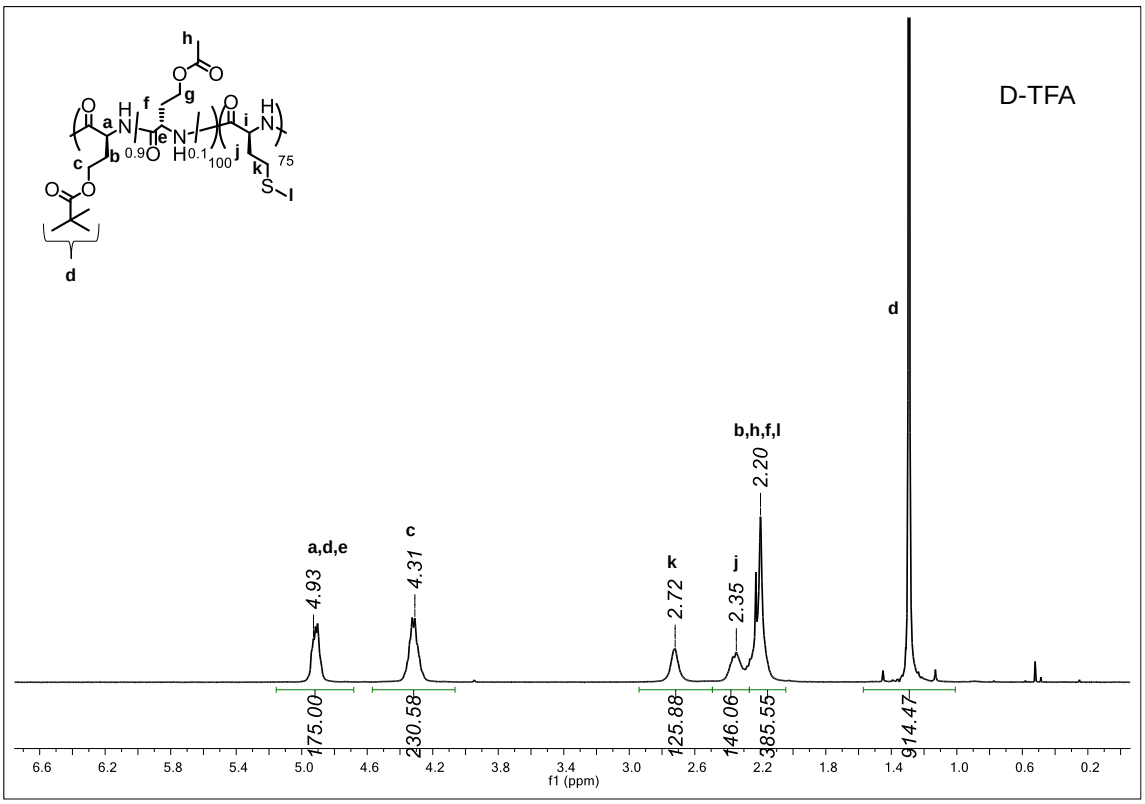
D-TFA
d
b,h,f,l
2.20
a,d,e
4.93
c
4.31
k
2.72
j
2.35
175.00
230.58
125.88
146.06
385.55
914.47
f1 (ppm)

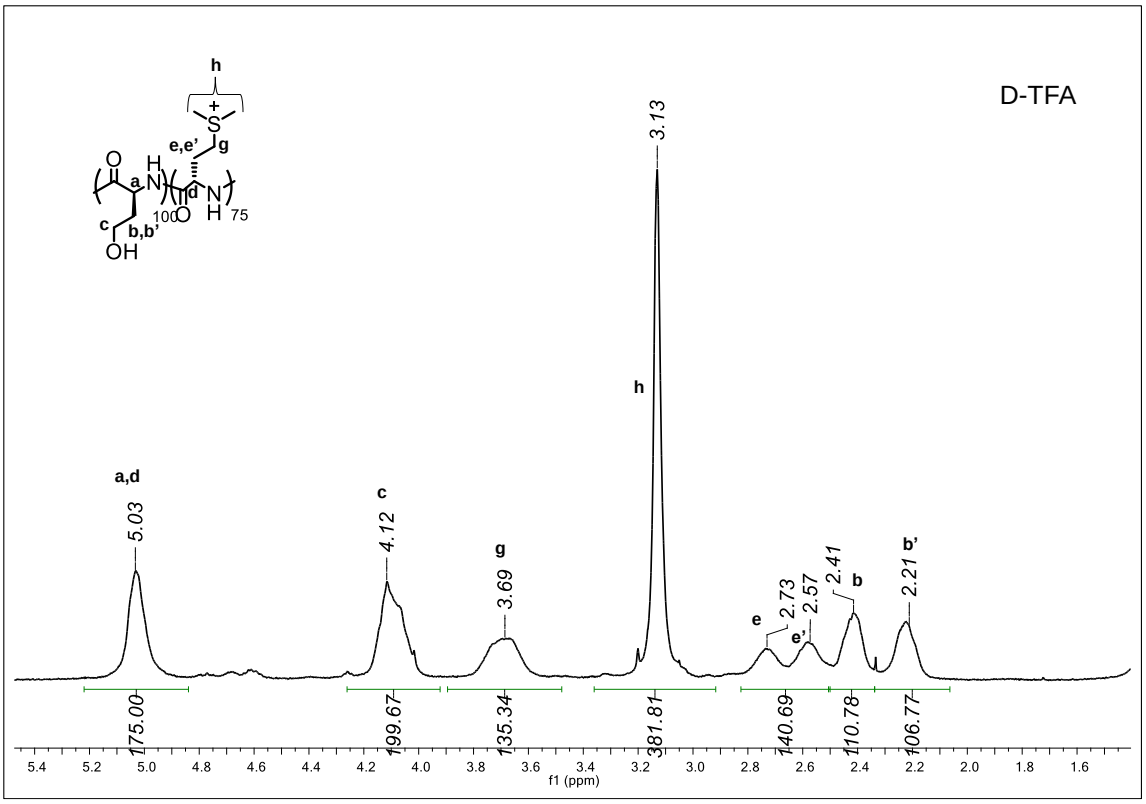
D-TFA
h
e,e'
g
a
d
c
b,b'
OH
100
75
3.13
h
a,d
5.03
c
4.12
g
3.69
e
2.73
e'
2.57
2.41
b
b'
2.21
175.00
199.67
135.34
381.81
140.69
110.78
106.77
f1 (ppm)

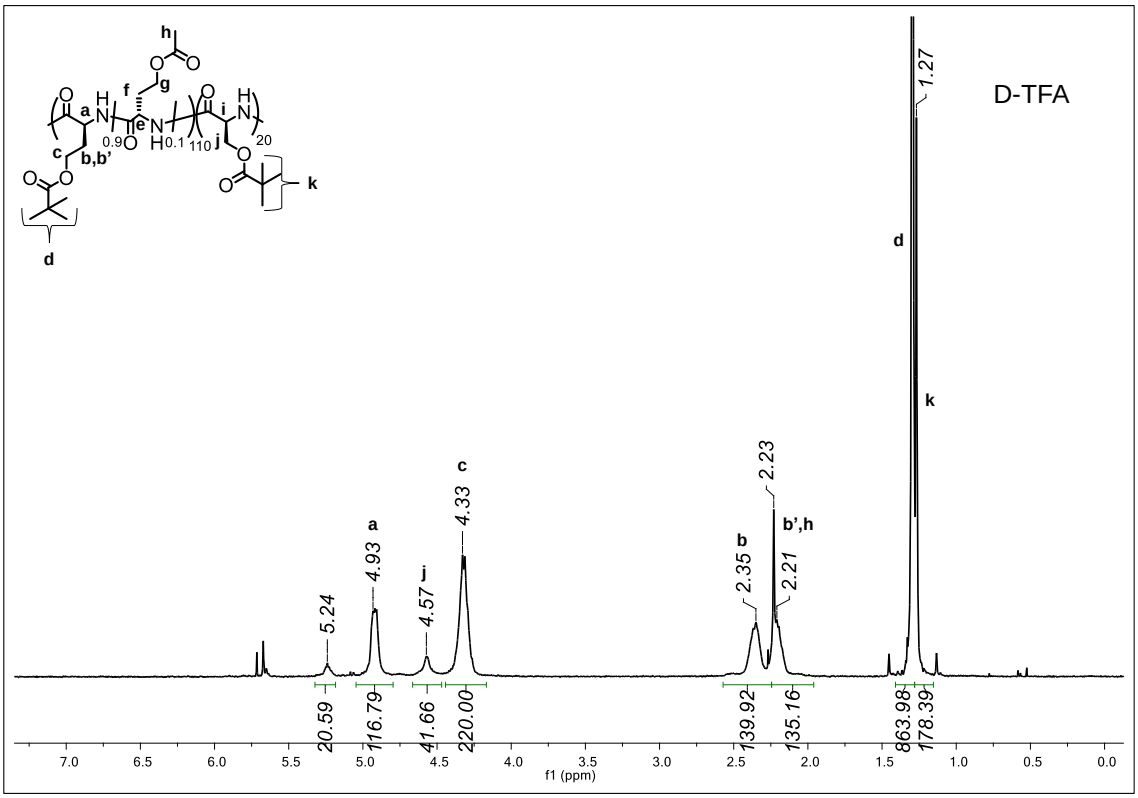
D-TFA
h
g
f
a
e
i
c
b,b'
0.9
0.1
110
j
20
k
d
1.27
d
k
c
4.33
a
4.93
5.24
j
4.57
2.23
b
2.35
b',h
2.21
20.59
116.79
41.66
220.00
139.92
135.16
863.98
178.39
f1 (ppm)

2.6 References

1. Love, R. J.; Jones, K. S. *J. Biomed. Mater. Res*. **2013,** *101A* (9), 2740-2752.

2. Peng, Z.; Shen, Y. *Polym. Plast. Techol. Eng*. **2011,** *50* (3), 245-250.

3. Viegas, T. X.; Fang, Z.; Yoon, K.; Weimer, R.; Dizman, B. 6 - Poly(oxazolines). In *Engineering of Biomaterials for Drug Delivery Systems*, Parambath, A., Ed. Woodhead Publishing: **2018**; pp 173-198.

4. Arciola, C. R.; Campoccia, D.; Montanaro, L. *Nat. Rev. Microbiol.* **2018,** *16* (7), 397-409.

5. Rudmann, D. G.; Alston, J. T.; Hanson, J. C.; Heidel, S. *Toxicol. Pathol.* **2013,** *41* (7), 970-983.

6. Bruusgaard-Mouritsen, M. A.; Johansen, J. D.; Garvey, L. H. *Clin. Exp. Allergy* **2021,** *51* (3), 463-470.

7. Sellaturay, P.; Nasser, S.; Islam, S.; Gurugama, P.; Ewan, P. W. *Clin Exp Allergy* **2021,** *51* (6), 861-863.

8. Jiang, Y.; Chen, Y.; Song, Z.; Tan, Z.; Cheng, J. *Adv. Drug Deliv. Rev.* **2021,** *170*, 261-280.

9. Song, Z.; Han, Z.; Lv, S.; Chen, C.; Chen, L.; Yin, L.; Cheng, J. *Chem. Soc. Rev.* **2017,** *46* (21), 6570-6599.

10. Lu, H.; Wang, J.; Song, Z.; Yin, L.; Zhang, Y.; Tang, H.; Tu, C.; Lin, Y.; Cheng, J. *Chem. Comm*. **2014,** *50* (2), 139-155.

11. Deng, C.; Zhang, Q.; Guo, J.; Zhao, X.; Zhong, Z. *Adv. Drug Deliv. Rev.* **2020**.

12. Deming, T. J. *Adv. Mater.* **1997,** *9* (4), 299-311.

13. Zhang, L.; Cao, Z.; Bai, T.; Carr, L.; Ella-Menye, J.-R.; Irvin, C.; Ratner, B. D.; Jiang, S. *Nat. Biotechnol.* **2013,** *31* (6), 553-556.

14. Bellomo, E. G.; Wyrsta, M. D.; Pakstis, L.; Pochan, D. J.; Deming, T. J. *Nat. Mater.* **2004,** *3* (4), 244-248.

15. Chen, C.; Wang, Z.; Li, Z. *Biomacromolecules* **2011,** *12* (8), 2859-2863.

16. Hwang, J.; Deming, T. J. *Biomacromolecules* **2001,** *2* (1), 17-21.

17. O'Shea, T. M.; Wollenberg, A. L.; Kim, J. H.; Ao, Y.; Deming, T. J.; Sofroniew, M. V. *Nat. Commun.* **2020,** *11* (1), 1-20.

18. Wollenberg, A.; O'shea, T.; Kim, J.; Czechanski, A.; Reinholdt, L. G.; Sofroniew, M.; Deming, T. *Biomaterials* **2018,** *178*, 527-545.

19. Rodriguez, A. R.; Kramer, J. R.; Deming, T. J. *Biomacromolecules* **2013,** *14* (10), 3610-3614.

20. Anderson, M. A.; O'Shea, T. M.; Burda, J. E.; Ao, Y.; Barlatey, S. L.; Bernstein, A. M.; Kim, J. H.; James, N. D.; Rogers, A.; Kato, B. *Nature* **2018,** *561* (7723), 396-400.

21. Bohak, Z.; Katchalski, E. *Biochem.* **1963,** *2* (2), 228-237.

22. Fasman, G.; Blout, E. *J. Am. Chem. Soc.* **1960,** *82* (9), 2262-2267.

23. Yang, Z.; Mao, Z.; Ling, J. *Polym. Chem.* **2016,** *7* (3), 519-522.

24. Sun, Y.; Liu, J.; Li, Z.; Wang, J.; Huang, Y. *ACS Appl. Mater. Interfaces* **2021,** *13* (16), 18454-18461.

25. Zhang, D.; Chen, Q.; Bi, Y.; Zhang, H.; Chen, M.; Wan, J.; Shi, C.; Zhang, W.; Zhang, J.; Qiao, Z.; Li, J.; Chen, S.; Liu, R. *Nat. Commun.* **2021,** *12* (1), 5327.

26. Zhang, D.; Chen, Q.; Zhang, W.; Liu, H.; Wan, J.; Qian, Y.; Li, B.; Tang, S.; Liu, Y.; Chen, S.; Liu, R. *Angew. Chem. Int. Ed.* **2020,** *59* (24), 9586-9593.

27. Frankel, M.; Cordova, S.; Breuer, M. *J. Chem. Soc.* **1953**, 1991-1994.

28. Miller, S. M.; Simon, R. J.; Ng, S.; Zuckermann, R. N.; Kerr, J. M.; Moos, W. H. *Drug Dev. Res.* **1995,** *35* (1), 20-32.

29. Yakovlev, I.; Deming, T. J. *J. Am. Chem. Soc.* **2015,** *137* (12), 4078-4081.

30. Schell, M. J.; Molliver, M. E.; Snyder, S. H. *PNAS* **1995,** *92* (9), 3948-3952.

31. Zhu, S.; Xue, R.; Yu, Z.; Zhang, X.; Luan, S.; Tang, H. *Biomacromolecules* **2021,** *22* (3), 1211-1219.

32. Perlin, P.; Gharakhanian, E. G.; Deming, T. J. *Chem. Comm*. **2018,** *54* (48), 6196-6199.

33. Song, Z.; Fu, H.; Wang, R.; Pacheco, L. A.; Wang, X.; Lin, Y.; Cheng, J. *Chem. Soc. Rev.* **2018,** *47* (19), 7401-7425.

34. Gharakhanian, E. G.; Bahrun, E.; Deming, T. J. *J. Amer. Chem. Soc.* **2019,** *141* (37), 14530-14533.

35. Zhang, Y.; Lu, H.; Lin, Y.; Cheng, J. *Macromolecules* **2011,** *44* (17), 6641-6644.

36. Zhang, R.; Zheng, N.; Song, Z.; Yin, L.; Cheng, J. *Biomaterials* **2014,** *35* (10), 3443-3454.

37. Hayakawa, T.; Kondo, Y.; Kobayashi, N. *Polym. J.* **1975,** *7* (5), 538-543.

38. Muhl, C.; Schäfer, O.; Bauer, T.; Räder, H.-J.; Barz, M. *Macromolecules* **2018,** *51* (20), 8188-8196.

39. Schäfer, O.; Huesmann, D.; Barz, M. *Macromolecules* **2016,** *49* (21), 8146-8153.

40. Fasman, G. D., Poly-[alpha]-amino acids; protein models for conformational studies. M. Dekker: New York, 1967.

41. Goodman, M.; Felix, A. M. *Biochem.* **1964,** *3*, 1529-1534.

42. Parrish, J. R., Jr.; Blout, E. R. *Biopolymers* **1971,** *10* (9), 1491-1512.

43. Elliott, A.; Wilson, A. H. *Proc. R. Soc. A: Math. Phys. Eng. Sci*. **1954,** *221* (1144), 104-114.

44. Guinn, R. M.; Margot, A. O.; Taylor, J. R.; Schumacher, M.; Clark, D. S.; Blanch, H. W. *Biopolymers* **1995,** *35* (5), 503-512.

45. Ahmed, A.; Tajmir-Riahi, H. A.; Carpentier, R. *FEBS Letters* **1995,** *363* (1), 65-68.

46. Brzezinska, K. R.; Curtin, S. A.; Deming, T. J. *Macromolecules* **2002,** *35* (8), 2970-2976.

47. Kramer, J. R.; Deming, T. J. *Biomacromolecules* **2010,** *11* (12), 3668-3672.

48. Deming, T. J. *Macromolecules* **1999,** *32* (13), 4500-4502.

49. Drauz, K.; Knaup, G.; Schwarm, M. Process for the preparation of 3-amino-2-oxo-pyrrolidines, novel intermediates and their use. **1998**, US6492541B2.

50. Previero, A.; Barry, L. G.; Coletti-Previero, M. A. *Biochim. Biophys. Acta Proteins Proteom.* **1972,** *263* (1), 7-13.

Chapter 3: Poly(dehydroalanine): Synthesis, Properties, and Functional Diversification of a Fluorescent Polypeptide†

† Experimental work was performed with equal contributions by Isaac Benavides and Dr. Eric Raftery. Computational studies for this project were performed by Alex Bell and Declan Evans.

Reprinted (adapted) with permission from Benavides, I.; Raftery, E.D.; Bell, A.G.; Evans, D.; Scott, W.A.; Houk, K.N.; Deming, T.J. *J. Am. Chem. Soc.* **2022**, *144* (9), 4214-4223.

3.1 Abstract

Via the design of a new, soluble poly(S-alkyl-L-cysteine) precursor, a route was developed for successful preparation of long chain poly(dehydroalanine), $\mathbf{A^{DH}}$, as well as the incorporation of dehydroalanine residues and $\mathbf{A^{DH}}$ segments into copolypeptides. Based on experimental and computational data, $\mathbf{A^{DH}}$ was found to adopt a previously unobserved 'hybrid coil' structure, which combines elements of 2_5-helical and 3_{10}-helical conformations. Analysis of the spectroscopic properties of $\mathbf{A^{DH}}$ revealed that it possesses strong inherent blue fluorescence, which may be amenable for use in imaging applications. $\mathbf{A^{DH}}$ also contains reactive electrophilic groups that allowed its efficient modification to functionalized polypeptides after reaction under mild conditions with thiol and amine nucleophiles. The combined structural, spectroscopic, and reactivity properties of $\mathbf{A^{DH}}$ make it a unique reactive and fluorescent polypeptide component for utilization in self-assembled biomaterials.

3.2 Introduction

Dehydroalanine (Dha) is an unsaturated amino acid that occurs naturally as a post-translational modification in peptides,[1,2] where it imparts unique conformational properties and electrophilic reactivity. Due to α,β-unsaturation, Dha residues prefer a planar conformation, which can induce inverse γ-turns in peptides.[3] In one study, peptides containing 3 to 6 consecutive Dha residues were found to adopt extended 2_5-helical conformations, where each chain possesses a striking, essentially flat conformation due to ϕ and ψ angles being *ca*. 180° for each residue.[4] Dha residues are

also potent electrophiles that react readily with thiol and amine nucleophiles.[5-8] Such reactions occur in the biosynthesis of cyclic peptide lantibiotics,[9] and have also been utilized as a strategy for site-specific functionalization of Dha residues in peptides and proteins.[10] In spite of the attractive conformation directing and reactivity properties of Dha, there has been no successful synthesis of long, repeating Dha sequences, i.e. poly(dehydroalanine), $\mathbf{A^{DH}}$.

The incorporation of multiple Dha residues into short peptides has been accomplished in a variety of examples.[11-14] The most significant were the flat peptides reported by Toniolo, where tri- through hexa-Dha peptides were synthesized and characterized.[4] In nearly all Dha containing peptides, the Dha residues were not incorporated during peptide synthesis, but were introduced post-synthesis by conversion of amino acid precursors into Dha residues.[1,2,11-14] This strategy, which mimics the biosynthesis of Dha from serine residues, is advantageous since it avoids the low nucleophilicity and instability of N-terminal enamine groups in Dha that hinder efficient peptide coupling (*vide infra*).[1,2] To date, hexa-Dha is the longest repeat of Dha residues that has been reported.[4] In the 1950s, Sakakibara attempted to prepare long chain $\mathbf{A^{DH}}$ via the direct ring-opening polymerization of Dha N-carboxyanhydride, Dha NCA (Fig. 3.1).[15.16] These reactions, utilizing primary amine or strong base initiators, gave low conversions (< 35%) of monomer, possibly due to both low reactivity of monomer and enamine chain-ends, and gave polymers that contained < 10 mol% of Dha residues. Further studies by Sakakibara revealed that a dominant reaction pathway was radical addition polymerization across the alkene bonds in Dha, either in monomer

or polymer, resulting in loss of unsaturation (Fig. 3.1).[15-17] Direct synthesis of **A^{DH}** via NCA polymerization was found to be unsuccessful.

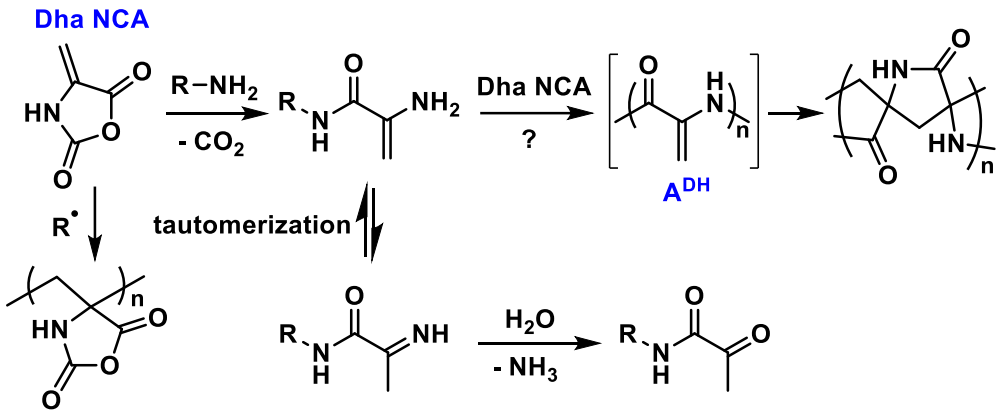

Figure 3.1. Reactions previously reported for dehydroalanine N-carboxyanhydride (Dha NCA).[15-17] Brackets indicate that product was not isolated. **A^{DH}** = poly(dehydroalanine).

A^{DH} is a desirable biopolymer since it should adopt a chain conformation different from most other polypeptides (e.g. α-helices and β-sheets),[4,18,19] and this difference may lead to unique physical properties and assembled structures. **A^{DH}** would also be a potentially valuable precursor to functional polypeptides via post-polymerization reactions with various nucleophiles.[10-14] Here, we have circumvented longstanding challenges in the synthesis of long chain **A^{DH}** by design of a readily prepared and soluble polypeptide precursor that can be efficiently modified to give **A^{DH}** of controlled length. The preparation of Dha containing block and statistical copolymers was also demonstrated using this approach. The Dha residues in these homo and copolypeptides were found to be efficiently derivatized by reaction with amine and thiol nucleophiles under mild conditions to yield the corresponding functionalized residues. Further, **A^{DH}** was found to adopt a previously unobserved “hybrid coil” structure in both solvents and in the solid-state, and **A^{DH}** chains were also found to exhibit inherent blue fluorescence.

The controlled synthesis of **A^{DH}** containing polypeptides and the unique properties of **A^{DH}** reported here are a promising combination for downstream development of reactive and 'label-free' fluorescent polypeptide materials.

3.3 Results and discussion

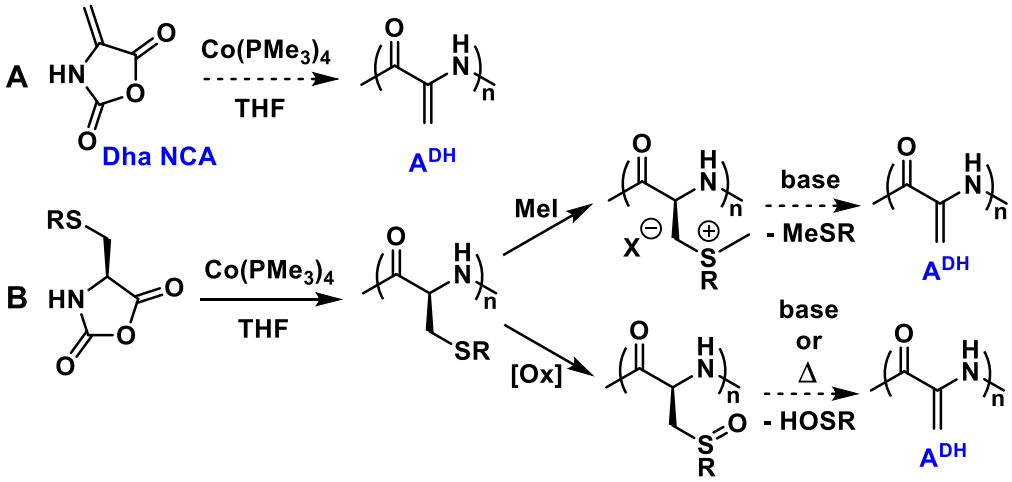

Figure 3.2. Potential synthetic routes to poly(dehydroalanine), **A^{DH}**. A) Direct polymerization of Dha NCA. B) Preparation of a poly(S-alkyl-L-cysteine) precursor followed by thioether alkylation or oxidation and subsequent base catalyzed or thermal elimination. R = alkyl group.

Since there have been considerable improvements in NCA polymerization methodology[20] since Sakakibara's work in the 1950s, we first sought to re-evaluate the polymerization of Dha NCA to determine if preparation of **A^{DH}** via this route was feasible (Fig. 3.2). Using a monomer to initiator ratio of 30 to 1, and either THF or DMF as solvent, polymerizations of Dha NCA were initiated using either $nBuNH_2$ or $Co(PMe_3)_4$ initiator[21] under air-free and anhydrous conditions at 20 °C. In all four polymerizations, Dha NCA consumption was sluggish as compared to other NCA monomers, and only small fractions of monomer were consumed after 24h. Reaction mixtures were diluted with water, and

after observation of no precipitates the samples were dialyzed against water to remove small molecules followed by lyophilization. Oligomeric products were then obtained as off-white solids in poor yields (11 to 16% for *n*$BuNH_2$, and 27 to 42% for $Co(PMe_3)_4$). Notably, only the product from *n*$BuNH_2$ initiation in DMF showed resonances in ^{1}H NMR assignable as alkene protons, and all products contained resonances consistent with aliphatic protons that should not be present in $\mathbf{A^{DH}}$ (Fig. 3.3). Overall, in agreement with Sakakibara's findings,[15-17] and the known poor reactivity and stability issues of enamine groups in Dha (Fig. 3.1),[1,2] our results confirmed that direct formation of $\mathbf{A^{DH}}$ via polymerization of Dha NCA was not feasible.

Consequently, we sought to develop an alternative route to $\mathbf{A^{DH}}$ based on a precursor polypeptide (Fig. 3.2b), similar to methods used to introduce Dha residues into peptides and proteins.[1,2,11-14,22-30] As shown in Fig. 3.4, many routes have been utilized to convert amino acid precursors into Dha residues in peptides and proteins. The most economical of these strategies rely on precursors based on natural cysteine or serine residues. While the methods in Scheme 3 work well for peptides and proteins, these molecules either contain few Dha residues or consist of short chains such that the solubility of the molecules is not compromised by incorporation of either precursor or Dha residues.[1,2,4,11-14] With polypeptides, a major challenge in development of a $\mathbf{A^{DH}}$ precursor is that nearly all derivatives of long chain poly(L-cysteine) or poly(L-serine) adopt stable β-sheet conformations, and consequently have low solubility in most solvents.[31] The poor solubility of these polypeptides prohibits controlled synthesis of high molecular weight chains, and can hinder their conversion to $\mathbf{A^{DH}}$.

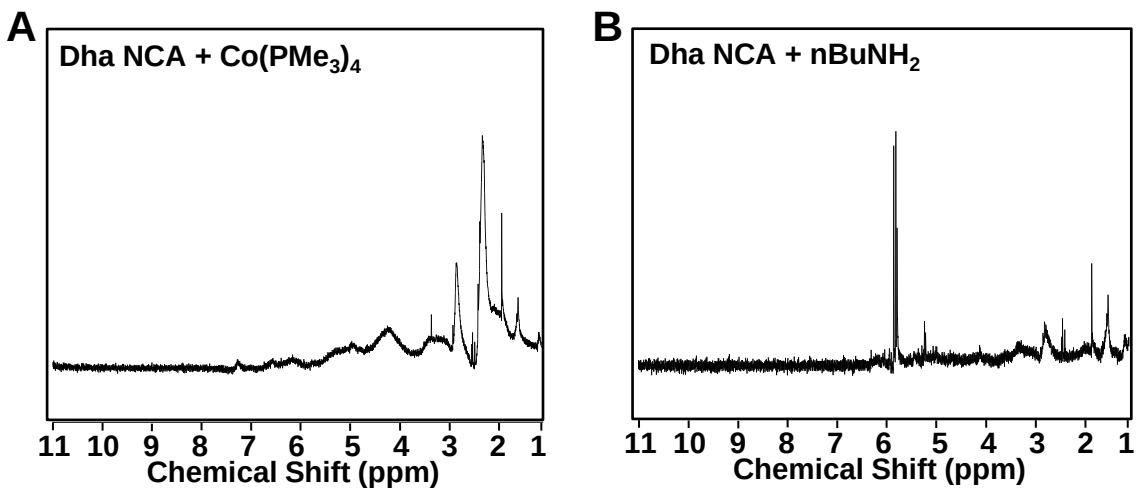

Figure 3.3. ^{1}H NMR spectra of products isolated from attempted Dha NCA polymerizations at 30:1 monomer to initiator ratios. A) Attempted polymerization of Dha NCA using $Co(Pme_3)_4$ in DMF. B) Attempted polymerization of Dha NCA using n-butyl amine in DMF. Polymerizations were performed in anhydrous DMF under N_2 atmosphere at 20 ^{o}C. ^{1}H NMR samples were prepared in D-TFA.

To address this challenge, we needed to develop a viable precursor to $\mathbf{A^{DH}}$ that possesses good solubility in solvents used for NCA polymerization to allow for controlled chain growth. Guided by prior observations, our efforts focused on derivatives of poly(L-cysteine). While most poly(L-cysteine) derivatives form poorly soluble β-sheets, e.g. protected poly(S-carboxyalkylcysteines),[32-36] protected poly(S-aminoalky-lcysteines),[39-43] and poly(S-alkyl-cysteines) we noted two examples had been reported that instead favor the soluble α-helical conformation. The first was poly(S-(L-menthyloxycarbonylmethyl)-L-cysteine),[44] and the second was a series of acetyl protected, monosaccharide functionalized poly(S-alkyl-L-cysteines) reported by our group.[45] Due to their lack of interchain H-bonding that would occur in β-sheet conformations,[31] these α-helical poly(L-cysteine) derivatives were found to possess

good solubility in organic solvents useful for NCA polymerization (e.g. THF), which allows preparation of high molecular weight chains.

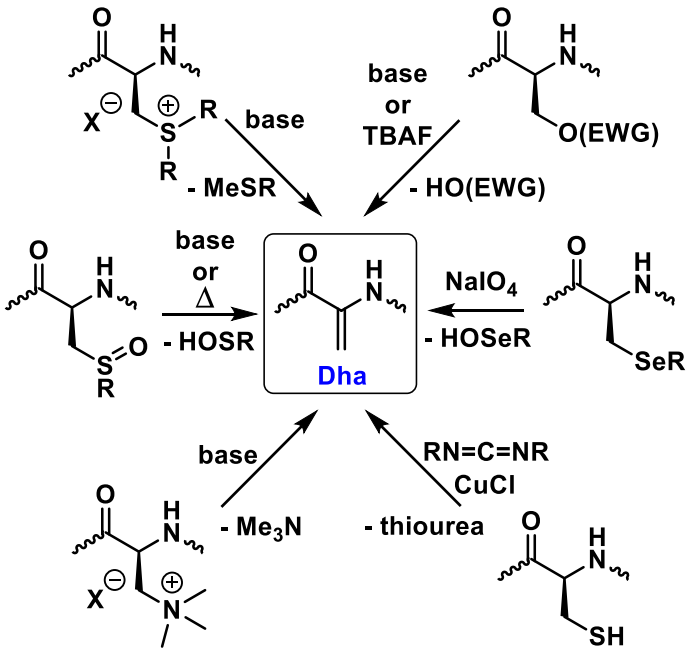

Figure 3.4 Common synthetic routes to Dha residues in peptides and proteins.[1,2,11-14,22-30] EWG = -Tosyl, -C(O)OR, or -PO_3^{2-}.

We observed that a common feature of these α-helical poly(L-cysteine) derivatives was the presence of sterically demanding groups (i.e. menthyl and tetra-acetyl monosaccharide) at the ends of the side chains, which may be responsible for their conformational preference. This observation led to a design concept for a simplified α-helical poly(L-cysteine) derivative to serve as an efficient precursor to **A**^{DH}. While poly(S-(benzyloxycarbonylmethyl)-L-cysteine) is well-known to adopt stable β-sheet conformations that precipitate or gel during polymerization,[32-34] we hypothesized that replacement of the benzyl groups with groups that were more sterically demanding could give α -helical polypeptides that would be soluble to high degrees of polymerization.[45] Further, although the hindered ester in poly(S-(L-menthyloxycarbonylmethyl)-L-cysteine) is difficult to hydrolyze, other alkoxycarbonyl

protecting groups may be more readily removed to give poly(S-carboxymethyl-L-cysteine), **C^{CM}**, which is water soluble when the carboxylates are deprotonated at pH > 4.[46-48] A water-soluble poly(S-carboxyalkyl-L-cysteine) precursor is desirable since both sulfonium and sulfoxide routes for its conversion to **A^{DH}** could be conducted under mild conditions in aqueous media (Fig. 3.4).[9,11,14,24,25,49] Hence, we designed and prepared a new L-cysteine based polypeptide, poly(S-(*tert*-butoxycarbonylmethyl)-L-cysteine), **C^{BCM}**, containing the sterically demanding *tert*-butyl group to both favor a helical conformation and allow facile deprotection.

L-Cysteine was converted to S-(*tert*-butoxycarbonylmethyl)-L-cysteine using standard procedures[50] and this amino acid was then converted to the corresponding N-carboxyanhydride under conditions that avoid the formation of HCl so that the *tert*-butyl esters remained intact (Fig. 3.5).[51] The purified S-(*tert*-butoxycarbonylmethyl)-L-cysteine NCA, *t*BuCM-Cys NCA, was then found to readily polymerize using $Co(PMe_3)_4$ in THF at 20 °C,[21] giving **C^{BCM}** that remained soluble in the reaction mixture. Chain lengths of **C^{BCM}** were readily controlled by variation of monomer to initiator ratio (Fig. 3.7a), and molecular weight distributions remained narrow and monomodal (Fig. 3.8a,b). Further, block and statistical copolypeptides of *t*BuCM-Cys NCA with a model co-monomer *tert*-butyl-L-glutamate NCA, *t*Bu-Glu NCA, were readily prepared (Fig. 3.6; Fig. 3.7; Fig. 3.8 a,b; Fig. 3.9; Fig. 3.10; Table 3.1; Table 3.2), which altogether confirmed the ability of *t*BuCM-Cys NCA to undergo living polymerization. Thus, it appeared that our design of **C^{BCM}** was successful in preventing formation of β-sheet conformations. Additional structure data was obtained from FTIR and circular dichroism studies on **C^{BCM}** (Fig. 3.8c,d), which are consistent with this polypeptide adopting an extended helical chain

conformation since these data are similar to those observed for the extended conformation of poly(α-GalNAc-L-serine).[52]

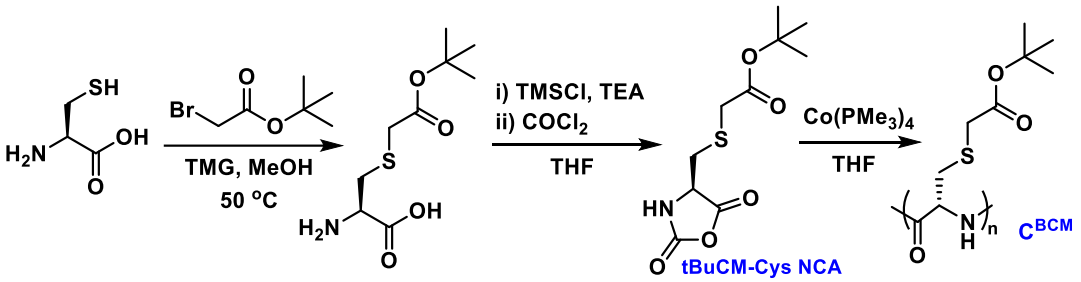

Figure 3.5 Preparation of S-(tert-butoxycarbonylmethyl)-L-cysteine N-carboxyanhydride, tBuCM-Cys NCA, and poly(S-(tert-butoxycarbonylmethyl)-L-cysteine), $\mathbf{C}^{\mathbf{BCM}}$.

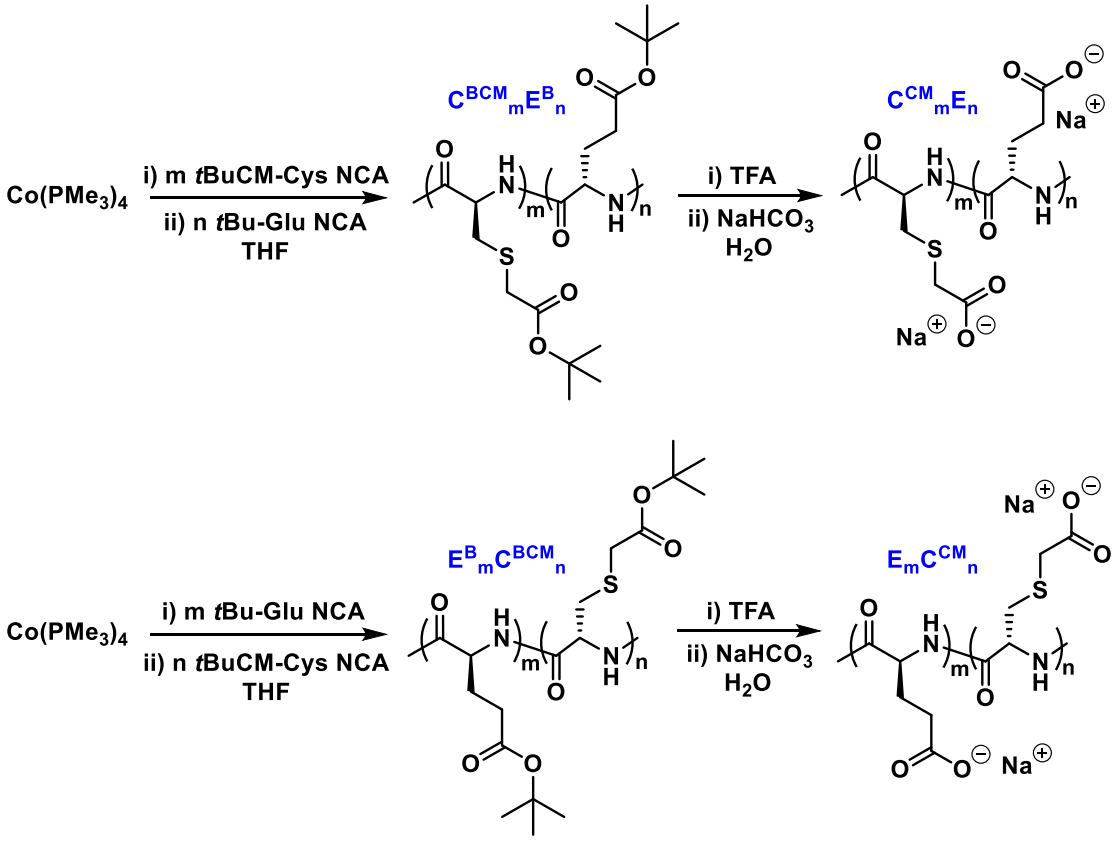

Figure 3.6. Preparation of block copolypeptides of opposite sequence using tBuCM-Cys and tBu-Glu NCAs via stepwise $Co(PMe_3)_4$ mediated polymerization in THF at 20 °C.

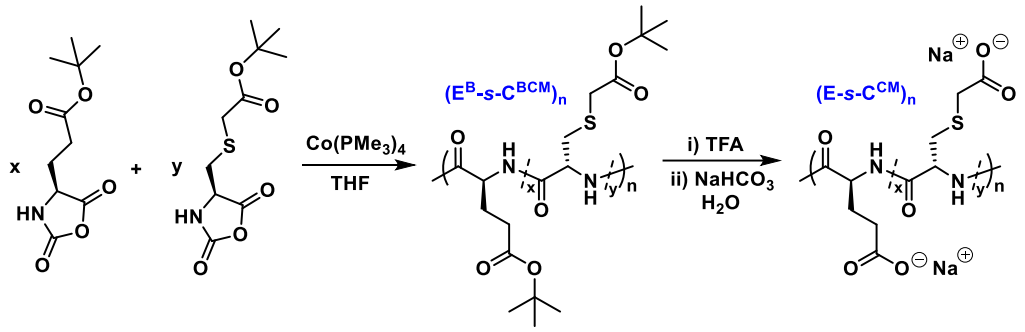

Figure 3.7. Preparation of statistical copolypeptides via combination of tBuCM-Cys and tBu-Glu NCAs and subsequent copolymerization using $Co(PMe^3)_4$ initiator in THF at 20 °C.

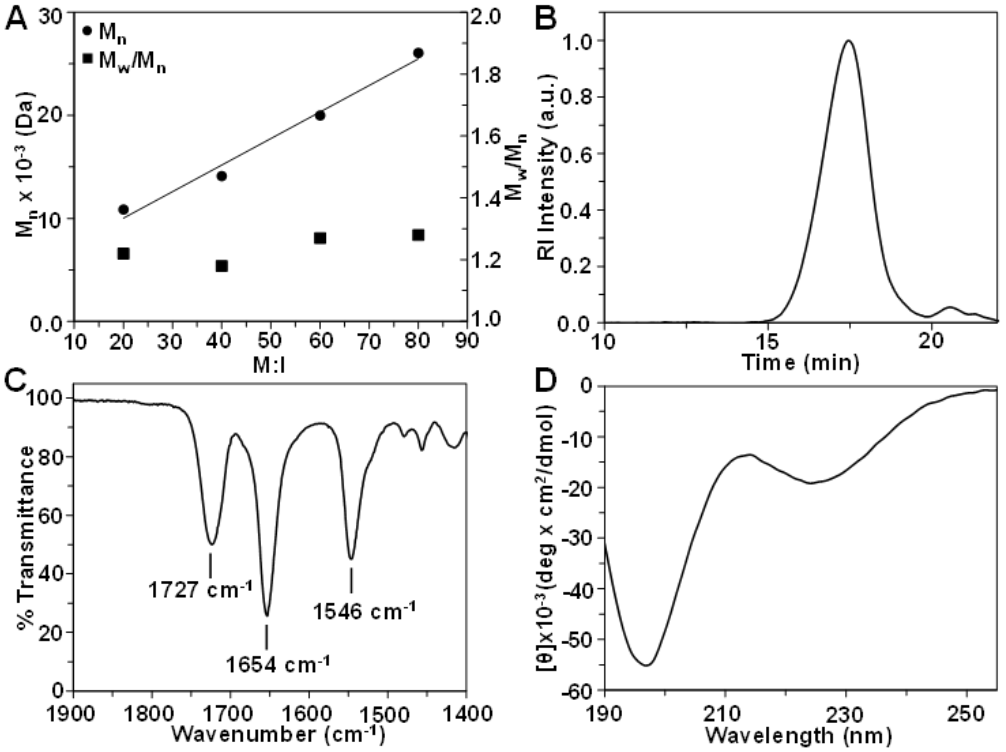

Figure 3.8. Properties of $\mathbf{C^{BCM}_{77}}$. a) Variation in molecular weight (M_n, determined by ^1H NMR) and dispersity (M_w/M_n, determined by GPC) of $\mathbf{C^{BCM}}$ as a function of monomer to initiator ratio (M:I) using $Co(PMe_3)_4$ mediated polymerization. b) GPC trace of $\mathbf{C^{BCM}_{77}}$ in HFIP containing 0.5% (w/w) KTFA. c) Solid State FTIR spectrum of the amide region for $\mathbf{C^{BCM}_{77}}$. The Amide I and II bands at 1654 and 1546 cm^{-1} are characteristic of a helical or disordered conformation. The band at 1727 cm^{-1} is the carbonyl stretch of *tert*-butyl ester groups. d) CD spectrum of $\mathbf{C^{BCM}_{77}}$ in HFIP. Minima at 197 and 224 nm suggest that the polymer is adopting an extended conformation in this solvent.[52]

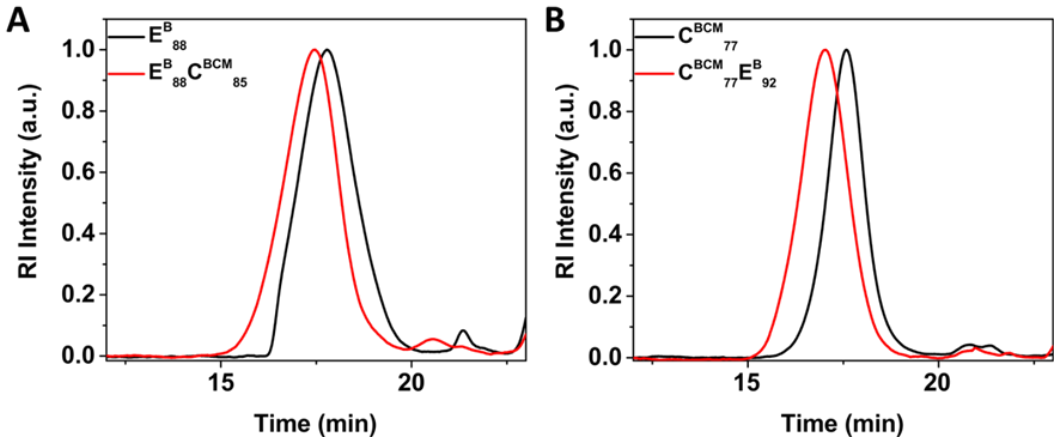

Figure 3.9. GPC analysis of $\mathbf{C^{BCM}}$ containing diblock copolypeptides a) Block copolymerization chain extension experiments for formation of $\mathbf{E^{B}_{88}C^{BCM}_{85}}$ analyzed via GPC in HFIP containing 0.5% (w/w) KTFA. b) Block copolymerization chain extension experiments for formation of $\mathbf{C^{BCM}_{77}E^{B}_{92}}$ analyzed via GPC in HFIP containing 0.5% (w/w) KTFA.

Monomer Feed Compositions		**First Segment[b]**			**Diblock copolymer[c]**			
First Monomer[a]	**Second Monomer[a]**	**M_n**	**DP**	***Đ***	**M_n**	**DP**	***Đ***	**Yield(%)[d]**
40 *t*Bu-Glu NCA	40 *t*BuCM-Cys NCA	20,172	88	1.28	42,381	173	1.29	96
40 *t*BuCM-Cys NCA	40 *t*Bu-Glu NCA	20,209	77	1.17	41,298	169	1.17	93

Table 3.1. Synthesis of diblock copolypeptides using $Co(PMe_3)_4$ initiator in THF.[a]First and second monomers added stepwise to the initiator at 20 ºC; number indicates equivalents of monomer per $Co(PMe_3)_4$. [b]Molecular weight (M_n) and dispersity ($Đ = M_w/M_n$) after polymerization of the first monomer determined by ^{1}H NMR and GPC. [c]Molecular weight and dispersity after polymerization of the second monomer determined by ^{1}H NMR and GPC. [d]Total isolated yield of deprotected diblock copolypeptide as the sodium salt. DP = number average degree of polymerization.

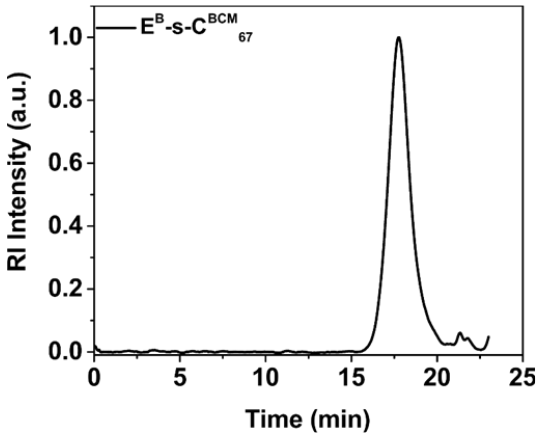

Figure 3.10. GPC chromatogram of **(E^B-*s*-C^{BCM})$_{67}$** in HFIP containing 0.5% (w/w) KTFA.

Comonomer I[a]	Comonomer II[a]	M:I[b]	DP[c]	*Đ*[d]	M_n[c]	Yield(%)[e]
50% Bu-Glu NCA	50% *t*BuCM-Cys NCA	40:1	67	1.28	42,381	90

Table 3.2. Preparation and characterization of a statistical copolypeptide using equimolar *t*BuCM-Cys and *t*Bu-Glu NCAs. [a]Both monomers were combined before initiator added; number indicates mol % of monomer in mixture. [b]Molar ratio of combined monomers to $Co(PMe_3)_4$ initiator. [c]Degree of polymerization and residue composition (49 mol% **E^B**; 51 mol% **C^{BCM}**) determined by ^{1}H NMR. [d]Dispersity (M_w/M_n) determined by GPC. [d]Total isolated yield of deprotected, purified copolypeptide.

With the successful controlled preparation of the soluble polypeptide precursor **C^{BCM}**, the next step was to attempt to convert this into **A^{DH}**. As shown in Fig. 3.11, we considered both oxidation-elimination and alkylation-elimination routes to convert **C^{BCM}** to **A^{DH}**. Some efforts were made initially to directly convert organic soluble **C^{BCM}** to **A^{DH}**, but these suffered from poor yields and negligible formation of **A^{DH}**. Consequently, **C^{BCM}** was readily deprotected using trifluoroacetic acid (TFA) to obtain, after neutralization, the water soluble poly(S-carboxymethyl-L-cysteine), **C^{CM}**, as its sodium salt (Fig. 3.11). The thioether groups in **C^{CM}** could either be fully methylated (Fig. 3.11a) or fully oxidized

(Fig. 3.11b) under mild conditions in aqueous media, similar to other thioether containing polypeptides.[53,54]

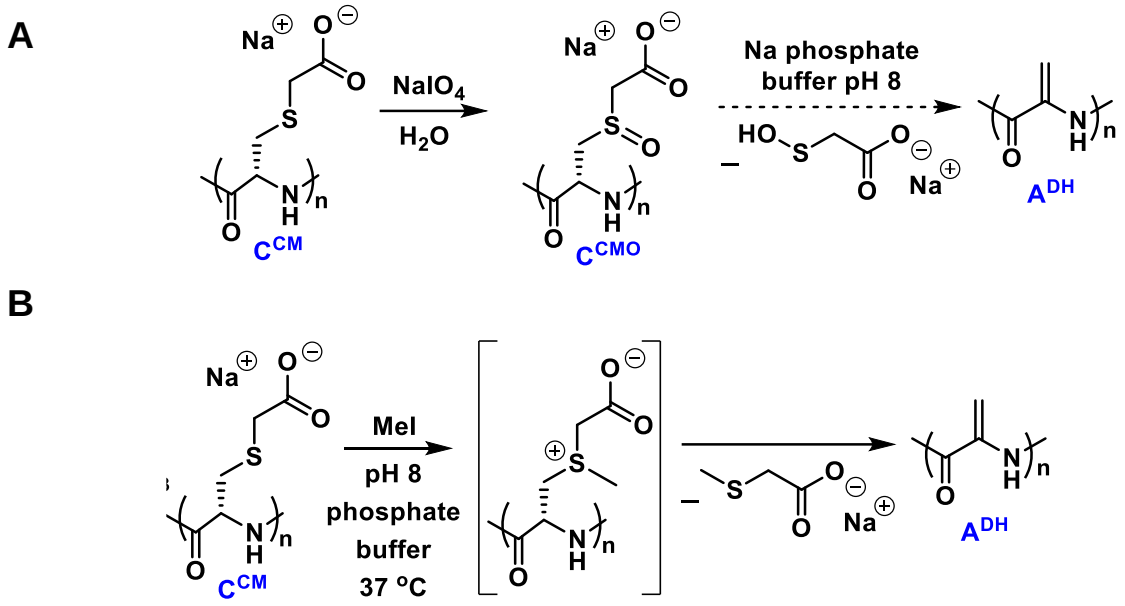

Figure 3.11. Synthetic routes to **A**^{DH} from **C**^{CM}. A) Oxidation of poly(S-carboxymethyl-L-cysteine), **C**^{CM}, to give poly(S-carboxymethyl-L-cysteine sulfoxide), **C**^{CMO}, and its subsequent attempted conversion to **A**^{DH} via base catalyzed elimination. B) Conversion of **C**^{CM} to **A**^{DH} via methylation and subsequent base catalyzed elimination.

While attempts to eliminate the sulfoxide groups at pH 8.0 and 37 °C were found to give only ca. 8% conversion to Dha residues, the elimination of sulfonium groups was found to proceed rapidly at pH 8.0 and 37 °C to give **A**^{DH} in high conversion and yield. Elimination occurred so rapidly at this pH that the sulfonium product was not isolated, and water insoluble **A**^{DH} precipitated directly from the reaction mixture. Thus, the methylation of **C**^{CM} was determined to be the most efficient method for preparation of **A**^{DH} (Fig. 3.12). Note that small amounts of butylated hydroxytoluene (BHT) were added to these reactions (0.01 mol% relative to Dha residues) in order to inhibit radical induced decomposition of the reactive Dha residues.

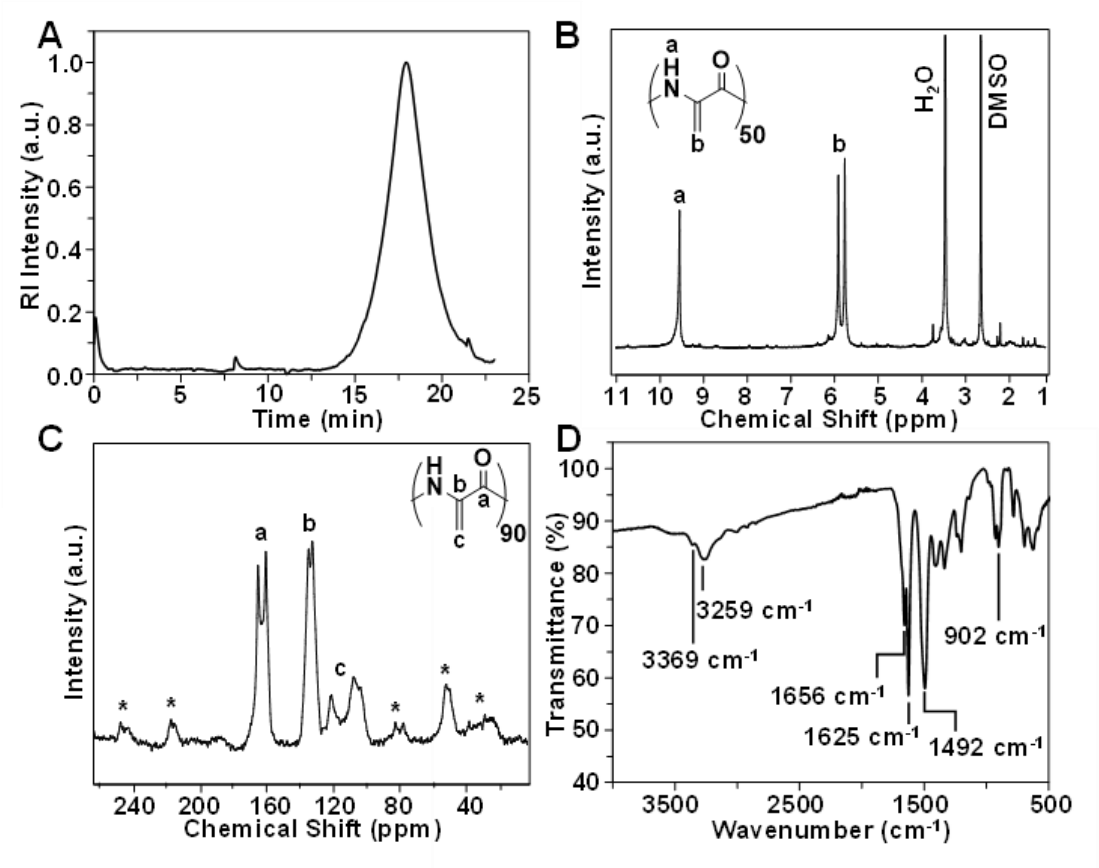

Figure 3.12. Characterization data for $\mathbf{A}^{\mathbf{DH}}$. A) GPC trace of $\mathbf{A}^{\mathbf{DH}}_{\mathbf{72}}$ in HFIP containing 0.5% (w/w) KTFA ($Đ$ = 2.30). B) ^{1}H NMR spectrum of $\mathbf{A}^{\mathbf{DH}}_{\mathbf{50}}$ in DMSO-d_6. C) Solid state CP-MAS ^{13}C NMR spectrum of $\mathbf{A}^{\mathbf{DH}}_{\mathbf{90}}$. Asterisks indicate spinning side bands. D) Solid state FTIR spectrum of $\mathbf{A}^{\mathbf{DH}}_{\mathbf{68}}$. The band at 897 cm^{-1} is consistent with alkene =C-H out of plane bends in $\mathbf{A}^{\mathbf{DH}}$.[57] The band at 1625 cm^{-1} is consistent with alkene stretches in $\mathbf{A}^{\mathbf{DH}}$. The bands at 1656 and 1492 cm^{-1} are consistent with Amide I and Amide II vibrations for peptides in the extended 2_5-helical conformation.[58]

Samples of $\mathbf{A}^{\mathbf{DH}}$ formed as off-white precipitates that were insoluble in water, but were found to disperse well in DMSO, TFA and hexafluoroisopropanol (HFIP) solvents. GPC analysis of $\mathbf{A}^{\mathbf{DH}}$ in HFIP showed a monomodal peak similar to the $\mathbf{C}^{\mathbf{CM}}$ precursor with apparent dispersity ($Đ$) of 2.30, which was likely inflated due to polypeptide aggregation (*vide infra*) (Fig. 3.12a). This result, combined with measurement of chain lengths of $\mathbf{C}^{\mathbf{CM}}$ and $\mathbf{A}^{\mathbf{DH}}$ segments relative to 1 kDa PEG endgroups via ^{1}H NMR

integration confirmed that no chain cleavage occurred during conversion of $\mathbf{C}^{\mathbf{CM}}$ to $\mathbf{A}^{\mathbf{DH}}$. The composition of $\mathbf{A}^{\mathbf{DH}}$ samples was confirmed by ^{1}H and ^{13}C NMR, as well as FTIR analysis (Fig 3.12b-d).

Contrary to the oligomers obtained above from attempted Dha NCA polymerizations, the ^{1}H NMR spectrum $\mathbf{A}^{\mathbf{DH}}$ derived from the $\mathbf{C}^{\mathbf{CM}}$ sulfonium precursor possessed intense resonances for the alkene protons of Dha residues (Fig. 3.12b).[4] The solid-state CP-MAS ^{13}C NMR spectrum of $\mathbf{A}^{\mathbf{DH}}$ was also consistent with the proposed structure, with resonances for carbonyl and alkene carbons that were analogous to those observed in Dha containing small molecules (Fig. 3.12c).[55] Observation of two resonances for each carbon may reflect different polypeptide conformations in the solid-state (*vide infra*). Finally, the FTIR spectrum of $\mathbf{A}^{\mathbf{DH}}$ contained bands consistent with Amide I and Amide II peptide vibrations, as well as bands at 1625 and 902 cm^{-1} that are consistent with an alkene stretch[56] and an alkene out of plane bend[57] in $\mathbf{A}^{\mathbf{DH}}$ (Fig. 3.12d). Altogether, these data confirm the successful preparation of long chain $\mathbf{A}^{\mathbf{DH}}$.

In addition to helping confirm its structure, FTIR analysis of $\mathbf{A}^{\mathbf{DH}}$ also provided valuable insights into the chain conformation of $\mathbf{A}^{\mathbf{DH}}$. As mentioned in the introduction, Toniolo and coworkers discovered that short oligomers of Dha adopt the flat 2_5-helical conformation,[4] and this group has also pioneered the study of other peptide motifs that adopt this structure.[58] These investigations led to the identification of signature FTIR bands for 2_5-helices, similar to those that are well known for α-helices, 3_{10}-helices and β-sheets.[59] Specifically, Toniolo and coworkers noted that peptides in the 2_5-helical conformation possess a strong Amide II band at *ca*. 1490 cm^{-1} and split Amide I bands

at *ca*. 1675 and 1650 cm^{-1}, where the Amide II band has greater intensity than the Amide I bands.[58] This pattern is distinct from the Amide bands of all other peptide conformations and is present in the $\mathbf{A^{DH}}$ samples prepared here, both in solid-state and in HFIP (Fig. 3.13) and strongly suggest that long chain $\mathbf{A^{DH}}$ also partially adopts the 2_5-helical conformation.

Figure 3.13. Comparison of FTIR spectra of $\mathbf{A^{DH}_{68}}$ in the solid state and in HFIP. Top: FTIR spectrum of $\mathbf{A^{DH}_{68}}$ in the solid state. Bottom: FTIR spectrum of $\mathbf{A^{DH}_{68}}$ in HFIP (50 mg/mL). The two sets of NH stretching bands between 3376 and 3259 cm^{-1} suggest that peptide NH groups are engaged in both strong and weak H bonding interactions.[4,58]

However, discrepancies do exist between 2_5-helical hexa-Dha and $\mathbf{A^{DH}}$ in the FTIR spectra. In the N-H stretching region, a band occurs at *ca*. 3380 cm^{-1} for hexa-Dha[4] and two bands appear for $\mathbf{A^{DH}}$ at 3369 and 3259 cm^{-1} (Fig. 3.13, Fig. 3.14a). The smaller $\mathbf{A^{DH}}$ N-H stretch at 3369 cm^{-1} is consistent with the 3380 cm^{-1} band for hexa-Dha since this band is known to shift to lower wavenumbers as the number of Dha repeats increases[4] and is due to weak intrachain H-bonding in a 2_5-helical conformation for $\mathbf{A^{DH}}$.[58] On the other hand, the larger $\mathbf{A^{DH}}$ N-H stretch at 3259 cm^{-1} indicates much stronger H-bonding than previously found in peptides with a 2_5-helical conformation.[58] A possible explanation for this additional N-H band may be the partial folding or aggregation of longer 2_5-helical chains in $\mathbf{A^{DH}}$ via interchain H-bonding. Such interactions would likely lead to conformational distortion of some chain segments and could also explain the presence of two sets of resonances observed in the solid-state CP-MAS ^{13}C NMR spectra (Fig. 3.12c). Also consistent with this hypothesis, weak shoulders are present in the Amide region of the $\mathbf{A^{DH}}$ FTIR spectra at *ca*. 1697 and

1519 cm^{-1} (Fig. 3.14b), which suggests that some fraction of $\mathbf{A^{DH}}$ chains may adopt conformations other than the fully extended 2_5-helix in the solid state and in HFIP.

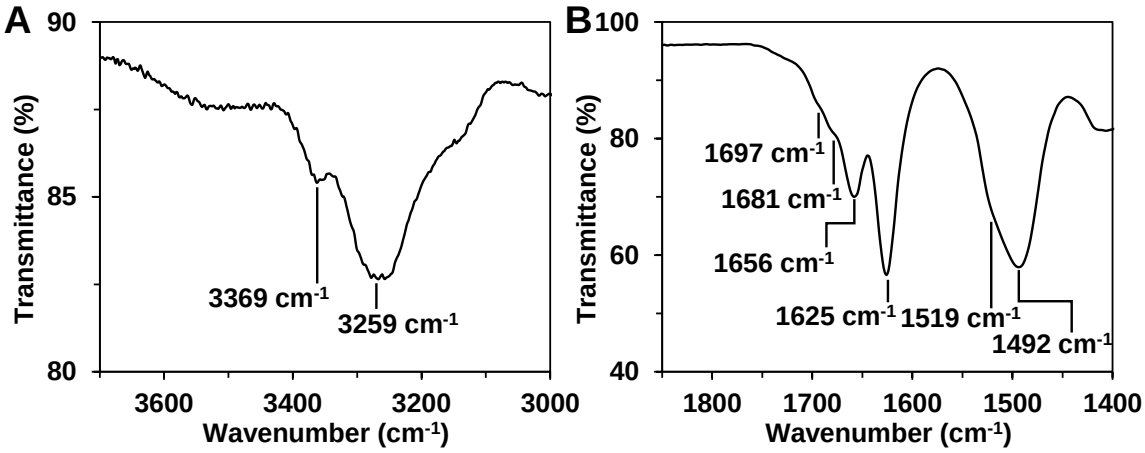

Figure 3.14. Conformational analysis of $\mathbf{A^{DH}_{68}}$ by solid state FTIR. (A) N-H stretching region of $\mathbf{A^{DH}_{68}}$ indicating intra- and interchain H-bonding.[4] (B) Amide I and II stretching region of $\mathbf{A^{DH}_{68}}$ suggesting interchain H-bonding interactions (shoulders at 1697 and 1519 cm^{-1}).[58]

To understand the conformational properties of $\mathbf{A^{DH}}$ in more detail, we performed computational analysis using density functional theory (DFT). Geometry optimizations and frequency calculations were performed at the B3LYP-D3/6-31G(d) level of theory and single point energies were calculated at the ωB97X-D/def2TZVP level of theory using the SMD solvation model for dimethyl sulfoxide (see SI). Models of $\mathbf{A^{DH}}$ with varying chain lengths were optimized in both the 2_5-helical conformation and the 3_{10}-helical conformation (Fig. 3.15a). The 3_{10}-helix was included here since it has also been proposed to be a stable conformation for $\mathbf{A^{DH}}$.[18,19] We found the 2_5-helical conformation to be clearly preferred in the shorter chains, with a free energy difference of 8.1 kcal/mol between the favored 2_5-helical conformation and the higher energy 3_{10}-helical conformation of $\mathbf{A^{DH}_4}$ (Fig. 3.15b). This energy difference varies linearly with polymer-

length, and the 3_{10}-helical conformation becomes preferred in the longer chains $\mathbf{A^{DH}_{16}}$, $\mathbf{A^{DH}_{20}}$, and $\mathbf{A^{DH}_{24}}$.

To better understand this trend, we performed noncovalent interaction (NCI) analyses on the DFT-optimized models (Fig. 3.15c). The NCI calculations show that the 2_5-helical conformation is stabilized by weak dispersion interactions between the methylidene groups of the side-chain and the amide groups of the backbone. Additionally, the linearized backbone dihedrals allow for weak intra-residue hydrogen bonding between the backbone carbonyl oxygens and amide hydrogens, sometimes referred to as C5 hydrogen bonds.[60-64] These noncovalent interactions, along with the extended p-electron conjugation, make the 2_5-helical conformation more stable in shorter $\mathbf{A^{DH}}$ chains. The 3_{10}-helical conformation is stabilized by dispersion interactions along the helix, and inter-residue hydrogen bonding between the *i* and *i+3* residue positions. These inter-residue hydrogen bonds have more linear N-H-O angles, making them stronger than the intra-residue hydrogen bonds observed in the 2_5-helical conformation. As the $\mathbf{A^{DH}}$ chain length increases, these inter-residue hydrogen bonds become more abundant, leading to the preference for the 3_{10}-helical conformation in these molecules.

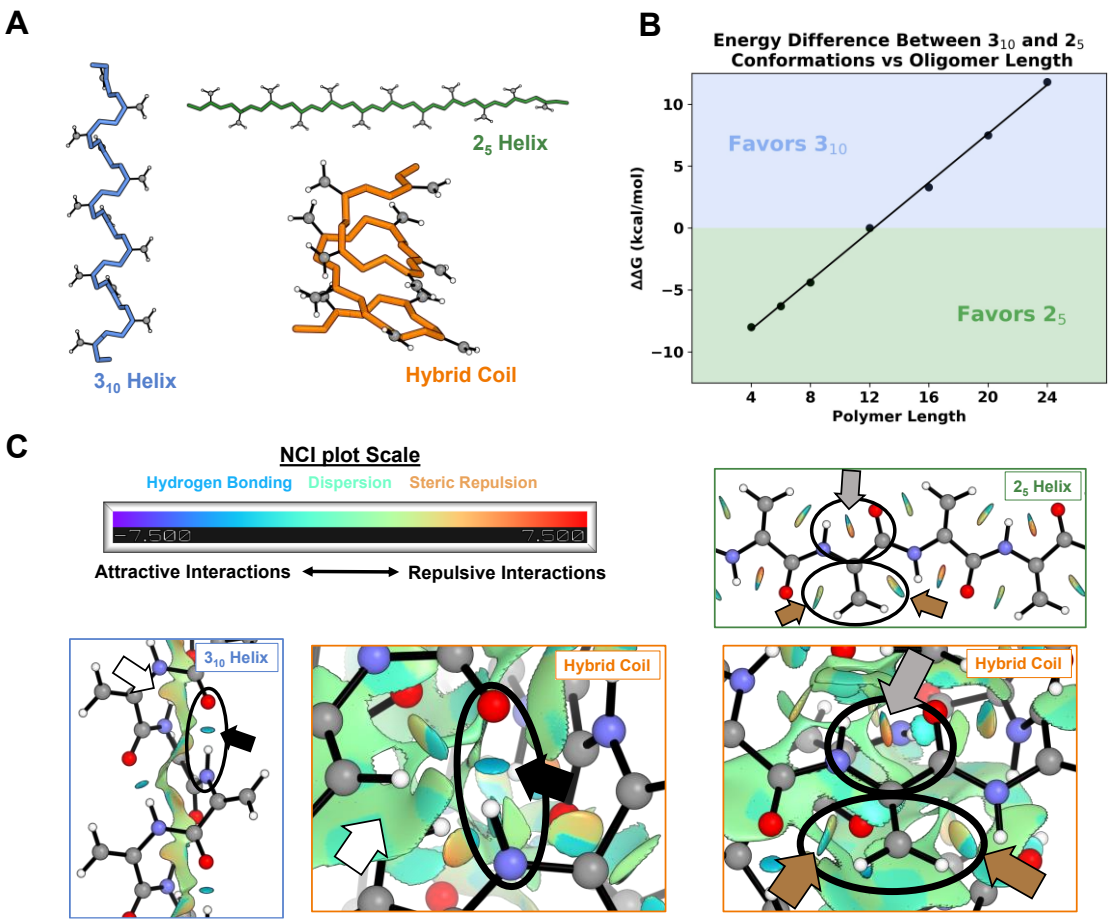

Figure 3.15. Computational analysis of ADH conformations. (A) Backbone traces of DFT-optimized models of $\mathbf{A^{DH}_{12}}$. The 2_5-helix conformation is shown in green, the 3_{10}-helix conformation is shown in blue, and the hybrid coil conformation is shown in orange. (B) Plot of polymer length versus the difference in free energy between the 2_5-helix and 3_{10}-helix conformations. Short repeats $\mathbf{A^{DH}_4}$, $\mathbf{A^{DH}_6}$, and $\mathbf{A^{DH}_8}$ favor the 2_5-helix conformation. Longer repeats $\mathbf{A^{DH}_{16}}$, $\mathbf{A^{DH}_{20}}$, and $\mathbf{A^{DH}_{24}}$ favor the 3_{10}-helix conformation. The energies are equivalent in $\mathbf{A^{DH}_{12}}$. (C) NCI plots of the DFT optimized structures of $\mathbf{A^{DH}_{12}}$. Scale is shown for colors that represent attractive interactions like hydrogen bonding and dispersion, along with repulsive interactions like steric repulsion. Weak dispersion interactions are observed along the helix in the 3_{10}-helix conformation and throughout the backbone in the hybrid coil conformation (white arrows). Additional weak dispersion interactions are observed between the sidechain and backbone in the 2_5-helix conformation and for flat residues in the hybrid coil conformation (brown arrows). Inter-residue hydrogen bonding is observed between *i* and *i+3* residue positions in the 3_{10}-helix conformation and throughout the hybrid coil conformation (black arrow). Intra-residue hydrogen bonding is observed between the backbone carbonyl oxygens and

amide hydrogens in the 2_5-helix conformation and in flat residues in the hybrid coil conformation (gray arrow).

In addition to the 2_5-helical and 3_{10}-helical conformations, we explored other possible conformations of $\mathbf{A^{DH}_{12}}$ using CREST, a conformational search algorithm which uses meta-dynamics to rapidly explore conformational space.[65] This led to the discovery of a third conformation type, where some residues adopt the 2_5-helical conformation, but other residues have bends in either the φ or ψ dihedral angles that cause the chain to fold into a loose coil-like structure (Fig. 3.15a). NCI plots show this new "hybrid coil" conformation has characteristics of both the 2_5-helical and 3_{10}-helical conformations (Fig. 3.15c). The nearly linearized backbone of many residues allows extended p-electron conjugation and the same intra-residue hydrogen bonding that stabilizes the 2_5-helical structure. The hybrid coil structure also allows for increased dispersion along the backbone and the same inter-residue hydrogen bonds that stabilize the 3_{10}-helical conformation. The free energy difference of 2.6 kcal/mol in favor of the hybrid coil conformer compared to either the 2_5-helical and 3_{10}-helical conformations of $\mathbf{A^{DH}_{12}}$ shows that this conformation is clearly preferred, although $\mathbf{A^{DH}_{12}}$ chains may exist in an equilibrium between conformations in solution. Altogether, this new hybrid coil conformation with elements of both 2_5-helical and 3_{10}-helical conformations fits well with our experimental data that shows evidence of both intra- and inter-chain H-bonding, and is the best model for the conformation of long $\mathbf{A^{DH}}$ chains.

When investigating the properties of $\mathbf{A^{DH}}$, we noted that the α,β-unsaturation and flat conformations of some residues may lead to extended π-electron conjugation.[1] Consequently, we measured the UV-visible absorption spectrum of $\mathbf{A^{DH}_{68}}$ in HFIP and compared this to an α-helical sample of poly(L-alanine)$_{53}$, $\mathbf{A_{53}}$, in HFIP as a control.

Contrary to **A$_{53}$**, which has only weak amide absorption above 200 nm, **A$^{DH}_{68}$** showed a strong absorption maximum at 220 nm with absorption extending to nearly 300 nm (Fig. 3.16a). The absorption of **A$^{DH}_{68}$** in this region is due to the known absorption properties of Dha residues[66]. The fluorescence spectra of both samples were also acquired. The **A$_{53}$** sample in HFIP showed weak absorption (λ_{max} = 302 nm) and emission (λ_{max} = 400 nm); while **A$^{DH}_{68}$** in HFIP showed considerably stronger absorption at higher wavelength (λ_{max} = 354 nm) and a remarkable strong blue emission (λ_{max} = 440 nm) (Fig. 3.16b,c).

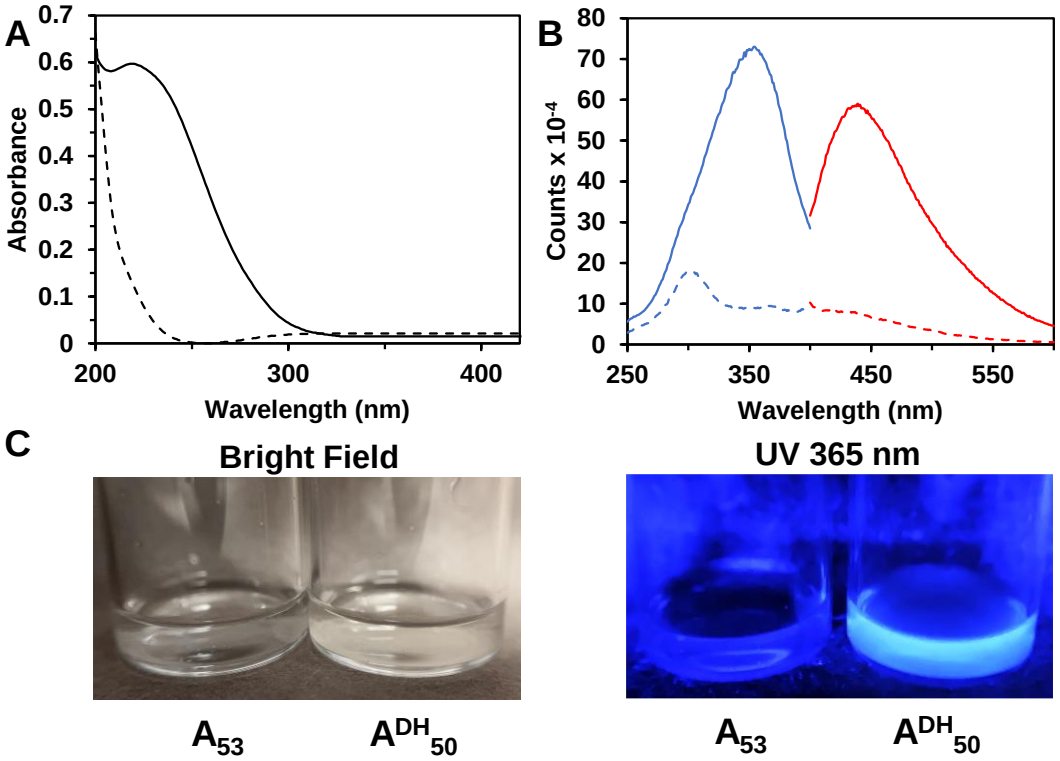

Figure 3.16. Spectroscopic properties of **A$^{DH}_{68}$** (solid lines) and poly(L-alanine)$_{53}$, **A$_{53}$** (dashed lines) in HFIP. a) UV/vis absorption spectra and b) excitation (blue) and emission (red) spectra. c) strong blue emission of **A$^{DH}_{68}$** at 1 mg/mL in HFIP upon UV excitation at 365 nm. All spectroscopic samples were prepared in HFIP (0.1 mg/mL) and spectra were acquired at 20 ºC.

Seeking to better understand the nature of **A^{DH}** fluorescence, we observed that while both polypeptides disperse well in HFIP to give limpid samples, we found using

dynamic light scattering that both $\mathbf{A_{53}}$ and $\mathbf{A^{DH}_{68}}$ form nanoscale aggregates in this solvent (Fig. 3.17a,b). Consequently, it is likely that the fluorescence properties of these samples arise from aggregation induced emission from the nanoparticles rather than from individual solvated chains.[67,68] Accordingly, we observed that solution samples of $\mathbf{A^{DH}_{68}}$ also showed strong blue emission upon excitation via hand-held UV lamp at 365 nm (Fig. 3.16c).

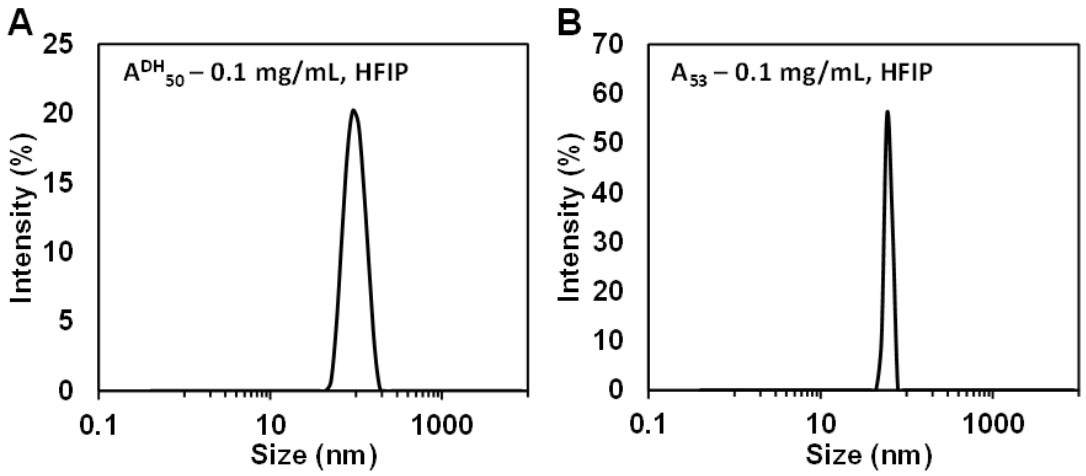

Figure 3.17. Dynamic light scattering data for (A) $\mathbf{A^{DH}_{50}}$ and (B) poly(L-alanine)$_{53}$, $\mathbf{A_{53}}$, in HFIP (0.1 mg/mL). Both samples were found to contain nanoscale aggregates with average diameters of 99 nm for $\mathbf{A^{DH}_{50}}$, and 59 nm for $\mathbf{A_{53}}$.

Regardless of its origin, the intrinsic blue fluorescence of $\mathbf{A^{DH}}$ has much higher intensity compared to that observed in other polypeptides that exhibit AIE.[67,68] This unique feature is potentially valuable for the development of label-free polypeptide nanocarriers and biomaterials for combination therapeutic and imaging applications.

Another feature of Dha containing polypeptides is the ability to functionally modify these residues by reaction with nucleophiles.[5-8] To evaluate the ability to functionally modify residues in $\mathbf{A^{DH}}$, we reacted homo, statistical, and block copolypeptides of $\mathbf{A^{DH}}$

with model thiol and amine nucleophiles in mixtures of DMSO and water (Fig. 3.19, Table 3.3). Addition of DMSO was necessary to disperse the $\mathbf{A}^{DH}$ segments of homo and block copolypeptides in aqueous media. All reactions proceeded in high yields with no sign of peptide chain cleavage (Table 3.3), and the use of hydrophilic nucleophiles resulted in fully water-soluble products. As expected, since the Dha precursors lack stereocenters, the resulting modified Dha residues possessed racemic stereochemistry as verified by circular dichroism spectroscopy (Fig. 3.20).[10] The facile modification of Dha residues in $\mathbf{A}^{DH}$ provides a new effective route to side-chain functional polypeptides, which have promise for a wide-range of applications. Since the products of reactions of $\mathbf{A}^{DH}$ with thiol nucleophiles are poly(S-alkyl-DL-cysteines), the racemic nature of these products likely provides an added benefit in enhancing their solubility by disfavoring the β-sheet formation commonly observed in poly(cysteine) derivatives.[69]

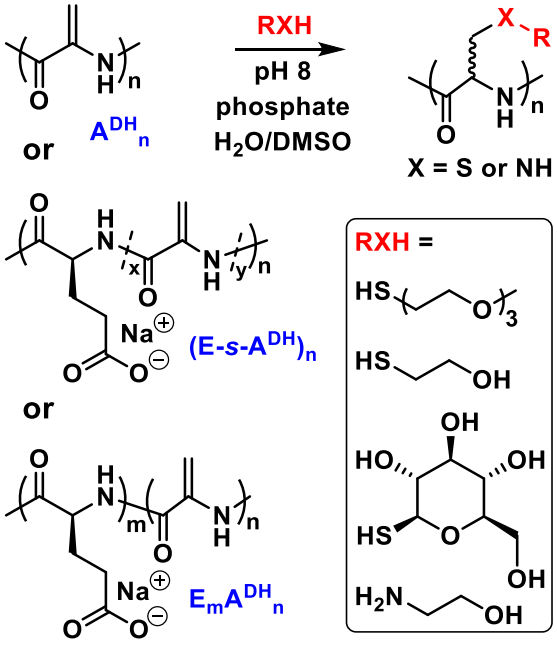

Figure 3.19. Functionalization of $\mathbf{A^{DH}}$ containing polypeptides using amine and thiol nucleophiles.

Starting Polymer	Nucleophile	Product	Functionalization (%)[a]	Yield (%)[b]
$\mathbf{A^{DH}_{72}}$	mEG_3SH	$\mathbf{(\textit{rac}\text{-}C^{EG3})_{72}}$	>99	86
$\mathbf{(E\text{-}\textit{s}\text{-}A^{DH})_{67}}$	mEG_3SH	$\mathbf{[E\text{-}\textit{s}\text{-}(\textit{rac}\text{-}C^{EG3})]_{67}}$	>99	89
$\mathbf{E_{88}A^{DH}_{85}}$	mEG_3SH	$\mathbf{E_{88}(\textit{rac}\text{-}C^{EG3})_{85}}$	>99	99
$\mathbf{E_{88}A^{DH}_{85}}$	$HOEtNH_2$	$\mathbf{E_{88}(\textit{rac}\text{-}A^{HEA})_{85}}$	>99	98
$\mathbf{E_{88}A^{DH}_{85}}$	HOEtSH	$\mathbf{E_{88}(\textit{rac}\text{-}C^{HE})_{85}}$	>99	99
$\mathbf{E_{88}A^{DH}_{85}}$	β-D-glcSH	$\mathbf{E_{88}(\textit{rac}\text{-}C^{GLC})_{85}}$	>99	95

Table 3.3. Preparation of functional derivatives of $\mathbf{A^{DH}}$ containing polypeptides. [a] Determined by ^1H NMR analysis of functionalized polypeptide. [b] Isolated yield of purified polypeptide.

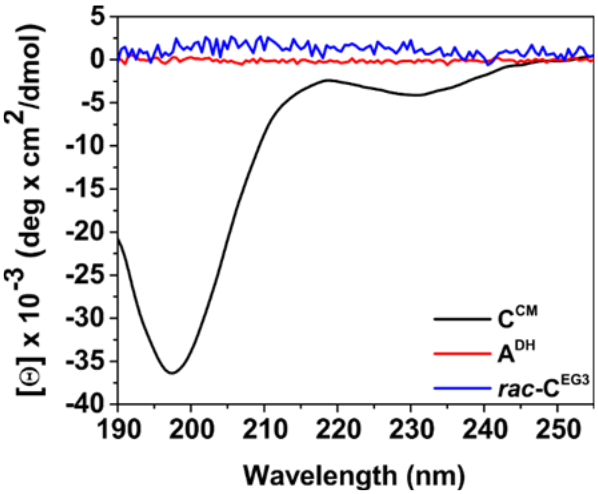

Figure 3.20. CD Spectra of $\mathbf{C^{CM}_{72}}$ (black) in DI H_2O, $\mathbf{A^{DH}_{72}}$ (red) in HFIP, and $(rac\text{-}C^{EG3})_{72}$ (blue) in DI H_2O (all samples 0.1 mg/mL) demonstrating the lack of optical activity after the conversion to $\mathbf{A^{DH}}$ and subsequent functionalization.

3.4 Conclusion

Via the design of a new, soluble poly(S-alkyl-L-cysteine) based precursor, we have developed a route for successful preparation of high molecular weight $\mathbf{A^{DH}}$, and the incorporation of Dha residues and $\mathbf{A^{DH}}$ segments into copolypeptides. Based on

experimental and computational data, $\mathbf{A^{DH}}$ was found to previously unobserved “hybrid coil” structure, which combines elements of both 2_5-helical and 3_{10}-helical conformation. Analysis of the spectroscopic properties of $\mathbf{A^{DH}}$ revealed that it possesses strong inherent blue fluorescence that may be amenable for use in downstream imaging applications. $\mathbf{A^{DH}}$ also contains reactive electrophilic groups that allowed its efficient modification to functionalized polypeptides after reaction under mild conditions with thiol and amine nucleophiles. The combined structural, spectroscopic, and reactivity properties of $\mathbf{A^{DH}}$ make it a unique polypeptide component for utilization in assemblies for therapeutic and diagnostic applications.

3.5 Experimental

3.5.1 Materials and Methods

The following chemicals were used as received from vendors: trifluoroacetic acid (Oakwood), L-cysteine (Sigma–Aldrich), tetramethyl guanidine (TMG) (Alfa Aesar), *tert*-butyl bromo acetate (Combi-Blocks), 15% phosgene in toluene (Sigma–Aldrich), iodomethane (Sigma-Aldrich). Triethylamine (TEA) (Fisher) was distilled from CaH_2 under N_2 and stored over 4 Å molecular sieves. TMSCl (Sigma–Aldrich) was purified by distillation under N_2. H_2O was purified by reverse osmosis. α-methoxy-ω-isocyanoethyl-poly(ethylene glycol), mPEG-NCO (1 kDa), was prepared as previously reported.[70] NCA purifications[71] and polymerizations[72] were performed in an N_2 filled glove box using established techniques. Reactions at elevated temperature were controlled using a Corning PC 420D thermostat controlled hotplate equipped with a thermocouple probe. Room temperature reactions were performed at *ca*. 20 ºC ambient temperature. All reactions were performed under N_2 at 20 ºC unless otherwise described. THF and

hexanes were degassed by sparging with nitrogen and water removed by passage through columns of dried alumina. Thin-layer chromatography was performed with EMD gel 60 F254 plates (0.25 mm thickness) and visualized using a UV lamp or ninhydrin stain. Column chromatography was performed using Silicycle Siliaflash G60 silica (60–200 mm). DART-MS spectra were collected on a Thermo Exactive Plus MSD (Thermo Scientific) equipped with an ID-CUBE ion source at the low desorption setting and a Vapur Interface (IonSense). Both the source and MSD were controlled by Excalibur v. 3.0. Analytes were dissolved at 1 mg/mL in 1:3 THF:MeCN and spotted onto OpenSpot sampling cards (IonSense). Ionization was accomplished using He plasma with no additional ionization agents. Mass calibration was carried out using Pierce LTQ Velos ESI (+) and (-) ion calibration solutions (Thermo Fisher Scientific). FTIR spectroscopy was performed on a PerkinElmer Spectrum RX spectrometer or a JASCO FT/IR-4100 spectrometer. NMR spectroscopy was performed on a Bruker AV400 spectrometer. CD spectra were collected using an OLIS RSM CD spectrophotometer (OLIS, USA) using conventional scanning mode. Samples were characterized by recording spectra (185-260 nm) within a quartz cuvette of 0.1 cm path length. ^{13}C cross polarization-magic angle spinning NMR was conducted on a Bruker AV III HD instrument with a magnetic field of 14.1 T, with contact time of 1.5 ms, recycle delay of 5 s, and sample spinning rate of 12.5 kHz. Tandem gel permeation chromatography/light scattering (GPC/LS) was performed using an SSI Accuflow Series III pump equipped with Wyatt DAWN EOS light scattering and Optilab REX refractive index detectors. Separations were achieved using 100 Å and 1000 Å PSS-PFG 7 μm columns at 30 ºC with 0.5% (w/w) potassium trifluoroacetate (KTFA) in 1,1,1,3,3,3-hexafluoroisopropanol (HFIP) as eluent and

sample concentrations of 10 mg/ml. Fluorescence spectroscopy was performed using a Horiba Instruments PTI QuantaMaster series Fluorometer using a quartz cuvette of 10 mm path length. Dynamic light scattering measurements were performed on a Malvern Zetasizer Nano ZS.

3.5.2 Synthesis of Amino Acids and NCA Monomers

S-(*tert*-butoxycarbonylmethyl)-L-cysteine[51]

L-Cysteine (2.4 g, 20 mmol, 1.0 eq.) was suspended in methanol (20 mL). Tetramethyl guanidine (TMG) (5 mL, 40 mmol, 2.0 eq.) in methanol (10 mL) was then added dropwise resulting in formation of a clear solution. Next, *tert*-butyl bromoacetate (3 mL, 20 mmol, 1.0 eq.) in THF (5 mL) was added dropwise to the solution. The reaction mixture was heated to 50 °C for 1h. The reaction was allowed to cool and the solvent was removed under vacuum. The resulting sticky residue was dissolved in water (30 mL) and then glacial acetic acid (1.1 mL, 20 mmol, 1.0 eq.) was added dropwise. Next, methanol was added dropwise until crystals began to appear (~10 mL). Crystallization was allowed to proceed overnight at 4 °C. The resulting white solid was filtered to remove excess water, and was then transferred to a 50 mL Falcon tube and washed with 95:5 Et_2O:MeOH exhaustively to obtain the product after solvent removal as a white solid. (2.4 g, 53% yield) ^{1}H NMR (400 MHz, D_2O, 25 °C): 3.81 (q, J=4.2 Hz, 1H), 3.26 (s, 2H), 3.10 (dd, J=4.2, 14.9 Hz, 1H), 2.97 (dd, J=7.9, 14.9 Hz, 1H), 1.36 (s, 9H). ^{13}C NMR (100 MHz, D_2O, 25 °C): 172.4, 171.8, 84.1, 53.4, 34.7, 32.7, 27.1 ppm.

S-(*tert*-butoxycarbonylmethyl)-L-cysteine N-carboxyanhydride (*t*BuCM-Cys NCA)

S-(*tert*-Butoxycarbonylmethyl)-L-cysteine (2.0 g, 8.5 mmol, 1.0 eq.) was suspended in THF (60 mL). Triethylamine (2.4 mL, 17 mmol, 2.0 eq.) and TMSCl (2.2 mL, 17 mmol,

2.0 eq.) were then added under N_2 and the turbid mixture was stirred for 1 h at room temperature. A 15% solution of phosgene in toluene (12 mL, 17 mmol, 2.0 eq.) was added and the mixture was heated to 45 °C under N_2 and allowed to react for 2 h. The resulting turbid mixture was then concentrated, filtered, and the crude product was purified by column chromatography (10:90 THF:hexanes to 30:70 THF:hexanes) all under inert atmosphere. After concentration, the resulting material was crystallized three times from 10:1 hexanes:THF to give the product as long, white needles (1.4 g, 60%).^{1}H NMR (400 MHz, $CDCl_3$, 25 °C): 6.98 (s, 1H), 4.53-4.49 (ddd, J=0.9, 3.3, 8.9 Hz 2H), 3.30-3.24 (m, 3H), 2.90-2.82 (dd, J=8.9, 14.8 Hz, 1H), 1.48 (s, 9H). ^{13}C NMR (100 MHz, $CDCl_3$, 25 °C): 170.5, 168.1, 83.3, 58.3, 36.0, 35.5, 27.9 ppm. FTIR (THF): 1860 and 1773 (NCA), 1717 (ester) cm^{-1}. DART-MS m/z = 260.06 $[M - H]^-$ (calcd for $C_{10}H_{14}NO_5S$: 260.06).

γ-*tert*-Butyl L-glutamate N-carboxyanhydride (*t*Bu-Glu NCA)

γ-*tert*-Butyl L-glutamic acid (2.0 g, 9.8 mmol, 1.0 eq.) was suspended in THF (60 mL). Triethylamine (2.8 mL, 20 mmol, 2.0 eq.) and TMSCl (2.5 mL, 20 mmol, 2.0 eq.) were added under N_2 and the turbid mixture was stirred for 1 h at room temperature. A 15% solution of phosgene in toluene (10 mL, 15 mmol, 1.5 eq.) was added and the mixture was heated to 45 °C and allowed to react for 2 h. The resulting turbid mixture was concentrated, filtered, and the crude product was purified by column chromatography (30:70 THF:hexanes to 50:50 THF:hexanes) all under inert atmosphere. After concentration, the resulting material was crystallized twice from 3:1 hexanes:THF to provide the product as a white fluffy solid (1.8 g, 68%). The FTIR and ^{1}H NMR spectral data for this material were in accordance with those previously reported.[74]

Dehydroalanine N-carboxyanhydride (Dha NCA)

Prepared according to a literature procedure.[73] N-(*tert*-Butoxycarbonyl)-L-serine methyl ester (2.0 g, 9.1 mmol, 1.0 eq) was dissolved in THF (20 mL) containing DMAP (220 mg, 1.8 mmol, 0.2 eq) and cooled to 0 ^{o}C in an ice-water bath. Boc anhydride (2.2 g, 10 mmol, 1.1 eq) was dissolved in THF (20 mL) and added slowly to the cooled reaction mixture, which was then stirred for 2 hours. The reaction was followed by TLC (1:1 hexanes:ethyl acetate) to monitor consumption of starting material over 1 to 2 hours. Once complete, the reaction mixture was concentrated by rotary evaporation and dissolved in ethyl acetate before washing with 1 M HCl followed by water. The organic layer was dried with anhydrous sodium sulfate and concentrated to an oil by rotary evaporation (1.8 g, 62%). This product, N,O-bis(*tert*-butoxycarbonyl)-L-serine methyl ester (1.8 g, 5.6 mmol, 1 eq) was redissolved in THF (36 mL) followed by addition of tetramethylguanidine (710 µL, 5.6 mmol, 0.7 eq) and was then stirred for 16 hours. The reaction mixture was concentrated via rotary evaporation, dissolved in EtOAc and washed with aqueous sodium bicarbonate, followed by brine, and then water before drying with sodium sulfate and concentrating via rotary evaporation. The crude product was then purified by column chromatography (1:1 hexanes:ethyl acetate) to obtain N-Boc-dehydroalanine methyl ester (700 mg, 62%). This product was then dissolved in 1:1 THF/H_2O (14 mL) and cooled to 0 ^{o}C before adding 2 eq of 5M NaOH followed by vigorous stirring for 4 hours. THF was removed by rotary evaporation before acidification of the reaction mixture to pH 1-2 followed by extraction with ethyl acetate. The solvent was removed by rotary evaporation to give N-Boc-dehydroalanine as a colorless oil (500 mg, 77%). The N-Boc-dehydroalanine was dissolved in dry DCM (10

mL) in a vacuum dried Schlenk flask fitted with a reflux condenser under nitrogen. To the Schlenk flask was added 2 eq. of α,α-dichloromethylmethyl ether via syringe under air-free conditions. The reaction was heated to 48 ^{o}C and stirred for 3 hours under N_2. DCM was then removed under vacuum before transferring the sealed Schlenk flask to a N_2 filled glove box. The crude Dha NCA was purified via column chromatography in the glove box using a gradient of 10-30% THF in hexanes. The isolated fractions containing the NCA were combined and solvent removed under vacuum to give a white solid. This crude Dha NCA was crystallized by dissolution in minimal THF, which was then layered under hexanes resulting in formation of long, needle-like colorless crystals (180 mg, 59%). The FTIR and ^{1}H NMR spectral data for this material were in accordance with those previously reported.[73] ^{1}H NMR (400 MHz, TFA-d) δ 5.89 (d, *J* = 3.3 Hz, 1H), 5.63 (d, *J* = 3.2 Hz, 1H). ^{13}C NMR (101 MHz, TFA-d) δ 160.61, 153.04, 130.18, 104.29.

3.5.3 Synthesis and Characterization of Polypeptides

Attempted polymerizations of Dha NCA

Co(PMe$_3$)$_4$ Initiator. Dha NCA was reacted with Co(PMe$_3$)$_4$ initiator (30 eq. of monomer per initiator) using conditions similar to those outlined below under “Example procedure for preparation of homopolypeptides” in either anhydrous DMF or anhydrous THF. Formation of solid precipitates was observed in both solvents within 30 minutes, and substantial Dha NCA remained in the mixtures at 24 hours when the reactions were stopped. The reaction mixtures were diluted tenfold with 0.1M aqueous NaCl resulting in the formation of clear solutions, which were then transferred to 2000 MWCO dialysis bags and dialyzed against DI H_2O for 48 hours with several water changes. A small amount of precipitation during dialysis was seen for both the THF and DMF reaction

products. The dialyzed suspensions were lyophilized to give off-white solids (DMF 27% yield; THF 42% yield as calculated for $\mathbf{A^{DH}}$).

Dha NCA + $Co(PMe_3)_4$ in THF: ^{1}H NMR (400 MHz, TFA-d) δ 2.74 (s, 1H), 2.20 (s, 2H).

Dha NCA + $Co(PMe_3)_4$ in DMF: ^{1}H NMR (400 MHz, TFA-d) δ 2.73 (s, 1H), 2.20 (s, 2H).

$nBuNH_2$ Initiator. Dha NCA was reacted with $nBuNH_2$ initiator (30 eq. of monomer per initiator) at 20 ^oC in either anhydrous DMF or anhydrous THF. Some precipitates formed in the THF reaction at 24 hours, while the DMF reaction remained clear with a deep, yellow color. Substantial Dha NCA remained in the mixtures at 4 days when the reactions were stopped. The reaction mixtures were diluted tenfold with 0.1M aqueous NaCl resulting in the formation of clear solutions, which were then transferred to 2000 MWCO dialysis bags and dialyzed against DI H_2O for 48 hours with several water changes. The dialyzed solutions were lyophilized to give off-white solids (DMF 11% yield; THF 16% yield as calculated for $\mathbf{A^{DH}}$).

Dha NCA + $nBuNH_2$ in DMF: ^{1}H NMR (400 MHz, TFA-d) δ 5.73 (s, 1H), 2.67 (s, 1H), 1.38 (s, 1H).

Dha NCA + $nBuNH_2$ in THF: ^{1}H NMR (400 MHz, TFA-d) δ 1.34 (s, 2H), 0.98 (s, 1H).

Example procedure for preparation of homopolypeptides

For preparation of polypeptide samples at *ca*. 100 mg scale in a N_2 filled glove box, a defined volume of initiator (20 mg/mL solution of $Co(PMe_3)_4$ in THF) was quickly added to a solution of *t*BuCM-Cys NCA in THF (50 mg/mL). After *ca*. 90 min, complete consumption of NCA was confirmed by FTIR spectroscopy. In order to determine polypeptide chain lengths a small aliquot of the reaction mixture (*ca*. 200 µL) was removed for end-group analysis after active chain-ends were reacted with mPEG-NCO

(*vide infra*). The remaining polypeptide was then precipitated by addition to DI H_2O (50 mL), centrifuged and the supernatant was removed. The polymer was then washed two additional times with DI H_2O and dried under reduced pressure to yield a light brown powder for $\mathbf{C^{BCM}}$. $\mathbf{C^{BCM}}$ samples were carried on immediately to deprotection.

General procedure for preparation of block copolypeptides using *t*BuCM-Cys NCA and *t*Bu-Glu NCA

For preparation of block copolypeptide samples at *ca*. 100 mg scale in a N_2 filled glove box, a defined volume of initiator (20 mg/mL solution of $Co(PMe_3)_4$ in THF) was quickly added to a solution of either *t*BuCM-Cys NCA or *t*Bu-Glu NCA as the first monomer in THF (50 mg/mL). After *ca*. 90 min, complete consumption of NCA was confirmed by FTIR spectroscopy. In order to determine the lengths and dispersities of the first segments, small aliquots (*ca*. 200 µL for end-group analysis (*vide infra*), and *ca*. 100 µL for GPC analysis) were removed. A defined volume of either *t*BuCM-Cys NCA or *t*Bu-Glu NCA in THF (50 mg/mL) as the second monomer was then added to the remaining polymerization solution and allowed to react for *ca*. 120 min. Consumption of the second NCA was confirmed by FTIR spectroscopy and a small aliquot (*ca*. 100 µL) was removed for GPC analysis. The copolypeptides were then precipitated by addition to DI H_2O (50 mL), centrifuged and the supernatant was removed. The block copolypeptides were then washed two additional times with DI H_2O and dried under reduced pressure to yield the products as light brown powders. These products were carried on immediately to deprotection.

General procedure for preparation of statistical copolypeptides using *t*BuCM-Cys NCA and *t*BuGlu-NCA

In a N_2 filled glove box, separate stock solutions of *t*BuCM-Cys NCA and *t*Bu-Glu NCA were prepared in THF at concentrations of 50 mg/mL each. Portions of each solution were combined to obtain the desired comonomer feed ratio. To the resultant comonomer solution was added a defined volume of initiator (20 mg/mL solution of $Co(PMe_3)_4$ in THF) to obtain the desired monomer to initiator ratio. After *ca*. 90 min an aliquot of the polymerization mixture was analyzed by FTIR spectroscopy to determine if consumption of NCA monomers was complete. In order to determine copolymer composition, chain length and dispersity, small aliquots (*ca*. 200 µL for end-group analysis (*vide infra*) and *ca*. 100 µL for GPC analysis) were removed. The copolypeptide was then precipitated by addition to DI H_2O (50 mL), centrifuged and the supernatant was removed. The copolypeptide was then washed two additional times with DI H_2O and dried under reduced pressure to yield the product as a light brown powder. This product was carried on immediately to deprotection.

General procedure for determination of polypeptide chain length using end-group analysis after active chain-ends are reacted with mPEG-NCO

A general procedure for polypeptide preparation was followed. Once the polymerization reaction was determined to be complete by FTIR, in a N_2 filled glove box a solution of α-methoxy-ω-isocyanoethyl-poly(ethylene glycol), mPEG-NCO (MW = 1000 Da, 4 eq per $Co(PMe_3)_4$) in THF was added to a *ca*. 200 µL aliquot of polymerization reaction mixture. The reaction was let stand overnight, and then removed from the glovebox and the reaction was precipitated with water, centrifuged at 3000 rpm and the supernatant was discarded. The pellet was washed 3 times with DI water to remove unconjugated mPEG-NCO, and the resulting pellet was then lyophilized to yield PEG-polypeptide

conjugates as white solids. To determine the molecular weight of the polypeptides (M_n), ^{1}H NMR spectra were obtained in deuterated trifluoroacetic acid (TFA-d) similar to procedures described in literature.[70] The integral of the methylene unit furthest from the backbone was compared to the integral of the polyethylene glycol resonance to obtain polypeptide lengths (see spectral data section and sample data below).

C^{BCM}-PEG: ^{1}H NMR (400 MHz, d-TFA, 25 °C): 5.03 (bs, 67H), 3.96 (bs, 88H), 3.56 (bs, 142H), 3.27 (bs, 134H), 1.66 (bs, 568H).

Polypeptide and copolypeptide deprotection

Protected polypeptides and copolypeptides were dissolved in TFA (20 mg/mL) and allowed to stand for 5 h. The crude reaction mixtures were each transferred to 2 kDa MWCO dialysis bags and dialyzed against aqueous 50 mM $NaHCO_3$ (24 h, 3 dialyzate changes) followed by DI H_2O (24 h, 4 dialyzate changes). The retentates were then lyophilized to provide the deprotected polypeptides and copolypeptides as white fluffy solids.

Poly(S-(carboxymethyl)-L-cysteine·Na)$_{72}$, C^{CM}_{72}

The general procedure for polypeptide deprotection was followed. **C^{BCM}_{72}** and TFA (3 mL) were used to prepare the product, obtained as a white fluffy solid (59 mg, 98% over 2 steps). The FTIR and ^{1}H NMR spectral data for this material were in accordance with those previously reported.[7] ^{1}H NMR (400 MHz, D_2O, 25 °C): 4.49 (bt, J= 7.6 Hz, 1H), 3.15 (bs, 2H), 2.93-2.85 (bm, 1H), 2.82-2.72 (bm, 1H).

Poly(L-glutamate·Na)$_{88}$-*block*-poly(S-(carboxymethyl)-L-cysteine·Na)$_{85}$, $E_{88}C^{CM}_{85}$

The general procedure for polypeptide deprotection was followed. **$E^{B}_{88}C^{BCM}_{85}$** and TFA (3 mL) were used to prepare the product, obtained as a white fluffy solid (50 mg, 96%

over 2 steps). ^{1}H NMR (400 MHz, D_2O, 25 °C): 4.63 (bs, 1H), 4.36 (bs, 1H), 3.30 (bs, 2H), 3.02 (bm, 1H), 2.92 (bm, 1H), 2.36 (bs, 2H), 2.06 (bm, 1H), 1.96 (bm, 1H).

Poly[(L-glutamate·Na)$_{0.49}$-*stat*-poly(S-(carboxymethyl)-L-cysteine·Na)$_{0.51}$]$_{67}$, (E-*s*-C^{CM})$_{67}$

The general procedure for polypeptide deprotection was followed. **(E^{B}-*s*-C^{BCM})$_{67}$** and TFA (3 mL) were used to prepare the product, obtained as a white fluffy solid (53 mg, 90% over 2 steps). ^{1}H NMR (400 MHz, D_2O, 25 °C): 4.47 (bs, 1H), 4.28 (bs, 1H), 3.16 (bs, 2H), 2.87 (bs, 1H), 2.77 (bs, 1H), 2.24 (bs, 2H), 1.96 (bs, 1H), 1.83 (bs, 1H).

Poly(S-(carboxymethyl)-L-cysteine sulfoxide·Na)$_{55}$, C$^{CMO}_{55}$

A sample of **C$^{CM}_{55}$** (40 mg, 0.22 mmol, 1 eq.) was dissolved in DI H_2O (40 mg/mL) and the reaction flask placed in an ice-water bath. Sodium periodate (0.26 mmol, 1.2 eq.) was dissolved in DI water (40 mg/mL), chilled in an ice-water bath, and then slowly added to the polypeptide solution. The reaction was stirred vigorously for 1.5 hours, allowing the ice-water bath to expire. The reaction was then transferred to a 2 kDa MWCO dialysis bag and dialyzed against DI H_2O (48 h, 4 dialyzate changes). The retentate was lyophilized to give a white, fluffy solid (43 mg, 99%). The FTIR and ^{1}H NMR spectral data for this material were in accordance with those previously reported. [2] FTIR (solid state): 1051 (sulfoxide) cm^{-1} ^{1}H NMR (400 MHz, D_2O) δ 4.74 (br s, 1H), 3.78 (br d, 2H), 3.52 – 3.09 (m, 2H).

Procedure for attempted formation of dehydroalanine residues from S-(carboxymethyl)-L-cysteine sulfoxide·Na residues in polypeptides

A sample of **C$^{CMO}_{55}$** was dissolved in 150 mM sodium phosphate buffer (pH 8) at a concentration of 20 mg/mL. The reaction flask was sealed and placed in a heating block

at 37 °C, covered in foil, and stirred for 3 days. The solution was transferred to a 2 kDa MWCO dialysis bag and dialyzed against DI H_2O (48 h, 4 dialyzate changes, dialysis jar covered in foil). The retentate was lyophilized to recover a fluffy, white solid. The degree of conversion to dehydroalanine residues was found to be *ca*. 8% with the remainder being unreacted S-(carboxymethyl)-L-cysteine sulfoxide·Na residues. ^{1}H NMR (400 MHz, D_2O) δ 5.66 (s, 0.08, alkene peak from $\mathbf{A^{DH}}$), 4.81 (s, 1H), 3.76 (d, *J* = 28.7 Hz, 2H), 3.53 – 3.09 (m, 2H).

General procedure for formation of dehydroalanine residues via alkylation of S-(carboxymethyl)-L-cysteine residues in polypeptides

Polypeptides containing S-(carboxymethyl)-L-cysteine residues were dissolved in 150 mM sodium phosphate buffer (pH 8) at a concentration of 20 mg/mL. Iodomethane (10 eq. per S-(carboxymethyl)-L-cysteine residue) was added and reaction flasks were sealed and placed in a heating block at 37 °C, covered in foil and allowed to react for 3 days. The resulting solutions (i.e. block and statistical copolymers) or suspensions (i.e. homopolymers) were mixed with a solution of BHT in dinitrogen sparged DMSO (0.2 mg/mL) to give a final 0.01 mol% ratio of BHT to polypeptide, and then transferred to 2 kDa MWCO dialysis bags and dialyzed against dinitrogen sparged DI H_2O (48 h, 4 dialyzate changes, dialysis jar covered in foil). The retentates were then lyophilized to provide the dehydroalanine containing polypeptides.

Poly(dehydroalanine)$_{72}$, $\mathbf{A^{DH}_{72}}$

The general procedure for formation of dehydroalanine residues via alkylation was followed. $\mathbf{C^{CM}_{72}}$ (58 mg) and methyl iodide (197 µL) were used to prepare the product, obtained as an off white powder (22 mg, 100%). ^{1}H NMR (400 MHz, DMSO-D_6, 25 °C):

9.51 (bs, 1H), 5.80 (bs, 1H), 5.65 (bs, 1H). ^{13}C NMR (CP-MAS, solid state, 10 kHz, 25 °C) sample appears to exist in two different conformations in the solid state: δ 166.4, 161.6, 136.3, 133.6, 122.2, 108.7.

Poly(L-glutamate·Na)$_{88}$-*block*-poly(dehydroalanine)$_{85}$, E$_{88}$A$^{DH}_{85}$

The general procedure for formation of dehydroalanine residues via alkylation was followed. **E$_{88}$C$^{CM}_{85}$** (29 mg) and methyl iodide (53 µL) were used to prepare the product, obtained as a white fluffy solid (16.5 mg, 86%). ^{1}H NMR (400 MHz, D_2O, 25 °C): 5.87 (bs, 0.16H), 5.75 (bs, 0.17H), 4.25 (bs, 1H), 2.46 (bs, 2H), 2.14 (bs, 2H). Note: since resonances for S-(carboxymethyl)-L-cysteine residues were absent in the product, the low integrations observed for alkene peaks of dehydroalanine residues were likely due to aggregation of hydrophobic **A^{DH}** segments in D_2O.

Poly[(L-glutamate·Na)$_{0.49}$-*stat*-poly(dehydroalanine)$_{0.51}$]$_{67}$, (E-*s*-A^{DH})$_{67}$

The general procedure for formation of dehydroalanine residues via alkylation was followed. **(E-*s*-C^{CM})$_{67}$** (20 mg) and methyl iodide (38 µL) were used to prepare the product, obtained as a white fluffy solid (11 mg, 83% conversion of **C^{CM}** to **A^{DH}**) ^{1}H NMR (400 MHz, D_2O, 25 °C): 5.60 (bm, 1.1 H), 4.26 (bs, 1H), 4.25 (bs, 1H), 2.33 (bs, 2H), 2.00 (bm, 2H). Note: due to the presence of resonances for S-(carboxymethyl)-L-cysteine residues, the low integration observed for the alkene peaks was due to incomplete conversion to **A^{DH}** (see NMR Spectra).

General procedure for modification of A^{DH} polypeptides

Dha containing polypeptides were dissolved in a defined volume of 150 mM, pH 8 phosphate buffer (Note: a mixture of 1:1 DMSO:buffer was used to fully solubilize **A^{DH}**). The desired small molecule thiol or amine reagent (5 eq. per Dha residue) was added

directly if a liquid or as a defined volume of a 50 mg/mL solution if a solid so that the final reaction volume had a polypeptide concentration of 10 mg/mL. The reactions were sealed and allowed to stir for 16 hours. Reactions were then transferred to 2 kDa MWCO dialysis bags and dialyzed against DI H_2O (48 h, 4 dialyzate changes). The retentates were then lyophilized to provide the modified polypeptides.

Poly(L-glutamate·Na)$_{88}$-*block*-poly(2-[2-(2-methoxyethoxy)ethoxy]ethyl-*rac*-cysteine)$_{85}$, E$_{88}$(*rac*-C^{EG3})$_{85}$

The general procedure for modification of **A^{DH}** polypeptides was followed. **E$_{88}$A$^{DH}_{85}$** (3 mg) and 2-[2-(2-methoxyethoxy)ethoxy]ethanethiol (mEG$_3$SH, 13 µL) were used to prepare the product, obtained as a white fluffy solid (6 mg, 100%). ^{1}H NMR (400 MHz, D_2O, 25 °C): 4.61 (bs, 1), 4.16 (bs, 1H), 3.64 (bm, 14H), 3.39 (s, 3H), 3.11 (bs, 2H), 2.98 (bs, 1H), 2.83 (bs, 1H), 2.58 (bs, 2H), 2.23 (bs, 2H).

Poly(L-glutamate·Na)$_{88}$-*block*-poly(β-(2-hydroxyethylamino)-*rac*-alanine)$_{85}$, E$_{88}$(*rac*-A^{HEA})$_{85}$ The general procedure for modification of **A^{DH}** polypeptides was followed. **E$_{88}$A$^{DH}_{85}$** (3 mg) and ethanolamine (5 µL) were used to prepare the product, obtained as a white fluffy solid (4 mg, 98%). ^{1}H NMR (400 MHz, D_2O, 25 °C): 4.20 (bs, 1H), 3.74 (bs, 1H), 3.67 (bt, J= 5.2 Hz, 1H), 3.53 (bs, 1H), 3.34 (bs, 1H), 3.13 (bs, 2H), 3.00 (bt, 1H), 2.58 (bt, J=5.2 Hz, 1H), 2.17 (bs, 2H), 1.92 (bs, 1H), 1.81 (bs, 1H).

Poly(L-glutamate·Na)$_{88}$-*block*-poly(S-(2-hydroxyethyl)-*rac*-cysteine)$_{85}$, E$_{88}$(*rac*-C^{HE})$_{85}$

The general procedure for modification of **A^{DH}** polypeptides was followed. **E$_{88}$A$^{DH}_{85}$** (3 mg) and β-mercaptoethanol (5 µL) were used to prepare the product, obtained as a white fluffy solid (4.3 mg, 99%). ^{1}H NMR (400 MHz, D_2O, 25 °C): 4.48 (bs, 1H), 4.20

(bs, 1H), 3.68 (bt, J=5.2 Hz, 1H), 3.63 (bt, J=5.6 Hz, 1H), 3.00 (bm, 2H), 2.86 (bs, 1H), 2.64 (bs, 2H), 2.18 (bs, 2H), 1.90 (bs, 1H), 1.81 (bs, 1H).

Poly(L-glutamate·Na)$_{88}$-*block*-poly(S-(*b*-D-glucosyl)-*rac*-cysteine)$_{85}$, E$_{88}$(*rac*-C^{GLC})$_{85}$ The general procedure for modification of **A^{DH}** polypeptides was followed. **E$_{88}$A$^{DH}_{85}$** (3 mg) and 1-thio-β-D-glucopyranoside sodium salt (β-D-glcSH, 283 μL) were used to prepare the product, obtained as a white fluffy solid (5.3 mg, 95%). ^{1}H NMR (400 MHz, D_2O, 25 °C): 4.67 (bm, 2H), 4.34 (bs, 1H), 3.94 (bm, 1H), 3.75 (bs, 1H), 3.59-2.95 (bm, 6H), 2.30 (bs, 2H), 2.03 (bs, 1H), 1.93 (bs, 1H).

poly(2-[2-(2-methoxyethoxy)ethoxy]ethyl-*rac*-cysteine)$_{72}$, (*rac*-C^{EG3})$_{72}$ The general procedure for modification of **A^{DH}** polypeptides was followed. **A$^{DH}_{72}$** (3 mg) and mEG$_3$SH (48 μL) were used to prepare the product, obtained as a white fluffy solid (11 mg, 86%). ^{1}H NMR (400 MHz, DMSO-D_6, 25 °C): 8.37 (bs, 1H), 4.55 (bs, 1H), 3.50 (bm, 12H), 3.49 (bs, 2H), 3.24 (bs, 3H), 2.92 (bs, 1H), 2.65 (bs, 3H).

Poly[(L-glutamate·Na)$_{0.49}$-*stat*-(2-[2-(2-methoxyethoxy)ethoxy]ethyl-*rac*-cysteine)$_{0.51}$]$_{67}$, [E-*s*-(*rac*-C^{EG3})]$_{67}$ The general procedure for formation of **A^{DH}** polypeptides was followed. **(E-*s*-A^{DH})$_{67}$** (3 mg) and mEG$_3$SH (39 μL) were used to prepare the product, obtained as a white fluffy solid (5.5 mg, 89%) ^{1}H NMR (400 MHz, D_2O, 25 °C): 4.59 (bs, 1 H), 4.40 (bs, 1H), 3.70 (bs, 12H), 3.39 (bs, 3H), 3.13 (bs, 2H), 3.01 (bs, 2H), 2.50 (bs, 2H), 2.17 (bs, 1H), 2.02 (bs, 1H).

3.5.4 Analysis of A^{DH} properties

Fluorescence spectroscopy of polypeptides

A sample of **A$^{DH}_{68}$** or **A$_{53}$** was dissolved in 0.1 μm filtered HFIP at 1.0 mg/mL before heating to 40 ^{o}C with stirring for 10 minutes until the sample appeared clear. Samples

were then diluted to 0.1 mg/mL in filtered HFIP and passed through a 0.1 μm pore size PTFE syringe filter before measuring fluorescence emission spectra (excitation wavelength: 365 nm) at ambient temperature.

Dynamic light scattering (DLS) analysis of polypeptides

A sample of $\mathbf{A^{DH}_{68}}$ or $\mathbf{A_{53}}$ was dissolved in 0.1 μm filtered HFIP at 1.0 mg/mL before heating to 40 ^{o}C with stirring for 10 minutes until the sample appeared clear. Samples were then diluted to 0.1 mg/mL in filtered HFIP and passed through a 0.1 μm pore size PTFE syringe filter before analysis using a Malvern Zetasizer Nano ZS at 23 ^{o}C.

3.5.5 Spectral Data

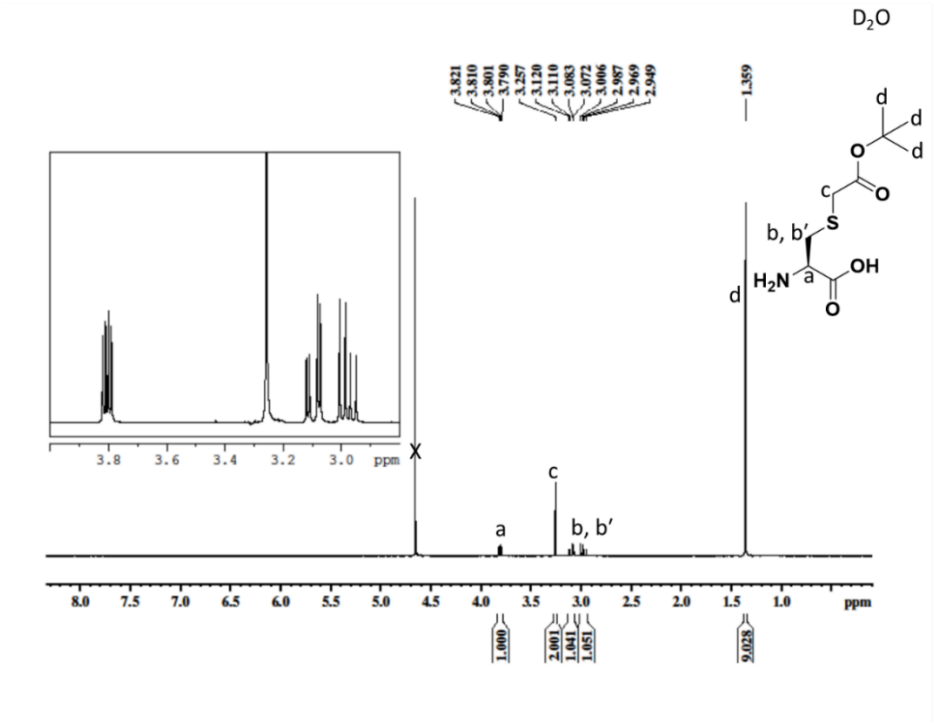

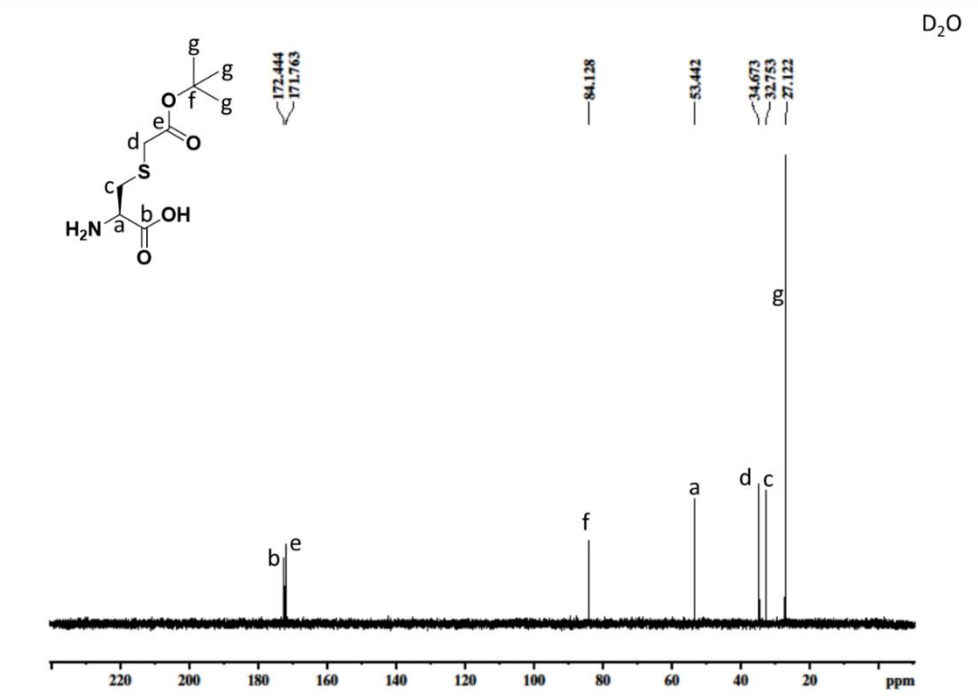

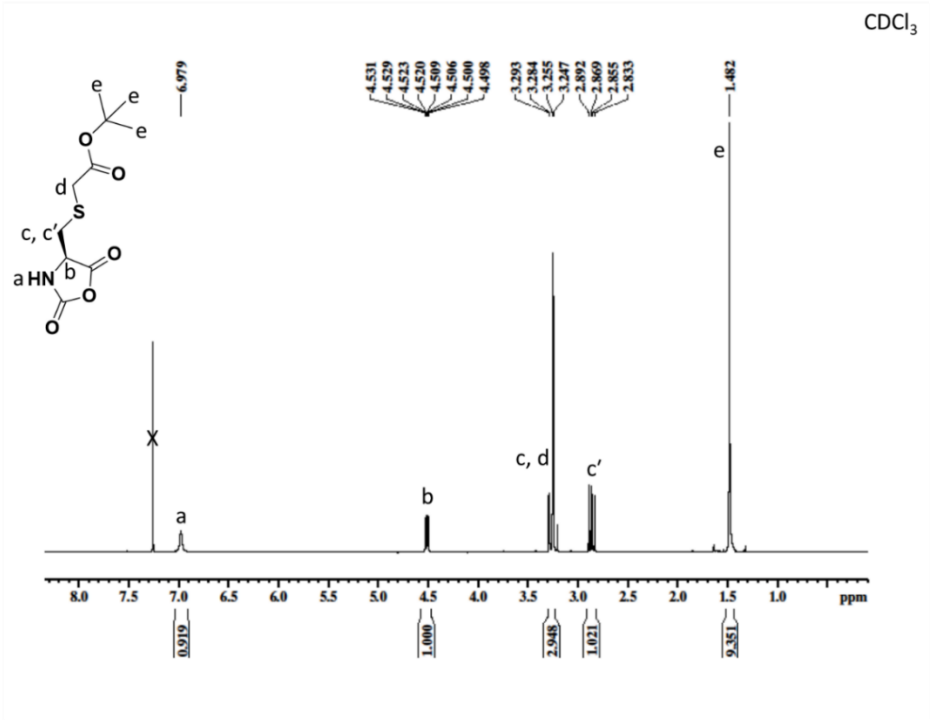
CDCl3
6.979
4.531
4.529
4.523
4.520
4.509
4.506
4.500
4.498
3.293
3.284
3.255
3.247
2.892
2.869
2.855
2.833
1.482
e
d
S
c, c′
a HN
b
O
X
a
b
c, d
c′
8.0
7.5
7.0
6.5
6.0
5.5
5.0
4.5
4.0
3.5
3.0
2.5
2.0
1.5
1.0
ppm
0.919
1.000
2.948
1.021
9.351

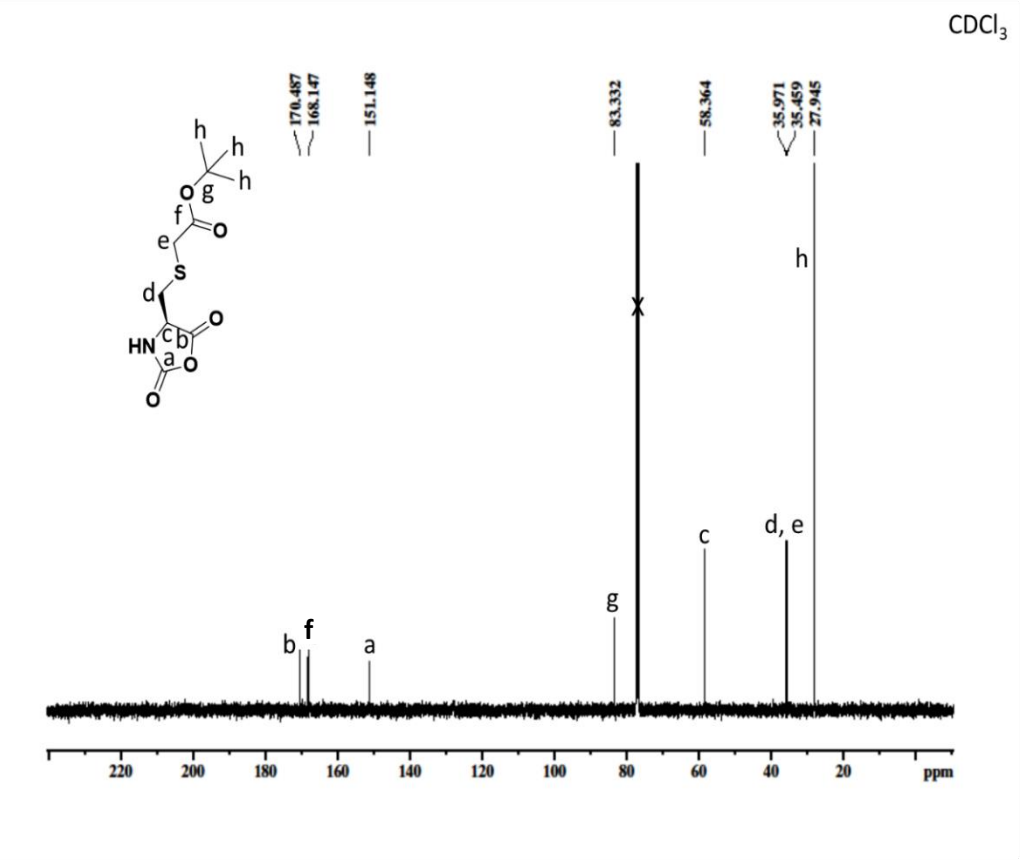
CDCl3
170.487
168.147
151.148
83.332
58.364
35.971
35.459
27.945
h
g
f
e
d
c
b
HN
a
X
d, e
c
g
b
f
a
220
200
180
160
140
120
100
80
60
40
20
ppm

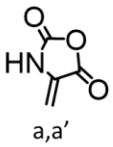
O
HN
O
O
a,a'

d-TFA

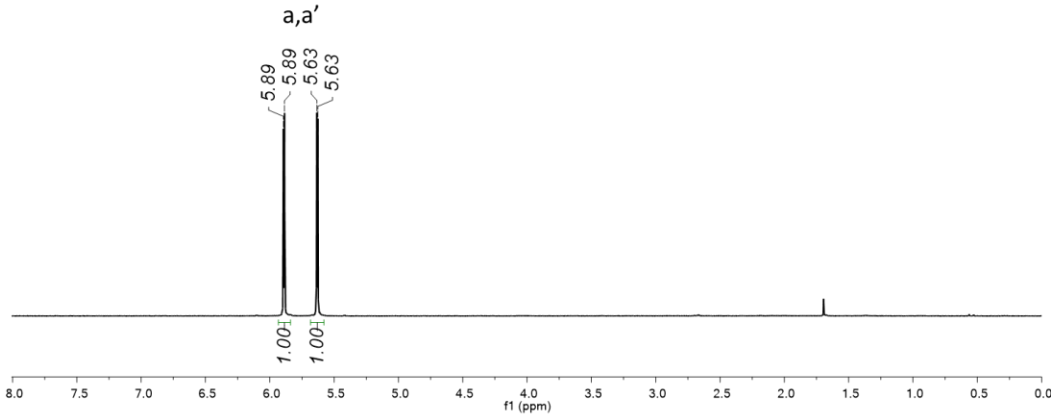
a,a'
5.89
5.89
5.63
5.63
1.00
1.00
8.0
7.5
7.0
6.5
6.0
5.5
5.0
4.5
4.0
3.5
3.0
2.5
2.0
1.5
1.0
0.5
0.0
f1 (ppm)

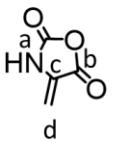
O
a
HN
c
O
b
O
d

d-TFA

160.61
153.04
170
165
160
155
150
f1 (ppm)
a
b
c
d
160.61
153.04
130.18
104.29
220
210
200
190
180
170
160
150
140
130
120
110
100
90
80
70
60
50
40
30
f1 (ppm)

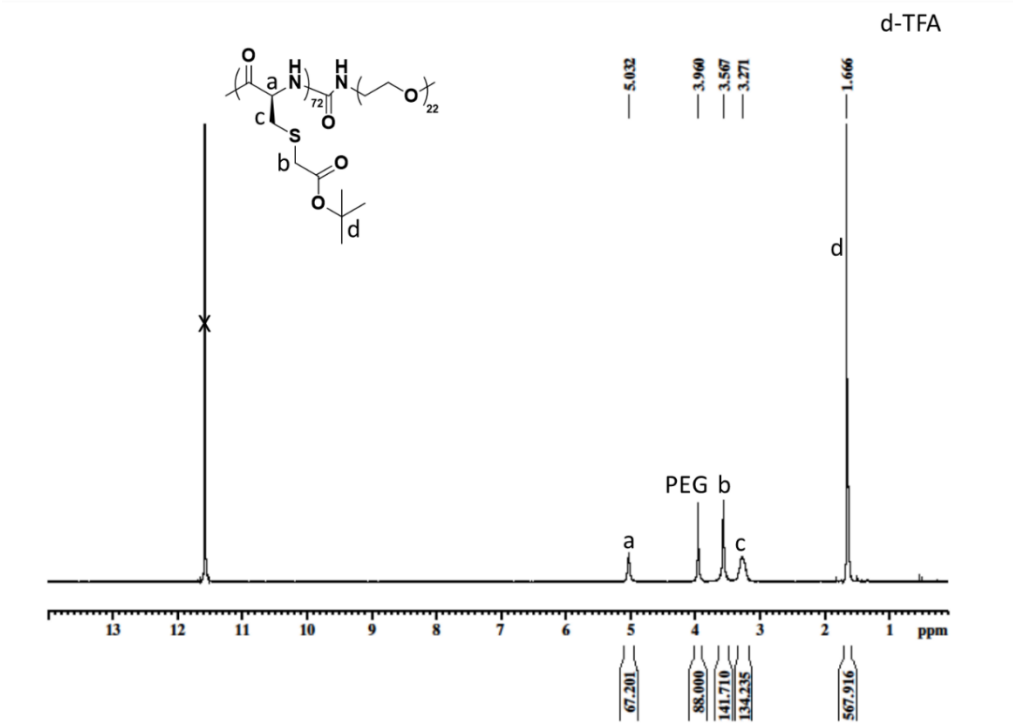
d-TFA
5.032
3.960
3.567
3.271
1.666
PEG
a
b
c
d
X
13 12 11 10 9 8 7 6 5 4 3 2 1 ppm
67.201
88.000
141.710
134.235
567.916

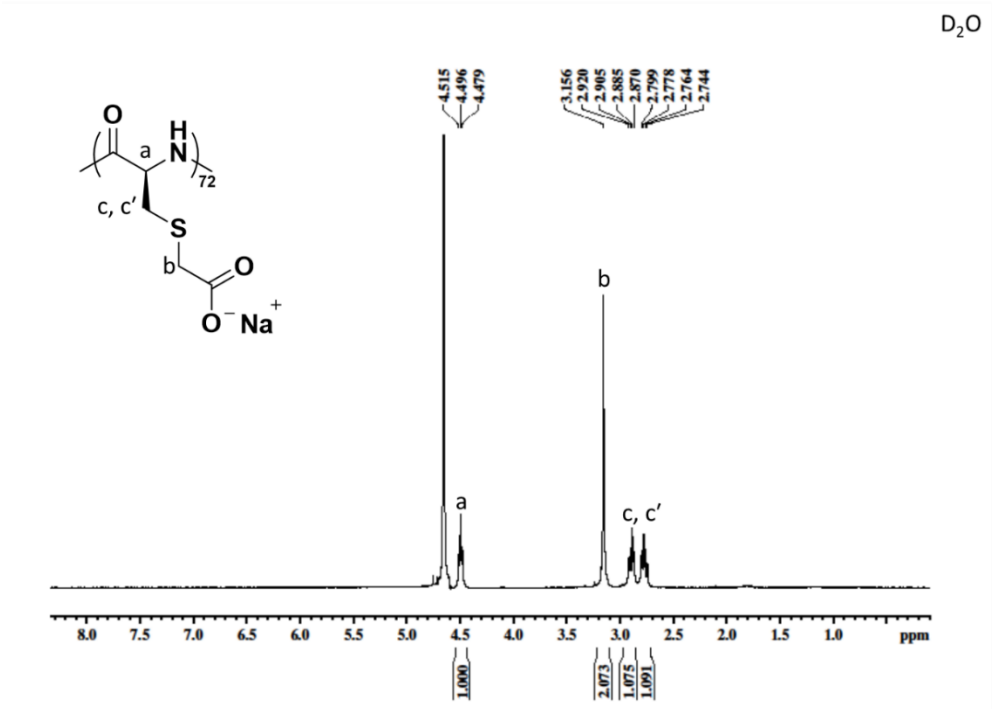
D2O
4.515
4.496
4.479
3.156
2.920
2.905
2.885
2.870
2.799
2.778
2.764
2.744
a
b
c, c′
8.0 7.5 7.0 6.5 6.0 5.5 5.0 4.5 4.0 3.5 3.0 2.5 2.0 1.5 1.0 ppm
1.000
2.073
1.075
1.091

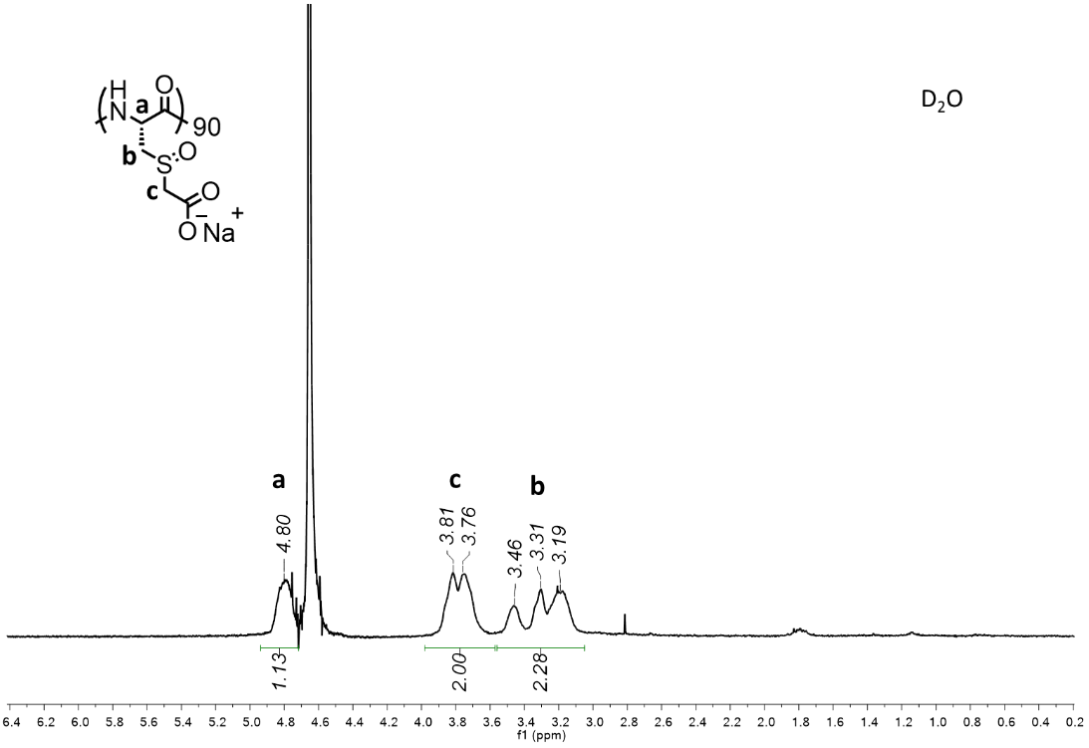
D2O
a
c
b
4.80
3.81
3.76
3.46
3.31
3.19
1.13
2.00
2.28
f1 (ppm)

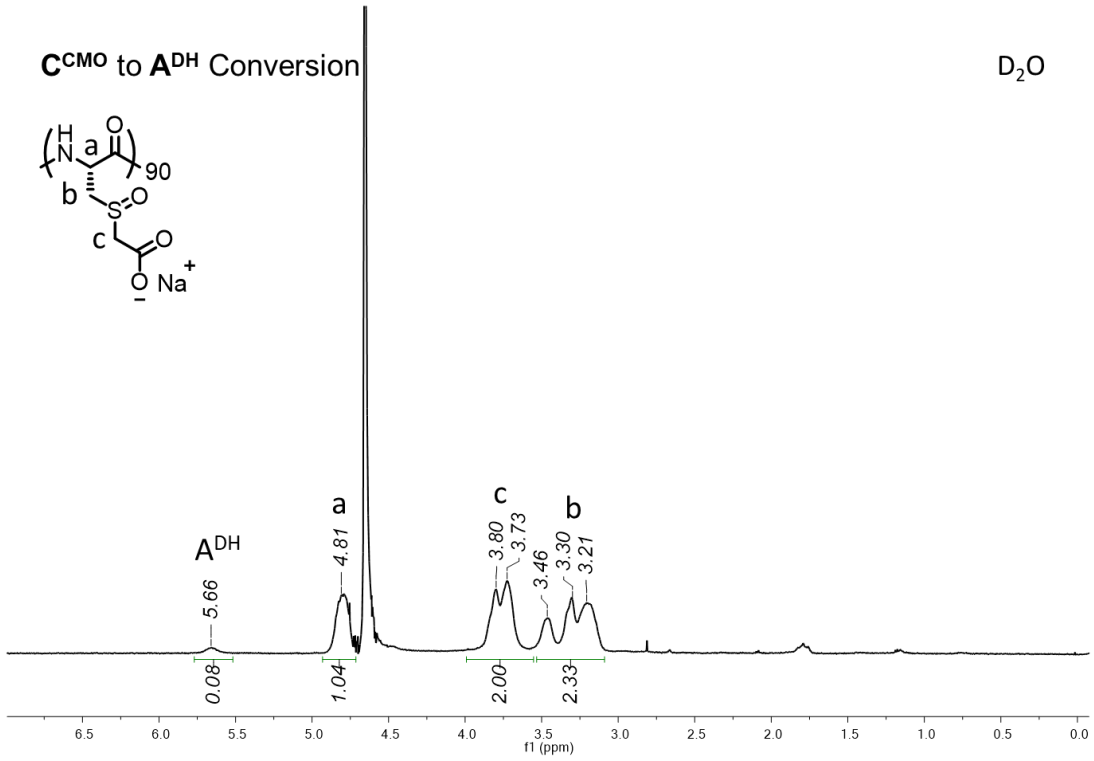
C^CMO to A^DH Conversion
D2O
A^DH
a
c
b
5.66
4.81
3.80
3.73
3.46
3.30
3.21
0.08
1.04
2.00
2.33
f1 (ppm)

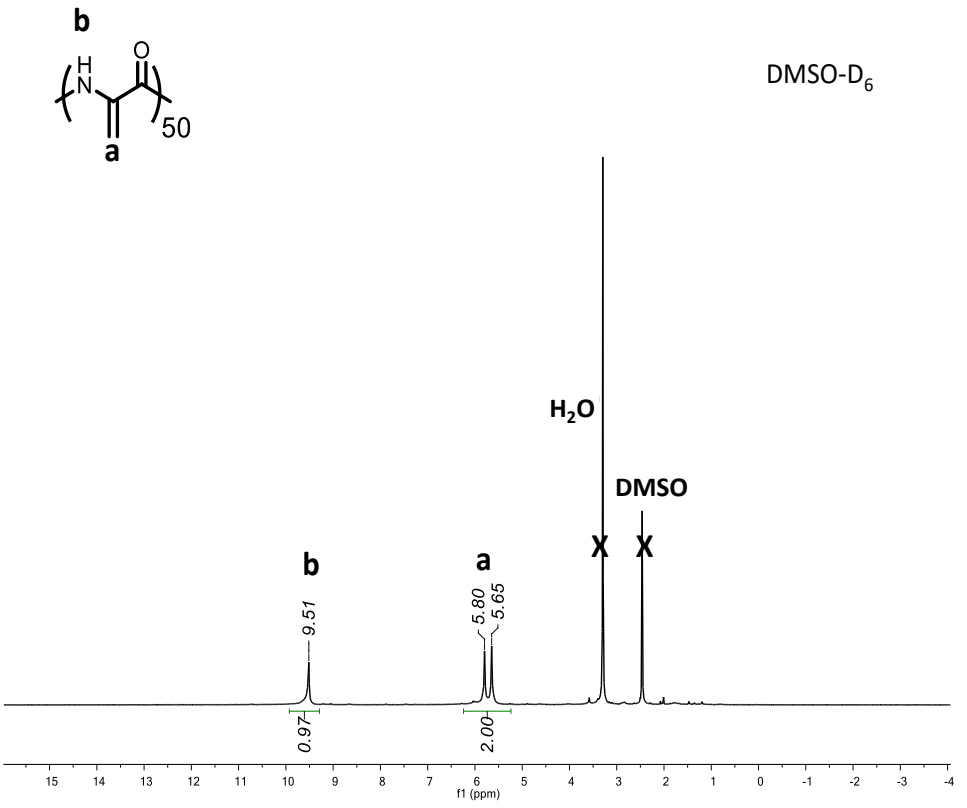
b
a
50
DMSO-D6
H2O
DMSO
b
a
9.51
5.80
5.65
0.97
2.00
f1 (ppm)

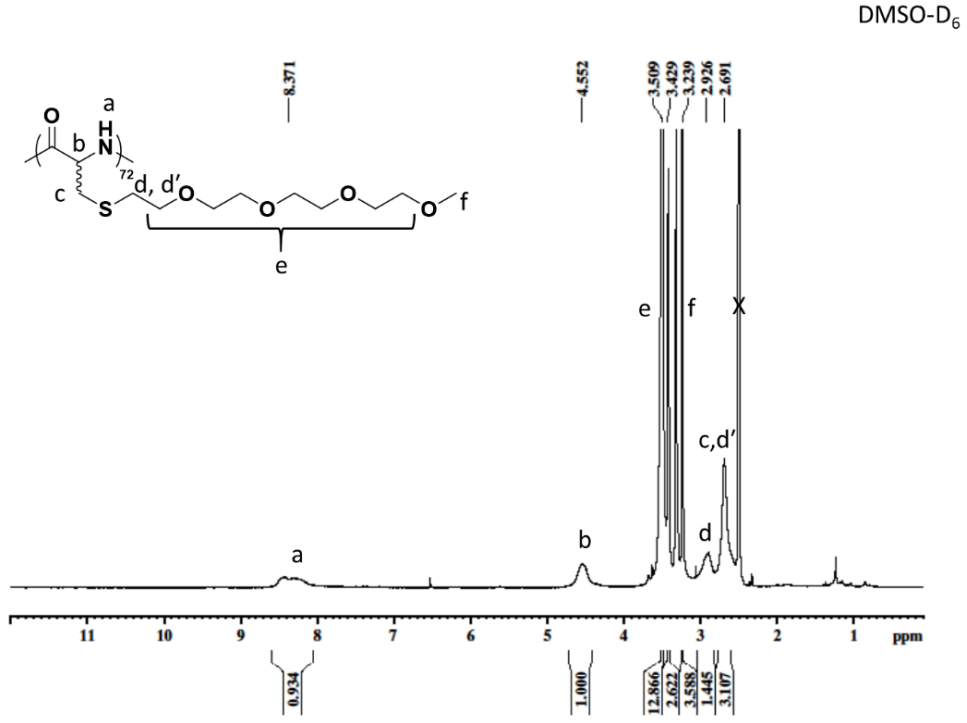
DMSO-D6
8.371
4.552
3.509
3.429
3.239
2.926
2.691
a
b
c
d, d'
e
f
X
c,d'
d
ppm
0.934
1.000
12.866
2.622
3.588
1.445
3.107

D_2O

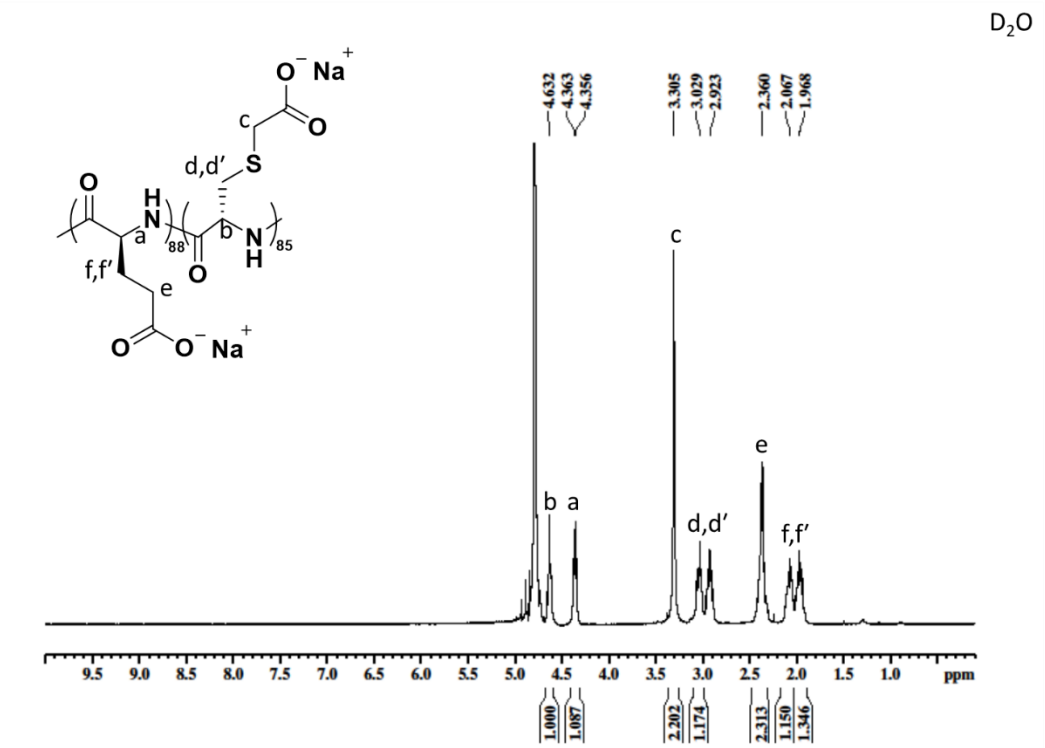
4.632
4.363
4.356
3.305
3.029
2.923
2.360
2.067
1.968
c
b a
d,d′
e
f,f′
9.5 9.0 8.5 8.0 7.5 7.0 6.5 6.0 5.5 5.0 4.5 4.0 3.5 3.0 2.5 2.0 1.5 1.0 ppm
1.000
1.087
2.202
1.174
2.313
1.150
1.346

D_2O

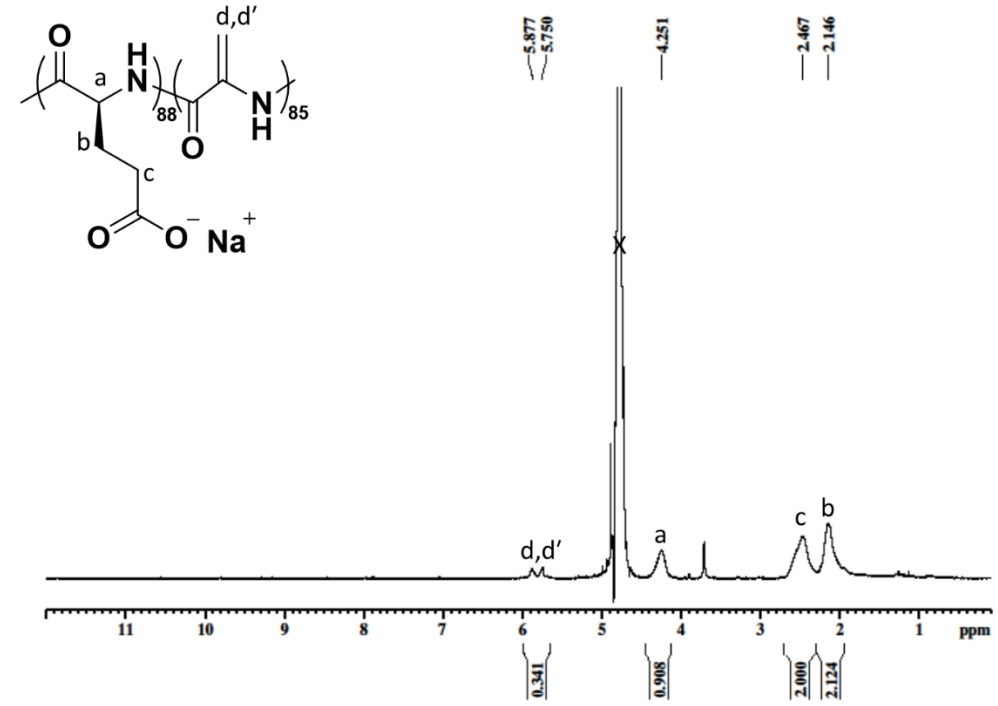
5.877
5.750
4.251
2.467
2.146
d,d′
a
c
b
11 10 9 8 7 6 5 4 3 2 1 ppm
0.341
0.908
2.000
2.124

D_2O

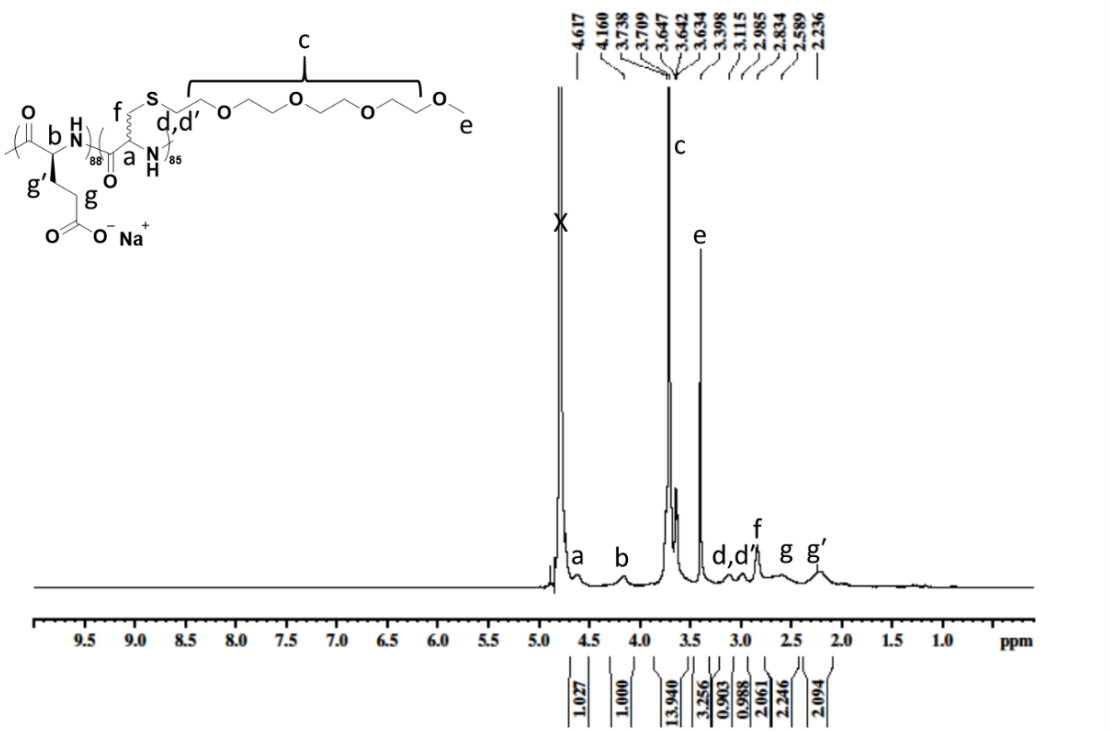
4.617
4.160
3.738
3.709
3.647
3.642
3.634
3.398
3.115
2.985
2.834
2.589
2.236
c
e
X
a
b
d,d′
f
g
g′
9.5 9.0 8.5 8.0 7.5 7.0 6.5 6.0 5.5 5.0 4.5 4.0 3.5 3.0 2.5 2.0 1.5 1.0 ppm
1.027
1.000
13.940
3.256
0.903
0.988
2.061
2.246
2.094

D_2O

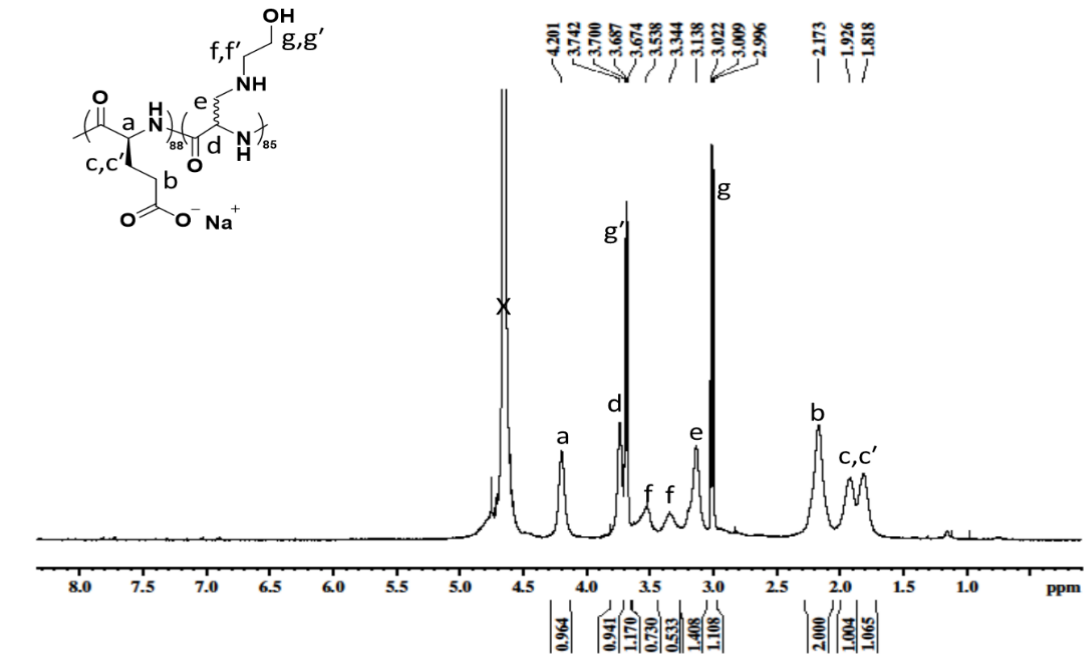
4.201
3.742
3.700
3.687
3.674
3.538
3.344
3.138
3.022
3.009
2.996
2.173
1.926
1.818
X
a
d
g′
g
e
f
f
b
c,c′
8.0 7.5 7.0 6.5 6.0 5.5 5.0 4.5 4.0 3.5 3.0 2.5 2.0 1.5 1.0 ppm
0.964
0.941
1.170
0.730
0.533
1.408
1.108
2.000
1.004
1.065

D_2O

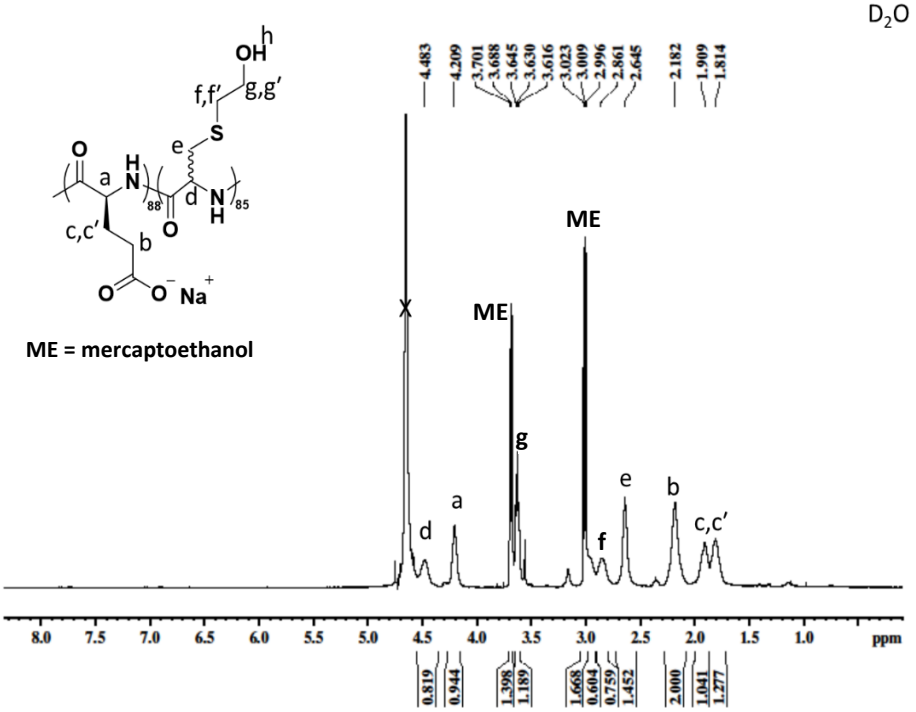

D_2O

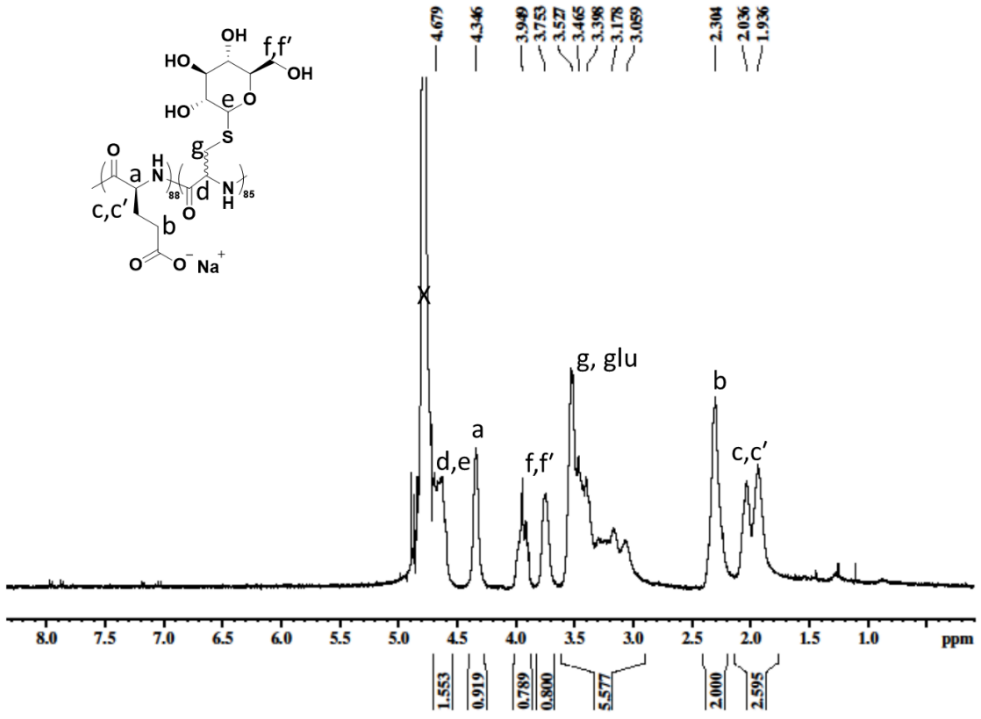

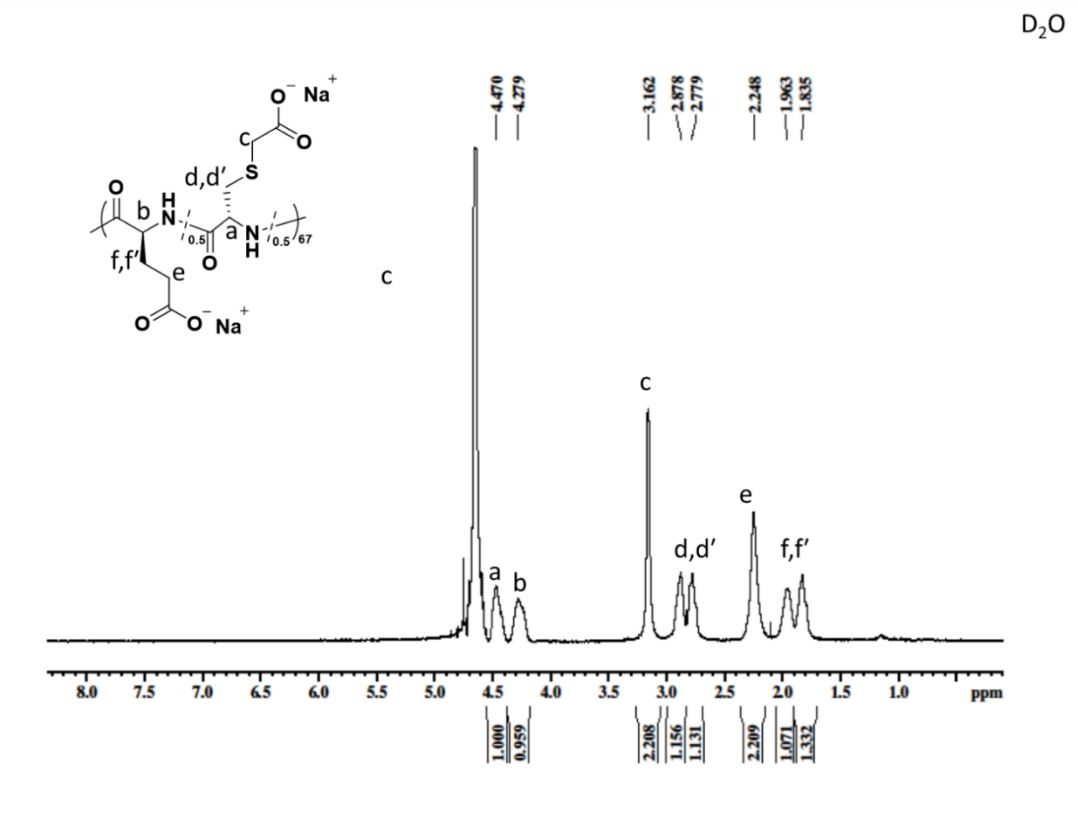
D2O
4.470
4.279
3.162
2.878
2.779
2.248
1.963
1.835
c
a
b
c
d,d′
e
f,f′
8.0
7.5
7.0
6.5
6.0
5.5
5.0
4.5
4.0
3.5
3.0
2.5
2.0
1.5
1.0
ppm
1.000
0.959
2.208
1.156
1.131
2.209
1.071
1.332

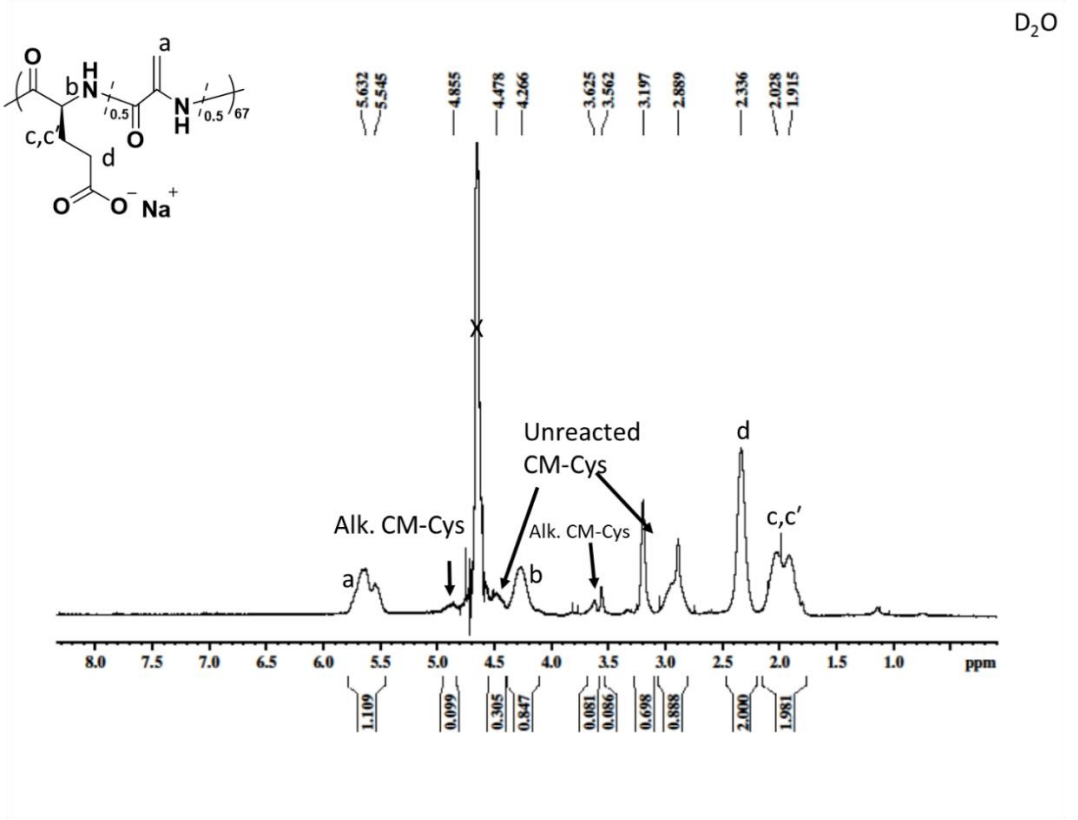
D2O
5.632
5.545
4.855
4.478
4.266
3.625
3.562
3.197
2.889
2.336
2.028
1.915
X
Unreacted
CM-Cys
Alk. CM-Cys
Alk. CM-Cys
a
b
d
c,c′
8.0
7.5
7.0
6.5
6.0
5.5
5.0
4.5
4.0
3.5
3.0
2.5
2.0
1.5
1.0
ppm
1.109
0.099
0.305
0.847
0.081
0.086
0.698
0.888
2.000
1.981

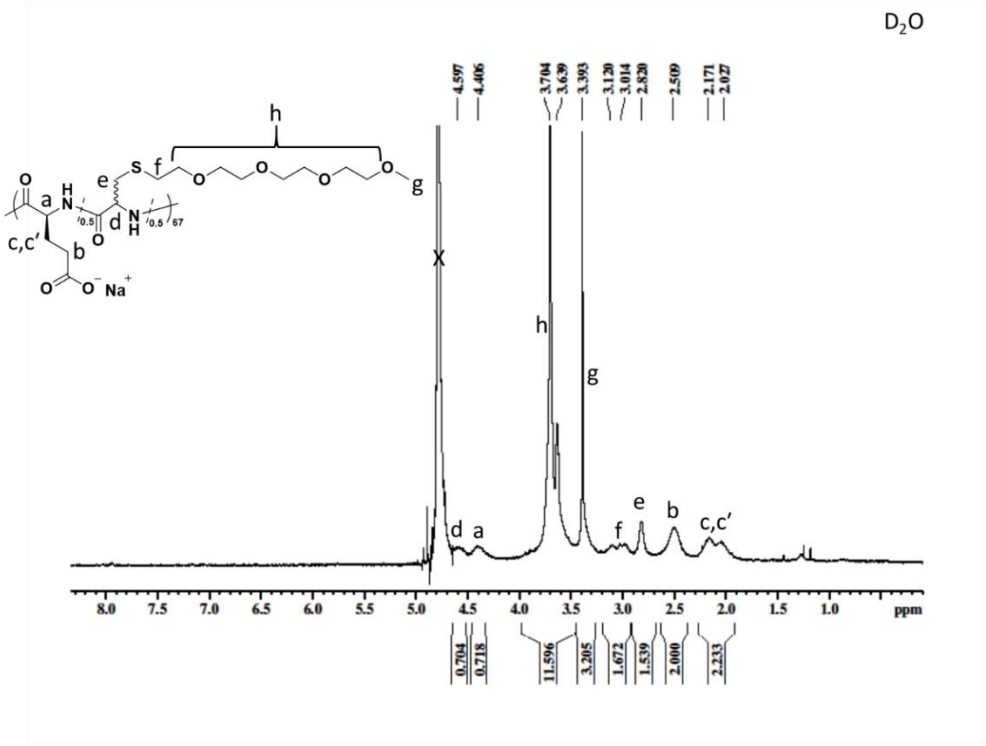
D2O
4.597
4.406
3.704
3.639
3.393
3.120
3.014
2.820
2.509
2.171
2.027
h
s
f
e
g
a
d
c,c′
b
X
h
g
d
a
f
e
b
c,c′
8.0
7.5
7.0
6.5
6.0
5.5
5.0
4.5
4.0
3.5
3.0
2.5
2.0
1.5
1.0
ppm
0.704
0.718
11.596
3.205
1.672
1.539
2.000
2.233

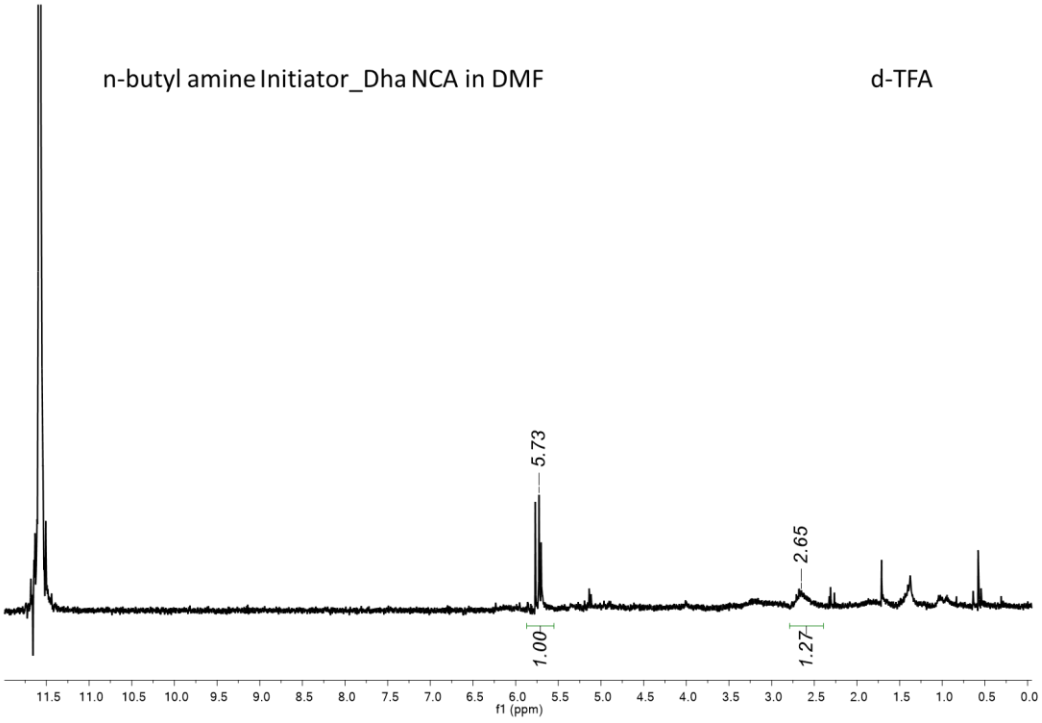
n-butyl amine Initiator_Dha NCA in DMF
d-TFA
5.73
2.65
1.00
1.27
11.5
11.0
10.5
10.0
9.5
9.0
8.5
8.0
7.5
7.0
6.5
6.0
5.5
5.0
4.5
4.0
3.5
3.0
2.5
2.0
1.5
1.0
0.5
0.0
f1 (ppm)

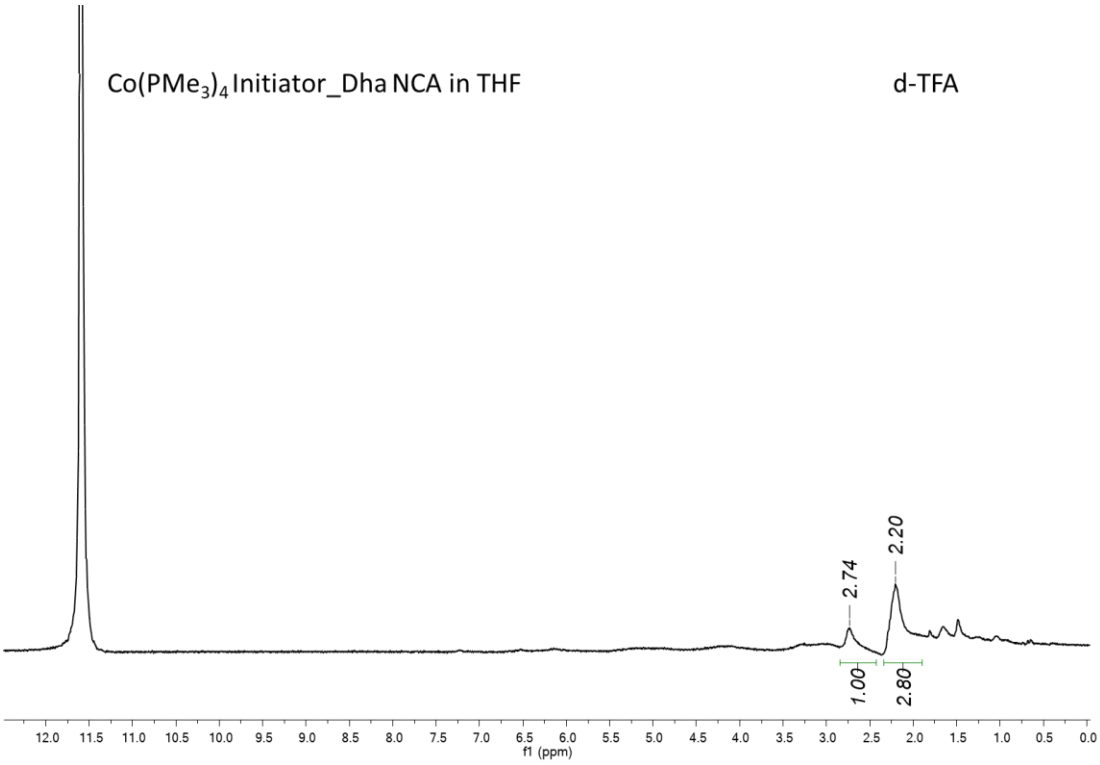
Co(PMe3)4 Initiator_Dha NCA in THF
d-TFA
2.74
2.20
1.00
2.80
12.0 11.5 11.0 10.5 10.0 9.5 9.0 8.5 8.0 7.5 7.0 6.5 6.0 5.5 5.0 4.5 4.0 3.5 3.0 2.5 2.0 1.5 1.0 0.5 0.0
f1 (ppm)

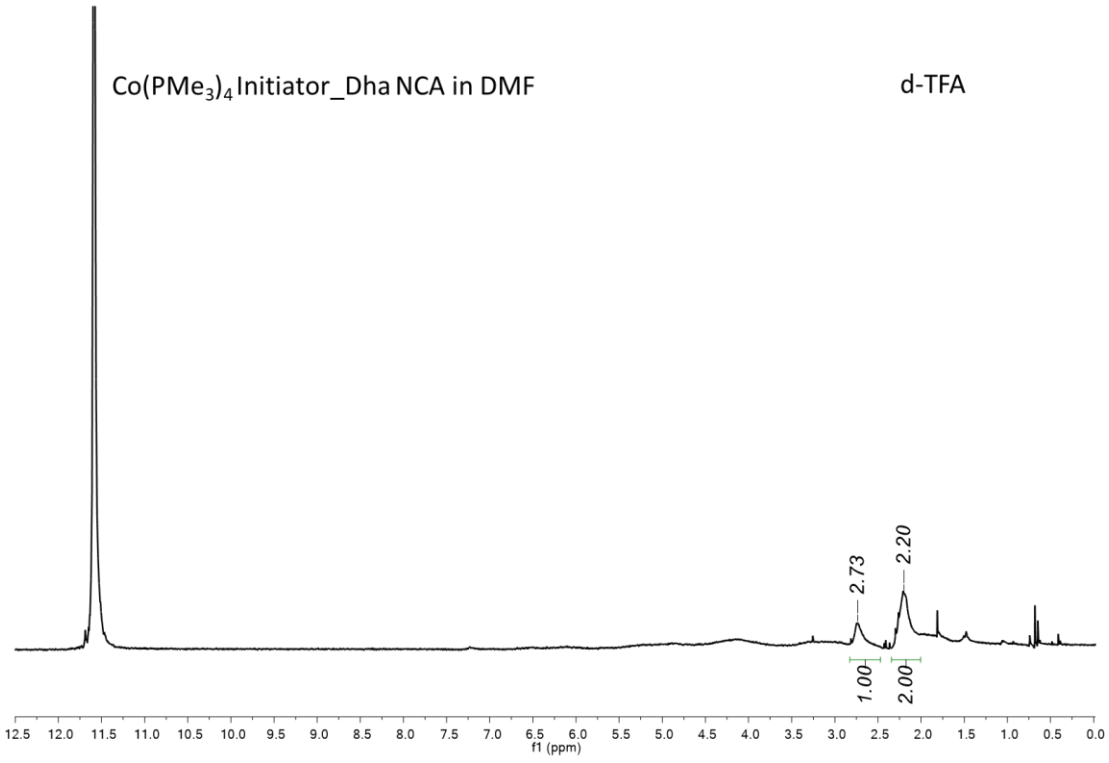
Co(PMe3)4 Initiator_Dha NCA in DMF
d-TFA
2.73
2.20
1.00
2.00
12.5 12.0 11.5 11.0 10.5 10.0 9.5 9.0 8.5 8.0 7.5 7.0 6.5 6.0 5.5 5.0 4.5 4.0 3.5 3.0 2.5 2.0 1.5 1.0 0.5 0.0
f1 (ppm)

3.6 References

1) Schmidt, U., Lieberknecht, A.; Wild, J. Didehydroamino Acids (DDAA) and didehydropeptides (DDP). *Synthesis* **1988**, 159-172.

2) Humphrey, J. M.; Chamberlin, A. R. Chemical synthesis of natural product peptides: Coupling methods for the incorporation of noncoded amino acids into peptides. *Chem. Rev*. **1997**, *97*, 2243-2266.

3) Palmer, D. E.; Pattaroni, C.; Nunami, K.; Chadha, R. K.; Goodman, M.; Wakamiya, T.; Fukase, K.; Horimoto, S.; Kitazawa, M.; Fujita, H.; Kubo, A.; Shiba, T. Effects of dehydroalanine on peptide conformations. *J. Am. Chem. Soc.* **1992**, *114*, 5634–5642.

4) Crisma, M.; Formaggio, F.; Toniolo, C.; Yoshikawa, T.; Wakamiya, T. Flat peptides. *J. Am. Chem. Soc.* **1999**, *121,* 3272-3278.

5) Fu, S-C. J.; Greenstein, J. P. Saturation of acetyldehydroalanine with benzylamine. *J. Am. Chem. Soc.* **1955**, *77,* 4412-4413.

6) Strumeyer, D. H.; White, W. N.; Koshland Jr., D. E. Role of serine in chymotrypsin action. Conversion of the active serine to dehydroalanine. *Proc. Nat. Acad. Sci. (USA)* **1963**, *50*, 931-935.

7) Zhu, Y.; van der Donk, W. A. Convergent synthesis of peptide conjugates using dehydroalanines for chemoselective ligations. *Org. Lett.* **2001**, *3,* 1189-1192.

8) Ferreira, P. M. T.; Maia, H. L. S.; Monteiro, L. S.; Sacramento, J. Michael addition of thiols, carbon nucleophiles and amines to dehydroamino acid and dehydropeptide derivatives. *J. Chem. Soc*. *Perkin Trans. 1* **2001**, 3167–3173.

9) Burrage, S.; Raynham, T.; Williams, G.; Essex, J. W.; Allen, C.; Cardno, M.; Swali, V.; Bradley. M. Biomimetic synthesis of lantibiotics. *Chem. Eur. J.* **2000**, *6*, 1455-1466.

10) Chalker, J. M.; Gunnoo, S. B.; Boutureira, O.; Gerstberger, S. C.; Fernández-González, M.; Bernardes, G. J. L.; Griffin, L.; Hailu, H.; Schofield, C. J.; Davis, B. G. Methods for converting cysteine to dehydroalanine on peptides and proteins. *Chem. Sci.* **2011**, *2*, 1666-1676.

11) Burrage, S. A.; Raynham, T.; Bradley, M. A highly efficient route to dehydroalanine containing peptides. *Tetrahedron Lett.* **1998**, *39*, 2831-2834.

12) Zhu, Y.; Gieselman, M. D.; Zhou, H.; Averin, O.; van der Donk, W. A. Biomimetic studies on the mechanism of stereoselective lanthionine formation. *Org. Biomol. Chem.* **2003**, *1,* 3304-3315.

13) Seebeck, F. P.; Szostak, J. W. Ribosomal synthesis of dehydroalanine-containing peptides. *J. Am. Chem. Soc.* **2006**, *128,* 7150-7151.

14) Morrison, P. M.; Foley, P. J.; Warriner, S. L.; Webb, M. E. Chemical generation and modification of peptides containing multiple dehydroalanines. *Chem. Commun.* **2015**, *51*, 13470-13473.

15) Sakakibara, S. Studies on dehydroalanine derivatives. I. Synthesis of N-carboxy-dehydroalanine anhydride. *Bull Chem. Soc. Jpn.* **1959**, *32*, 13-17.

16) Sakakibara, S. Studies on dehydroalanine derivatives. II. Synthesis of polydehydroalanine. *Bull Chem. Soc. Jpn.* **1960**, *33*, 814-818.

17) Sakakibara, S. Studies on dehydroalanine derivatives. V. Radical polymerization of N-carboxy-dehydroalanine anhydride and of N-phthaloyl-dehydroalanine. Synthesis of a new amphoteric polymer. *Bull Chem. Soc. Jpn.* **1961**, *34*, 174-177.

18) Nandel, F. S.; Malik, N.; Singh, B.; Jain, D. V. S. Conformational structure of peptides containing dehydroalanine: Formation of β-bend ribbon structure. *Int. J. Quantum Chem.* **1999**, *72*, 15-23.

19) Zanuy, D.; Casanovas, J.; Alemán, C. The conformation of dehydroalanine in short homopeptides: molecular dynamics simulations of a 6-residue chain. *Biophys. Chem*. **2002**, *98*, 301-312.

20) Deming, T. J. Synthesis and self-assembly of well-defined block copolypeptides via controlled NCA polymerization. *Adv. Polymer Sci.* **2013**, *262*, 1-37.

21) Deming, T. J. Cobalt and iron initiators for the controlled polymerization of α-amino acid-N-carboxyanhydrides. *Macromolecules* **1999**, *32*, 4500-4502.

22) Walter, R.; Roy, J. Selenomethionine, a potential catalytic antioxidant in biological systems. *J. Org. Chem.* **1971**, *36*, 2561-2563.

23) Rich, D. H.; Tam, J. P.; Mathiaparanam, P.; Grant, J. A.; Mabuni, C. General synthesis of didehydroamino-acids and peptides. *J. Chem. Soc. Chem. Commun.* **1974**, *0*, 897-898.

24) Rich, D. H.; Tam, J. P. Synthesis of didehydropeptides from peptides containing 3-alkylthio-amino acid residues. *Tetrahedron Lett.* **1975**, *16*, 211-212.

25) Rich, D. H.; Tam, J. P. Synthesis of dehydroamino acids and peptides by dehydrosulfenylation. Rate enhancement using sulfenic acid trapping agents. *J. Org. Chem.* **1977**, *42*, 3815-3820.

26) Nomoto, S.; Sano, A.; Shiba, T. A new synthetic method for dehydroalanine peptides through hofmann degradation of α,β-diaminopropionyl residue. *Tetrahedron Lett.* **1979**, *20*, 521-522.

27) Miller, M. J. Isourea-mediated preparation of dehydro amino acids. *J. Org. Chem.* **1980**, *45*, 3131-3132.

28) Okeley, N. M.; Zhu, Y.; van der Donk, W. A. Facile chemoselective synthesis of dehydroalanine-containing peptides. *Org. Lett.* **2000**, *2*, 3603-3606.

29) You, Y. O.; Levengood, M. R.; Ihnken, L. A. F.; Knowlton, A. K.; van der Donk, W. A. Lacticin 481 synthetase as a general serine/threonine kinase. *ACS Chem. Biol.* **2009**, *4*, 379-385.

30) Ramapanicker, R.; Mishra, R.; Chandrasekaran, S. An improved procedure for the synthesis of dehydroamino acids and dehydropeptides from the carbonate derivatives of serine and threonine using tetrabutylammonium fluoride. *J. Peptide Sci.* **2010**, *16*, 123-125.

31) Deming, T. J. Synthesis of side-chain modified polypeptides. *Chem. Rev.* **2016**, *116*, 786–808.

32) Hayakawah, T.; Nishi, H.; Noguchi, J.; Ikeda, S.; Yamashita, T.; Isemeura, T. The synthesis of protein analogue. XXIII-XXV. XXIV. The syntheses of ω-benzyl esters of α-amino-α, co-dicarboxylic acids and the properties of their polymers. *Nippon kagaku zassi* **1961**, *82*, 601–604.

33) Harrap, B. S.; Stapleton, I. W. Poly-S-carbobenzoxymethyl-l-cysteine: A model system for the denaturation of non-helical proteins. *Biochim. Biophys. Acta* **1963**, *75*, 31-36.

34) Ikeda, S.; Maeda, H.; Isemura, T. The β-structure of poly-S-carbobenzoxymethyl-l-cysteine in solution. *J. Mol. Biol.* **1964**, *10*, 223-234.

35) Xiao, J.; Li, M.; Liu, W.; Li, Y.; Ling, Y.; Tang, H. Synthesis and thermoresponsive properties of poly(L-cysteine)s bearing imidazolium salts. *Eur. Poly. J.* **2017**, *88*, 340-348.

36) Xiao, J.; Tan, J.; Jiang, R.; He, X.; Xu, Y.; Ling, Y.; Luan, S.; Tang, H. A pH and redox dual responsive homopolypeptide: synthesis, characterization, and application in “smart” single-walled carbon nanotube dispersion. ***Polym. Chem.*** **2017**, ***8***, 7025-7032.

37) Hayakawa, T.; Kondo, Y.; Murakami, Y. Syntheses and conformational studies of poly(S-aminoalkyl-L-cysteines) and their benzyloxycarbonyl derivatives. *Polym. J.* **1974**, *6*, 424–430.

38) Liu, H.; Wang, R.; Wei, J.; Cheng, C.; Zheng, Y.; Pan, Y.; He, X.; Ding, M.; Tan, H.; Fu, Q. Conformation-directed micelle-to-vesicle transition of cholesterol-decorated polypeptide triggered by oxidation. *J. Amer. Chem. Soc.* **2018**, *140*, 6604-6610.

39) Frankel, M.; Zilkha, A. Synthesis of poly-S-allylcysteine (poly-deoxo-alliin). *Nature* **1955**, *175*, 1045–1046.

40) Hayakawa, T; Matsuyama, M.; Inoue, K. Poly (S-alkyl-L-cysteines) containing long aliphatic side chains. *Polymer* **1977**, *18*, 854-855.

41) Fu, X.; Shen, Y.; Fu, W.; Li, Z. Thermoresponsive oligo(ethylene glycol) functionalized poly-l-cysteine. *Macromolecules* **2013**, *46*, 3753–3760.

42) Akbulut, H.; Yamada, S.; Endo, T. Phosgene-free synthesis of poly(l-cysteine) containing styrene moiety as a reactive function. *Macromol. Chem. Phys.* **2017**, *218*, 1700078.

43) Yi, L.; Wang, Y.; Lin, G.; Lin, D.; Chen, W.; Huang, Y.; Ye, G. Synthesis of conformation switchable cationic polypeptides based on poly (S-propargyl-cysteine) for use as siRNA delivery. *Int. J. Biol. Macromol.* **2017**, *101*, 758-767.

44) Hayakawa, T.; Kondo, Y.; Matsuyama, M. Syntheses and conformational studies of poly (S-menthyloxycarbonylmethyl L-and D-cysteines). *Polymer* **1976**, *17*, 1009-1012.

45) Kramer, J. R.; Deming, T. J. Glycopolypeptides with a redox-triggered helix-to-coil transition. *J. Amer. Chem. Soc.* **2012**, *134*, 4112-4115.

46) Ikeda, S.; Fasman, G. D. Optical rotatory dispersion of poly-S-carboxymethyl-l-cysteine in aqueous solutions: A beta ⇌ random coil transition. *J. Mol. Biol.* **1967**, *30*, 491-505.

47) Ikeda, S. Molecular conformation of poly-S-carboxymethyl-L-cysteine in aqueous solutions. *Biopolymers* **1967**, *5*, 359-374.

48) Ikeda, S.; Fukutome, A.; Imae, T.; Yoshida, T. Circular dichroism and the pH-induced β-coil transition of poly(S-carboxymethyl-L-cysteine) and its side-chain homolog. *Biopolymers* **1979**, *18*, 335-349.

49) Holmes, T. J.; Lawton, R. G. Cysteine modification and cleavage of proteins with 2-methyl-N1-benzenesulfonyl-N4-bromoacetylquinonediimide. *J. Amer. Chem. Soc.* **1977**, *99*, 1984-1986.

50) Włostowski, M.; Czarnocka, S.; Maciejewski, P. Efficient S-alkylation of cysteine in the presence of 1,1,3,3-tetramethylguanidine. *Tetrahedron Lett.* **2010**, *51*, 5977-5979.

51) Lavilla, C.; Byrne, M.; Heise, A. Block-sequence-specific polypeptides from α-amino acid N-carboxyanhydrides: Synthesis and influence on polypeptide properties. *Macromolecules* **2016**, *49*, 2942-2947.

52) Kramer, J. R.; Onoa, B.; Bustamante, C.; Bertozzi, C. R. Chemically tunable mucin chimeras assembled on living cells. *Proc. Nat. Acad. Sci. (USA)* **2015**, *112*, 12574-12579.

53) Aujard-Catot, J.; Nguyen, M.; Bijani, C.; Pratviel, G.; Bonduelle, C. Cd 2+ coordination: an efficient structuring switch for polypeptide polymers. *Polym. Chem*. **2018**, *9*, 4100–4107.

54) Kramer, J. R.; Deming, T. J. Multimodal switching of conformation and solubility in homocysteine derived polypeptides. *J. Amer. Chem. Soc.* **2014, *136*,** 5547–5550.

55) Henzler Wildman, K. A.; Ramamoorthy, A.; Wakamiya, T.; Yoshikawa, T.; Crisma, M.; Toniolo, C.; Formaggio, F. A study of a $C^{\alpha,\beta}$-didehydroalanine homo-oligopeptide series in the solid-state by ^{13}C cross-polarization magic angle spinning NMR. *J. Peptide Sci.* **2004**, *10*, 336-341.

56) Siodłak, D.; Macedowska-Capiga, A.; Broda, M. A.; Kozioł, A. E.; Lis, T. The cis-trans isomerization of N-methyl-α,β-dehydroamino acids. *Biopolymers* **2012**, *98*, 466-478.

57) Malek, K.; Makowski, M.; Królikowska, A.; Bukowska, J. Comparative studies on IR, Raman, and surface enhanced Raman scattering spectroscopy of dipeptides containing ΔAla and ΔPhe. *J. Phys. Chem. B* **2012**, *116*, 1414−1425.

58) Peggion, C.; Moretto, A.; Formaggio, F.; Crisma, M.; Toniolo, C. Multiple, consecutive, fully-extended 2.0_5-helix peptide conformation. *Biopolymers* **2013**, *100*, 621-636.

59) Katchalski, E.; Sela, M.; Silman, H. I.; Berger, A. Polyamino acids as protein models. In *The Proteins Composition, Structure, and Function, Volume 2*; Neurath, H., Ed.; Academic Press: New York, **1964**; pp 405–601.

60) Avignon, M. Huong, P. V.; Lascombe, J.; Marraud, M. Neel, J. Etude, par spectroscopie infra-rouge, de la conformation de quelques composés peptidiques modèles. *Biopolymers* **1969**, *8*, 69–89.

61) Toniolo, C. Intramolecularly hydrogen-bonded peptide conformations. *Crit. Rev. Biochem.* **1980**, *9*, 1–44.

62) Burgess, A. W.; Scheraga, H. A. Stable conformations of dipeptides. *Biopolymers* **1973**, *12*, 2177–2183.

63) Scheiner, S. Relative strengths of NH••O and CH••O hydrogen bonds between polypeptide chain segments. *J. Phys. Chem. B* **2005**, *109*, 16132-16141.

64) Newberry, R. W.; Raines, R. T. A prevalent intraresidue hydrogen bond stabilizes proteins. *Nat. Chem. Biol.* **2016**, *12*, 1084-1088.

65) Grimme, S. Exploration of chemical compound, conformer, and reaction space with meta-dynamics simulations based on tight-binding quantum chemical calculations. *J. Chem. Theory Comput.* **2019**, *15*, 2847−2862.

66) Carter, C. E.; Greenstein, J. P. Spectrophotometric determination of dehydropeptidase activity. *J. Natl. Cancer Inst.* **1946**, *7*, 51-56.

67) Ye, R.; Liu, Y.; Zhang, H.; Su, H.; Zhang, Y.; Xu, L.; Hu, R.; Kwok, R. T. K.; Wong, K. S.; Lam, J. W. Y.; Goddard, III, W. A.; Tang, B. Z. Non-conventional fluorescent biogenic and synthetic polymers without aromatic rings. *Polym. Chem*. **2017**, *8*, 1722-1727.

68) Chen, X.; Luo, W.; Ma, H.; Peng, Q.; Yuan, W. Z.; Zhang, Y. Prevalent intrinsic emission from nonaromatic amino acids and poly(amino acids). *Sci. China Chem.* **2018**, *61*, 351–359.

69) Bauer, T. A.; Muhl, C.; Schollmeyer, D.; Barz, M. Racemic S-(ethylsulfonyl)-dl-cysteine N-carboxyanhydrides improve chain lengths and monomer conversion for β-sheet-controlled ring-opening polymerization. *Macromol. Rapid Commun.* **2021**, *42*, 2000470.

70) Brzezinska, K. R.; Curtin, S. A.; Deming, T. J. Polypeptide end-capping using functionalized isocyanates: preparation of pentablock copolymers. *Macromolecules* **2002,** *35*, 2970-2976.

71) Kramer, J. R.; Deming, T. J. General method for purifaction of α-amino acid-*N*-carboxyanhydride using flash chromatography. *Biomacromolecules* **2010,** *11*, 3668-3672.

72) Deming, T. J. Cobalt and iron initiators for the controlled polymerization of α-amino acid-*N*-carboxyanhydrides. *Macromolecules* **1999,** *32*, 4500-4502.

73) Schäfer, G.; Bode, J. W. Synthesis of sterically hindered N-acylated amino acids from N-carboxyanhydrides. *Org. Lett.* **2014,** *16*, 1526-1529.

Chapter 4. Complex coacervate core micelles based on PEG-*b*-poly(S-alkyl-L-homocysteine) block copolymers for oligonucleotide encapsulation and delivery †

† The work presented in this chapter was performed equally by Wendell Scott and Isaac Benavides. The cryoEM images were taken by Dr. Xiaoying Cai. The submitted manuscript will list both Wendell Scott and Isaac Benavides as co-first authors.

4.1 Abstract

In the search for more efficient means to deliver therapeutic oligonucleotides, we investigated the possibility of using complex coacervate core micelles, C3Ms, to facilitate that delivery. Polypeptide-based C3Ms were prepared and characterized for single-stranded RNA (ssRNA) encapsulation efficiency and size stability as model carriers for gene delivery. N-Terminal pegylated cationic, α-helical polypeptides, **PEG$_{113}$-*b*-5b$_x$** and **PEG$_{113}$-*b*-5c$_x$**, were designed and prepared to study formation of nanoparticles upon binding of polyvalent anions. Both sodium tripolyphosphate (TPP) and the model ssRNA sequence polyadenylic acid (poly(A)) were used as polyanions to determine the optimal polypeptide composition and chain length for the formation of monomodal-size distributions of C3Ms. **PEG$_{113}$-*b*-5c$_{27}$** was selected for further study of ssRNA complexation and release since it provided monomodal distributions of C3Ms with low size dispersity as well as nanoparticles that were stable for up to 16 days at room temperature. The particle size distribution was stable at physiological ionic strength and pH as measured by DLS, and spherical morphology was confirmed by AFM and cryoEM measurements. Characterization of C3Ms revealed over 90% encapsulation of poly(A) in complexes that possessed good stability against both dissolution and high ionic strength. Study of their stimuli-responsive properties showed that up to 40% of encapsulated poly(A) was released from C3Ms in the presence of other anionic polymers or in media at basic pH.

4.2 Introduction

In recent years, the delivery of biologics such as proteins and oligonucleotides has become increasingly popular in the pharmaceutical industry. Biologics are an attractive

alternative to small molecule drugs due to their improved potency and specificity.[1] With the discovery of DNA came the first conceived uses of oligonucleotides for gene therapy: the replacement of defective genetic material.[2,3] In addition to the use of plasmid DNA (pDNA) for gene therapy, oligonucleotide-based therapeutics have been expanded to include messenger RNA (mRNA), small interfering RNA (siRNA), micro RNA (miRNA), and antisense oligonucleotides (ASO).

When administered alone, these mechanistically diverse oligonucleotide therapeutics all encounter high vulnerability to degradation and difficulty entering cells.[4–6] Chemical modifications to the nucleotide backbone can remedy some of these problems but can also increase the prevalence of off-target effects. Alternative approaches involve encapsulation of oligonucleotides in viral capsid vehicles[7] or in nonviral vehicles such as lipid nanoparticles[8] and polyelectrolyte complexes (PEC), sometimes referred to as polyplexes.[9] All of these encapsulation strategies increase oligonucleotide circulation lifetime and aid in cell internalization, but they often require complex formulations that can cause significant adverse side effects.[10,11]

Polycations are ideal candidates for the formation of PECs with anionic oligonucleotides. The formation of PECs is driven by a combination of coulombic interactions between oppositely charged polyelectrolytes (PEs) and an entropic gain from the release of bound monovalent counterions from each charged residue along the polymer backbones.[12,13] When a PEC in aqueous media undergoes a liquid-liquid phase separation (LLPS) upon complexation, it is considered a complex coacervate (CC).[14] These CC phases have physical properties that are sensitive to the pH and ionic strength of the solution,[15–17] possess low interfacial surface tension[18,19] and have the ability to

stabilize their cargos against degradation,[20,21] which makes them valuable for oligonucleotide delivery applications. Charged synthetic polypeptides have been used frequently to form PECs for oligonucleotide delivery due to their biocompatibility and biodegradability.[22–26] Cationic polypeptides widely used for PEC formation with oligonucleotides include poly-L-lysine (**K**), poly-L-arginine, and poly-L-ornithine.[27,28]

A general limitation in synthetic cationic polypeptides used for gene delivery is the inability to fine-tune or add multiple functionalities to each residue. Both **K** and poly(L-glutamate) (**E**) have undergone side chain modification to enhance the delivery of oligonucleotides in a variety of ways. Amidation of the primary amine side chains of pLL offers a means for further modification to add ligands,[29] hydrophobic groups,[30] thiols,[31] and imidazole moeties;[32] These modifications have been used to tune PEC particle properties such as targeting capabilities, particle stability, and stimuli responsiveness. Cationic, α-helical polypeptides can also be prepared by post-polymerization modification of pLG chains at the carboxylic acid of each residue side chain via esterification.[33–35] These approaches, however, only allow for modification of one functional element at each amino acid residue.

Another strategy to improve polypeptide-mediated delivery of oligonucleotides is the incorporation of a polyethylene glycol (PEG) block as a hydrophilic segment. Incorporating a PEG segment into one[36] or both[37] PEC components has been found to result in colloidally stable PECs that are coated with PEG chains. The size and morphology of both types of assemblies are dependent on the ratio of the PEG segment to the charged segment(s) and thus can be controlled by varying the length of the PEG block relative to the charged block on each copolymer.[38–40] Additionally, different

nanoscale particle morphologies can be obtained depending on the hybridization of the oligonucleotide component (i. e., single-stranded or double-stranded).[33,41–43] When PEG-polycations are used promote CC formation, the resulting sterically stabilized PEC micelles are known as complex coacervate core micelles (C3Ms).[43]

Herein we explored the ability of block copolymers of PEG and new synthetic α-helical polypeptide segments to form C3Ms when mixed with a model single-stranded oligonucleotide, polyadenylic acid (poly(A)). The abundance of examples of PEG-polypeptide-based materials for delivery of oligonucleotides such as pDNA,[44,45] siRNA,[46,47] and ASOs,[48] shows the broad potential utility of this type of non-ionic-*b*-cationic double hydrophilic block copolymer architecture. In this study, we improve upon this well-established approach by preparing PEG-*b*-poly(L-methionine) copolymers that were readily derivatized into a wide variety of different block copolymers containing multifunctional and switchable cationic polypeptide segments.

4.3 Results and Discussion

The Deming group has developed a “click”-type reaction for modification of the thioether groups in poly(L-methionine), **M**, that can be used to introduce a range of side-chain functionalities onto an α-helical polypeptide backbone.[49,50] This methodology has been expanded in recent work to develop a library of side-chain amino acid containing cationic poly(S-alkyl-L-homocysteine)s that undergo LLPS in aqueous media upon mixing with oppositely charged multivalent anions (Figure 4.1).[51] By alkylating **M** with epoxides bearing different amino acids, a variety of derivatives were obtained that allow tuning of the conditions for coacervate formation. Previous work by the Deming group has shown the potential for cationic, α-helical amino acid-modified poly(S-alkyl-L-homocysteine)s as

versatile polypeptides for coacervate formation via PEC in aqueous media (Figure 4.1). While the previous study introduced these novel synthetic polypeptides as a model system to study membraneless organelles (MLO), this current work shows the potential of these coacervate-forming polypeptide segments for aqueous self-assembly of C3Ms with applications in gene delivery. Different copolymer compositions and block lengths of PEG-amino acid-containing poly(S-alkyl-L-homocysteine) copolymers were utilized to study coacervation and properties of the resulting self-assembled C3Ms.[52]

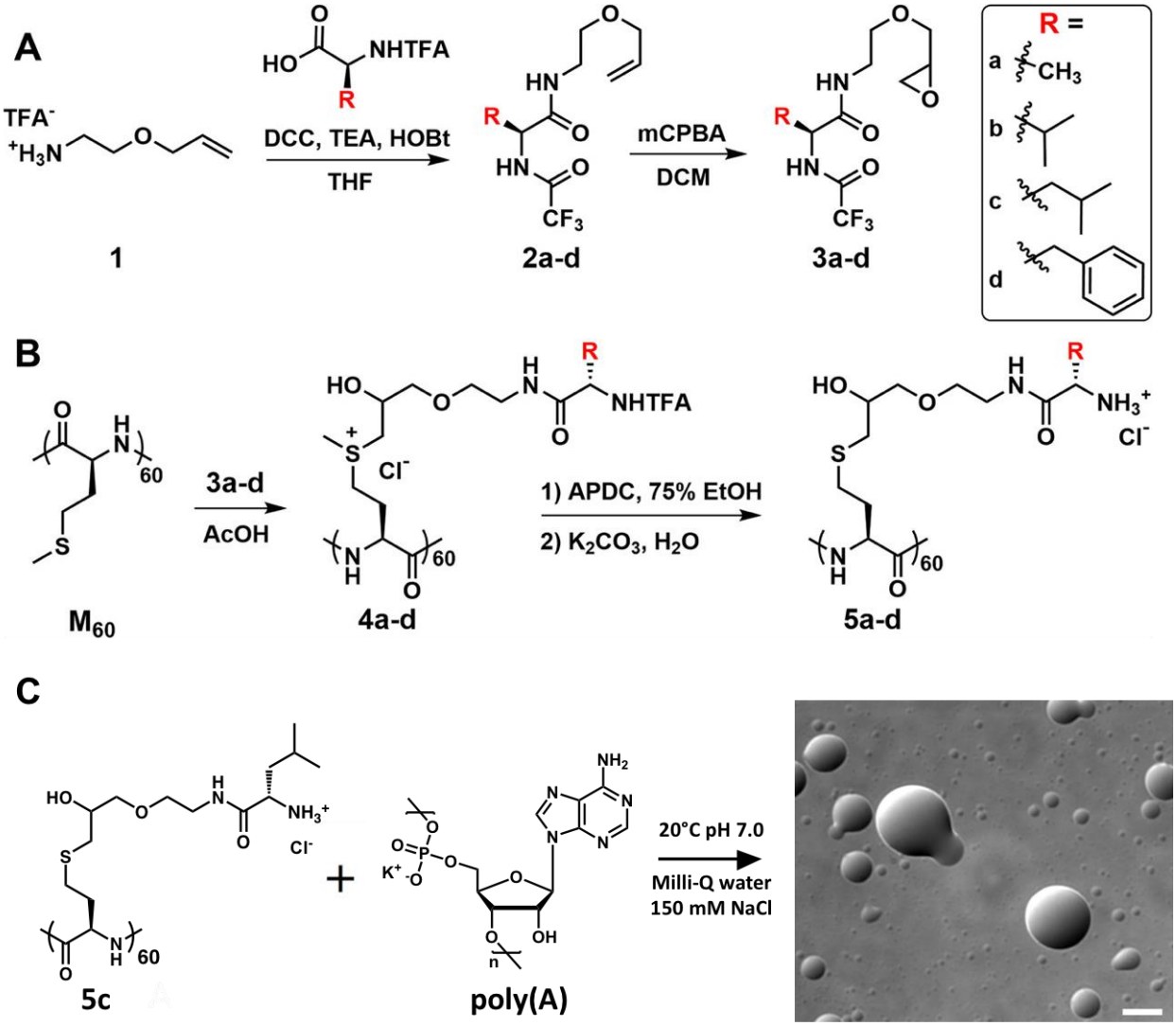

Figure 4.1 Preparation of side-chain amino acid containing cationic poly(S-alkyl-L-homocysteine)s for LLPS. (A) Synthesis of intermediates and epoxide alkylating agents **3a-d**. (B) Synthesis of intermediates and polypeptide samples **5a-d**. (C) Optical

micrograph of coacervate phase resulting from mixing of homopolypeptide **5c** and polyadenylic acid (poly(A)). A freshly prepared mixture of **5c** at 5.0 mg/mL and poly(A) (5.0 mg/mL) at 20 °C and pH 7.0 was allowed to settle onto a glass slide. Scale bar = 20 μm. Adapted with permission from Wendell A. Scott, Eric G. Gharakhanian, Alexandra G. Bell, Declan Evans, Ehab Barun, K. N. Houk, and Timothy J. Deming *Journal of the American Chemical Society* **2021** *143* (43), 18196-18203. *Copyright © 2021, American Chemical Society.*

Using previously established methods for the living ring-opening polymerization of L-methionine N-carboxyanhydride (NCA), **M** chains with average degrees of polymerization (DP) of 27 and 51 were synthesized, and both were subsequently end-capped with α-methoxy-ω-isocyanoethyl-poly(ethylene glycol) (**PEG**, DP = 113) to give **PEG$_{113}$-*b*-M$_{27}$** and **PEG$_{113}$-*b*-M$_{51}$** copolymers (Figure 4.2a). These two precursor copolymers were then separately functionalized with the epoxides **3b** or **3c** followed by demethylation and deprotection to provide four different copolymers: **PEG$_{113}$-*b*-5b$_{27}$**, **PEG$_{113}$-*b*-5c$_{27}$**, **PEG$_{113}$-*b*-5b$_{51}$**, and **PEG$_{113}$-*b*-5c$_{51}$** (Figure 4.2b). The resulting copolymers were isolated as hydrochloride salts in high yields (Table 4.1), and the quantitative functionalization of methionine residues was verified via ^{1}H NMR characterization. Compositions of the coacervate-forming polypeptide segments were chosen based on the properties of homopolypeptides evaluated in previous studies: **5b** and **5c** were hydrophobic enough for robust coacervate formation yet sufficiently hydrophilic to provide good solubility for formulation purposes.[53–55]

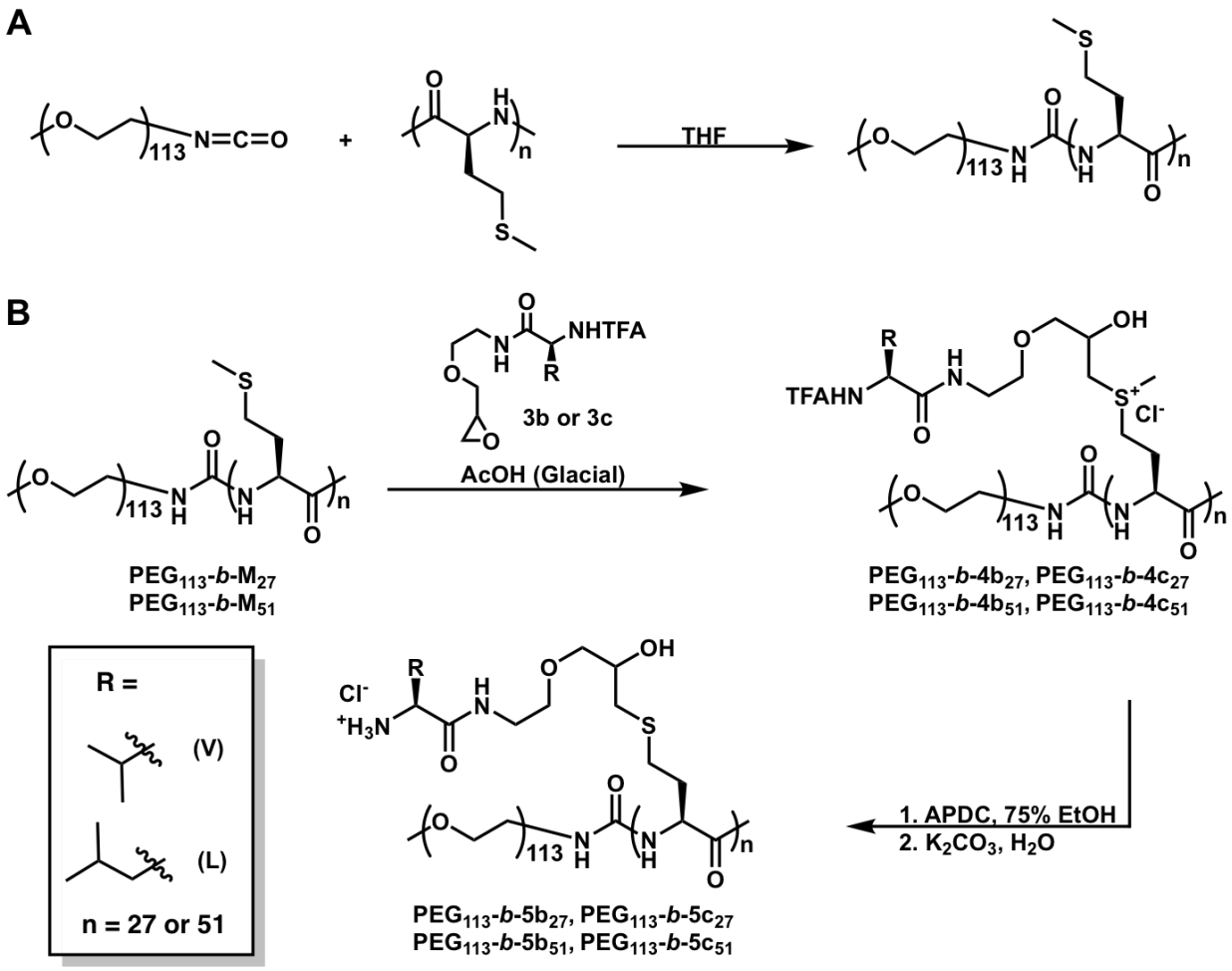

Figure 4.2 (A) Synthesis of **PEG$_{113}$-*b*-M$_x$** copolymers. (B) Synthesis of **PEG$_{113}$-*b*-5b$_x$** and **PEG$_{113}$-*b*-5c$_x$** copolymers and intermediates. x = 27 or 51.

Intermediate Copolymer	Isolated Yield (%)	Final Copolymer	Isolated Yield (%)
PEG$_{113}$-*b*-4b$_{27}$	88	**PEG$_{113}$-*b*-5b$_{27}$**	72
PEG$_{113}$-*b*-4c$_{27}$	87	**PEG$_{113}$-*b*-5c$_{27}$**	72
PEG$_{113}$-*b*-4b$_{51}$	84	**PEG$_{113}$-*b*-5b$_{51}$**	75
PEG$_{113}$-*b*-4c$_{51}$	90	**PEG$_{113}$-*b*-5c$_{51}$**	82

Table 4.1 Isolated yields of **PEG$_{113}$-*b*-5b$_x$** and **PEG$_{113}$-*b*-5c$_x$** copolymers and intermediates.

The chain length and hydrophobicity of a polyelectrolyte are both important parameters that can be used to tune coacervate formation. Indeed, our goal here was to identify copolymer compositions capable of forming monomodal populations of C3Ms that are stable against bulk coalescence. For initial evaluation of coacervate forming properties of our four copolymers, sodium tripolyphosphate (TPP) was chosen as a model multivalent anion to promote coacervation via polyelectrolyte complexation. We hypothesized that successful coacervate formation with small multivalent counterions such as TPP could be used to predict the formation of similar coacervates with single-stranded RNA (ssRNA). In the presence of 13 mM TPP in DI water, all four copolymers were found to phase separate as TPP-complex coacervate core micelles (TPP-C3Ms). Using dynamic light scattering (DLS) to monitor self-assembly, we discovered that both **PEG$_{113}$-*b*-5b$_{27}$** and **PEG$_{113}$-*b*-5b$_{51}$** formed multimodal size distributions of particles (Figure 4.3a, b, and Table 4.2) that mainly consisted of unimers (Figure 4.4a, b, and Table 4.3). Both **PEG$_{113}$-*b*-5c$_{27}$** and **PEG$_{113}$-*b*-5c$_{51}$** initially formed particles with monomodal size distributions in the presence of TPP (Figure 4.3c, d, and Table 4.2), although the larger particles formed from **PEG$_{113}$-*b*-5c$_{51}$** were observed to settle from suspension, leaving behind only unimers in solution (Figure 4.4d and Table 4.3). In contrast, particles formed from **PEG$_{113}$-*b*-5c$_{27}$** remained as a stable suspension over the entire 28-day period (Figure 4.4c and Table 4.3). The inability of the **PEG$_{113}$-*b*-5c$_{51}$** TPP-C3Ms to remain stable over this period was likely due to their larger size and the failure of the PEG chains to stabilize the nanoparticles against coalescence, which was confirmed by optical microscopy imaging (Figure 4.5b). The best results were obtained with the TPP-C3Ms based on **PEG$_{113}$-*b*-5c$_{27}$** that maintained a consistent, uniform size over 28 days by DLS

(Figure 4.3c, Figure 4.4c, Table 4.2, and Table 4.3), which was also confirmed using AFM imaging (Figure 4.5a).

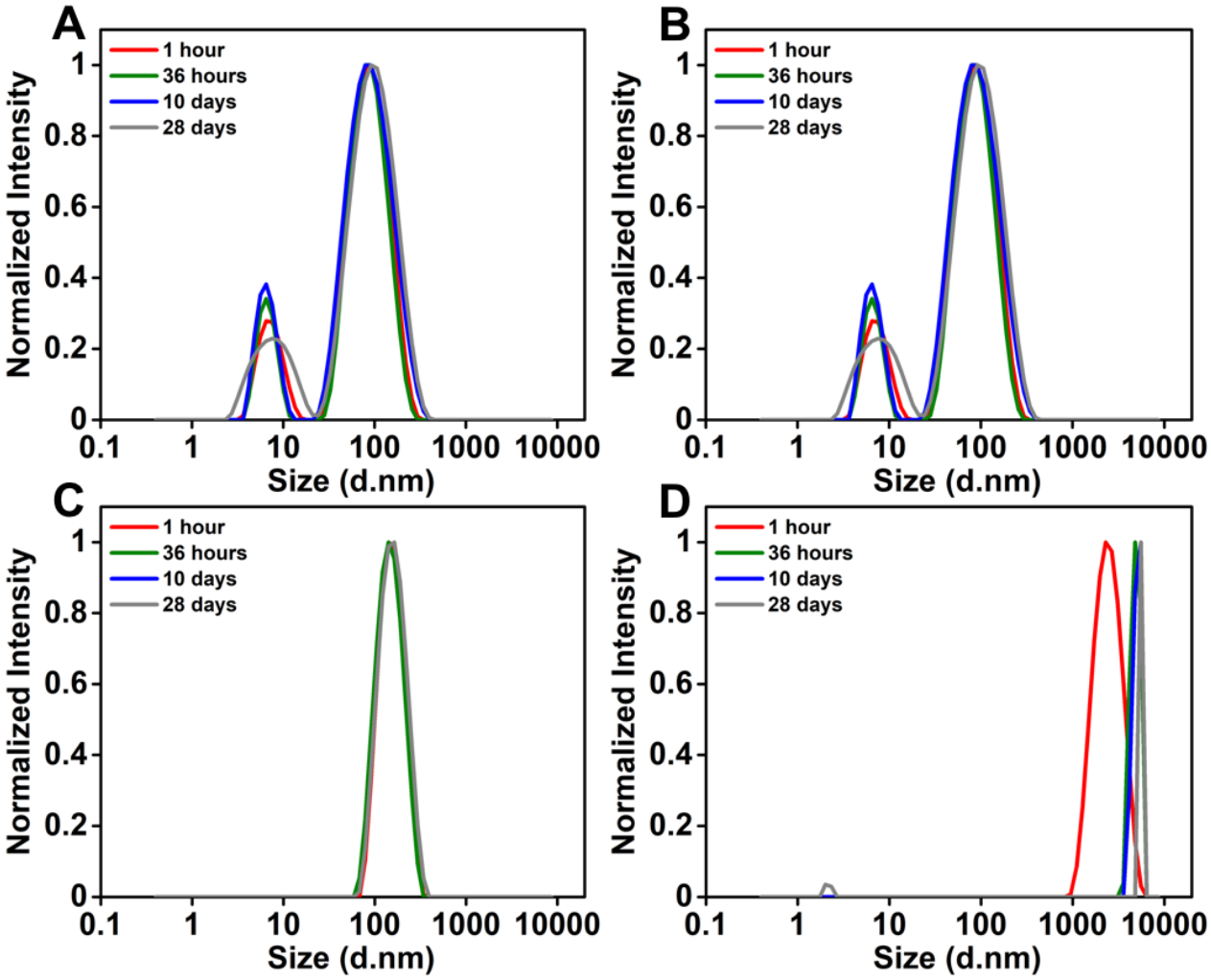

Figure 4.3. Normalized intensity size distributions of TPP-C3M populations from DLS analysis. Aqueous suspensions of TPP-C3Ms were prepared from (A) **PEG$_{113}$-*b*-5b$_{27}$**, (B) **PEG$_{113}$-*b*-5b$_{51}$**, (C) **PEG$_{113}$-*b*-5c$_{27}$**, and (D) **PEG$_{113}$-*b*-5c$_{51}$** at 5 mg/mL (9, 8.8, 10.7, and 10.1 mM **5x** polypeptide residue concentrations, respectively) in DI water with sodium tripolyphosphate (13 mM) in the presence of 150 mM NaCl at room temperature. d.nm = average hydrodynamic diameter in nanometers.

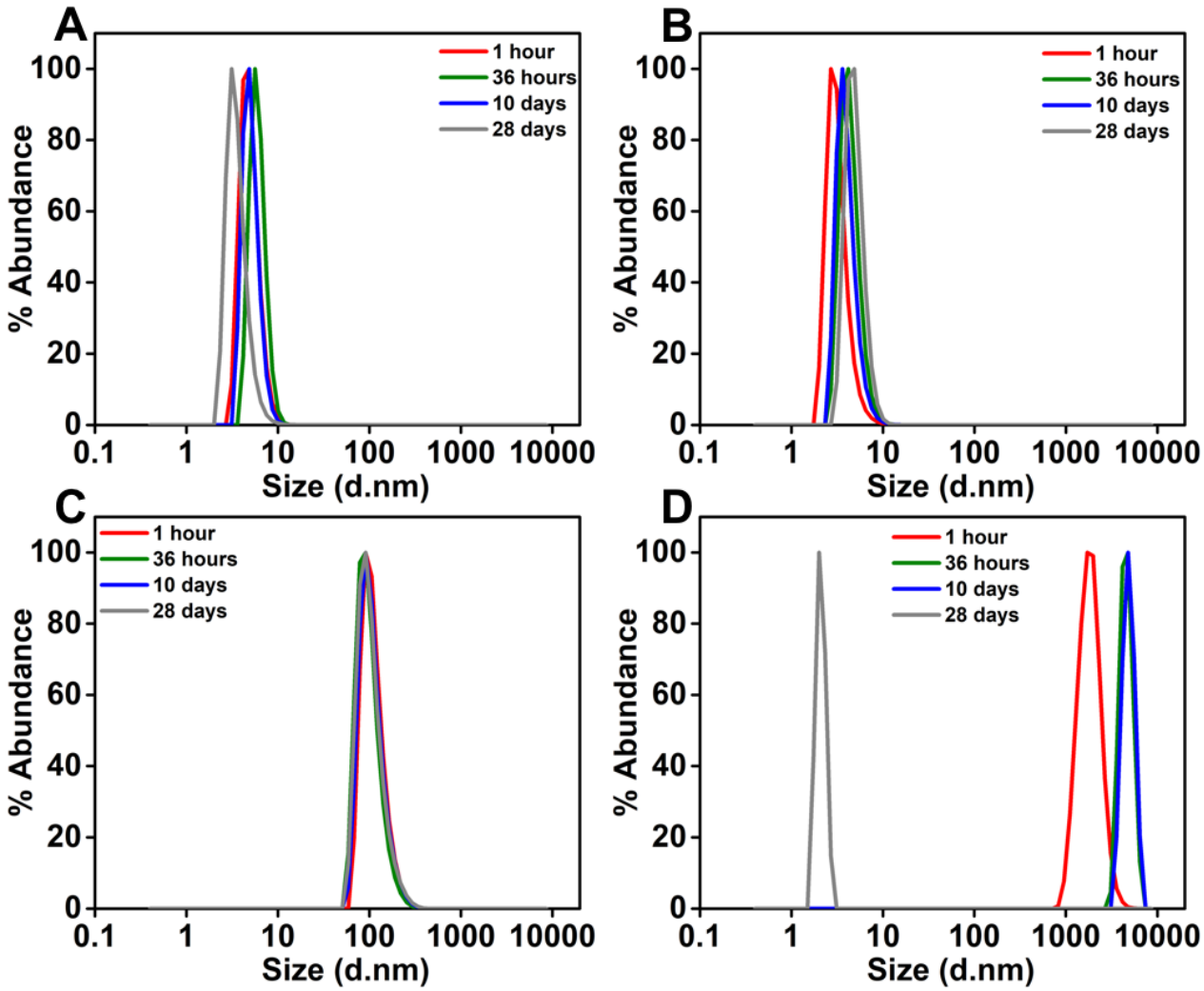

Figure 4.4. Normalized number distributions of TPP-C3M populations from DLS analysis. Aqueous suspensions of TPP-C3Ms were prepared from (A) **PEG$_{113}$-*b*-5b$_{27}$**, (B) **PEG$_{113}$-*b*-5b$_{51}$**, (C) **PEG$_{113}$-*b*-5c$_{27}$**, and (D) **PEG$_{113}$-*b*-5c$_{51}$** at 5 mg/mL (9, 8.8, 10.7, and 10.1 mM **5x** polypeptide residue concentrations, respectively) in DI water with sodium tripolyphosphate (13 mM) in the presence of 150 mM NaCl at room temperature. d.nm = average hydrodynamic diameter in nanometers.

DLS intensity distribution for TPP-C3M		Hydrodynamic diameter (nm)			
		PEG$_{113}$-*b*-5b$_{27}$	**PEG$_{113}$-*b*-5c$_{27}$**	**PEG$_{113}$-*b*-5b$_{51}$**	**PEG$_{113}$-*b*-5c$_{51}$**
1 hour	**Peak 1**	97±45	160±49	140±66	2500±880
	Peak 2	7.5±15	******	7.9±3.4	**
36 hours	**Peak 1**	94±42	150±49	160±80	4900±560
	Peak 2	6.7±1.6	**	8.0±3.5	**
10 days	**Peak 1**	100±55	170±55	150±72	5100±510
	Peak 2	6.7±1.7	**	8.1±3.3	**
28 days	**Peak 1**	110±58	170± 61	140±67	5600±6.1E-5
	Peak 2	8.1±3.7	**	7.1±1.9	2.16±0.16

Table 4.2 Hydrodynamic diameters of **PEG$_{113}$-*b*-5b$_{27}$**, **PEG$_{113}$-*b*-5b$_{51}$**, **PEG$_{113}$-*b*-5c$_{27}$**, and **PEG$_{113}$-*b*-5c$_{51}$** TPP-C3M populations determined from DLS intensity distributions. Aqueous suspensions of TPP-C3Ms were prepared from copolymers at 5.0 mg/mL (9, 8.8, 10.7, and 10.1 mM **5x** polypeptide residue concentrations, respectively) in DI water with sodium tripolyphosphate (13 mM) in the presence of 150 mM NaCl at room temperature. ** indicates no peak detected.

DLS number distribution for TPP-C3M		Hydrodynamic diameter (nm)			
		PEG$_{113}$-*b*-5b$_{27}$	**PEG$_{113}$-*b*-5c$_{27}$**	**PEG$_{113}$-*b*-5b$_{51}$**	**PEG$_{113}$-*b*-5c$_{51}$**
1 hour	**Peak**	5.0±1.2	110±35	3.2±0.97	1900±550
36 hours	**Peak**	6.0±1.2	100±32	4.4±1.2	4600±740
10 days	**Peak**	5.1±1.1	110±37	4.0±1.1	4900±740
28 days	**Peak**	3.6±1.0	110±38	5.0±1.2	2.1±0.23

Table 4.3. Hydrodynamic diameters of **PEG$_{113}$-*b*-5b$_{27}$**, **PEG$_{113}$-*b*-5b$_{51}$**, **PEG$_{113}$-*b*-5c$_{27}$**, and **PEG$_{113}$-*b*-5c$_{51}$** TPP-C3M populations determined from DLS number distributions. Aqueous suspensions of TPP-C3Ms were prepared from copolymers at 5.0 mg/mL (9, 8.8, 10.7, and 10.1 mM **5x** polypeptide residue concentrations, respectively) in DI water with sodium tripolyphosphate (13 mM) in the presence of 150 mM NaCl at room temperature.

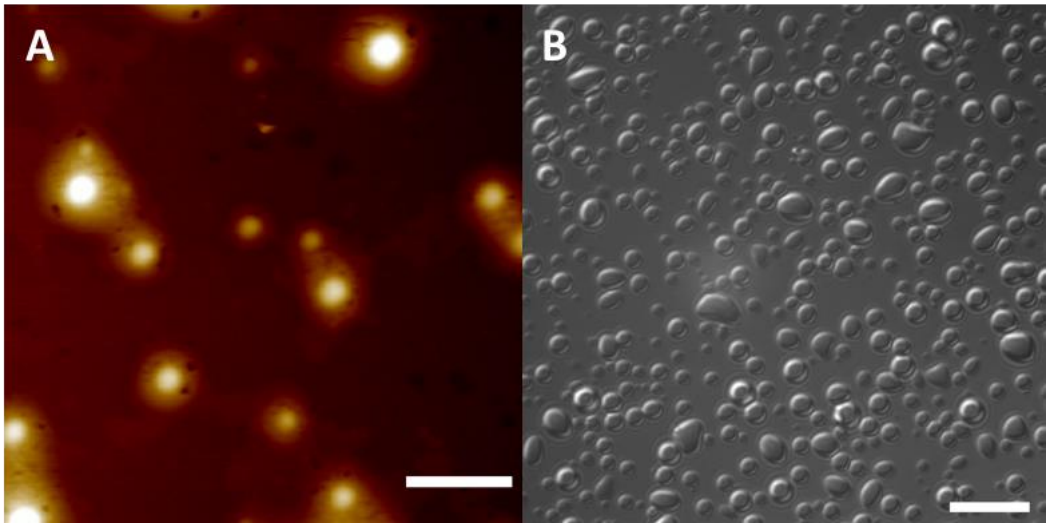

Figure 4.5. Characterization of TPP-C3Ms prepared from **PEG$_{113}$-*b*-5c$_x$**. (A) Atomic force microscopy image of TPP-C3Ms. An aqueous suspension of TPP-C3Ms prepared from **PEG$_{113}$-*b*-5c$_{27}$** at 5.0 mg/mL (8.8 mM **5c** residue concentration), and sodium tripolyphosphate (13 mM) in the presence of 150 mM NaCl was diluted in nuclease-free water to a final copolymer concentration of 0.1 mg/mL and then dropcast onto a freshly cleaved mica surface and permitted to dry. Scale bar = 400 nm (B) Optical micrograph of TPP-C3Ms. An aqueous suspension of TPP-C3Ms prepared from **PEG$_{113}$-*b*-5c$_{51}$** at 5.0 mg/mL and sodium tripolyphosphate (13 mM) in the presence of 150 mM NaCl was transferred to a glass slide and allowed to settle before imaging. Scale bar = 20 μm.

In the next phase of the study, we wanted to determine how results obtained with TPP would translate to complexation with poly(A). We used both lengths of **PEG$_{113}$-*b*-5c$_x$** to provide a comparison. Here, single-stranded poly(A) was used as a model ssRNA sequence to drive the formation of C3Ms with **PEG$_{113}$-*b*-5c$_{27}$** and **PEG$_{113}$-*b*-5c$_{51}$**. The selection of ssRNA as a model genetic payload was influenced by the propensity of flexible single-stranded oligonucleotides to form spherical C3Ms.[41,56] Additionally, poly(A) was previously found to form coacervates when mixed with **5c** homopolymer.[51] When an aqueous solution of poly(A) was mixed with a solution of **PEG$_{113}$-*b*-5c$_x$** at an equimolar charge ratio relative to the charged **5c** residues, the mixture immediately became cloudy, indicative of coacervate formation. To evaluate nanoparticle assembly and stability, the

suspensions of poly(A)-complex coacervate core micelles (poly(A)-C3Ms) were monitored by DLS for 16 days. The poly(A)-C3Ms obtained from complexation of **PEG$_{113}$-*b*-5c$_{27}$** with poly(A) were found to equilibrate to an average hydrodynamic diameter (D_h) of 107 ± 26 nm within one hour and were stable against coalescence over the duration of the experiment (Figure 4.6a, Table 4.4, Figure 4.7a, and Table 4.5). In comparison, the particles obtained from complexation of **PEG$_{113}$-*b*-5c$_{51}$** with poly(A) possessed a broad distribution of average D_h, which continued to change over the course of the study (Figure 4.6b, Table 4.4, Figure 4.7b, and Table 4.5).

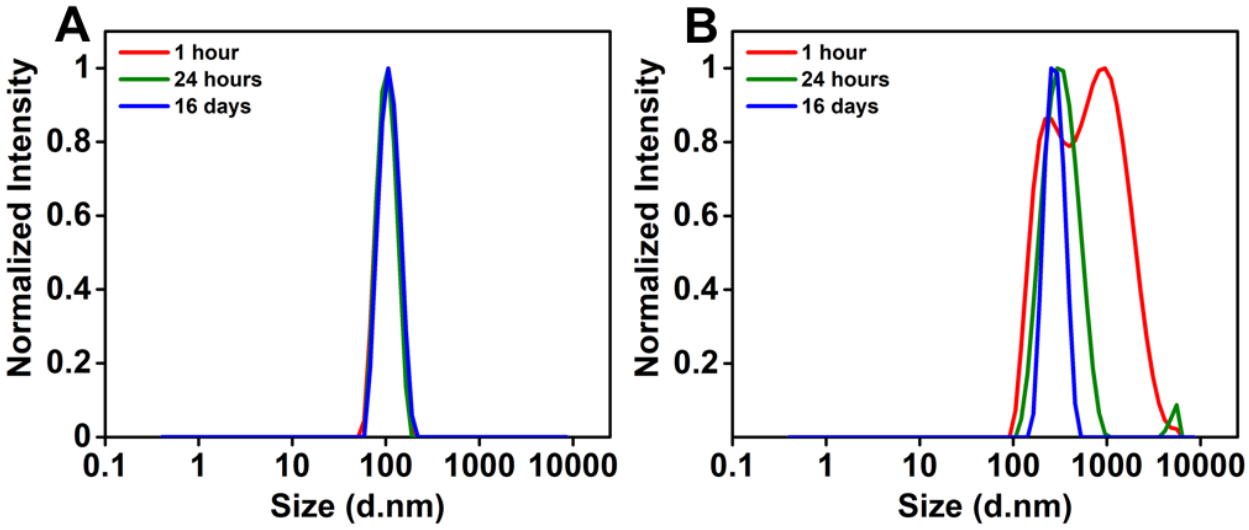

Figure 4.6 Normalized intensity size distributions of poly(A)-C3M populations from DLS analysis. Aqueous suspensions of poly(A)-C3Ms were prepared from (A) **PEG$_{113}$-*b*-5c$_{27}$** and (B) **PEG$_{113}$-*b*-5c$_{51}$** at 5.0 mg/mL (8.8 and 10.4 mM **5c$_x$** residue concentrations, respectively) in nuclease-free water with an equimolar concentration of poly(A) residues relative to the charged **5c** residues (8.8 and 10.4 mM poly(A) residue concentrations, respectively) in the presence of 150 mM NaCl at room temperature.

DLS intensity distribution poly(A)-C3Ms		Hydrodynamic diameter (nm)	
		PEG$_{113}$-b-5c$_{27}$	**PEG$_{113}$-b-5c$_{51}$**
1 hour	**Peak 1**	107±26	1100±550
	Peak 2	**	232±68
24 hours	**Peak 1**	105±23	360±120
	Peak 2	**	4900±650
16 days	**Peak 1**	112±27	280±137
	Peak 2	**	**

Table 4.4 Hydrodynamic diameters of **PEG$_{113}$-*b*-5c$_{27}$** and **PEG$_{113}$-*b*-5c$_{51}$** poly(A)-C3M populations determined from DLS intensity distributions. Aqueous suspensions of poly(A)-C3Ms were prepared from copolymers at 5.0 mg/mL (8.8 and 10.4 mM **5c$_x$** residue concentrations, respectively) in nuclease-free water with an equimolar concentration of poly(A) residues relative to the charged **5c** residues (8.8 and 10.4 mM poly(A) residue concentrations, respectively) in the presence of 150 mM NaCl at room temperature.** indicates no peak detected

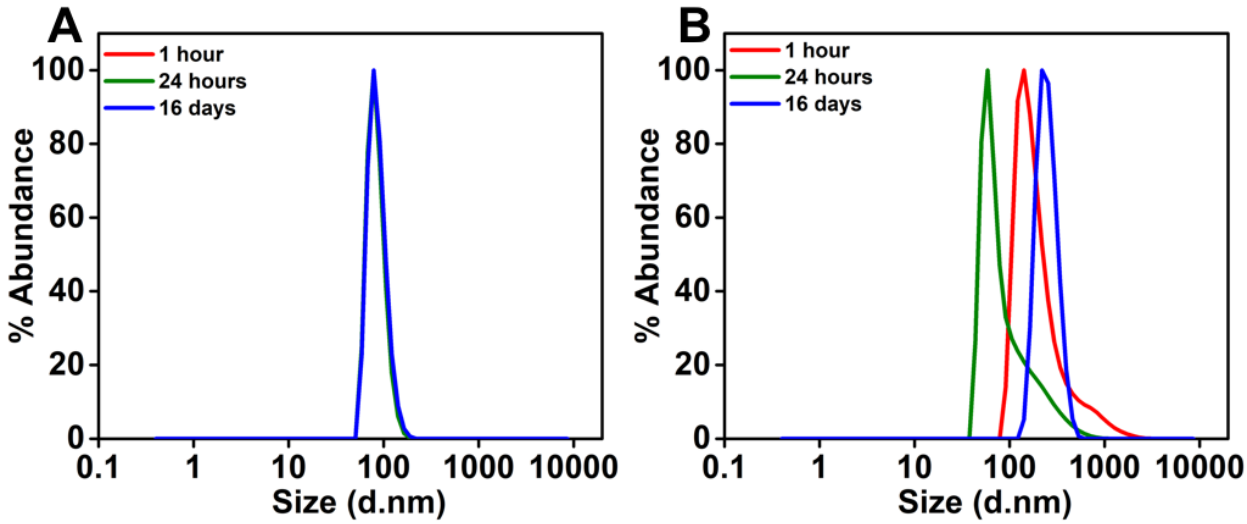

Figure 4.7 Normalized number distributions of poly(A)-C3M populations from DLS analysis. Aqueous suspensions of poly(A)-C3Ms were prepared from (A) **PEG$_{113}$-*b*-5c$_{27}$** and (B) **PEG$_{113}$-*b*-5c$_{51}$** at 5.0 mg/mL (8.8 and 10.4 mM **5c$_x$** residue concentrations, respectively) in nuclease-free water with an equimolar concentration of poly(A) residues relative to the charged **5c** residues (8.8 and 10.4 mM poly(A) residue concentrations, respectively) in the presence of 150 mM NaCl at room temperature.

DLS number distribution poly(A)-C3Ms		Hydrodynamic diameter (nm)	
		PEG_{113}-*b*-$5c_{27}$	**PEG_{113}-*b*-$5c_{51}$**
1 hour	**Peak**	82±20	240±220
24 hours	**Peak**	85±19	106±91
16 days	**Peak**	87±20	253±64

Table 4.5 Hydrodynamic diameters of **PEG_{113}-*b*-$5c_{27}$** and **PEG_{113}-*b*-$5c_{51}$** poly(A)-C3M populations determined from DLS number distributions. Aqueous suspensions of poly(A)-C3Ms were prepared from copolymers at 5.0 mg/mL (8.8 and 10.4 mM **$5c_x$** residue concentrations, respectively) in nuclease-free water with an equimolar concentration of poly(A) residues relative to the charged **5c** residues (8.8 and 10.4 mM poly(A) residue concentrations, respectively) in the presence of 150 mM NaCl at room temperature

Since poly(A)-C3Ms made using **PEG_{113}-*b*-$5c_{27}$** gave particles that were both uniform and stable, this formulation was selected for further characterization by AFM and cryo-EM (Figure 4.8a, b). Both techniques showed the presence of primarily spherical particles with size ranges similar to the D_h distributions observed by DLS. These results show that the results obtained via complexation with TPP translate well to poly(A) complexation and confirmed that copolymer **PEG_{113}-*b*-$5c_{27}$** was the best candidate for poly(A)-C3M formation.

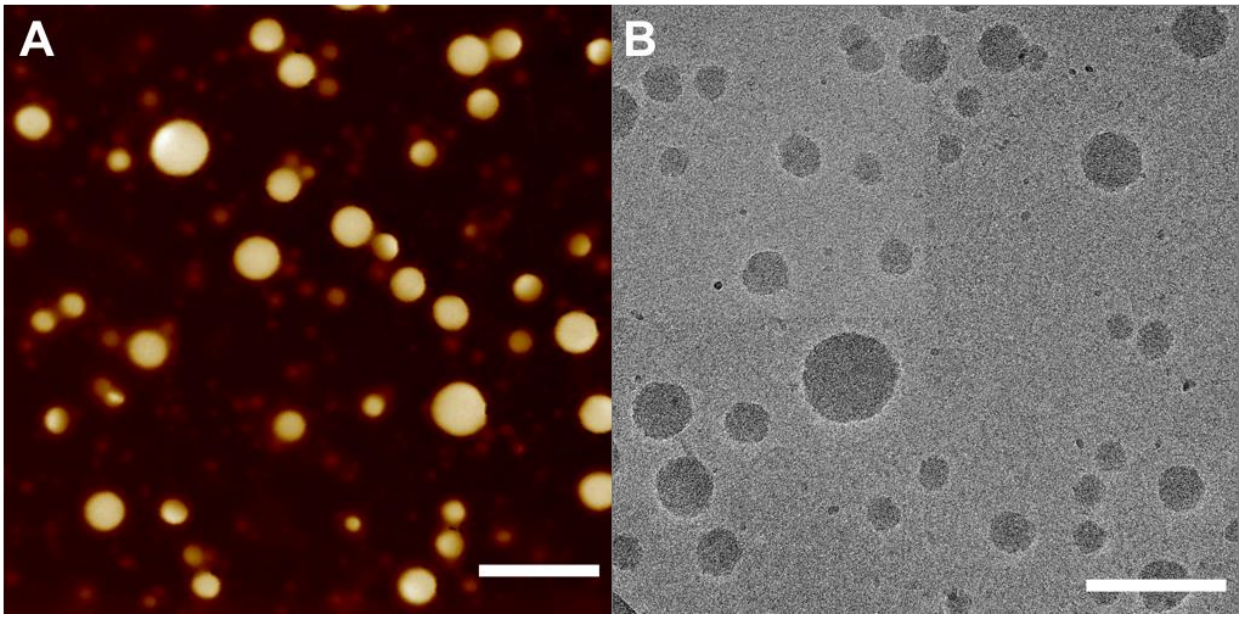

Figure 4.8. Characterization of poly(A)-C3Ms. (A) Atomic force microscopy image of poly(A)-C3Ms. An aqueous suspension of poly(A)-C3Ms prepared from **PEG$_{113}$-*b*-5c$_{27}$** at 1.0 mg/mL (1.76 µM **5c** residue concentration) in nuclease-free water with an equimolar concentration of poly(A) residues relative to the charged **5c** residues (1.76 µM poly(A) residue concentration) in the presence of 150 mM NaCl was diluted in nuclease-free water to a final polymer concentration of 0.1 mg/mL, dropcast onto a freshly cleaved mica surface and permitted dry. Scale bar = 400 nm. (B) CryoEM Image of poly(A)-C3Ms. A suspension of poly(A)-C3Ms prepared from **PEG$_{113}$-*b*-5c$_{27}$** at 25 mg/mL (44 mM **5c** residue concentration) in nuclease-free water with an equimolar concentration of poly(A) residues relative to the charged **5c** residues (44 mM poly(A) residue concentration) in the presence of 150 mM NaCl was diluted in nuclease-free water containing 150 mM NaCl to a final copolymer concentration of 2.5 mg/mL. Scale bar = 200 nm.

To better understand the complexation of poly(A) with **PEG$_{113}$-*b*-5c$_{27}$** and resulting assembly into poly(A)-C3Ms, the efficiency of the ability of **PEG$_{113}$-*b*-5c$_{27}$** to sequester poly(A) was determined. The encapsulation efficiency of poly(A) within the C3Ms was measured using a RyboGreen fluorescent probe, which binds to RNA. When poly(A) was complexed with **PEG$_{113}$-*b*-5c$_{27}$** to form the poly(A)-C3M, the fluorescent signal from soluble poly(A) binding to RyboGreen was greatly diminished when compared to a solution of free poly(A) in the absence of **PEG$_{113}$-*b*-5c$_{27}$** (Figure 4.9a). This significant decrease in fluorescence was due to inability of RyboGreen to bind to the complexed

poly(A) within poly(A)-C3Ms, allowing us to measure poly(A) encapsulation and release. The fluorescent signal of the supernatant containing free poly(A) after removal of poly(A)-C3Ms by centrifugation was compared to a calibration curve of RyboGreen complexed with free poly(A) at known concentrations (see Experimental), which allowed us to determine that 95% of the poly(A) was encapsulated within poly(A)-C3Ms over 24 hours (Figure 4.9b).

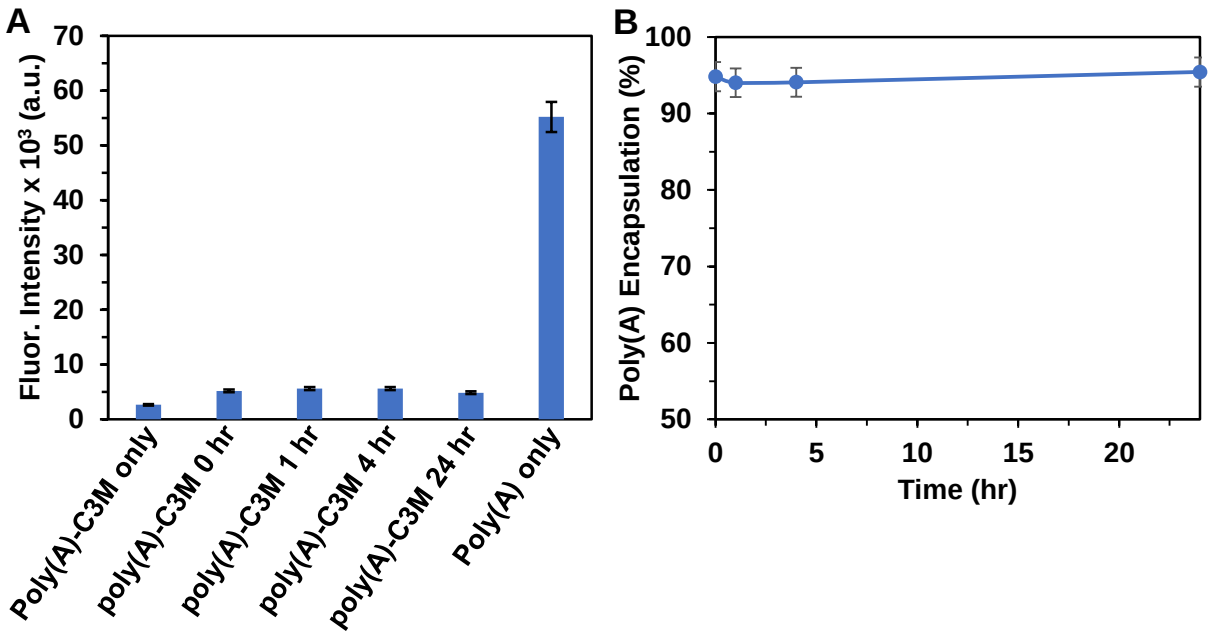

Figure 4.9. Encapsulation efficiency of poly(A)-C3M. (A) RyboGreen:poly(A) fluorescence over time for poly(A)-C3Ms prepared with **PEG-*b*-5c$_{27}$** at equimolar charge ratios (B) poly(A)-C3M encapsulation efficiency over 24 hours indicating stable poly(A) complexation after mixing equimolar charge ratios of 1 mg/mL **PEG$_{113}$-*b*-5c$_{27}$** with 0.58 mg/mL poly(A) and diluting to 0.1 mg/mL in 150 mM NaCl.

Previous studies on the stability of C3Ms in response to increasing ionic strength revealed behavior ranging from dissolution[36,40,57] to swelling[40,55,58], indicating that the effects of ionic strength on C3Ms are highly variable between different systems and need to be evaluated empirically. Consequently, the D_h of our **PEG$_{113}$-*b*-5c$_{27}$** based poly(A)-C3Ms at two different concentrations were monitored using DLS over a range of NaCl

concentrations in water to evaluate their stability against increasing ionic strength. Suspensions of poly(A)-C3Ms were prepared at two different to determine the effect of copolymer concentration on ionic-strength mediated micelle morphology. Samples were prepared in NaCl solutions ranging from 0 to 1000 mM for **PEG$_{113}$-*b*-5c$_{27}$** concentrations of 1.0 mg/mL (Figure 4.10a), as well as NaCl concentrations ranging from 0 to 2000 mM NaCl for **PEG$_{113}$-*b*-5c$_{27}$** concentrations of 4.0 mg/mL (Figure 4.11a). For samples with **PEG$_{113}$-*b*-5c$_{27}$** concentrations of 1.0 mg/mL, particle size increased linearly as ionic strength increased from 75 mM to 300 mM NaCl (Figure 4.10a). For samples with **PEG$_{113}$-*b*-5c$_{27}$** at concentrations of 4.0 mg/mL particles size increased linearly from 150 to 500 mM NaCl (Figure 4.11a) indicating a slight concentration dependence on poly(A)-C3Ms behavior upon increasing ionic strength. The small increase of D_h across the linear region can likely be attributed to swelling of the micelles caused by increased hydration at the core of the poly(A)-C3Ms. While the linear range for the two copolymer concentrations was slightly different, the D_h for both was found to increase dramatically at higher NaCl concentrations (Figure 4.10a and Figure 4.11a). This observed inflection point is likely correlated with a change in micelle morphology where size changes were the result of increased aggregation number as opposed to micelle swelling due to increased core hydration.[28] At both concentrations, initial submicron-size C3Ms were found to increase to over 5 microns in diameter at NaCl concentrations above 750 mM (Figure 4.10a and Figure 4.11a). Optical microscopy (performed on samples at 4.0 mg/L copolymer concentration) at 1.0 and 2.0M NaCl showed that the smaller micelles had coalesced into larger compound micelles (Figure 4.11b and c), which then settled out of suspension resulting in decreased sample turbidity (Figure 4.11a). These changes in particle size and

morphology at high salt concentrations are consistent with observations reported for other C3M systems.[40,55,58] Increased micelle diameter has been attributed to a combination of swelling of the C3M core due to increased hydration and to a decrease in the overall aqueous solubility of the PEG block resulting in condensation of these chains, both of which lead to increased aggregation number for each C3M.[40] Despite the large increases in D_h at high ionic strength, the C3Ms reported here were found to remain stable at physiologically relevant ionic strength.

Next, it was necessary to determine how changes to micelle morphology affected the retention of the poly(A) cargo. The poly(A)-C3M suspensions were prepared as previously described in 150 mM NaCl at 1.0 mg/mL **PEG$_{113}$-*b*-5c$_{27}$** concentrations. These suspensions then underwent a 10x dilution (0.1 mg/mL poly(A)-C3Ms, 176 µM **5c** residue concentration, 6.51 µM total **PEG$_{113}$-*b*-5c$_{27}$** concentration) in 150 mM, 500 mM and 1000 mM solutions of nuclease-free water before quantification of free poly(A) at zero, one, and four hours. The fluorescence signals of the different NaCl concentration samples were compared to a poly(A):RyboGreen calibration curve to determine extent of poly(A) release from poly(A)-C3Ms in response to the increasing ionic strength. While NaCl concentrations above 150 mM are higher than physiologically relevant ionic strength, the goal was to determine if the observed changes in micelle morphology were related to release of poly(A) cargo. Interestingly, despite a significant increase in size of the poly(A)-C3Ms at elevated NaCl concentrations (Figure 4.10a and Figure 4.11a), the amount of poly(A) released was less than 10% in 1M NaCl after four hours (Figure 4.10b). The observation that the initial release of poly(A) cargo was consistent over the range of ionic strength studied suggests that the morphology change of these micelles at increasing

ionic strength is unrelated to poly(A) cargo release. The increase in D_h is therefore likely attributed to formation of larger compound micelles from the combination of individual poly(A)-C3Ms.

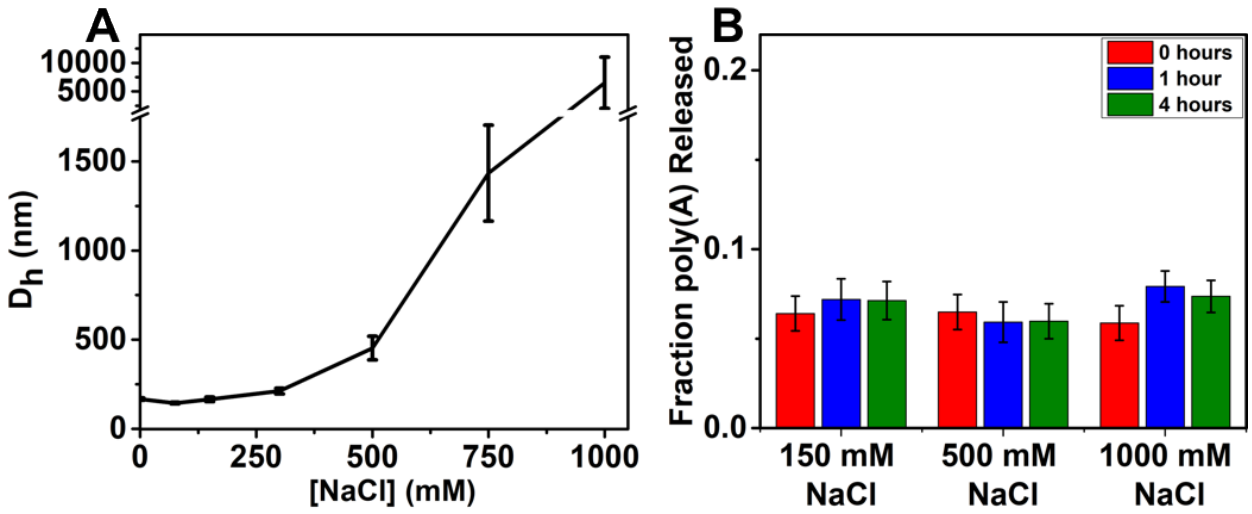

Figure 4.10 Poly(A)-C3Ms stability and poly(A) release against increasing ionic strength media. (A) Stability of poly(A)-C3Ms in aqueous media with increasing ionic strength. Aqueous suspensions of poly(A)-C3Ms were prepared from **PEG$_{113}$-*b*-5c$_{27}$** at 1.0 mg/mL (1.76 mM **5c** residue concentration) in nuclease-free water with an equimolar concentration of poly(A) residues relative to the charged **5c** residues (1.76 mM poly(A) residue concentration) in the desired concentration of aqueous NaCl. (B) Fraction of poly(A) released from complexes over time when exposed to different increase in NaCl concentration. Aqueous suspensions of poly(A)-C3Ms were prepared from **PEG$_{113}$-*b*-5c$_{27}$** at 10 mg/mL (17.6 mM **5c** residue concentration) in nuclease-free water with an equimolar concentration of poly(A) residues relative to charged **5c** residues (17.6 mM poly(A) residue concentration) in the presence of 150mM NaCl and were then diluted in the different aqueous media (150, 500 and 1000 mM NaCl concetrations) to give final polymer concentrations of 0.1 mg/mL (176 µM **5c** residue concentration, 6.51 µM total **PEG$_{113}$-*b*-5c$_{27}$** concentration).

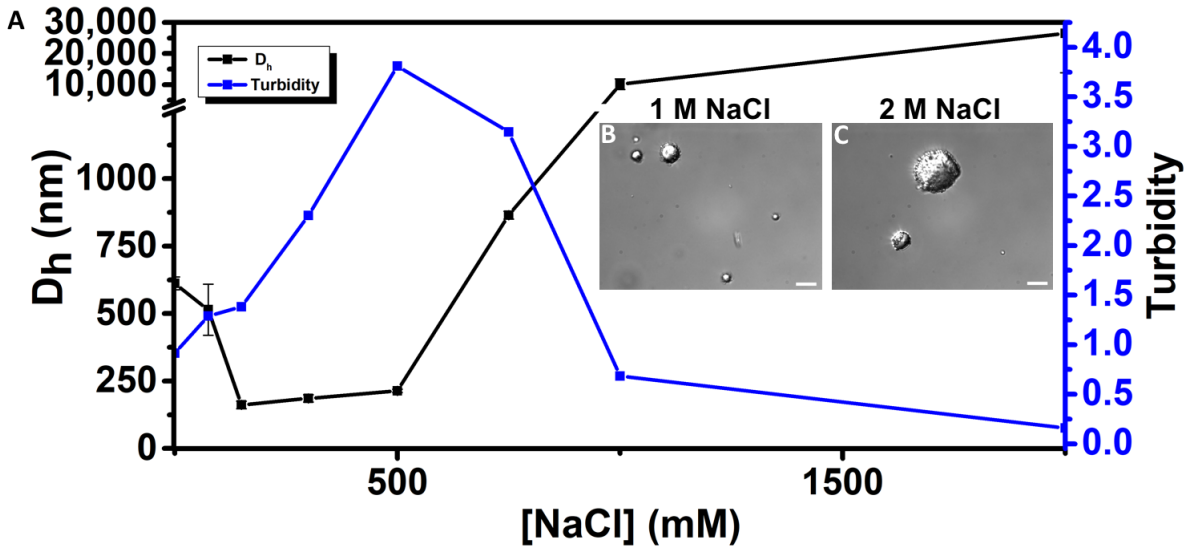

Figure 4.11. Behavior of poly(A)-C3Ms prepared with **PEG$_{113}$-*b*-5c$_{27}$** at increasing ionic strength characterized by DLS, UV-Vis spectroscopy, and DIC microscopy. Aqueous suspensions of poly(A)-C3Ms were prepared from **PEG$_{113}$-*b*-5c$_{27}$** at 4 mg/mL (7.04 mM **5c** residue concentration) in nuclease-free water with an equimolar concentration of poly(A) residues relative to charged **5c** residues (7.04 mM poly(A) residue concentration) in the desired concentration of aqueous NaCl. After confirming particle size by DLS, these samples were transferred to a quartz cuvette for analysis by UV-vis spectroscopy. (A) D_h obtained from DLS studies (black) and sample turbidity was determined by monitoring UV-Vis absorbance at 500 nm and measured in absorption units (a.u.) (Blue). For optical microscopy images of compound micelles, samples at ionic strengths of (B) 1 M NaCl and (C) 2 M NaCl were transferred onto glass slides and allowed to settle before imaging. Scale bars = 20 μm.

Having found that stable C3Ms with nanoscale diameters could be prepared using **PEG$_{113}$-*b*-5c$_{27}$** and poly(A), we continued to evaluate their suitability for polynucleotide delivery by examining their stability and morphology across a range of solution pH. Consequently, C3Ms of **PEG$_{113}$-*b*-5c$_{27}$** and poly(A) were prepared in the presence of acidic, neutral, or basic pH adjusted PBS buffer. These poly(A)-C3Ms were found to maintain an average D_h between 150 – 200 nm between pH 6.0 and pH 6.8 that fluctuated slightly but remained below 200 nm (Figure 4.12a). Between a pH of 7.3 and 7.7 these poly(A)-C3Ms experienced slight linear increase in D_h from 200 to 240 nm before a drastic increase in average D_h above pH 7.7 to about 450 nm (Figure 4.12a). Considering that

the pK_a of side-chain amine groups in the poly(S-alkyl-L-homocysteine) segment of the copolymers has been observed to be between pH 7.0 and 8.0,[51] the differences in D_h at different pH can likely be attributed to the amount of charge present on the cationic block. Below pH 7.0, the ammonium groups of the **5c$_{27}$** segment remain fully charged, which explains why the D_h of the poly(A)-C3Ms that did not increase above 200 nm. Between pH 7.3 and 7.7, deprotonation of the cationic segment starts to decrease the charge density of **5c$_{27}$** segments, which could explain the resulting increase in D_h. Indeed, as the charge of the cationic block is decreased while the anionic charge of the poly(A) remains constant, more **PEG$_{113}$-*b*-5c$_{27}$** polymer chains are needed to maintain charge neutrality at the core of the C3Ms. Above a pH of 8.0, the charge of the cationic block is minimal resulting in reduced ability to complex with the anionic poly(A). However, rather than complete dissolution of the complexes, the poly(A)-C3Ms swell but persist, likely indicating non-electrostatic association occurring between the polypeptide blocks at the center of the C3Ms (Figure 4.12a).[59] While these results are interesting, it was important to determine the extent of poly(A) encapsulation across this pH range to better understand the basis for the change in D_h of these poly(A)-C3Ms.

The morphology of these poly(A)-C3Ms was observed by DLS across a range of physiologically relevant pH and showed that these C3Ms remain stable. Changes in pH are a commonly used stimulus for triggering nanoparticle payload release due to differences in pH between the acidic environment of unhealthy tissues and intracellular compartments, and the neutral physiological pH of the extracellular space.[60] For this reason, it was important to study the relationship between encapsulation of poly(A) in acidic environments and the changes in poly(A)-C3M morphology (Figure 4.12b). The

encapsulation of poly(A) within the poly(A)-C3Ms (0.1 mg/mL, 176 µM **5c** residue concentration, 6.51 µM total **PEG$_{113}$-*b*-5c$_{27}$** concentration) at acidic pH of 5.4 and 6.5 were measured to simulate the acidic environment in the late-stage endosome which is a commonly utilized means of nanoparticle cargo release. At pH < 6.5, most of the side-chain ammonium groups in **5c** segments remain protonated, and so anionic poly(A) should remain complexed. Indeed, only 5% of the encapsulated poly(A) was released from the poly(A)-C3Ms based on the RyboGreen assay. Next, the relationship between poly(A) encapsulation and poly(A)-C3M morphology was probed at pH 7.3, representative of physiological pH. Above pH 7.0, deprotonation of the side-chain ammonium groups in **5c** segments becomes significant, which weakens the polyelectrolyte complexation of **PEG$_{113}$-*b*-5c$_{27}$** with poly(A) leading to destabilization of the C3Ms and an increase in particle D_h. Here, the D_h increase of the poly(A)-C3Ms at neutral and basic pH noted by DLS is correlated with an increase in poly(A) release (Figure 4.12a,b). At pH 7.3, over 20% of the poly(A) was released immediately based on the RyboGreen assay. Interestingly, when the poly(A)-C3M was exposed to pH 7.3 and poly(A) levels were measured over four hours, poly(A) release diminished from 20% at zero hours to 10% after four hours (figure 4.12b). Further studies will be needed to better understand this trend. Following the trend of deprotonation of the **5c** segment and destabilizing the poly(A) complexation at elevated pH, up to 40% of poly(A) was released at pH 8.3 (Figure 4.12b). Thus, the poly(A)-C3Ms were found to be stable at acidic pH and destabilized at basic pH, resulting in particle swelling, decomplexation, and poly(A) release. While these poly(A)-C3Ms will not release poly(A) cargo in response to physiologically relevant pH changes, future modifications to include appropriate pH responsive side-chain groups in

the polypeptide segments may enable the release of poly(A) in response to physiological triggers.

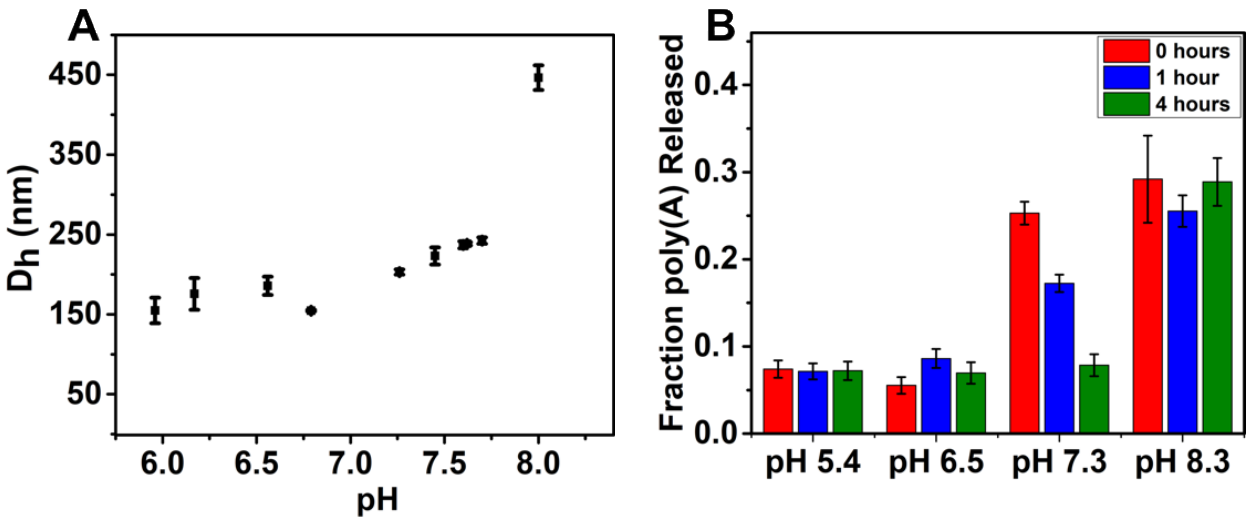

Figure 4.12. pH effect on poly(A)-C3Ms. (A) Stability of poly(A)-C3Ms in PBS buffer over a range of pH. Aqueous suspensions of poly(A)-C3Ms made from **PEG$_{113}$-*b*-5c$_{27}$** at 1.0 mg/mL (1.76 mM **5c** residue concentration) in nuclease-free water with poly(A) (0.58 mg/mL final concentration) were prepared using stock solutions of PBS buffer that had been adjusted to different pHs (150 mM final PBS concentration). The pH of poly(A)-C3M suspensions were determined after the DLS measurements were taken. (B) Fraction of poly(A) released from complexes over time when exposed to increases in pH. Aqueous suspensions of poly(A)-C3Ms were prepared from **PEG$_{113}$-*b*-5c$_{27}$** at 10 mg/mL (17.6 mM **5c** residue concentration) in nuclease-free water with an equimolar concentration of poly(A) relative to charged **5c** residues (17.6 mM poly(A) residue concentration) in the presence of 150mM NaCl and were then diluted in the different aqueous media (150 mM PBS buffer at pH 5.4, 6.5, 7.3 and 8.3) to give final polymer concentrations of 0.1 mg/mL (176 µM **5c** residue concentration, 6.51 µM total **PEG$_{113}$-*b*-5c$_{27}$** concentration).

To further investigate the stability of poly(A)-C3Ms, we studied the effect of added multivalent anions on C3M size and poly(A) release. Both intracellular and extracellular spaces *in vivo* are filled with multivalent anions that can exchange with the complexed

poly(A) in the C3Ms, resulting in the release of poly(A). The extracellular matrix is composed of highly charged anionic proteoglycans and glycosaminoglycans, including heparan sulfate-containing proteins and hyaluronic acid, that may potentially interact with C3Ms.[61] Additionally, cellular membranes are overall anionic due to the presence of anionic phospholipids, and will bind polycations, such as polyplexes used for gene delivery.[62,63] TPP and sodium alginate were used as model polyanions to study the interactions between multivalent anions and poly(A)-C3Ms (Figure 4.12c and d).[64] TPP was previously shown to complex with **PEG$_{113}$-*b*-5c$_{27}$** and form C3Ms. Here, poly(A)-C3M stability against exchange with TPP was studied by suspending poly(A)-C3Ms in increasing concentrations of TPP and quantifying release of poly(A). The TPP concentrations selected were based on the cationic **5c$_{27}$** residue concentration within the poly(A)-C3M to probe polyanion exchange at equimolar charge ratios. 25 μM TPP and 250 μM TPP are equivalent to a 0.5:1 and 5:1 anionic to cationic charge ratio, respectively. Data in Figure 4.13a showed that *ca.* 20% of the complexed poly(A) was released from poly(A)-C3Ms in the presence of TPP within one hour at all TPP concentrations, compared to less than 10% in 0mM TPP with 150 mM NaCl (Figure 4.3a). This indicates that the poly(A) release is due to TPP interactions with **PEG-*b*-5c$_{27}$** rather than a function of increased overall salt concentration. Interestingly, despite a 10-fold increase in TPP concentration between the samples with 25 μM and 250 μM TPP, similar levels of poly(A) release were measured (between 25-30% release) after four hours (Figure 4.13a). The similar levels of poly(A) release over a wide range of TPP concentration showed that the small molecule TPP was only partially effective in

exchanging with poly(A) within the C3Ms, likely due to the higher molecular weight and polymer chain of poly(A) forming a more stable C3M with **PEG-*b*-5c$_{27}$**.

To test this hypothesis, poly(A)-C3Ms were next mixed with increasing concentrations of polymeric sodium alginate in the presence of 150 mM NaCl (Figure 4.13b). The large excess of sodium alginate (4.6 to 23 mM) relative to poly(A) in the C3Ms (0.025 mM) was expected to favor displacement of poly(A) from the C3Ms. However, at 4.6 mM sodium alginate, only *ca*. 17% of the poly(A) was released after four hours. At 23 mM sodium alginate *ca*. 40% of the poly(A) was released, which showed that the poly(A)-C3Ms possess good stability against polyanion exchange, but counterion exchange may allow limited release of poly(A) cargo from these C3Ms. Thus, poly(A)-C3Ms exhibited considerable stability against decomplexation and dissolution in the presence of elevated salt and polyanions. This stability may help extend extracellular circulation time *in vivo* while further modification of the **5c** pH responsive groups may enable a pH responsive trigger for intracellular oligonucleotide release.

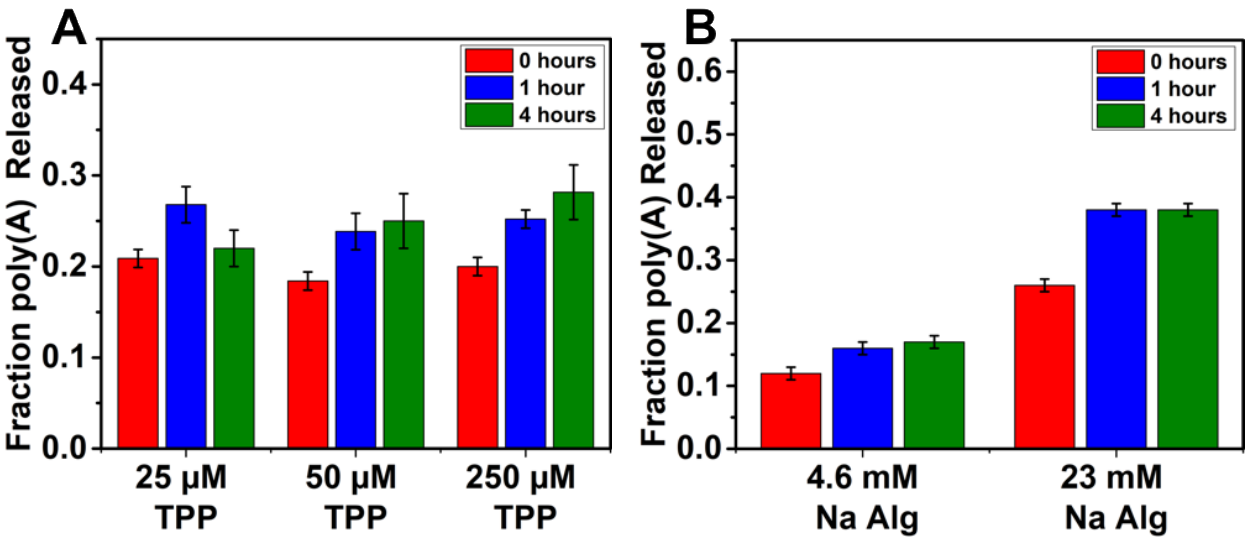

Figure 4.13. Polyanion exchange and release of poly(A) from **PEG$_{113}$-*b*-5c$_{27}$** containing poly(A)-C3Ms complexes. Fraction of poly(A) released from complexes over time when

exposed to (A) increasing TPP concentration and (B) increase in polymeric sodium alginate (Na Alg) polyanion concentration. Aqueous suspensions of poly(A)-C3Ms were prepared from **PEG$_{113}$-*b*-5c$_{27}$** at 10 mg/mL (17.6 mM **5c** residue concentration) in nuclease-free water with an equimolar concentration of poly(A) relative to charged **5c** residues (17.6 mM poly(A) residue concentration) in the presence of 150mM NaCl and were then diluted in the different aqueous media (25, 50, and 250 mM TPP and 4.6 and 23 mM Na Alg) to give final polymer concentrations of 0.1 mg/mL (176 μM **5c** residue concentration, 6.51 μM total **PEG$_{113}$-*b*-5c$_{27}$** concentration).

4.4 Conclusions

Previous work by the Deming group on cationic, α-helical amino acid side-chain modified poly(S-alkyl-L-homocysteine)s has shown the utility of these polypeptides for coacervate formation through PEC. In this study, spherical C3Ms were formulated by complexation of PEG-***b***-polypeptides, where the polypeptide segments are composed of coacervate forming, cationic, α-helical segments, with TPP or poly(A) in aqueous media. Variation of the polypeptide segment lengths and compositions of the amino acid side-chains was used to identify copolymers capable of forming uniform nanoparticles. These C3Ms were characterized by DLS, AFM, and cryoEM and were found to be stable in size over time. Notably, these **PEG-*b*-5c$_{27}$** copolymers were able to efficiently complex single-stranded poly(A), and the resulting poly(A)-C3Ms were stable against dilution to below 10 μM **PEG-*b*-5c$_{27}$** and physiologically relevant ionic strength, highlighting the potential of C3Ms as gene delivery vehicles. At basic pH or in the presence of multivalent anions, up to 40% of the oligonucleotide cargo could be released, which showed that complexation of poly(A) was reversible. Future *in vitro* studies will be necessary to evaluate the potential of these C3Ms for intracellular delivery. Collectively, these results demonstrate the potential of coacervate-forming cationic α-helical polypeptides for complexation and release of oligonucleotides for gene therapy.

4.5 Experimental

4.5.1 Materials and Methods

Tetrahydrofuran (THF) and dichloromethane (DCM) were each degassed with dinitrogen and passed through an activated alumina column before use. Unless otherwise specified, all post-polymerization modification chemistry was performed in glass vials under ambient atmosphere. $Co(PMe_3)_4$ and L-methionine N-carboxyanhydride (NCA) were prepared according to the literature procedures.[65] Reactions of **PEG$_{113}$-*b*-M$_x$** with epoxides were performed in scintillation vials under ambient atmosphere and temperature, unless otherwise specified. Small molecule chemistry was performed in heat-dried glassware under a nitrogen atmosphere, unless otherwise specified. All other reagents and solvents were used as received. In-house deionized water was used for all aqueous chemistry and dialysis unless otherwise specified. Thin-layer chromatography was performed with EMD gel 60 F254 plates (0.25 mm thickness) and spots were visualized using a UV lamp or $KMnO_4$ stain. Silicycle Siliaflash G60 silica (60−200 μm) was used for all column chromatography. Silica used for chromatographic purification of NCA monomers was dried under vacuum at 250 °C for 72 hrs and then stored in a dinitrogen-filled glovebox. Compositions of mobile phases used for chromatography are given in volume ratios. Dialysis was performed with regenerated cellulose tubing obtained from Spectrum laboratories with 2000 Da molecular weight cutoff. NMR spectra of solution samples were recorded on Bruker AV400 and Bruker AV300 instruments with chemical shifts reported relative to the deuterated solvent used. Dynamic light scattering (DLS) measurements were collected using a Malvern Zetasizer NanoZS. Turbidity measurements were recorded at a wavelength of 500 nm on an HP 8453 UV-vis

spectrophotometer. Atomic Force Microscopy (AFM) was performed using a Bruker Dimension FastScan. Differential interface contrast (DIC) images were taken using a Zeiss Axiovert 200 DIC/fluorescence inverted optical microscope. Negative-stain Transmission Electron Microscopy (TEM) was performed using a JEOL JEM 1200 EX. Cryoelectron microscopy (CryoEM) was performed using a TF20 (FEI Tecnai G2). Sample preparation and imaging was performed at the Electron Imaging Center for Nanomachines (EICN) at the UCLA California NanoSystems Institute (CNSI). Fluorescence readings were taken on a BioTek Synergy H1 Hybrid Reader. Quant-iT RyboGreen RNA Reagent and Kit was purchased from Invitrogen and used as indicated by the included protocol.

4.5.2 Synthesis of Small Molecules and PEG-*b*-polypeptides

General procedure for synthesis of N-TFA-amino acids

The desired amino acid (2 g) was suspended in methanol (MeOH, 30 mL). Triethylamine (2 eq, TEA) was then added, and the suspension was stirred for 15 min. Ethyl trifluoroacetate (1.1 eq, ETFA) was then added dropwise and the suspension was stirred overnight. The solvent was removed *in vacuo* and the residue was resuspended in ethyl acetate (EtOAc) (50 mL/g of starting amino acid) and washed 3x with 0.1 N HCl before drying with sodium sulfate. The resulting EtOAc solution was concentrated *in vacuo* to give an oil that was dried under high vacuum overnight to afford the product as a slightly yellow solid.

General procedure for synthesis of N-TFA-amino acid (2-allyloxy)ethyl amides

A round bottom flask was charged with a stirbar, the desired TFA-amino acid (1 eq, TFA-AA), THF (to give 0.38 M solution), and hydroxybenzotriazole (1 eq, HOBt). The

mixture was cooled to 0 °C in an ice bath, and then a 3.6 M solution of N,N′-dicyclohexylcarbodiimide (DCC) (1.2 eq) in THF was added dropwise to the stirred mixture. The mixture was let stir on ice for 30 min, and a 3.3 M solution of 2-(allyloxy)ethylammonium trifluoroacetate (1.1 eq) in THF was then added to the mixture dropwise followed by dropwise addition of TEA (2 eq). The mixture was let stir in the ice bath, which was allowed to warm to ambient temperature overnight. The next day, the resulting suspension in THF was filtered into a round bottom flask and the THF was removed *in vacuo*. The residue was thereafter dissolved in EtOAc to give a 0.30 M solution with respect to the starting quantity of TFA-AA. This solution was then left in a freezer overnight and any further precipitate was removed by filtration. The resulting solution was purified using flash chromatography at a solvent ratio of 2:1 hexanes (hex) to EtOAc to afford the product as a white solid.

General procedure for synthesis of N-TFA-amino acid (2-glycidyloxy)ethyl amides

The following procedure was taken from the literature with some modifications.[50] The desired TFA-amino acid (2-allyloxy)ethyl amide (1 eq) was dissolved in DCM (3.3 mL/mmol alkene). Commercial 70 % mCPBA (1.5 eq) was then added and the mixture was stirred. After full conversion of alkene was confirmed by TLC (24 - 36 hrs), the suspension was cooled in an ice bath. The mixture was treated with 10% Na_2SO_3 (aq) (1.5 eq) followed by 10% Na_2CO_3 (aq) (1.3 eq); it was then stirred for 5 min. The reaction mixture was diluted with EtOAc and washed 2x with sat. $NaHCO_3$ (aq) followed by brine. The organic layer was dried over Na_2SO_4, concentrated *in vacuo* and purified by flash chromatography with a solvent ratio of 1:1 hex to EtOAc to afford the product as a white solid.

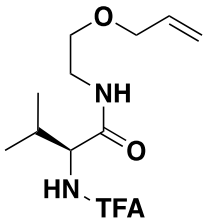

N-TFA-L-valine (2-allyloxy)ethyl amide, 2b

Prepared from TFA-Val using the *General procedure for synthesis of TFA-amino acid (2-allyloxy)ethyl amides*. Spectral data matches previously reported literature procedures.[51]

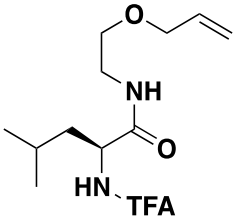

N-TFA-L-leucine (2-allyloxy)ethyl amide, 2c

Prepared from TFA-Leu using the *General procedure for synthesis of TFA-amino acid (2-allyloxy)ethyl amides*. Spectral data matches previously reported literature procedures.[51]

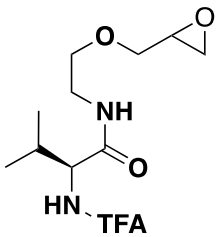

N-TFA-L-valine (2-glycidyloxy)ethyl amide, 3b

Prepared from N-TFA-L-valine (2-allyloxy)ethyl amide using the *General procedure for synthesis of TFA-amino acid (2-glycidyloxy)ethyl amides*. Spectral data matches previously reported literature procedures.[51]

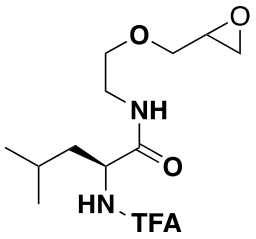

N-TFA-L-leucine (2-glycidyloxy)ethyl amide, 3c

Prepared from N-TFA-L-leucine (2-allyloxy)ethyl amide using the *General procedure for synthesis of TFA-amino acid (2-glycidyloxy)ethyl amides*. Spectral data matches previously reported literature procedures.[51]

Preparation of mPEG$_{113}$-NCO

α-methoxy-ω-isocyanoethyl-poly(ethylene glycol), mPEG-NCO (DP = 113) was synthesized by direct amination of α-methoxy-poly(ethylene glycol), mPEG$_{113}$-OH, and subsequent phosgenation, following literature procedures.[66] Briefly described here, mPEG$_{113}$-OH (6.0 g, 1 eq) was dissolved in 20 mL dry THF and stored under N_2. Separately, diisopropyl azodicarboxylate (DIAD) (710 uL, 3 eq) was dissolved in 1 mL dry THF and added dropwise under N_2 to an ice-water bath cooled solution of triphenyl phosphine (940 mg, 3 eq) in 5 mL dry THF. The reaction was stirred for 1 hr under N_2 before the mPEG$_{113}$-OH solution was transferred via cannula into the DIAD/triphenyl phosphine solution, allowing the reaction mixture to stir for an additional hr. Next, phthalimide (530 mg, 3 eq) was added as a powder to the reaction under positive N_2 pressure and the reaction mixture was allowed to stir overnight at 50 ^{o}C. After conjugation of the phthalimide to mPEG, hydrazine (850 uL, 15 eq) was added to the reaction, which was refluxed for 3 hrs to generate mPEG$_{113}$-NH_2. The crude product was evaporated under reduced pressure to give a yellow oil, which was then dissolved in cold 5 M HCl and filtered to remove water-insoluble impurities. The acidified solution was then

neutralized with an equivalent amount of 5 M NaOH and transferred to a 2000 Da MWCO dialysis bag for further purification. $mPEG_{113}$-NH_2 was dialyzed extensively against isopropanol, isopropanol/DI water (1:1), and finally DI water to remove small molecule impurities, and the solution was lyophilized to give the product as a solid (3.5 g, 58% yield). Amination was confirmed using ^1H NMR to quantify shifts of resonances of methylene protons closest to the amine functional group.

^1H NMR (400 MHz, $CDCl_3$) δ 3.67 (s, 440H), 3.41 (s, 2H), 2.97 – 2.90 (m, 3H**).**

To prepare $mPEG_{113}$-NCO, $mPEG_{113}$-NH_2 (3.5 g) was dissolved in dry THF under N_2 followed by addition of phosgene (2 eq per amine group) and allowing the mixture to stir overnight at 35 ^oC. The $mPEG_{113}$-NCO crude product was dried in vacuo and transferred to a N_2 filled glove box for further purification. Here, the crude oil was redissolved in THF and precipitated into hexanes twice before drying under vacuum to recover the product as a white solid (2.5 g, 71% yield).

Preparation of poly(ethylene glycol)$_{113}$-*b*-poly(L-methionine)$_x$, PEG_{113}-*b*-M_x

For preparation of polypeptide samples at 500 mg scale in a N_2 filled glove box, a defined volume of $Co(PMe_3)_4$ initiator (20 mg/mL solution in THF) was added to the reaction flask with stirring. Met NCA (50 mg/mL in THF) was quickly added to the stirring initiator solution. After *ca*. 90 min, consumption of the NCA was confirmed by FTIR by monitoring loss of the anhydride bands at 1790 cm^{-1} and 1850 cm^{-1}. A 200 µL aliquot of the reaction mixture was removed for end-group analysis (*vide infra*). To the remaining polypeptide was added $mPEG_{113}$-NCO in THF (100 mg/mL, 3 eq per $Co(PMe_3)_4$) and the reaction mixture was stirred for 48 hrs. Next, the copolymer was precipitated into ether and dried, followed by resuspension in DI H_2O and transferred to a 300 kDa MWCO

dialysis bag. The polymer was dialyzed against 1M HCl and DI H_2O (5 days, 2 dialysate changes/day). The retentate was then filtered through a 0.45 µm polypropylene syringe filter before lyophilization to give the product as a white solid.

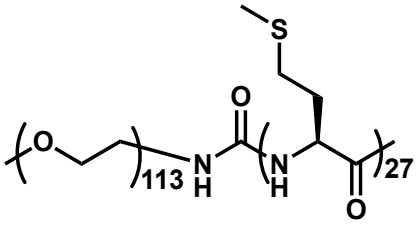

PEG_{113}-*b*-poly(L-methionine)$_{27}$, PEG_{113}-*b*-M_{27}

Prepared using the *Preparation of poly(ethylene glycol)$_{113}$-b-poly(L-methionine)$_x$.* 80% yield.

^{1}H NMR (400 MHz, TFA-d) δ 4.91 (br s, 27H), 3.96 (br s, 440H), 2.74 (br s, 60H), 2.24 (br m, 135H).

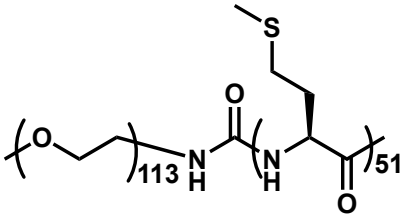

PEG_{113}-*b*-poly(L-methionine)$_{51}$, PEG_{113}-*b*-M_{51}

Prepared using the *Preparation of poly(ethylene glycol)$_{113}$-b-poly(L-methionine)$_x$.* 60% yield.

^{1}H NMR (400 MHz, $CDCl_3$) δ 4.16 (s, 51H), 3.69 (s,440H), 2.80 (br s, 55H), 2.61 (s, 62H), 2.16 (br m, 282H).

General procedure for determination of polypeptide chain length using end-group analysis after active chain-ends are reacted with mPEG-NCO

The procedure for *Preparation of poly(ethylene glycol)$_{113}$-b-poly(L-methionine)$_x$* was followed. Once the polymerization completion was confirmed by FTIR, a solution of

α-methoxy-ω-isocyanoethyl-poly(ethylene glycol), mPEG-NCO (DP = 22, 3 eq per $Co(PMe_3)_4$) in THF was added to a *ca*. 200 µL aliquot of polymerization reaction mixture in a N_2 filled glove box. The reaction was let stand overnight before removing from the glovebox, followed by precipitation of polymer by addition to excess 0.1 M HCl. The precipitate was stirred vigorously for 1 hr followed by centrifugation to recover the pellet, and the supernatant was discarded. The pellet was washed and centrifuged 3 times with DI H_2O to remove excess mPEG-NCO before lyophilization to give the product as a white solid. ^{1}H NMR in deuterated TFA (d-TFA) was used to determine the molecular weight of the polypeptide segment (M_n), according to literature procedures.[67]

4.5.3 Post-Polymerization Modifications

General procedure for alkylation of PEG_{113}-*b*-M_x (x = 27 and 51)

This procedure was modified from a related procedure in the literature.[50] **PEG_{113}-*b*-M_x** was suspended in glacial AcOH (50 mg/mL). The desired epoxide (3 eq per methionine residue) was added and the mixture was stirred vigorously at 38 °C. After 4 to 6 hrs, additional epoxide (3 eq per methionine residue) was added to the reaction mixture, followed by additional AcOH to give a polypeptide concentration of 25 mg/mL. After 48 hrs, the limpid solution was transferred to a 2000 Da MWCO dialysis bag and dialyzed against 3 mM HCl (aq) (24 hrs, 3 changes) and then DI water (24 hrs, 3 changes). The retentate was lyophilized to provide the **PEG_{113}-*b*-4b$_x$** and **PEG_{113}-*b*-4c$_x$** sulfonium salts as white solids. Yields provided in Table 4.1.

General procedure for demethylation and deprotection of PEG_{113}-*b*-*4*b$_x$ and PEG_{113}-*b*-*4*c$_x$ sulfonium salts

This procedure was modified from a related procedure in the literature.[49] A solution of the desired alkylated **PEG$_{113}$-*b*-4b$_x$** or **PEG$_{113}$-*b*-4c$_x$** sulfonium salt in 75% EtOH (aq) ([alkylated methionine residues] = 20 mM) was prepared in a vial and then treated with ammonium pyrrolidinedithiocarbamate (APDC, 5.0 eq per methionine residue). The headspace of the vial was briefly flushed with a stream of N_2 and the vial was immediately capped. The mixture was vortexed until homogenous, then allowed to stand for 24 hrs at ambient temperature. To the mixture was added H_2O (7.5 mL per mmol of alkylated methionine residues) and K_2CO_3 (10 eq per alkylated methionine residue). The reaction was allowed to stir vigorously at 50 °C for 5 days and the solution was then transferred to a 2000 Da MWCO dialysis bag and dialyzed against 50% MeOH (aq) containing 3 mM HCl (24 hrs, 3 changes), followed by 3mM HCl (24 hrs, 3 changes) and then H_2O (8 hrs, 3 changes). The retentate was lyophilized to provide the amino acid functionalized poly(S-alkyl-L-homocysteine) product: **PEG$_{113}$-*b*-*5*b$_{27}$**, **PEG$_{113}$-*b*-*5*c$_{27}$**, **PEG$_{113}$-*b*-*5*b$_{51}$**, or **PEG$_{113}$-*b*-*5*c$_{51}$**. For all four products additional processing was required to facilitate their dissolution in H_2O. A minimal amount of TFA was added to lyophilized copolymer obtain complete dissolution. The solution was then diluted by addition of 10 volumes of DI H_2O and then transferred to a 2000 Da MWCO dialysis bag and dialyzed against 1 M NaCl containing 3 mM HCl (24 hrs, 1 change), followed by 3 mM HCl (24 hrs, 2 changes), and DI H_2O (24 hrs, 3 changes). The retentate was lyophilized again to provide the desired product as a fluffy white solid. ^{19}F NMR was used to confirm complete removal of TFA counterions. Yields provided in Table 4.1.

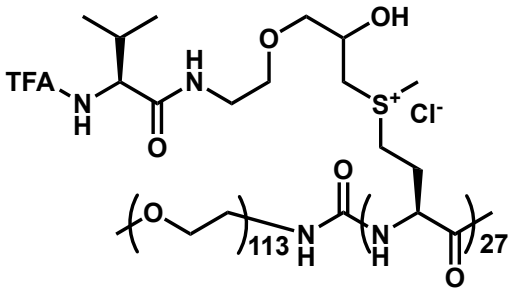

PEG$_{113}$-*b*-poly(*S*-(3-(2-(N-trifluoroacetyl-L-valine amido)ethoxy)-2-hydroxypropyl)-L-methionine sulfonium chloride)$_{27}$, PEG$_{113}$-*b*-4b$_{27}$

Prepared using the *General procedure for alkylation of* ***PEG$_{113}$-b-M$_x$*** *(x = 27 and 51)*

Yield given in Table 4.1.

^{1}H NMR (400 MHz, TFA-*d*) δ 4.95 (br s, 27H), 4.58 (br s, 27H), 4.35 (br d, 27H), 3.91 (s, 452H), 3.86 – 3.56 (br m, 273H), 3.19 – 3.09 (br m, 81H), 2.60 (br d, 54H), 2.26 – 2.16 (m, 27H), 1.06 (dd, 162H).

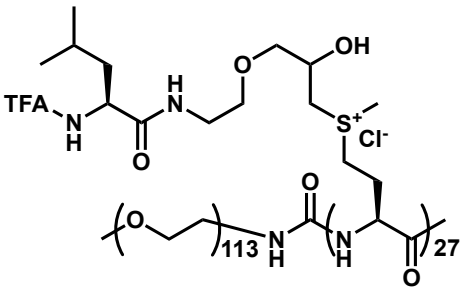

PEG$_{113}$-*b*-poly(*S*-(3-(2-(N-trifluoroacetyl-L-leucine amido)ethoxy)-2-hydroxypropyl)-L-methionine sulfonium chloride)$_{27}$, PEG$_{113}$-*b*-4c$_{27}$

Prepared using the *General procedure for alkylation of* ***PEG$_{113}$-b-M$_x$*** *(x = 27 and 51).*

Yield given in Table 4.1.

^{1}H NMR (400 MHz, TFA-*d*) δ 4.97 (br s, 27H), 4.68 (br s, 27H), 4.57 (br s, 27H), 3.91 (s, 452H), 3.88 – 3.57 (br m, 273H), 3.22 – 3.08 (br m, 81H), 2.61 (br d, 54H), 1.88 – 1.79 (br m, 27H), 1.72 (br m, 54H), 0.98 (dd, 162H).

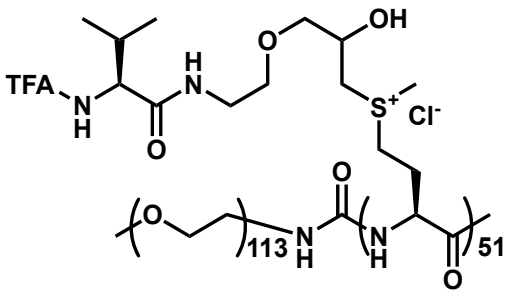

PEG$_{113}$-*b*-poly(*S*-(3-(2-(N-trifluoroacetyl-L-valine amido)ethoxy)-2-hydroxypropyl)-L-methionine sulfonium chloride)$_{51}$, PEG$_{113}$-*b*-4b$_{51}$

Prepared using the *General procedure for alkylation of* ***PEG$_{113}$-b-M$_x$*** *(x = 27 and 51).*

Yield given in Table 4.1.

^{1}H NMR (400 MHz, TFA-*d*) δ 4.96 (br s, 51H), 4.59 (br s, 51H), 4.36 (br s, 51H), 3.91 (s, 452H), 3.85 – 3.55 (br m, 513H), 3.14 (br m, 153H), 2.60 (br d, 102H), 2.26 – 2.16 (br m, 51H), 1.08 – 1.05 (br m, 306H).

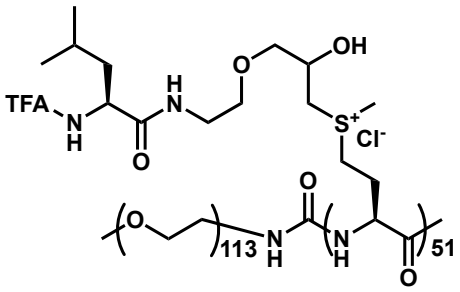

PEG$_{113}$-*b*-poly(*S*-(3-(2-(N-trifluoroacetyl-L-leucine amido)ethoxy)-2-hydroxypropyl)-L-methionine sulfonium chloride)$_{51}$, PEG$_{113}$-*b*-4c$_{51}$

Prepared using the *General procedure for alkylation of* ***PEG$_{113}$-b-M$_x$*** *(x = 27 and 51).*

Yield given in Table 4.1.

^{1}H NMR (400 MHz, TFA-*d*) δ 4.94 (br s, 51H), 4.67 (br s, 51H), 4.56 (br s, 51H), 3.91 (br s, 452H), 3.88 – 3.56 (br m, 513H), 3.17 – 3.08 (br m, 153H), 2.57 (br d, 102H), 1.88 – 1.79 (br m, 51H), 1.78 – 1.66 (br m, 102H), 0.98 (dd, 306H).

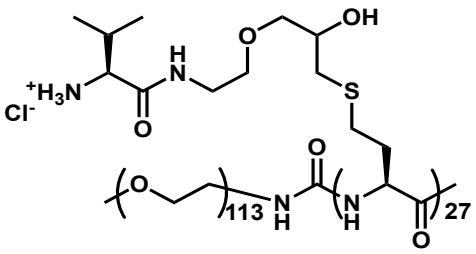

PEG$_{113}$-*b*-poly(*S*-(3-(2-L-valine amido)ethoxy)-2-hydroxypropyl)-L-homocysteine hydrochloride)$_{27}$, PEG$_{113}$-*b*-5b$_{27}$

Prepared using the *General procedure for demethylation and deprotection of* ***PEG$_{113}$-b-4b$_x$*** *and* ***PEG$_{113}$-b-4c$_x$*** *sulfonium salts.* Yield given in Table 4.1.

^{1}H NMR (400 MHz, TFA-*d*) δ 4.86 (br s, 27H), 4.23 (br s, 27H), 4.18 (br s, 27H), 3.91 (s, 452H), 3.76 – 3.57 (m, 165H), 2.78 (br s, 108H), 2.36 (br m, 27H), 2.18 (br s, 54H), 1.16 (d, 162H).

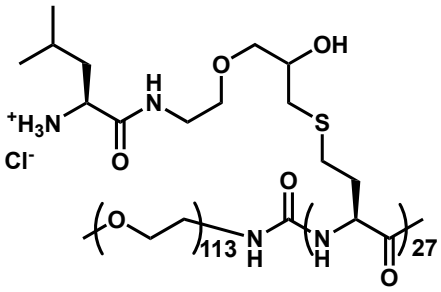

PEG$_{113}$-*b*-poly(*S*-(3-(2-L-leucine amido)ethoxy)-2-hydroxypropyl)-L-homocysteine hydrochloride)$_{27}$, PEG$_{113}$-*b*-5c$_{27}$

Prepared using the *General procedure for demethylation and deprotection of* ***PEG$_{113}$-b-4b$_x$*** *and* ***PEG$_{113}$-b-4c$_x$*** *sulfonium salts.* Yield given in Table 4.1.

^{1}H NMR (400 MHz, TFA-*d*) δ 4.86 (br s, 27H), 4.36 (br t, 27H), 4.23 (br s, 27H), 3.91 (s, 452H), 3.86 – 3.54 (m, 165H), 2.78 (br s, 108H), 2.19 (br s, 54H), 1.88 (br m, 54H), 1.78 (br m, 27H), 1.03 (t, 162H).

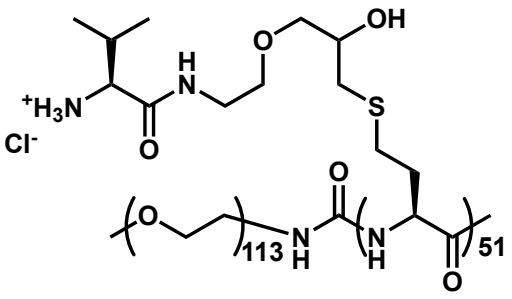

PEG_{113}-*b*- poly(*S*-(3-(2-L-valine amido)ethoxy)-2-hydroxypropyl)-L-homocysteine hydrochloride)$_{51}$, PEG_{113}-*b*-5b$_{51}$

Prepared using the *General procedure for demethylation and deprotection of* ***PEG_{113}-b-4b$_x$*** *and* ***PEG_{113}-b-4c$_x$*** *sulfonium salts.* Yield given in Table 4.1.

^{1}H NMR (400 MHz, TFA-*d*) δ 4.85 (br s, 51H), 4.23 (br s, 51H), 4.16 (br d, 51H), 3.91 (s, 452H), 3.87 – 3.62 (br m, 309H), 2.78 (br s, 204H), 2.40 – 2.32 (br m, 51H), 2.18 (br s, 102H), 1.16 (d, 306H).

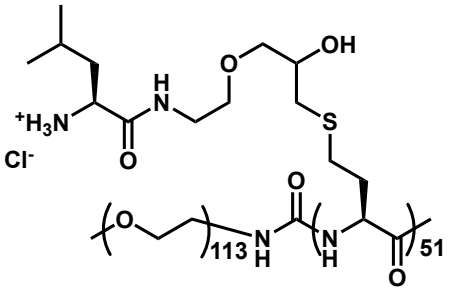

PEG_{113}-*b*-poly(*S*-(3-(2-L-leucine amido)ethoxy)-2-hydroxypropyl)-L-homocysteine hydrochloride)$_{51}$, PEG_{113}-*b*-5c$_{51}$

Prepared using the *General procedure for demethylation and deprotection of* ***PEG_{113}-b-4b$_x$*** *and* ***PEG_{113}-b-4c$_x$*** *sulfonium salts.* Yield given in Table 4.1.

^{1}H NMR (400 MHz, TFA-*d*) δ 4.86 (br s, 51H), 4.33 (t, 51H), 4.22 (br s, 51H), 3.91 (s, 452H), 3.87 – 3.54 (br m, 309H), 2.77 (br s, 204H), 2.16 (br s, 102H), 1.88 (br m, 102H), 1.78 (br m, 51H), 1.03 (t, 306H).

4.5.4 Procedures for Formulation of C3Ms

Preparation of tripolyphosphate-complex coacervate core micelle (TPP-C3M) suspensions for DLS stability studies

Stock solutions of **PEG$_{113}$-*b*-5b$_{27}$**, **PEG$_{113}$-*b*-5c$_{27}$**, **PEG$_{113}$-*b*-5b$_{51}$**, and **PEG$_{113}$-*b*-5c$_{51}$** were separately prepared at 10 mg/mL (18, 17.6, 21.4 and 20.1 mM **5x** polypeptide residue concentrations, respectively) in DI water and filtered through 0.45 μm PTFE filters. These were each mixed in a 1:1 ratio (v:v) with a filtered stock solution of 26 mM sodium tripolyphosphate (TPP) with 300 mM NaCl in DI water at pH 7.0 to give final concentrations of 5 mg/mL copolymer (9, 8.8, 10.7 and 10.1 mM **5x** polypeptide residue concentrations, respectively), 13 mM TPP and 150 mM NaCl. Each sample was lightly agitated by tapping the vial and permitted to equilibrate for 1 hr before taking the first measurements. These samples were used for DLS studies as well as DIC microscopy experiments.

Preparation of poly(A)-complex coacervate core micelle (poly(A)-C3M) suspensions for DLS stability studies

All stock solutions were prepared using nuclease-free water and filtered through 0.45 μm PTFE syringe filters prior to use. Stock solutions of **PEG$_{113}$-*b*-5c$_{27}$** and **PEG$_{113}$-*b*-5c$_{51}$** were separately prepared at 10 mg/mL concentration (17.6 mM and 20.7 mM **5c** residue concentrations, respectively) in 300 mM aqueous NaCl. Stock solutions of poly(A) were prepared at concentrations of 5.8 and 6.8 mg/mL (17.6 mM and 20.7 mM poly(A) residue concentrations, respectively). Stock solutions of **PEG$_{113}$-*b*-5c$_{27}$** and **PEG$_{113}$-*b*-5c$_{51}$** were separately mixed in a ratio of 1:1 (v:v) with 5.8 and 6.8 mg/mL poly(A) solutions, respectively, to achieve an equal stoichiometric ratios of [**5c** residues]:[poly(A) residues] for both samples. Final sample concentrations were 5 mg/mL copolymer (8.8 mM and

10.4 mM **5c** residue concentrations, respectively), 2.9 mg/mL poly(A) (8.8 mM poly(A) residue concentration) for **PEG$_{113}$-*b*-5c$_{27}$**, and 3.4 g/mL poly(A) (10.4 mM poly(A) residue concentration) for **PEG$_{113}$-*b*-5c$_{51}$** all at final NaCl concentrations of 150 mM. Each sample was lightly agitated by tapping the vial and was permitted to equilibrate for 1 hr before taking the first measurements.

Preparation of poly(A)-C3M suspensions for salt studies

All stock solutions were prepared using nuclease-free water and filtered through 0.45 µm PTFE syringe filters prior to mixing. Stock solutions in water were prepared for **PEG$_{113}$-*b*-5c$_{27}$** at 10 mg/mL (17.6 mM **5c** residue concentration), for poly(A) at 5.8 mg/mL (17.6 mM poly(A) residue concentration) and for NaCl (5 M). Samples were prepared by mixing the stock solutions of **PEG$_{113}$-*b*-5c$_{27}$**, poly(A) and NaCl in a 1:1:x (v/v/v) ratio with x corresponding to the appropriate amount of NaCl solution to give final salt concentrations of 0, 0.075, 0.15, 0.3, 0.5, 0.75, 1.0 and 2.0 M. Particle suspensions were diluted with necessary amounts of nuclease-free water to give final polymer concentrations of either 1 mg/mL or 4 mg/mL. Each sample was lightly agitated by tapping the vial and was permitted to equilibrate for 1 hr before taking the first measurements.

Preparation of poly(A)-C3M suspensions for pH studies

All stock solutions were prepared using nuclease-free water and filtered through a 0.45 µm PTFE syringe filter prior to mixing. Stock solutions were prepared for **PEG$_{113}$-*b*-5c$_{27}$** at 10 mg/mL (17.6 mM **5c** residue concentration), for poly(A) at 5.8 mg/mL (17.6 mM poly(A) residue concentration) and for 10x PBS buffer adjusted to different pH ranging between pH 5.0 and 9.0. Samples were prepared by mixing the stock solutions of **PEG$_{113}$-*b*-5c$_{27}$**, poly(A) and 1.5 M PBS in a 1:1:1 (v/v/v) ratio. These suspensions were then

diluted with nuclease free water to give final **PEG$_{113}$-*b*-5c$_{27}$** concentrations of 1.0 mg/mL (1.76 mM **5c** residue concentration), poly(A) concentrations of 0.58 mg/mL (1.76 mM poly(A) residue concentration) and 150 mM PBS. Each sample was lightly agitated by tapping the vial and was permitted to equilibrate for 1 hr before taking the first measurements. The pH of each sample was determined using a pH probe after DLS measurements.

Preparation of complex coacervate core micelle (C3M) suspensions for atomic force microscopy (AFM) studies

Aqueous suspensions of TPP-C3Ms and poly(A)-C3Ms made using **PEG$_{113}$-*b*-5c$_{27}$** were prepared as described in *Preparation of tripolyphosphate-complex coacervate core micelle (TPP-C3M) suspensions for DLS stability studies* or *Preparation of poly(A)-complex coacervate core micelle (poly(A)-C3M) suspensions for DLS stability studies*. The formation of C3Ms was confirmed by DLS and then the suspensions were diluted in nuclease-free water to final copolymer concentrations of 0.1 mg/mL before imaging.

Preparation of poly(A)-C3M suspensions for transition electron microscopy (TEM) studies

A stock solution of **PEG$_{113}$-*b*-5c$_{27}$** at 50 mg/mL (88 mM **5c** residue concentration), in 300 mM aqueous NaCl was prepared using nuclease-free water and was filtered through a 0.45 µm PTFE filter. This solution was mixed in a 1:1 (v:v) ratio with a 29 mg/mL solution of poly(A) (88 mM poly(A) residue concentration) in nuclease-free water to give to a final copolymer concentration of 25 mg/mL. This sample was then further diluted with a stock solution of 150 mM NaCl (in nuclease-free water) filtered through a 0.45 µm PTFE filter to prepare samples for TEM measurements.

4.5.5 Characterization of C3Ms

Dynamic light scattering (DLS) measurements

Dynamic light scattering measurements were performed on a Malvern Panalytical Zetasizer Nano ZS and measured using a non-invasive backscattering angle of 173°. Samples were prepared in disposable plastic cuvettes (ZEN0118 and ZEN0040) and analyzed using the intensity distribution, number distribution and z-average cumulant method.

Turbidity measurements

Turbidity measurements were recorded using a HP 8453 UV-vis spectrophotometer at a wavelength of 500 nm using a quartz cuvette with a path length of 1 cm. The turbidity is defined as $-\ln(I/I_0)$, where I_0 = incident light intensity and I = intensity of light transmitted through the sample volume. The turbidity was measured in absorption units (a.u.). Samples were prepared as described in *Preparation of poly(A)-C3M suspensions for salt studies* at final **PEG$_{113}$-*b*-5c$_{27}$** concentrations of 4 mg/mL.

AFM measurements

Atomic force microscopy measurements on air-dried samples were performed on a Dimension FastScan Bruker AFM system. The topography images of the nanoparticles were obtained with ScanAsyst^{TM} mode using a silicon tip on a nitride lever (SCANASYST-AIR-HPI, Bruker) with cantilever resonance of 55 kHz, a spring constant of 0.25 N/m and a nominal tip radius of 2 nm and a maximum radius of 10 nm. Samples were prepared by dropcasting 5 µL of the C3M suspension onto freshly cleaved mica and then permitting the sample to dry before imaging. A final concentration of 0.1 mg/mL relative to **PEG$_{113}$-*b*-5c$_{27}$** was found to provide the best conditions for imaging.

Cryogenic transmission electron microscopy of poly(A)-C3Ms

A drop of a suspension of poly(A)-C3Ms at 2.5 mg/mL relative to **PEG$_{113}$-*b*-5c$_{27}$** was placed on a 300 mesh Quantifoil R1.2/1.3 holey copper grid. The sample was allowed to sit for 10 s before blotting to remove residual fluid. The grid was then placed in a liquid ethane cryogenic bath before storing under liquid nitrogen; it was then placed on a cold stage for imaging using a TF20 (FEI Tecnai G2) electron microscope with an accelerating voltage of 200 kV.

Differential interference contrast microscopy of TPP-C3Ms

Stock solutions of **PEG$_{113}$-*b*-5b$_{27}$**, **PEG$_{113}$-*b*-5c$_{27}$**, **PEG$_{113}$-*b*-5b$_{51}$**, and **PEG$_{113}$-*b*-5c$_{51}$** were prepared at 10 mg/mL mL (18, 17.6, 21.4 and 20.1 mM polypeptide residue concentrations, respectively) in DI water. A stock solution of TPP (26 mM) and NaCl (300 mM) was mixed with a stock solution of copolymer in a 1:1 (v/v) ratio to give a final TPP concentration of 13 mM, NaCl concentration of 150 mM NaCl, and copolymer concentration of 5.0 mg/mL (9, 8.8, 10.7, and 10.1 mM **5x** polypeptide residue concentrations, respectively). Upon mixing, each sample formed a milky suspension, which was quickly transferred to a Fisherbrand Superfrost slide prepared with a Secure-Seal Image Spacer with a thickness of 0.12 mm and then sealed using a 1.5 mM Fisherbrand coverslip. Each sample was allowed to stand for 5 min to allow liquid coacervate droplets to condense, or for precipitate to settle, onto the glass surface. Samples were then imaged using a Zeiss Axiovert 200 DIC/Fluorescence Inverted Optical Microscope. Only copolymer **PEG$_{113}$-*b*-5c$_{51}$** resulted in TPP-C3Ms visible by optical microscopy.

Poly(A) calibration curve and encapsulation efficiency

All buffers and salt solutions were prepared in nuclease-free water and filtered through 0.45 µm PES filters. To prepare the calibration curve of poly(A) with RyboGreen, a stock solution of poly(A) (5.8 mg/ml) in 150 mM NaCl was diluted to 1 µg/mL in 1X TE buffer (Invitrogen) and then this mixture was serially diluted to obtain a series of lower concentrations. 60 µL of each concentration of poly(A) was dispensed in triplicate into a 96 well plate before adding 60 µL of 1X RyboGreen RNA Reagent (Invitrogen). The plate was then covered in foil and incubated for 5 min before placing on a fluorescence plate reader (Excitation 480 nm, Emission 520 nm).

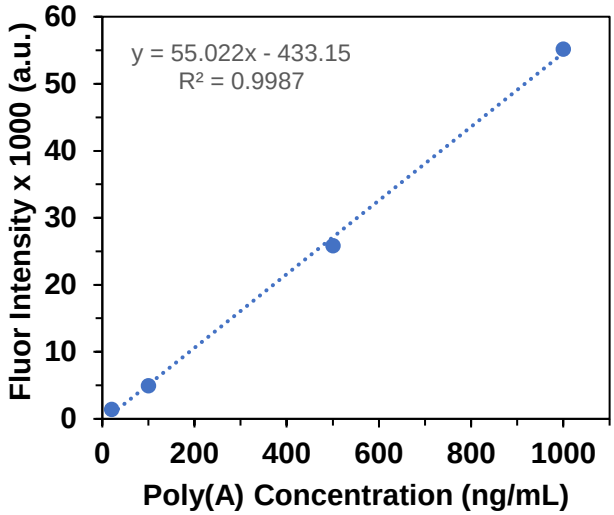

Equation to calculate encapsulation efficiency:

$$Fraction\ poly(A)\ released = \frac{\left(\frac{(Sample\ signal - 2080) + 433.15}{55.02}\right)}{1000}$$

Sample signal is fluorescent signal from supernatant containing unencapsulated poly(A)

2080 is background signal from poly(A)-C3M fluorescence (Figure 4.9a)

1000 ng/mL is maximum concentration of poly(A) present after dilution in TE buffer

The poly(A)-C3M suspensions were prepared by mixing 500 µL of a 10 mg/mL **PEG$_{113}$-*b*-5c$_{27}$** (17.6 mM **5c** residue concentration) copolymer solution in water with 500 µL of poly(A) solution at 5.84 mg/mL (17.6 mM poly(A) residue concentration) in 150 mM aqueous NaCl, at a 1:1 stoichiometric charge ratio, to create a 5 mg/mL copolymer stock C3M suspension. This C3M suspension was further diluted to 1 mg/mL copolymer in 150 mM aqueous NaCl to create the working C3M stock and was let equilibrate overnight at ambient temperature. To measure poly(A) encapsulation efficiency, 10 µL of working poly(A)-C3M stock suspension was diluted in 90 µL of 150 mM aqueous NaCl for suspensions with a final copolymer concentration of 0.1 mg/mL (176 µM **5c** residue concentration) and poly(A) concentration of 0.58 mg/mL (176 µM poly(A) residue concentration) and was then centrifuged at 13000 rpm for 30 min to concentrate the poly(A)-C3Ms while any unencapsulated poly(A) was retained in the supernatant. 17 µL of the supernatant was removed and diluted in 983 uL 1X TE buffer, RNase-free (Invitrogen) before dispensing 60 µL of the resulting suspension in triplicate into a 96 well plate and adding 60 µL of RiboGreen. The encapsulation efficiency was calculated using the calibration curve for poly(A) + RyboGreen described above.

General procedure for study of release of poly(A) from poly(A)-C3Ms

All buffers and salt solutions were prepared in nuclease-free water and filtered through 0.45 µm PES filters. The C3M complexes were prepared by mixing 500 µL of 10 mg/mL **PEG$_{113}$-*b*-5c$_{27}$** copolymer solution in water with 500 µL of poly(A) solution at 5.84 mg/mL in 150 mM aqueous NaCl, at a 1:1 stoichiometric charge ratio, to create a 5 mg/mL copolymer stock C3M suspension. This C3M suspension was further diluted to 1 mg/mL copolymer in 150 mM aqueous NaCl to create the working C3M stock and was let

equilibrate overnight at ambient temperature. For each buffer and salt condition (diluent), 10 µL of working C3M stock was diluted in 90 µL of diluent, to give a final copolymer concentration of 0.1 mg/mL (176 µM **5c** residue concentration and 176 µM poly(A) residue concentration). The suspensions were then incubated at 37 ^{o}C for the desired amount of time.

To quantify release of poly(A), the C3M suspension was centrifuged at 13000 rpm for 30 min, followed by removal of 17 µL of the supernatant and then diluting this in 983 µL 1X TE buffer, RNase-free (Invitrogen). 60 µL of each sample was dispensed in triplicate into a 96 well plate before adding 60 µL of RyboGreen RNA Reagent (Invitrogen) at its working concentration. The plate was covered in foil and incubated for 5 min before placing on a fluorescence plate reader (Excitation 480 nm, Emission 520 nm).

4.5.6 Spectral Data

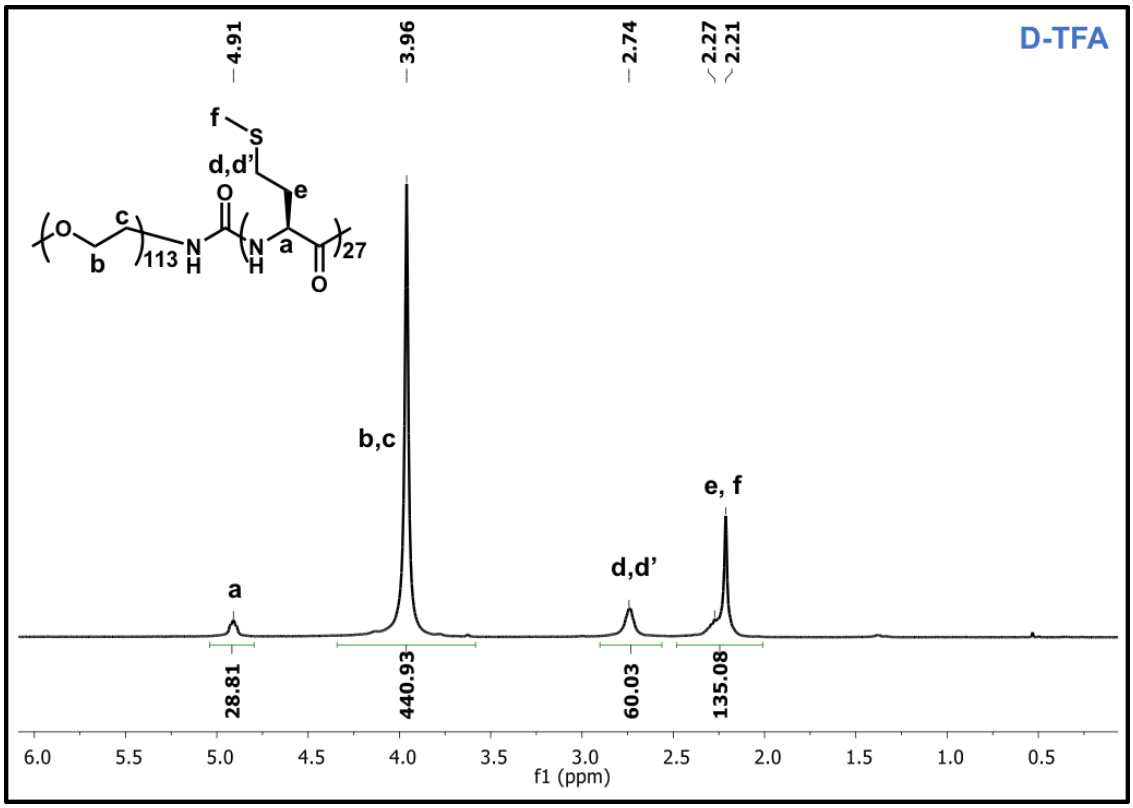
D-TFA
4.91
3.96
2.74
2.27
2.21
f
S
d,d'
e
O
c
O
b
113
N
H
N
H
a
27
O
b,c
e, f
d,d'
a
28.81
440.93
60.03
135.08
6.0
5.5
5.0
4.5
4.0
3.5
3.0
2.5
2.0
1.5
1.0
0.5
f1 (ppm)

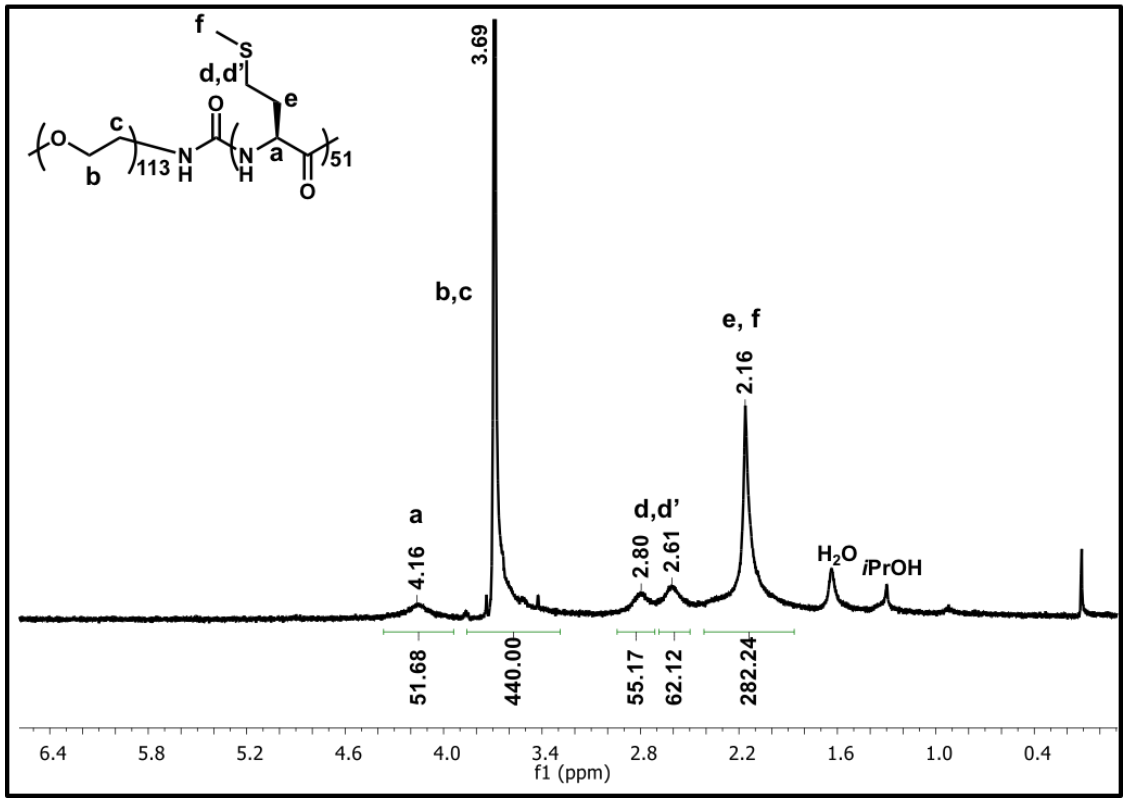
f
S
d,d'
e
O
c
O
b
113
N
H
N
H
a
51
O
3.69
b,c
e, f
2.16
a
4.16
d,d'
2.80
2.61
H2O
iPrOH
51.68
440.00
55.17
62.12
282.24
6.4
5.8
5.2
4.6
4.0
3.4
2.8
2.2
1.6
1.0
0.4
f1 (ppm)

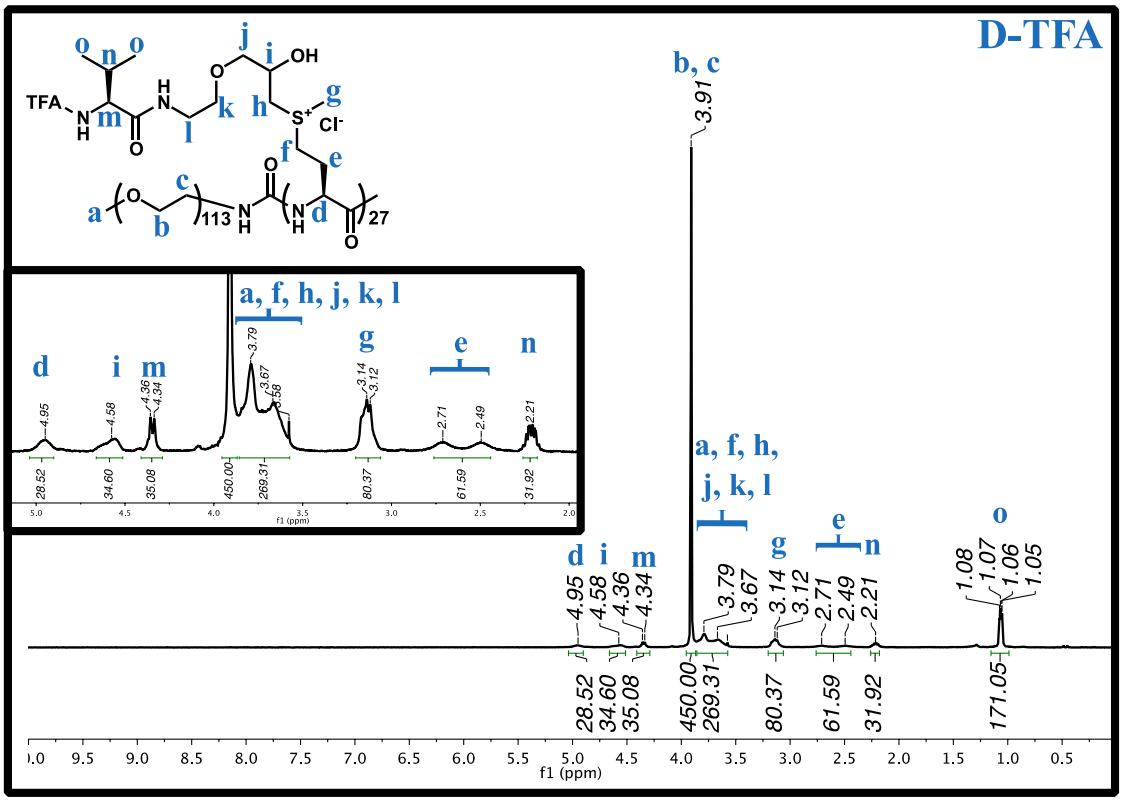
D-TFA
TFA
Cl-
OH
113
27
b, c
3.91
a, f, h, j, k, l
d i m g e n o
4.95 4.58 4.36 4.34 3.79 3.67 3.14 3.12 2.71 2.49 2.21 1.08 1.07 1.06 1.05
28.52 34.60 35.08 450.00 269.31 80.37 61.59 31.92 171.05
f1 (ppm)

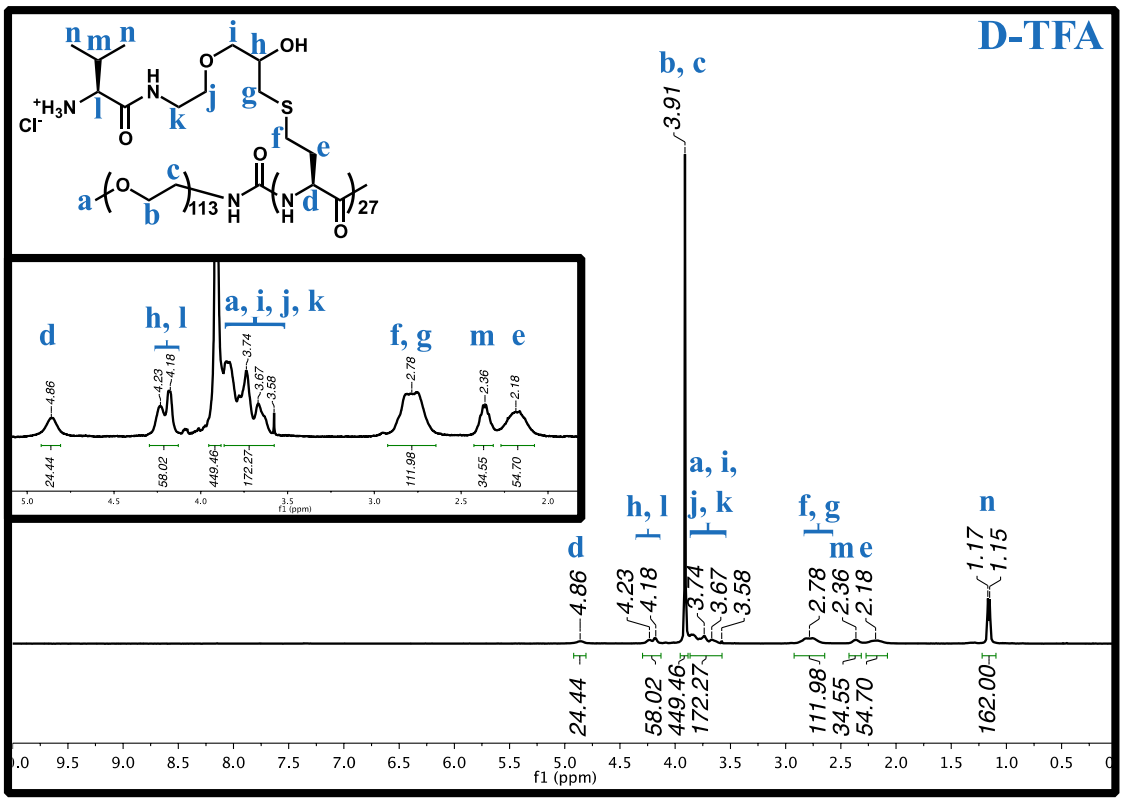
D-TFA
Cl-
OH
113
27
b, c
3.91
a, i, j, k
h, l
d
f, g
m e
n
4.86 4.23 4.18 3.74 3.67 3.58 2.78 2.36 2.18 1.17 1.15
24.44 58.02 449.46 172.27 111.98 34.55 54.70 162.00
f1 (ppm)

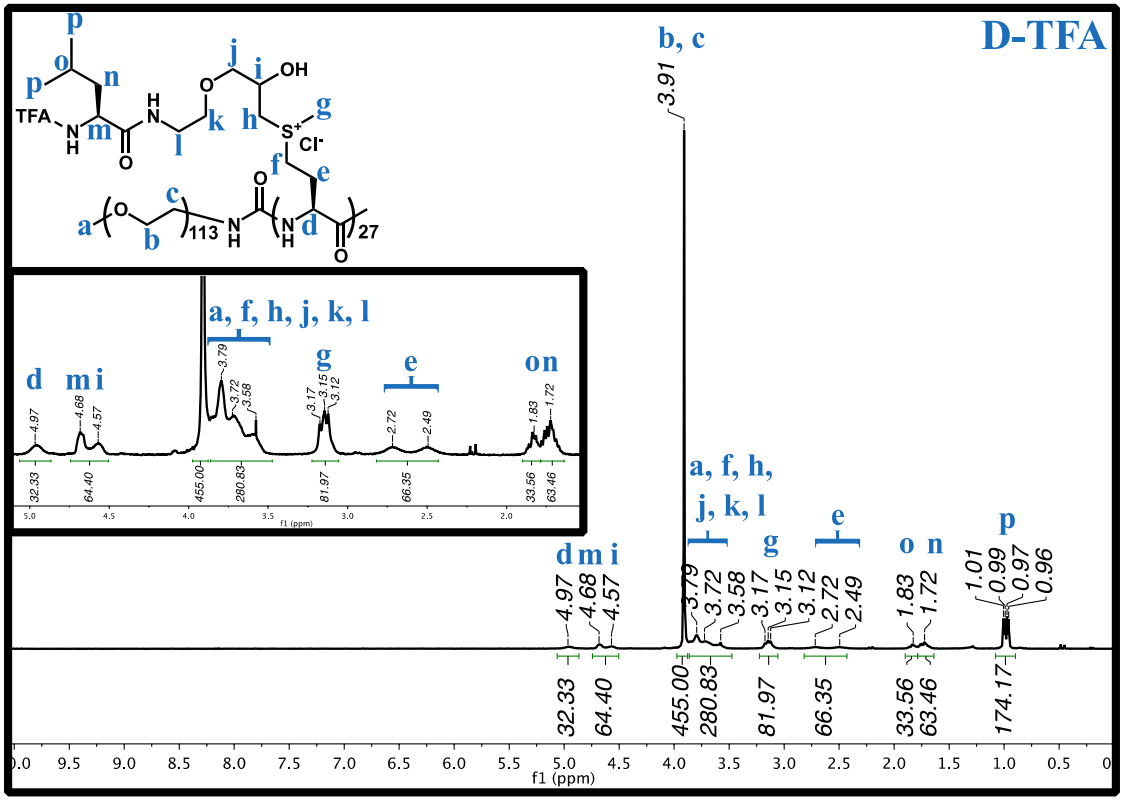
D-TFA
b, c
3.91
a, f, h, j, k, l
d m i
g
e
o n
p
4.97
4.68
4.57
3.79
3.72
3.58
3.17
3.15
3.12
2.72
2.49
1.83
1.72
1.01
0.99
0.97
0.96
32.33
64.40
455.00
280.83
81.97
66.35
33.56
63.46
174.17
f1 (ppm)

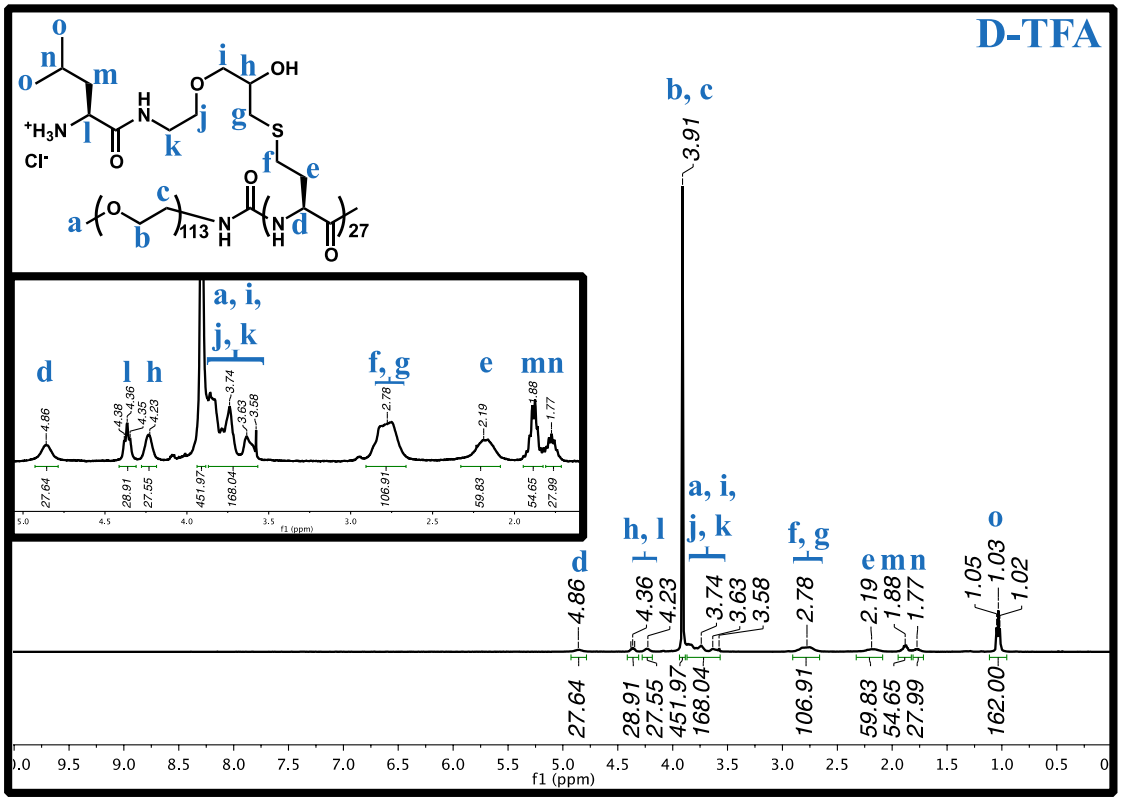
D-TFA
b, c
3.91
a, i, j, k
h, l
f, g
e m n
o
d
4.86
4.36
4.23
3.74
3.63
3.58
2.78
2.19
1.88
1.77
1.05
1.03
1.02
27.64
28.91
27.55
451.97
168.04
106.91
59.83
54.65
27.99
162.00
f1 (ppm)

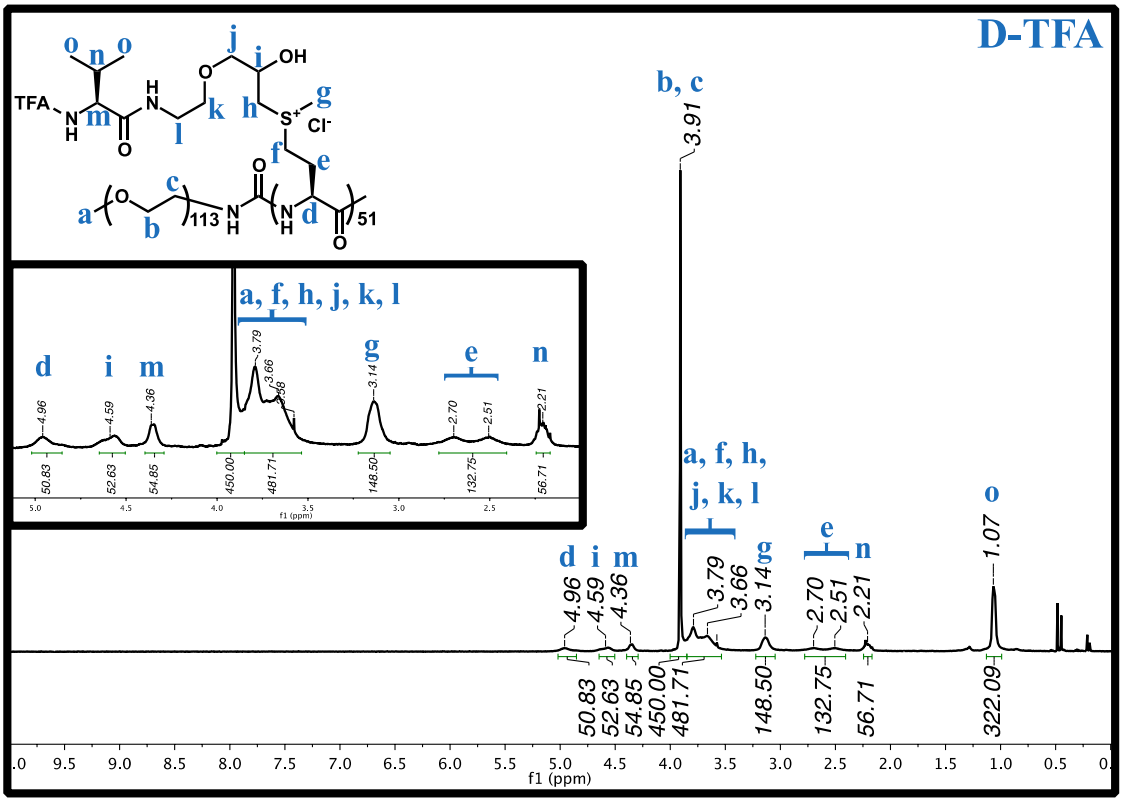
D-TFA
TFA
OH
Cl-
113
51
b, c
3.91
a, f, h, j, k, l
o
1.07
d i m
4.96
4.59
4.36
3.79
3.66
3.14
g
e
n
2.70
2.51
2.21
50.83
52.63
54.85
450.00
481.71
148.50
132.75
56.71
322.09
f1 (ppm)

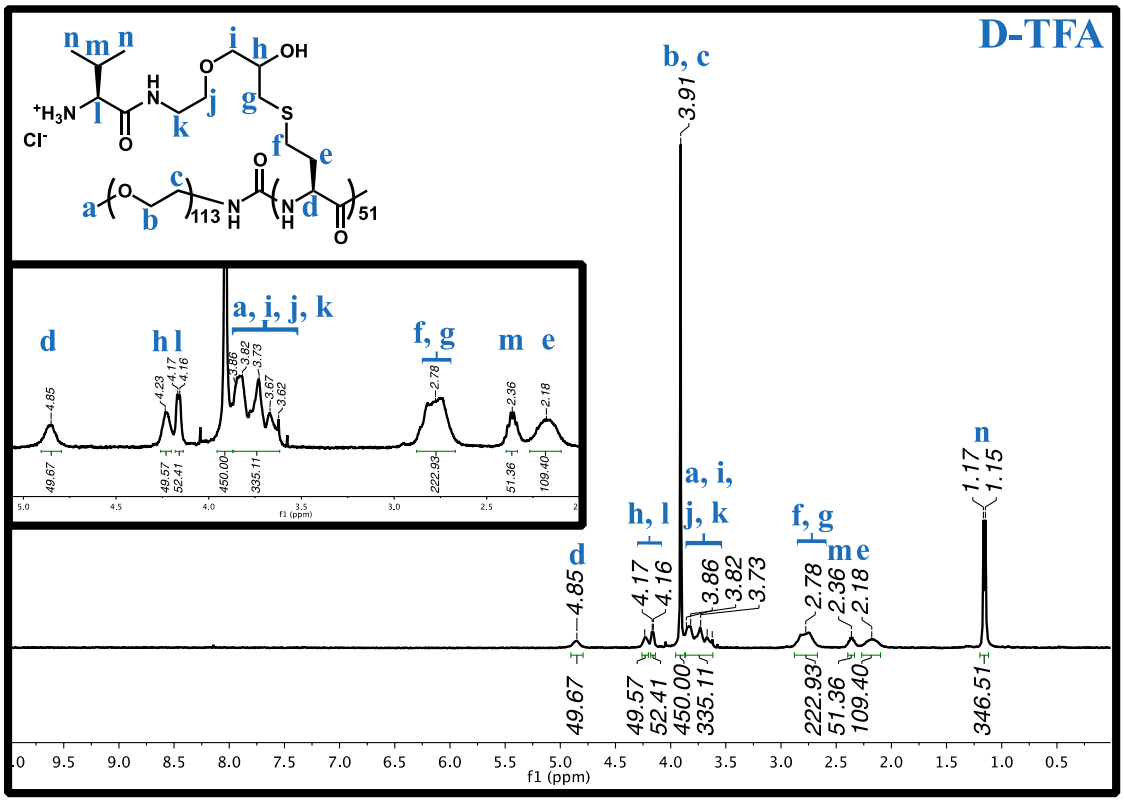
D-TFA
OH
Cl-
113
51
b, c
3.91
a, i,
j, k
h, l
f, g
m e
d
4.85
4.17
4.16
3.86
3.82
3.73
2.78
2.36
2.18
n
1.17
1.15
49.67
49.57
52.41
450.00
335.11
222.93
51.36
109.40
346.51
f1 (ppm)

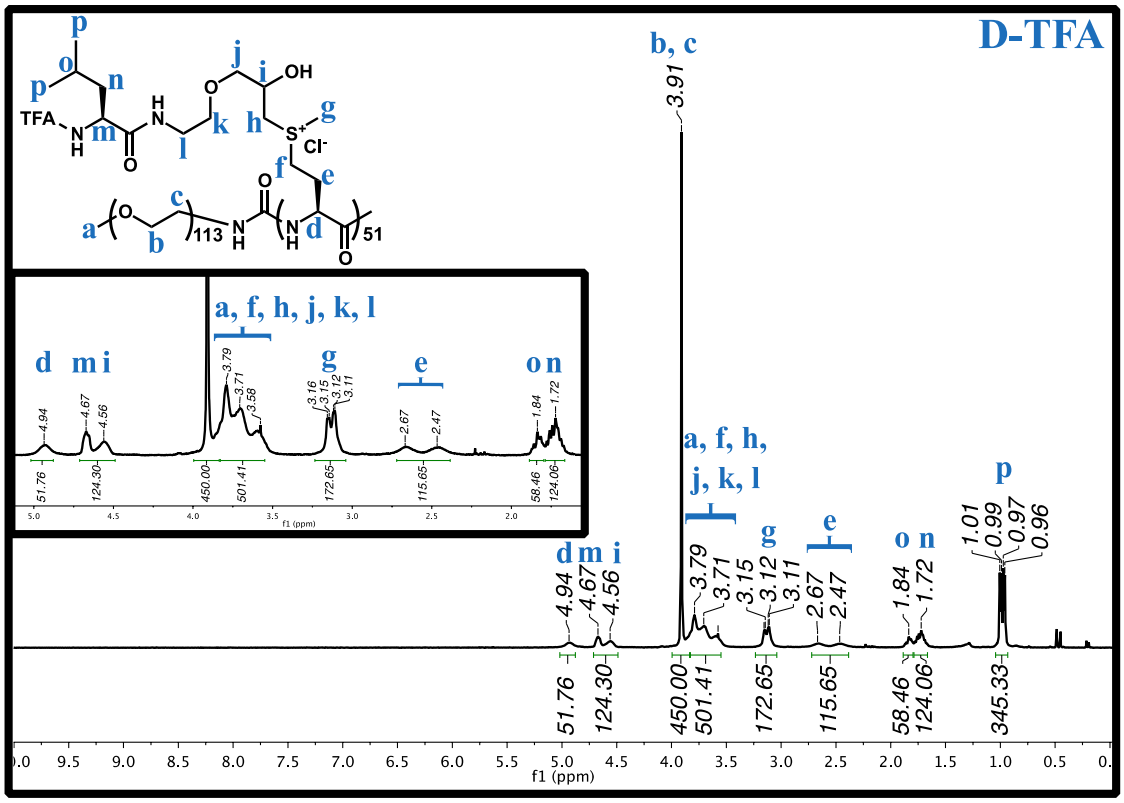
D-TFA
b, c
3.91
a, f, h,
j, k, l
p
g
e
o n
d m i
4.94
4.67
4.56
3.79
3.71
3.15
3.12
3.11
2.67
2.47
1.84
1.72
1.01
0.99
0.97
0.96
51.76
124.30
450.00
501.41
172.65
115.65
58.46
124.06
345.33
f1 (ppm)
TFA
OH
Cl-
113
51
a, f, h, j, k, l
d m i
g
e
o n

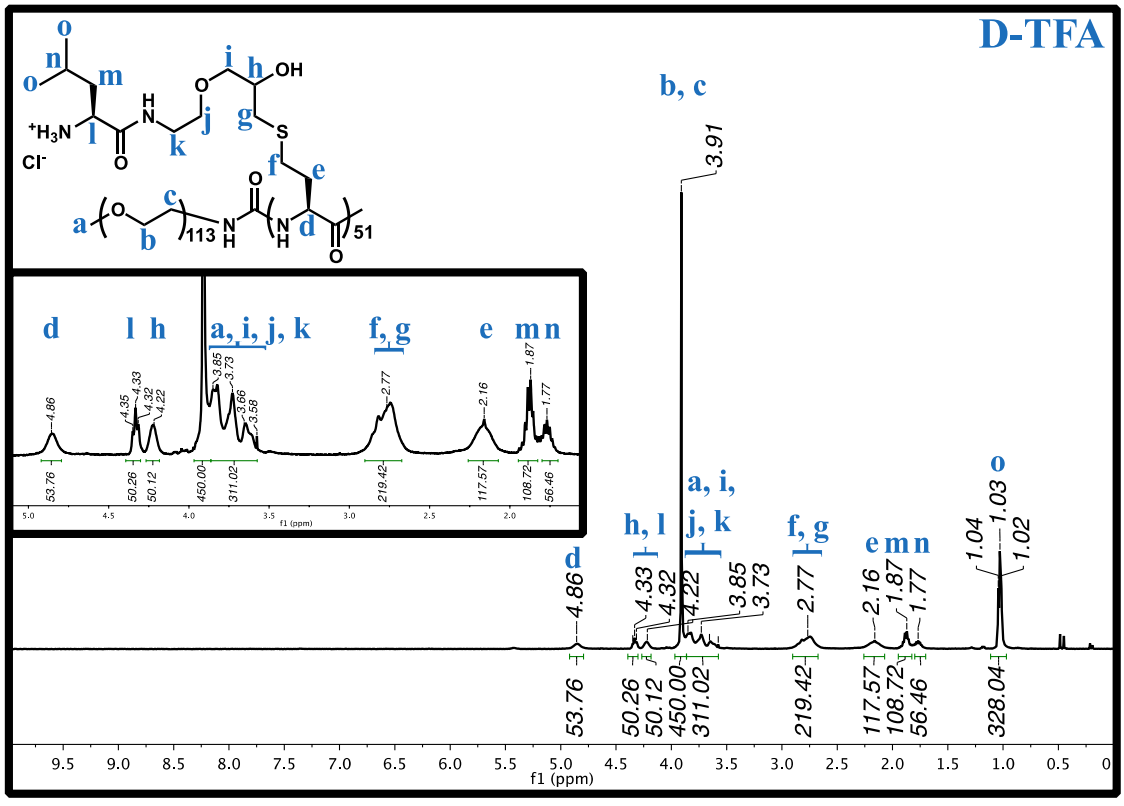
D-TFA
b, c
3.91
a, i,
j, k
h, l
f, g
e m n
d
o
4.86
4.33
4.32
4.22
3.85
3.73
2.77
2.16
1.87
1.77
1.04
1.03
1.02
53.76
50.26
50.12
450.00
311.02
219.42
117.57
108.72
56.46
328.04
f1 (ppm)
Cl-
113
51
d l h
a, i, j, k
f, g
e m n

4.6 References

(1) Mitragotri, S.; Burke, P. A.; Langer, R. *Nat. Rev. Drug Discov.* **2014**, *13* (9), 655–672.

(2) Friedmann, T.; Roblin, R. *Science* **1972**, *175* (4025), 949–955.

(3) Mulligan, R. C. *Science* **1993**, *260*, 926–932.

(4) Bertrand, J. R.; Pottier, M.; Vekris, A.; Opolon, P.; Maksimenko, A.; Malvy, C. *Biochem. Biophys. Res. Commun.* **2002**, *296* (4), 1000–1004.

(5) Lorenzer, C.; Dirin, M.; Winkler, A. M.; Baumann, V.; Winkler, J. *J. Control. Release* **2015**, *203*, 1–15.

(6) Kawabata, K.; Takakura, Y.; Hashida, M. *Pharm. Res.* **1995**, *12* (6), 825–830.

(7) Chen, S. H.; Haam, J.; Walker, M.; Scappini, E.; Naughton, J.; Martin, N. P. *Curr. Protoc. Neurosci.* **2019**, *87* (1), 1–11.

(8) Hou, X.; Zaks, T.; Langer, R.; Dong, Y. *Nat. Rev. Mater.* **2021**, *6* (12), 1078–1094.

(9) Lächelt, U.; Wagner, E. *Chem. Rev.* **2015**, *115* (19), 11043–11078.

(10) Verdera, H. C.; Kuranda, K.; Mingozzi, F. *Mol. Ther.* **2020**, *28* (3), 723–746.

(11) Lonez, C.; Vandenbranden, M.; Ruysschaert, J. M. *Prog. Lipid Res.* **2008**, *47* (5), 340–347.

(12) Priftis, D.; Megley, K.; Laugel, N.; Tirrell, M. *J. Colloid Interface Sci.* **2013**, *398*, 39–50.

(13) Priftis, D.; Laugel, N.; Tirrell, M. *Langmuir* **2012**, *28* (45), 15947–15957.

(14) Bungenberg De Jong, H. G.; Kruyt, H. R. *Proc. K. Ned. Akad. Wet* **1929**, *32*, 849–856.

(15) Singh, A. N.; Yethiraj, A. *J. Phys. Chem. B* **2020**, *124* (7), 1285–1292.

(16) Krogstad, D. V.; Lynd, N. A.; Choi, S. H.; Spruell, J. M.; Hawker, C. J.; Kramer, E. J.; Tirrell, M. V. *Macromolecules* **2013**, *46* (4), 1512–1518.

(17) Hunt, J. N.; Feldman, K. E.; Lynd, N. A.; Deek, J.; Campos, L. M.; Spruell, J. M.; Hernandez, B. M.; Kramer, E. J.; Hawker, C. J. *Adv. Mater.* **2011**, *23* (20), 2327–2331.

(18) Spruijt, E.; Sprakel, J.; Cohen Stuart, M. A.; Van Der Gucht, J. *Soft Matter* **2009**, *6* (1), 172–178.

(19) Priftis, D.; Farina, R.; Tirrell, M. *Langmuir* **2012**, *28* (23), 8721–8729.

(20) Kawamura, A.; Harada, A.; Kono, K.; Kataoka, K. *Bioconjug. Chem.* **2007**, *18* (5), 1555–1559.

(21) Water, J. J.; Schack, M. M.; Velazquez-Campoy, A.; Maltesen, M. J.; Van De Weert, M.; Jorgensen, L. *Eur. J. Pharm. Biopharm.* **2014**, *88* (2), 325–331.

(22) Deming, T. J. *Prog. Polym. Sci.* **2007**, *32* (8–9), 858–875.

(23) He, C.; Zhuang, X.; Tang, Z.; Tian, H.; Chen, X. *Adv. Healthc. Mater.* **2012**, *1* (1), 48–78.

(24) Lu, H.; Wang, J.; Song, Z.; Yin, L.; Zhang, Y.; Tang, H.; Tu, C.; Lin, Y.; Cheng, J. *Chem. Commun.* **2014**, *50* (2), 139–155.

(25) Shen, Y.; Fu, X.; Fu, W.; Li, Z. *Chem. Soc. Rev.* **2015**, *44* (3), 612–622.

(26) Liu, Y.; Yin, L. *Adv. Drug Deliv. Rev.* **2021**, *171*, 139–163.

(27) Vaheri, A.; Pagano, J. S. *Virology* **1965**, *27* (3), 434–436.

(28) Farber, F. E.; Melnick, J. L.; Butel, J. S. *Biochim. Biophys. Acta* **1975**, *390* (3), 298–311.

(29) Zauner, W.; Ogris, M.; Wagner, E. *Adv. Drug Deliv. Rev.* **1998**, *30* (1–3), 97–113.

(30) Kim, J. S.; Kim, B. Il; Maruyama, A.; Akaike, T.; Wan Kim, S. *J. Control. Release.* **1998**, *53* (1–3), 175–182.

(31) Kakizawa, Y.; Harada, A.; Kataoka, K. *J. Am. Chem. Soc.* **1999**, *121* (48), 11247–11248.

(32) Bello Roufaï, M.; Midoux, P. *Bioconjug. Chem.* **2001**, *12* (1), 92–99.

(33) Priftis, D.; Leon, L.; Song, Z.; Perry, S. L.; Margossian, K. O.; Tropnikova, A.; Cheng, J.; Tirrell, M. *Angew. Chem. Int. Ed.* **2015**, *54* (38), 11128–11132.

(34) Yen, J.; Zhang, Y.; Gabrielson, N. P.; Yin, L.; Guan, L.; Chaudhury, I.; Lu, H.; Wang, F.; Cheng, J. *Biomater. Sci.* **2013**, *1* (7), 719–727.

(35) Yen, J.; Ying, H.; Wang, H.; Yin, L.; Uckun, F.; Cheng, J. *ACS Biomater. Sci. Eng.* **2016**, *2* (3), 326–335.

(36) Kabanov, A. V.; Bronich, T. K.; Kabanov, V. A.; Yu, K.; Eisenberg, A. *Macromolecules* **1996**, *29* (21), 6797–6802.

(37) Harada, A.; Kataoka, K. *Macromolecules* **1995**, *28* (15), 5294–5299.

(38) Harada, A.; Kataoka, K. *Macromolecules* **2003**, *36* (13), 4995–5001.

(39) Marras, A. E.; Campagna, T. R.; Vieregg, J. R.; Tirrell, M. V. *Macromolecules* **2021**, *54* (13), 6585–6594.

(40) Van Der Kooij, H. M.; Spruijt, E.; Voets, I. K.; Fokkink, R.; Cohen Stuart, M. A.; Van Der Gucht, J. *Langmuir* **2012**, *28* (40), 14180–14191.

(41) Hayashi, K.; Chaya, H.; Fukushima, S.; Watanabe, S.; Takemoto, H.; Osada, K.; Nishiyama, N.; Miyata, K.; Kataoka, K. *Macromol. Rapid Commun.* **2016**, *37* (6), 486–493.

(42) Kim, Y. H.; Lee, K.; Li, S. *Chem. Mater.* **2021**, *33* (20), 7923–7943.

(43) Marras, A. E.; Ting, M.; Stevens, K. C.; Tirrell, M. V. *J. Phys. Chem. B* **2021**, *125* (26), 7076–7089.

(44) Fukushima, S.; Miyata, K.; Nishiyama, N.; Kanayama, N.; Yamasaki, Y.; Kataoka, K. *J. Am. Chem. Soc.* **2005**, *127* (9), 2810–2811.

(45) Ge, Z.; Chen, Q.; Osada, K.; Liu, X.; Tockary, T. A.; Uchida, S.; Dirisala, A.; Ishii, T.; Nomoto, T.; Toh, K.; Matsumoto, Y.; Oba, M.; Kano, M. R.; Itaka, K.; Kataoka, K. *Biomaterials* **2014**, *35* (10), 3416–3426.

(46) Christie, R. J.; Matsumoto, Y.; Miyata, K.; Nomoto, T.; Fukushima, S.; Osada, K.; Halnaut, J.; Pittella, F.; Kim, H. J.; Nishiyama, N.; Kataoka, K. *ACS Nano* **2012**, *6* (6), 5174–5189.

(47) Kuo, C. H.; Leon, L.; Chung, E. J.; Huang, R. T.; Sontag, T. J.; Reardon, C. A.; Getz, G. S.; Tirrell, M.; Fang, Y. *J. Mater. Chem. B* **2014**, *2* (46), 8142–8153.

(48) Min, H. S.; Kim, H. J.; Naito, M.; Ogura, S.; Toh, K.; Hayashi, K.; Kim, B. S.; Fukushima, S.; Anraku, Y.; Miyata, K.; Kataoka, K. *Angew. Chem. Int. Ed.* **2020**, *59* (21), 8173–8180.

(49) Gharakhanian, E. G.; Deming, T. J. *Chem. Commun.* **2016**, *52* (30), 5336–5339.

(50) Gharakhanian, E. G.; Deming, T. J. *Biomacromolecules* **2015**, *16* (6), 1802–1806.

(51) Scott, W. A.; Gharakhanian, E. G.; Bell, A. G.; Evans, D.; Barun, E.; Houk, K. N.; Deming, T. J. *J. Am. Chem. Soc.* **2021**, *143* (43), 18196–18203.

(52) Van Der Burgh, S.; De Keizer, A.; Cohen Stuart, M. A. *Langmuir* **2004**, *20* (4), 1073–1084.

(53) Tabandeh, S.; Leon, L. *Molecules* **2019**, *24* (5), 868.

(54) Sadman, K.; Wang, Q.; Chen, Y.; Keshavarz, B.; Jiang, Z.; Shull, K. R. *Macromolecules* **2017**, *50* (23), 9417–9426.

(55) Yuan, X.; Harada, A.; Yamasaki, Y.; Kataoka, K. *Langmuir* **2005**, *21* (5), 2668–2674.

(56) Lueckheide, M.; Vieregg, J. R.; Bologna, A. J.; Leon, L.; Tirrell, M. V. *Nano Lett.* **2018**, *18* (11), 7111–7117.

(57) Park, J. S.; Akiyama, Y.; Yamasaki, Y.; Kataoka, K. *Langmuir* **2007**, *23* (1), 138–146.

(58) Lindhoud, S.; Voorhaar, L.; Vries, R. De; Schweins, R.; Stuart, M. A. C.; Norde, W. *Langmuir* **2009**, *25* (19), 11425–11430.

(59) Li, L.; Srivastava, S.; Meng, S.; Ting, J. M.; Tirrell, M. V. *Macromolecules* **2020**, *53* (18), 7835–7844.

(60) Liu, Y.; Wang, W.; Yang, J.; Zhou, C.; Sun, J. *Asian J. Pharm. Sci.* **2013**, *8* (3), 159–167.

(61) Walimbe, T.; Panitch, A. *Front. Pharmacol.* **2020**, *10*, 1661.

(62) Zheng, N.; Yin, L.; Song, Z.; Ma, L.; Tang, H.; Gabrielson, N. P.; Lu, H.; Cheng, J. *Biomaterials* **2014**, *35* (4), 1302–1314.

(63) Gabrielson, N. P.; Lu, H.; Yin, L.; Li, D.; Wang, F.; Cheng, J. *Angew. Chem. Int. Ed.* **2012**, *51* (5), 1143–1147.

(64) Xu, Y.; Szoka, F. C. *Biochemistry* **1996**, *35* (18), 5616–5623.

(65) Kramer, J. R.; Deming, T. J. *Biomacromolecules* **2012**, *13* (6), 1719–1723.

(66) Kim, M.; Cha, C. *Biomacromolecules* **2020**, *21* (9), 3693–3703.

(67) Brzezinska, K. R.; Curtin, S. A.; Deming, T. J. *Macromolecules* **2002**, *35* (8), 2970–2976.